



GEORG-AUGUST-UNIVERSITÄT
GÖTTINGEN

**Specific ubiquitin-dependent protein degradation
requires a trimeric CandA complex in
*Aspergillus nidulans***

Dissertation

for the award of the degree

“Doctor rerum naturalium”

of the Georg-August Universität Göttingen

within the doctoral program “Microbiology and Biochemistry” of the
Georg-August University School of Science (GAUSS)

submitted by

Anna Maria Köhler

from Fritzlar

Göttingen, 2018

For my grandma Anna Wagner.

Thesis Committee and members of the Examination Board

Referee: Prof. Dr. Gerhard Braus

Department of Molecular Microbiology and Genetics,
Georg-August-Universität Göttingen

2nd referee: Prof. Dr. Kai Tittmann

Department of Molecular Enzymology
Georg-August-Universität Göttingen

3rd referee: Dr. Achim Dickmanns

Department of Molecular Structural Biology
Georg-August-Universität Göttingen

Further members of the Examination Board

Prof. Dr. Stefanie Pöggeler

Department of Genetics and Eukaryotic Microorganisms, Georg-August-Universität Göttingen

Jun.-Prof. Dr. Kai Heimel

Department of Molecular Microbiology and Genetics, Georg-August-Universität Göttingen

PD Dr. Michael Hoppert

Department of General Microbiology, Georg-August-Universität Göttingen

Date of oral examination:

Declaration of independence

Herewith I declare that the dissertation entitled “**Specific ubiquitin-dependent protein degradation requires a trimeric CandA complex in *Aspergillus nidulans***” was written on my own and independently without any other aids and sources than indicated.

Anna Maria Köhler

Göttingen, 2018

This work was conducted in the group of Prof. Dr. Gerhard H. Braus at the Department of Molecular Microbiology and Genetics, Institute of Microbiology and Genetics, Georg-August-Universität Göttingen.

Parts of this work will be published or are published:

Anna M. Köhler, Rebekka Harting, Annika E. Langeneckert, Oliver Valerius, Jennifer Gerke, Cindy Meister and Gerhard H. Braus (2019). Integration of fungal specific CandA-C1 into a trimeric CandA complex allowed splitting of the gene for the conserved receptor exchange factor of CullinA E3 ubiquitin ligases in *Aspergilli*. Submitted.

Köhler, A.M., Meister, C., and Braus, G.H. (2016) *In vitro* Deneddylation Assay. *Bio-protocol* 6(6): e1756. DOI: 10.21769/BioProtoc.1756.

Meister, C*, Kolog Gulko, M*, **Köhler, A.M.***, and Braus, G.H. (2016) The devil is in the details: comparison between COP9 signalosome (CSN) and the LID of the 26S proteasome. *Curr Genet* 62: 129–136 (* equally contributed)

Beckmann, E.A., **Köhler, A.M.**, Meister, C., Christmann, M., Draht, O.W., Rakebrandt, N., Valerius, O., and Braus, G. H. (2015) Integration of the catalytic subunit activates deneddylase activity in vivo as final step in fungal COP9 signalosome assembly. *Mol Microbiol* 97: 110–124

Table of contents

Summary.....	1
Zusammenfassung.....	2
1 Introduction	4
1.1 Fungi and the genus <i>Aspergillus</i>	4
1.1.1 <i>Aspergillus nidulans</i> and <i>Aspergillus fumigatus</i>	5
1.1.2 Germination and vegetative growth.....	6
1.1.3 Asexual development of <i>A. nidulans</i>	8
1.1.4 Sexual development of <i>A. nidulans</i>	8
1.1.5 Regulation of fungal growth and development	9
1.1.6 Secondary metabolism	12
1.2 Protein homeostasis.....	13
1.2.1 Posttranslational protein modification as functional signaling groups of proteins.	13
1.2.2 Ubiquitin and Nedd8	13
1.2.3 The E1, E2, E3 enzyme cascade – a PTM labelling apparatus	15
1.2.4 The ubiquitin proteasome system	18
1.3 Regulation of the ubiquitin proteasome system	20
1.3.1 CSN and DenA – two deneddylating isopeptidases	23
1.3.2 Canda – a substrate adaptor-receptor exchange factor	26
1.4 Aim of this work.....	30
2 Materials and Methods	31
2.1 Chemicals and materials	31
2.2 Media and growth conditions.....	33
2.2.1 Bacterial growth.....	33
2.2.2 Fungal growth.....	33
2.2.3 <i>Aspergillus fumigatus</i>	34
2.2.4 <i>Aspergillus nidulans</i>	35
2.3 Computational methods	37
2.4 Morphological methods	37
2.5 Nucleic acid methods	38
2.5.1 Isolation of fungal genomic DNA.....	38
2.5.2 Isolation of fungal genomic RNA.....	38
2.5.3 Isolation and purification of plasmid DNA, PCR products and linearized DNA fragments.....	39
2.5.4 Polymerase chain reaction.....	39
2.5.5 Agarose gel electrophoresis.....	39

Table of contents

2.5.6	Quantitative real-time polymerase chain reaction.....	40
2.5.7	cDNA amplification assay	41
2.6	Plasmid construction for genetic manipulation of <i>A. nidulans</i> , <i>A. fumigatus</i> and <i>E. coli</i>	41
2.6.1	Self-excising marker cassettes as selection markers	42
2.6.2	Primer and plasmid design	43
2.6.3	Plasmid and strain construction of <i>A. nidulans</i> mutant strains.....	48
2.6.4	Plasmid and strain construction of <i>A. fumigatus</i> mutant strains.....	55
2.6.5	Plasmid construction for protein expression in <i>E. coli</i>	56
2.7	Genetic manipulation of microorganisms.....	57
2.7.1	Transformation of <i>E. coli</i>	57
2.7.2	Transformation of <i>A. nidulans</i> and <i>A. fumigatus</i>	57
2.8	Southern hybridization.....	58
2.9	Protein methods.....	59
2.9.1	Protein extraction from <i>A. nidulans</i>	59
2.9.2	<i>In vitro</i> protein pull-down.....	59
2.9.3	SDS-PAGE	60
2.9.4	Western hybridization	60
2.9.5	Heterologous protein overexpression in <i>E. coli</i> and purification	61
2.9.6	Lysis of <i>E. coli</i> cell material.....	61
2.9.7	Affinity purification via HisTrap and GSTrap.....	62
2.9.8	Dialysis and GST-tag cleavage.....	62
2.9.9	Size-exclusion chromatography.....	62
2.10	Microscopy.....	63
2.11	Secondary metabolite extraction	63
2.12	Bottom-up protein analysis with mass spectrometry after pull-down experiments...64	
2.12.1	<i>In-gel</i> digest of proteins with trypsin	64
2.12.2	Sample clean-up of peptide samples with <i>C18 StageTips</i>	65
2.12.3	Peptide analysis with LC-MS	65
3	Results.....	67
3.1	Organization of <i>canA/canda</i> genes in Aspergilli	67
3.1.1	<i>A. fumigatus</i> carries an N-terminal extension of the CanA protein	67
3.1.2	<i>A. nidulans</i> carries an additional separate gene <i>canda-C1</i> corresponding to <i>A. fumigatus</i> N-terminal extension of CanA.....	69
3.1.3	<i>A. nidulans canda-C1</i> and <i>canda-C</i> express different transcripts	73
3.1.4	<i>A. fumigatus</i> expresses a CanA protein corresponding to the combined molecular weight of <i>A. nidulans</i> CandA-C1 with CandA-C.....	76

3.2	Cellular CanA/CandA functions	78
3.2.1	<i>A. nidulans</i> CandA proteins are mainly localized in the nucleus.....	78
3.2.2	<i>A. nidulans</i> CandA-N, CandA-C1 and CandA-C can physically interact and presumably form a trimeric complex.....	82
3.2.3	<i>A. nidulans</i> CandA interacts exclusively with cullin-1 (CulA)	84
3.2.4	<i>A. fumigatus</i> CanA interacts with CulA and CulC	90
3.2.5	<i>A. nidulans</i> CandA subunits but not recombinant CandA-N and CandA-C proteins activate CulA SCFs of <i>A. nidulans</i>	92
3.2.6	CandA-C1 contributes to SCF activation.....	97
3.2.7	CandA-C and CandA-N predominantly interact with each other and with Nedd8	99
3.3	The CandA-complex and fungal growth, development and secondary metabolism	106
3.3.1	CandA promotes spore germination.....	106
3.3.2	CandA-C1 specifically promotes vegetative growth and can be exchanged between <i>A. nidulans</i> and <i>A. fumigatus</i>	111
3.3.3	CsnE and CandA are required for vegetative growth and development in <i>A. nidulans</i>	117
3.3.4	<i>A. nidulans</i> CandA promotes accurate mitochondria development	119
3.3.5	<i>A. nidulans</i> CandA-C1 promotes conidia formation.....	120
3.3.6	CandA-N and CandA-C promote early phase of sexual development and repress orcinol SM-production, whereas CandA-C1 and DenA support later phases of cleistothecia formation	122
4	Discussion.....	130
4.1	The subunit composition of the CandA complex differs between eukaryotes.....	130
4.1.1	CandA-C1 is a separate protein in <i>A. nidulans</i> but an N-terminally extension of CanA C-terminal subunit in <i>A. fumigatus</i>	130
4.1.2	CandA-C1 and CanA N-terminally extension share the same sequence features in <i>A. nidulans</i> and <i>A. fumigatus</i>	131
4.1.3	CandA-C1 and the N-terminal CanA extension are conserved in <i>Aspergillus</i> and <i>Penicillium</i> spp. and might be bifunctional.....	134
4.1.4	The <i>candA</i> genes encountered a DNA rearrangement in a common ancestor of <i>Aspergillus</i> spp.	136
4.1.5	CandA-C1 and CandA-C are expressed from separate transcripts in <i>A. nidulans</i>	138
4.2	CandA proteins are required for growth and development in <i>A. nidulans</i> and <i>A. fumigatus</i> and the <i>A. nidulans</i> CandA complex is connected to secondary metabolism	140

Table of contents

4.2.1	CandA-N and CandA-C but not CandA-C1 repress the production of orsellinic acid derivatives in <i>A. nidulans</i>	140
4.2.2	<i>Aspergillus</i> CandA is required for development	141
4.2.3	<i>A. nidulans</i> CandA-C1 and the <i>A. fumigatus</i> CanA N-terminal domain are required for germination and vegetative growth	143
4.2.4	The <i>Aspergillus</i> specific CanA N-terminal extension and CandA-C1 are putative candidates for invasive aspergillosis treatment	145
4.3	CandA facilitates CulA neddylation.....	146
4.3.1	<i>A. nidulans</i> CandA mediates substrate-receptor-adaptor release on CulA containing SCFs	146
4.3.2	CandA might protect CRLs from autoubiquitination by a mechanism similar to CSN	148
4.3.3	<i>A. nidulans</i> CandA-N might modulate the cullin-Nedd8 binding site to facilitate neddylation	149
4.3.4	<i>A. nidulans</i> CandA physically interacts with Nedd8.....	150
4.3.5	CandA mediated protein quality control is observed at the nucleus, in the cytosol and at mitochondria in <i>A. nidulans</i>	151
4.4	Conclusion and Outlook	154
	Literature.....	157
	List of abbreviations	176
	List of figures.....	178
	List of tables	181
	Acknowledgements	182
	<i>Curriculum vitae</i>	184

Summary

E3 cullin-RING ubiquitin ligase complexes are activated by modification of their cullin scaffold protein with the ubiquitin-like modifier Nedd8. Deneddylases as the COP9 signalosome (CSN) or Den1/A interact and destabilize these complexes by cleaving the isopeptide bond between Nedd8 and cullin. Non-neddylated cullins can bind Cand1/A, which is the exchange factor for the substrate recognition subunits of the E3 RING ligases. Most eukaryotes possess a single Cand1 polypeptide. The mold *Aspergillus nidulans* and its relatives encountered a DNA rearrangement, which resulted in separate genes for two CandA polypeptides. CandA-N corresponds to N-terminal Cand1, blocking the neddylation site and CandA-C inhibits the interaction to the adaptor and substrate recognition subunits and thereby corresponds to the C-terminal Cand1. The Nedd8 blocking and adaptor-receptor exchange features are conserved in all eukaryotes. *A. nidulans* CandA proteins are required for asexual conidia production, sexual fruiting body formation, coordinated secondary metabolism and E3 ligase activity. Double deletion strains of *candA-N/denA*, *candA-N/csnE* and *candA-C/csnE* resulted in strains without the potential of cleistothecia formation and with reduced asexual development. A triple deletion strain of *candA-N/C/csnE* was additionally reduced in vegetative growth. These observations underline the importance of deneddylation and the exchange of substrate recognition subunits to allow E3 ligase activity towards a variety of substrates. The gene *candA-C* is located five open reading frames upstream of *candA-N*. This thesis shows that the CandA-C ortholog of the human pathogen *A. fumigatus* includes an additional fungal specific N-terminal 190 amino acid extension encoded by an extra exon, which is not present in human Cand1. This extension of *A. fumigatus* corresponds to *A. nidulans* CandA-C1 as a third CandA protein of 19 kDa encoded by a third *candA* gene 269 bp upstream of *candA-C*. The three fungal CandA-C1, CandA-C and CandA-N proteins form a trimeric complex mainly in the nucleus. This complex specifically interacts with CulA, supporting its neddylation but does not interact with other cellular cullins. *A. fumigatus* CanA is different and interacts with CulA as well as CulC E3 ligases. The *Aspergillus* specific CandA-C1 subunit has common but also distinct cellular functions in comparison to the other CandA proteins. This work shows that CandA-C1 of *A. nidulans* is required for vegetative growth, cleistothecia maturation including ascospore formation and activation of the ubiquitin labeling machinery. However, unlike the other CandA proteins, CandA-C1 does not affect the secondary metabolism of orcinol derivatives. *A. fumigatus* CanA N-terminal extension is as important for germination and vegetative growth as CandA-C1 in *A. nidulans*. These results make the *Aspergillus*-specific CandA/CanA subunit an interesting candidate for a drug-based approach to control fungal spreading in immunocompromised patients that are infected with e.g. *A. fumigatus* caused bronchopulmonary aspergillosis without affecting the human ubiquitin-proteasome system.

Zusammenfassung

E3-Cullin-RING-Ubiquitin-Ligase-Komplexe werden durch die kovalente Modifikation ihres Grundgerüst-Proteins Cullin mit dem ubiquitin-ähnlichem Modifizierer Nedd8 aktiviert. Deneddylasen, wie das COP9 Signalosom (CSN) und DenA interagieren und destabilisieren diese Komplexe durch die Trennung der Isopeptidbindung zwischen Nedd8 and Cullin. Nicht-neddylierte Culline können Cand1/A binden, welches der Austauschfaktor für die Substrat-Erkennungsmodule der E3 RING Ligasen ist. Die meisten Eukaryoten besitzen ein einzelnes Cand1 Polypeptit. Veränderungen in der Gen Anordnung führten bei dem Schimmelpilz *Aspergillus nidulans* und seinen Verwandten zur Trennung des CandA Gens in zwei separate Gene, die für jeweils eine CandA Protein-Untereinheit kodieren. CandA-N entspricht dem N-terminalen Cand1 und verdeckt die Neddylierungsstelle. CandA-C entspricht dem C-terminalen Cand1 und inhibiert die Bindung der Substratadapter-Proteine. Die Blockierung der Nedd8-Bindestelle und der Substratadapter-Austausch sind in allen Eukaryoten konserviert. Die *A. nidulans* CandA Proteine werden für die asexuelle Konidiosporenbildung, die sexuelle Fruchtkörperentwicklung, für einen koordinierten Sekundärmetabolismus und für E3 Ligase-Aktivität benötigt. Doppeldeletionsmutanten von *candA-N/denA*, *candA-N/csnE* und *candA-C/csnE* können keine Kleistothecien bilden und zeigen eine reduzierte asexuelle Entwicklung. Eine Dreifachdeletion von *candA-N/C/csnE* zeigt zusätzlich ein eingeschränktes vegetatives Wachstum. Diese Beobachtungen zeigen, dass die Deneddylierung und der Austausch der Substratadaptoren für die Variabilität von Substraten der E3 Ligasen von großer Bedeutung sind. Das Gen *candA-C* liegt fünf offene Leserahmen vor dem Gen *candA-N*. Diese Dissertation zeigt, dass das CandA-C orthologe Protein in *A. fumigatus* eine zusätzliche pilzspezifische N-terminale Verlängerung von 190 Aminosäuren hat, welche in einem separaten Exon kodiert ist, aber im menschlichen Cand1 fehlt. In *A. fumigatus* entspricht diese Erweiterung dem CandA-C1 protein von *A. nidulans*. Dieses ist ein drittes CandA Protein von 19 kDa und wird von einem dritten *candA* Gen kodiert, welches 269 bp vor dem *candA-C* Gen liegt. Die drei CandA-C1, CandA-C und CandA-N Proteine bilden einen Dreierkomplex der hauptsächlich im Zellkern zu finden ist. Dieser Komplex interagiert spezifisch mit CulA und unterstützt dessen Neddylierung. Der Komplex bindet jedoch keine anderen Culline. CanA von *A. fumigatus* bindet neben CulA auch CulC E3 Ligasen. Die *Aspergillus*-spezifische CandA-C1 Untereinheit hat im Vergleich zu den anderen beiden CandA Proteinen gemeinsame und unterschiedliche Funktionen. Diese Arbeit zeigt, dass CandA-C1 von *A. nidulans* für das vegetative Wachstum, die Reifung der Kleistothecien und der damit verbundenen Ascosporenbildung sowie der Aktivierung der Ubiquitinmarkierungssysteme verantwortlich ist. Anders als CandA-N und CandA-C hat CandA-C1 keinen Einfluss auf den Sekundärmetabolismus von Orsellinsäure-Derivaten. Der N-terminale Bereich des *A. fumigatus* CanA ist genauso wichtig für die Sporenkeimung und das vegetative Wachstum

wie CandA-C1 von *A. nidulans*. Diese Ergebnisse machen die *Aspergillus*-spezifische CandA/CanA Untereinheit zu einem interessanten Kandidaten für die Medikamentenforschung gegen Pilzinfektionen bei zum Beispiel immungeschwächten Patienten mit bronchopneumonaler Aspergillose verursacht durch *A. fumigatus*, ohne dabei das menschliche Ubiquitin-Proteasome-System zu beeinträchtigen.

1 Introduction

1.1 Fungi and the genus *Aspergillus*

Fungi belong to the domain of eukaryotes and are closely related to animals and plants. The term *fungus* (English: mushroom), is a word of Latin origin, which in term originated from the Greek word *sphóngos* (sponge). One subkingdom of Fungi is the Dikarya, which is often called “higher fungi”. *Dikarya* (Greek: *di* = two, *karyon* = *nucleus*) are split into Ascomycota and Basidiomycota, which form filamentous or unicellular structures that can have two different haploid nuclei in certain phases of development. Filamentous fungi are characterized as asexual and sexual spore-producing organisms that grow as branching filamentous structures, called hyphae, which have a thick cell wall containing chitin and/or cellulose and many other complex compounds (Adams *et al.*, 1998; Bartnicki-Garcia, 2002; Steinberg, 2007). Ascomycota are the largest phylum of fungi, which contains about 64 000 described species (Abinsworth and Bisby, 2008) including for example the penicillin producing fungus *Penicillium chrysogenum* and the genetic model organism *Aspergillus nidulans*. The name of this phylum derives from the sac-like (Greek: *askus* = sac) structures formed under the sexual life style produced by most of the phylum members (Pöggeler *et al.*, 2018). The probably best studied genus is *Aspergillus*. The name *Aspergillus* was given by Micheli (Micheli, 1729) because the appearance of the asexual spore-bearing structure that looks like an *asperges*, which is a device for sprinkling holy water during Roman Catholic clergy (Bennett, 2010). The 350 known *Aspergillus* species (de Vries *et al.*, 2017) are ubiquitously distributed mostly saprophytic in soil and can have harmful as well as beneficial properties to plants, animals and humankind. They can produce different enzymes and secondary metabolites, such as mycotoxins (e.g. aflatoxin by *A. flavus*), which cause food spoilage (Bossou *et al.*, 2017). They are useful in many different fields such as biotechnology (e.g. citric acid production by *A. niger*, soy sauce production by *A. oryzae*) and pharma industry (e.g. lovastatin synthesis, a cholesterol reducing agent from *A. terreus*) but can cause health risks as for example pulmonary aspergillosis (human pathogens like *A. fumigatus* and *A. flavus*) (Gerke and Braus, 2014; Samson *et al.*, 2014; Challa, 2018). Besides those fields, *Aspergillus* species are of great interest in science to studying the eukaryotic cell biology, genetics and physiology (Pontecorvo *et al.*, 1953). *A. nidulans* has a fast propagation by vegetative hyphal growth from germinating spores in 12 to 20 hours and competence for asexual and sexual life style as well as the property of easy genetic manipulation which are ideal features for a model organism. *A. fumigatus* is a close relative of *A. nidulans* and is used in science as sophisticated model to study aspergillosis. The nomenclature for genes and proteins in *Aspergillus* species uses a letter code, which most often corresponds to mammalian number code (e.g. CuiA – Cullin-1) (Howard and Gow, 2001).

1.1.1 *Aspergillus nidulans* and *Aspergillus fumigatus*

Aspergillus nidulans is a self-fertilizing homothallic fungus (Raper and Fennell, 1965) and studied as model organism for understanding the science of a eukaryotic cell. Besides selfing, *A. nidulans* can also reproduce with a opposite mating-type partner, which makes it beneficial for crossing with a suitable partner (Todd *et al.*, 2007). It has eight chromosomes and a total genome size of 31 Mb. The genome is completely sequenced but only 19 % of the 10 560 encoded genes are characterized (Bayram *et al.*, 2016). *Emericella nidulans* is an alternative name, whereby *Emericella* describes the capability for sexual reproduction. This double nomenclature is based on the fact that *Aspergillus* describes the asexual reproduction and the sexual cycle is not known for all *Aspergillus* species. Therefore subgenera like *Emericella* were introduced but reversed to have a 'one-fungus: one name' nomenclature (Samson *et al.*, 2014; Chen *et al.*, 2016). Therefore, *Emericella* and *Aspergillus* are the same genera. *A. nidulans* has an asexual life style producing conidiophores. Conidiophores are built of different cell types: a hypha swells to become a foot cell, which develops a vertically growing stalk with a vesicle cell at its tip. On top of the vesicle is one layer of metulae followed by a layer of phialide cells that then bud to form the characteristic green pigmented conidiospores (Figure 1A). *A. nidulans* has a vegetative hyphal growth prior to the sexual and asexual developmental programs. Exposure to air is a prerequisite for asexual conidiospore formation whereas carbon dioxide and dark conditions support sexual fruiting body formation (Adams *et al.*, 1998).

Aspergillus fumigatus is a heterothallic fungus. Until 2009, when its sexual cycle was discovered, only an asexual life cycle of *A. fumigatus* had been described (O'Gorman *et al.*, 2009) (Figure 1B). Conidiophores of *A. fumigatus* lack metulae cells, thus spores develop from phialide cells, different to conidiophores of *A. nidulans* (Figure 1) (Yu, 2010). *A. fumigatus* usually grows as saprophyte in compost or other degrading matter being of importance in recycling carbon and nitrogen. Furthermore, *A. fumigatus* is the major cause of invasive fungal infection causing aspergillosis (mold pneumonia) in immunocompromised patients that inhale the airborne conidia (Figure 1B). Conidia of *A. fumigatus* are hydrophobic and only 2-3 μm in diameter, which make them readily airborne (Paulussen *et al.*, 2017). Inhalation of conidia appears daily, and healthy individuals have an immune system that is capable of recognizing conidia resulting in conidia clearance (Shlezinger *et al.*, 2017). The spores can bind to the lung alveoli surface in immunocompromised patients, which leads to altered conidial hydrophobicity and invading of the spores into the lung tissue (Dagenais and Keller, 2009; Oliveira, 2014). The spores gain metabolic activity within 30 min, and germinate within six to eight hours (Kwon-Chung and Sugui, 2013). The fungus can also invade blood vessels whereby it distributes throughout the host (Sheppard and Filler, 2014; Paulussen *et al.*, 2017). The mortality rate of aspergillosis caused by specific strains can be up to 90%. Increased resistance to common fungicides like azoles arises for example due to high application doses in

agriculture (Verweij *et al.*, 2009; Gsaller *et al.*, 2016; Zhang *et al.*, 2017). *A. fumigatus* pathogenicity deficient mutants are extensively used in scientific studies to find virulence factors that might be good targets for drug design (Dagenais and Keller, 2009; Lin *et al.*, 2015; Jöhnk *et al.*, 2016; Thammahong *et al.*, 2017).

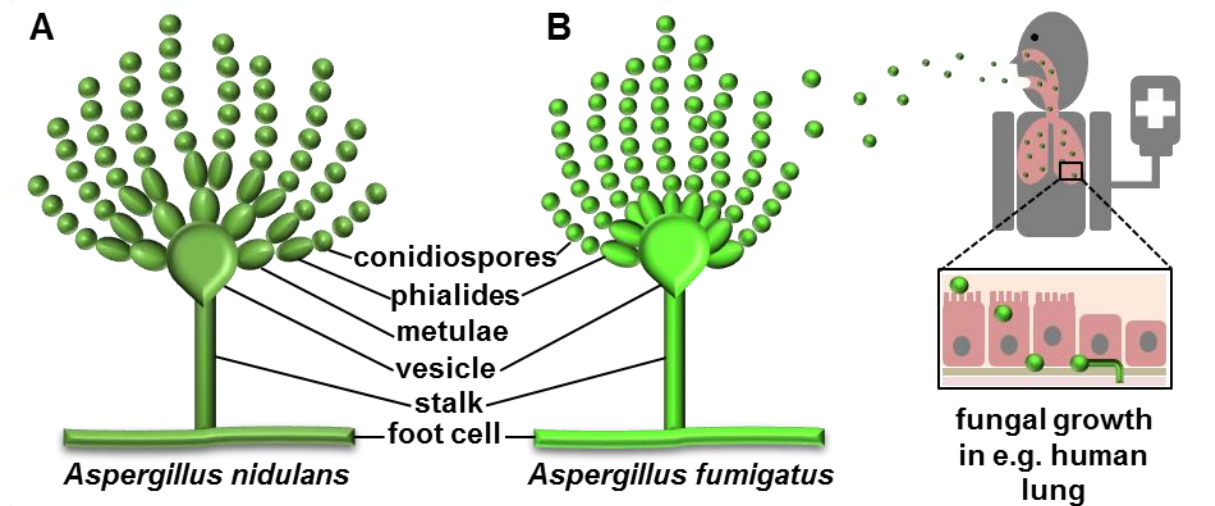


Figure 1. Conidia of *A. nidulans* and *A. fumigatus*. **A** *A. nidulans* conidiophores develop from a foot cell, forming a stalk and vesicle, from which metulae cells are budding and further budding processes produce the spore-forming phialides resulting in asexual conidiospores. Each conidia has a size of about $2.4 \times 2.7 \mu\text{m}$ in diameter. **B** *A. fumigatus* conidiophores lack metulae and spores are smaller ($1.3 \times 1.8 \mu\text{m}$). Conidia from *A. fumigatus* can cause pneumonic diseases like aspergillosis in case the spores are not detected by a weak immune system and then propagate in lung tissue (partially modified from Dagenais and Keller, 2009; Yu, 2010).

1.1.2 Germination and vegetative growth

Vegetative growth of *Aspergillus* species includes chains of tubular cells that expand at their hyphal tip. Vegetative propagation starts with the germination of spores, which form tubular filaments. (Horio and Oakley, 2005; Steinberg, 2007). Spores can easily survive long periods in distilled water without having metabolic activity (Osheroov and May, 2000). Germination is initiated as soon as spores are exhibited to a nutrient source and other conditions, such as an appropriate spore density are as well given. Activity of trehalose breakdown and translational activity can be measured already after 20 min of germination inducing conditions, which is a disaccharide for energy supply (Hagiwara *et al.*, 2017). In consequence the spore swells and the nucleus divides already 360 min after induction which finally results in polarized hyphal growth (Bainbridge, 1971). This hyphal extension requires the polarized transport on actin and

microtubule filaments as well as exocytosis of vesicles containing cell wall components, ribosomes and mRNAs for apical protein synthesis (Horio and Oakley, 2005; Steinberg, 2007; Taheri-Talesh *et al.*, 2008). The tip of this organized polarisome is called the *Spitzenkörper* (Harris *et al.*, 2005). The shape of the hyphae is supported by the internal turgor, cell wall containing polysaccharides and membrane proteins (Bartnicki-Garcia *et al.*, 2000). Hyphal compartments are separated by septa, which are positioned after multiple rounds of nuclear division (Fiddy and Trinci, 1976). The vegetative growth is the simplest form of fungal propagation. A complex hyphal network is developed after 16 to 20 hours and is called mycelium. This is the same time when the fungus reaches developmental competence as hyphae become sensitive to external stimuli (e.g. light, nutrients, fungal pheromones, oxygen), which determine the induction of the asexual and/or sexual developmental program (Figure 2) (Axelrod *et al.*, 1973; Champe and Simon, 1992; Bayram and Braus, 2012).

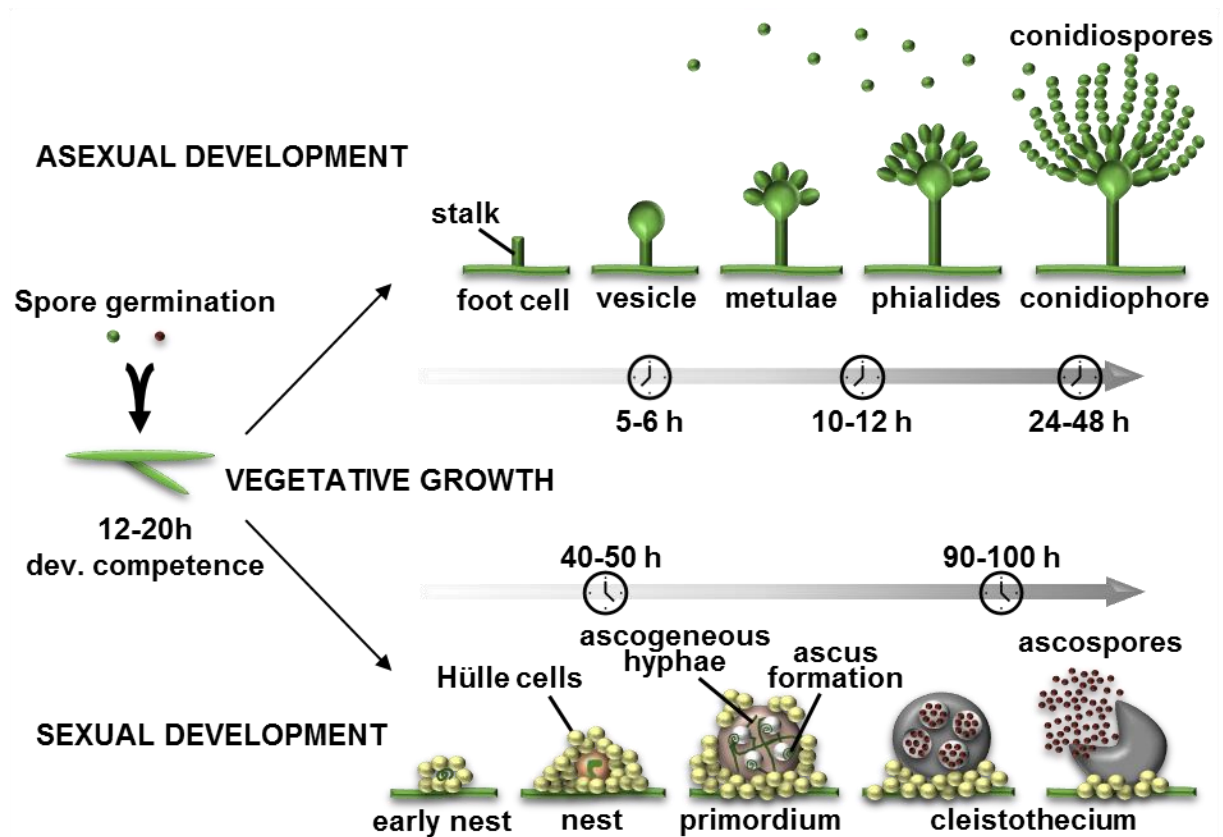


Figure 2. *Aspergillus nidulans* life cycle. Asexual or sexual spores germinate upon nutrient supply and form a network of polarized growing hyphae. After 12-20 hours of vegetative growth, cells reach developmental competence. The asexual development includes the formation of conidiophores from a swelling foot cell, which forms a stalk and then a vesicle. The vesicle undergoes mitotic nuclear divisions and by apical budding processes metulae, phialides and conidia are formed. In the sexual development nest-like structures are formed by Hülle cells covering the fusing ascogoneous hyphae, differentiating into young asci, called primordium. Several rounds of meiosis and mitosis result in several thousand asci each containing eight ascospores. Cleistothecia are designated as the overwintering structures of the fungus.

1.1.3 Asexual development of *A. nidulans*

Asexual development is favored mainly by light and oxygen supply when the fungus grows on solid media/surfaces after it gained developmental competence (Adams *et al.*, 1998; Krijgsheld *et al.*, 2013). Asexual development results in structures called conidiophores, which harbor mitotically derived conidiospores 24 to 48 hours after germination (Figure 2) (Yu, 2010). A vegetative hypha grows an aerial hyphal branch that is called the conidiophore stalk. The basal hyphal compartment is a swelling, thick-walled foot cell connecting the stalk to the rest of the mycelium (Adams *et al.*, 1998). The stalk tip begins to swell and forms one compartment with a vesicle structure at the tip five to six hours post induction of asexual development. Division of multiple nuclei and budding of the cell wall at the surface of the vesicle form a primary layer of about 60 uninucleated metulae cells (Mims *et al.*, 1988; Fischer and Timberlake, 1995). In the following, each metula undergoes two polar, apical budding events producing a secondary layer of about 120 cylindrical phialide cells after 10 to 12 hours of starting development (Adams *et al.*, 1998; Etxebeste *et al.*, 2010). The phialides perform a series of asymmetric divisions producing chains of uninucleated spores. By this more than 10 000 spores are produced by one conidiophore that are capable for a new cycle of growth and development (Figure 2) (Adams *et al.*, 1998).

1.1.4 Sexual development of *A. nidulans*

The knowledge of sexual development is limited to some *Aspergillus* species (Krijgsheld *et al.*, 2013; Pöggeler *et al.*, 2018). The sexually derived closed fruiting bodies of *A. nidulans* are called cleistothecia. Their function is to protect the sexual spores by many layers of different cell types and are therefore an overwintering structure for those ascomycetes (Braus *et al.*, 2002). Whereas asexual conidiophores are similar in all ascomycetes, sexual fruiting body morphology differs between species (e.g. cleistothecia in *A. nidulans* and perithecia in *S. macrospora* (Pöggeler *et al.*, 2018)). Sexual development in Aspergilli is initiated by fusion of hyphae of opposite mating partners (e.g. in *A. fumigatus*) or by selfing (e.g. in *A. nidulans*). The developing fruiting body is surrounded by differentiating mycelium and Hülle cells, which together form the so-called nest (Krijgsheld *et al.*, 2013) (Figure 2). The mycelium is involved in the formation of the fruiting body envelope and the Hülle cells are thick-walled nursing cells emerging either at hyphal tips or intercalary positions (Ellis *et al.*, 1973; Carvalho *et al.*, 2002). The ascogenous hyphae form hooks in which the nuclei divide several times synchronously, developing to dikaryotic cells, the crozier cells. Two nuclei fuse (karyogamy), which results in diploid young asci appearing around 70 to 80 hours after germination (Pontecorvo *et al.*, 1953). Karyogamy is followed by meiosis resulting in four nuclei that are further divided by a first mitosis

into eight nuclei (Braus *et al.*, 2002). The immature fruiting body is named primordium and contains ascogenous hyphae that build a membrane surrounding the asci (Pöggeler *et al.*, 2006, 2018). A second round of mitosis forms binuclear, red-pigmented ascospores. Meanwhile the cleistothecial wall surrounding the asci matures and the Hülle cells are degenerated. Each cleistothecium is around 200 µm in size and contains around 80 000 spores 100 hours after germination of the initial spore (Braus *et al.*, 2002) (Figure 2).

1.1.5 Regulation of fungal growth and development

Developmental decisions are required to adapt a fungus to environmental changes. External and internal stimuli regulate signaling cascades involving heterotrimeric G-protein complex coupled receptors or light-dependent receptors and transcription factors that induce germination, vegetative growth and asexual or sexual development.

Spores are the resting structures of fungi. They can be exhibited to various stress conditions, but germination is prevented under unfavorable circumstances by different mechanisms and is described as dormancy (Herrero-Garcia *et al.*, 2011; Novodvorska *et al.*, 2013). Growth of *Aspergillus* species starts with a germinating spore. Germination triggers are for example a carbon source (e.g. glucose) recognized by a receptor and in turn the cAMP/PKA (cyclic adenosine monophosphate, protein kinase A) pathway is activated, which results in activation of a downstream cascade inducing trehalose degradation by TreB (trehalase B) to glucose (Lafon *et al.*, 2005; Krijgsheld *et al.*, 2013; Svanström and Melin, 2013). This supplies energy for the germination process, which includes swelling of the spore followed by germ tube formation. The switch of isotropic swelling to polarized germ tube formation is mediated by inactivation of the Ras GTPase RasA (rat sarcoma). The GTPase-activating protein GapA mediates the hydrolysis of GTP from RasA, which inactivates RasA and in turn actin cytoskeleton polymerization is initiated for polarized growth (Harispe *et al.*, 2008). The velvet transcription factors VelB (velvet-like B) and VosA (viability of spores A) are required for trehalose biosynthesis and have direct influence on spore viability and stress tolerance (Figure 3) (Sarıkaya Bayram *et al.*, 2010). VelB was also shown to act downstream of the G-protein GanB inhibiting germination (Park *et al.*, 2012, 2015).

Growth is regulated by heterotrimeric G-protein complexes by stimulating vegetative growth and repressing conidiation (Shimizu and Keller, 2001; Yu, 2006). Activation of the MAPK kinase cascade leads to phosphorylation of transcription factors that in consequence influence downstream factors. One important downstream factor is BrIA (bristle A), which is required for vesicle and metulae formation (Figure 3) (Dickman and Yarden, 1999; Bayram *et al.*, 2012).

BrlA is a major regulator of asexual development and is required for processes after conidiophore stalk production, which involves a series of different additional transcription factors (Adams *et al.*, 1988). The central regulatory pathway of asexual development is proposed to start with a putative extracellular FluG (fluffy G) signal (Figure 3) (Yu, 2010). FluG has repressing effects on *sfgA* (s_u_ppressor of *fluG*), whereby the *flb* (fluffy low *brlA*) genes are activated (Seo *et al.*, 2006). Deletion of *fluG*, *sfgA* and *flb* genes results in the production of mainly aerial hyphae without conidiospores and low *brlA* expression levels (Adams *et al.*, 1992; Seo *et al.*, 2006).

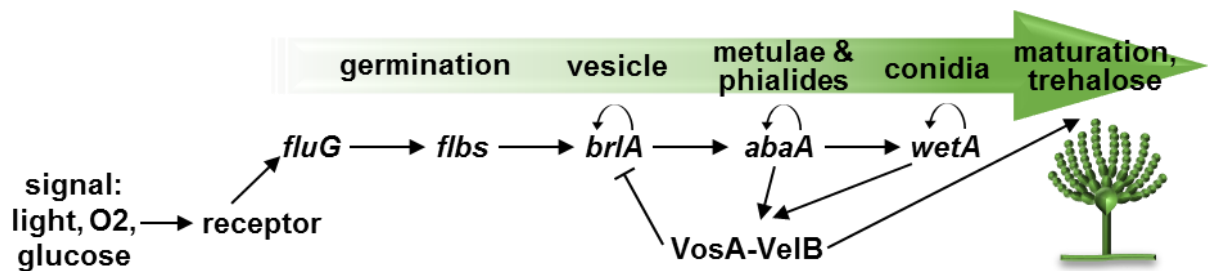


Figure 3. The central regulatory pathway of *A. nidulans* asexual development. Asexual development is induced by external signals like light, oxygen and nutrients such as glucose. Those stimuli are sensed by receptors that activate signal transduction into the nucleus where the transcription factor cascade of *fluG* → *flbs* → *brlA* → *abaA* → *wetA* is activated. The single pathway components exhibit different autoregulatory feedback loops. VosA-VelB heterodimer represses *brlA* expression but has positive effect on spore maturation and trehalose synthesis (modified from Yu, 2010).

FibB and FibE are found as heterodimer at the tip of vegetative growing hyphae until gain of developmental competence (Oartzabal-Arano *et al.*, 2015). As consequence, FibB is supposed to be modified by FibE and then transported from the apical tip into nuclei where it activates *flbD* expression (Garzia *et al.*, 2009; Oartzabal-Arano *et al.*, 2015). Expression of *brlA* is activated on the one hand by the release of the VosA and NsdD (n_ever in s_exual d_evelopment D) repressors as well as by FibD and FibB/E complex binding to the *brlA* promoter (Lee *et al.*, 2014). Two other Fib proteins, FibA and FibC act independently from FibB/D/E. FibA is a regulator of G-protein signaling and allows indirect *brlA* expression by inactivation of the G α FadA, which in turn is unable to activate the MAPK kinase pathway required for vegetative growth (Ruger-Herreros *et al.*, 2011). FibC induces *fluG* and *brlA* expression (Ruger-Herreros *et al.*, 2011; Krijgsheld *et al.*, 2013). Production of BrlA results in transcriptional activation of *abaA* (a_bacus A), which deletion causes apically budding of metulae forming metulae-like cell chains (Figure 3) (Sewall *et al.*, 1990). The *abaA* gene

product is as well a transcription factor inducing the *wetA* (wet white A) gene expression (Figure 3) (Adams and Timberlake, 1990). Strains defective in *wetA* produce conidia, which are not pigmented and not water repellent. AbaA and WetA induce VosA and VelB expression, which contributes to spore maturation and trehalose production (Figure 3) (Park *et al.*, 2012; Garzia *et al.*, 2013).

The balance between asexual and sexual development is coordinated by environmental conditions, hormone factors, availability of mating partners, and a complex cross-talk between regulatory pathways. Sexual development is favored in dark and under carbon dioxide pressure and limited oxygen supply, whereas the external factors light and oxygen induce asexual development (Pöggeler *et al.*, 2006; Busch and Braus, 2007; Pöggeler *et al.*, 2018). The underlying mechanism of light sensing is based on photoreceptors FphA (fungal phytochrome A) for sensing red light, the white collar complex blue-light receptors LreA and LreB (light response A/B) and the photolyase/cryptochrome A CryA for sensing blue light and UVA (Bayram *et al.*, 2010). These receptors are tightly coupled to downstream regulatory events mediated by velvet proteins. The photoreceptors FphA and LreA/B build a complex with the transcription factor VeA in the nucleus stimulating asexual development under light conditions (Blumenstein *et al.*, 2005; Purschwitz *et al.*, 2009; Ruger-Herreros *et al.*, 2011; Bayram *et al.*, 2012). The methyltransferase LaeA (lack of *afIR* expression A) reduces VosA/VelB expression levels (Sarıkaya Bayram *et al.*, 2010). CryA reduces VeA RNA amount and combined with lower levels of VelB, the heterotrimeric VelB-VeA-LaeA complex cannot be formed (Bayram *et al.*, 2008b). This complex supports sexual development dependent on α -importin KapA (karyopherin A) mediated nuclear transport of VelB-VeA (Bayram *et al.*, 2008a; Sarıkaya Bayram *et al.*, 2010).

The complex cross-talk of developmental regulatory pathways is also controlled by different endogenous factors like psi factors and pheromones. Pheromones are interconnected with the mating type in heterothallic *Aspergillus* species like *A. fumigatus* as the strain of one mating type contains the receptor for the other mating type pheromone and *vice versa* (Szewczyk and Krappmann, 2010; Krijgsheld *et al.*, 2013). Pheromone signaling is independent from the mating type in homothallic species like *A. nidulans*. Psi factors and pheromones are recognized by G-protein coupled receptors and leads to MAPK cascade signaling (Seo *et al.*, 2004; Busch and Braus, 2007). The MAPK cascade phosphorylates the transcription factors SteA (sterile12-like A) and NsdD, which are required for the production of sexual structures (Vallim *et al.*, 2000; Han *et al.*, 2001; Pöggeler *et al.*, 2006; Krijgsheld *et al.*, 2013). Sexual development is induced by nuclear localized VeA, where it activates genes required for sexual development (Vienken *et al.*, 2005; Vienken and Fischer, 2006).

1.1.6 Secondary metabolism

Fungal development is connected to secondary metabolism (Busch *et al.*, 2003; Nahlik *et al.*, 2010; Helmstaedt *et al.*, 2011). Secondary metabolites are non-essential, small molecular weight compounds and are produced by almost all filamentous fungi (Gerke *et al.*, 2012; Gerke and Braus, 2014). The compounds range from beneficial to harmful for mammals, plants, other fungi or bacteria (Samson *et al.*, 2014). Secondary metabolites with positive aspects for humans include penicillin's, which have antibacterial effects, caspofungin with antifungal effect, lovastatin against high cholesterol levels or anticancer substances like taxol (Gerke and Braus, 2014). Mycotoxins, such as aflatoxins or gliotoxin are secondary metabolites, which can cause carcinogenic or allergic effects (Bossou *et al.*, 2017). Secondary metabolites are also found in form of pigments (e.g. melanin) or with positive effect on spore formation (e.g. austinol/dehydroaustinol) (Calvo *et al.*, 2002; Rodríguez-Urra *et al.*, 2012). Most secondary metabolites derive from primary metabolite precursors and belong to product families consisting of different derivatives or intermediates. Genes encoding secondary metabolite catalyzing enzymes are often clustered and mostly silent during laboratory conditions (Schroeckh *et al.*, 2009; Gerke *et al.*, 2012). Secondary metabolism is regulated by a plethora of gene products and environmental factors. The methyltransferase LaeA was described as master regulator of secondary metabolism and development. Together with VeA-VelB LaeA controls for example sterigmatocystin and penicillin synthesis and the formation of Hülle cells (Sarıkaya Bayram *et al.*, 2010; Sarıkaya-Bayram *et al.*, 2015). This underlines the complexity and interconnection of the secondary metabolism and developmental network.

1.2 Protein homeostasis

Adaptation to altered environmental or internal conditions is dependent on the change of the protein content of a cell (Portbury *et al.*, 2012; Chowdhury and Enenkel, 2015). Posttranslational protein modifications and selective protein degradation (Karve and Cheema, 2011) are next to transcription, alternative splicing and translation of proteins two other possibilities of protein diversity regulation. All processes of protein homeostasis are highly connected with each other, for example in the ubiquitin proteasome system (UPS).

1.2.1 Posttranslational protein modification as functional signaling groups of proteins

The functional diversity of a proteome can be influenced by posttranslational protein modifications (PTMs). PTMs are covalent conjugations of chemical groups or small proteins to single amino acid residues of a protein, whereby several amino acids can be modified with the same or different PTMs dependent on the required function (Komander, 2009; Karve and Cheema, 2011; Vierstra, 2012). These modifications can affect protein folding or electrostatic properties that lead to changes in interaction partners, stability, activity or localization (Duan and Walther, 2015). The different types of PTMs are dependent on their functional group. Stable modifications include glycosylation or lipidation of membrane proteins. PTMs like phosphorylation, methylation, acetylation, ubiquitination or modification with ubiquitin-like proteins (UBLs) are dynamic because their conjugation depends on temporal and spatial circumstances (Deribe *et al.*, 2010; Karve and Cheema, 2011; Zheng and Shabek, 2017). Dynamic modifications require enzymes for conjugation (kinases, methyltransferases, acetyltransferases, E3 ligases) and cleavage (phosphatases, demethylases/amine oxidases, deacetylases, deubiquitinases) (Sarikaya-Bayram *et al.*, 2015; Schinke *et al.*, 2016; Swatek and Komander, 2016; Chou *et al.*, 2017).

1.2.2 Ubiquitin and Nedd8

The ubiquitin family of protein modifiers includes ubiquitin and ubiquitin-like proteins, such as Nedd8 (neural precursor cell expressed, developmentally down-regulated 8; in *A. nidulans* also NeddH, in plants Rub1/2), SUMO (small ubiquitin-like modifier), Atg8 or Atg12 (autophagy related proteins 8 or 12) (van der Veen and Ploegh, 2012; Vierstra, 2012; Harting *et al.*, 2013). These signaling molecules label designated proteins by covalent posttranslational isopeptide

modification, which regulates a plethora of important cellular processes (Hershko and Ciechanover, 1998).

Nedd8 is the most similar UBL to ubiquitin (Whitby *et al.*, 1998; Swatek and Komander, 2016). Both are comprised of 76 amino acids (processed Nedd8) having a molecular weight of 9 kDa. Human ubiquitin and Nedd8 share 58% identity and both proteins share 55% identity in *A. nidulans* (Figure 4) (Shin *et al.*, 2017). Comparison of human to *A. nidulans* ubiquitin and Nedd8 comprise 96% and 76% identity, respectively underlining the conservation of both proteins throughout eukaryotes. Ubiquitin has seven lysine residues (Lys (K) 6, 11, 27, 29, 33, 48 and 63, highlighted in green Figure 4) that are targets for cross-ubiquitination, which results in different polyubiquitin chains varying in chain length and linkage-type and modification can also occur at its N-terminus (Met1) (Komander and Rape, 2012; Swatek and Komander, 2016). Furthermore, ubiquitin can itself be modified with e.g. Nedd8, SUMO or phosphate-groups, which increases the complexity of the ubiquitin code (Komander and Rape, 2012; Swatek and Komander, 2016). The most predominant linkage type is the Lys48 linked poly-ubiquitin chain that targets substrates for degradation by the 26S proteasome (Hershko and Ciechanover, 1998). For long period it was assumed that a ubiquitin chain of four units is the minimum signal required for recognition by the proteasome (Thrower *et al.*, 2000). It was reported that Lys48/Lys11 branched chains are even better targets for proteasomal degradation and that the tetraubiquitin chain is only the base for further cross-linkages (Lu *et al.*, 2015).

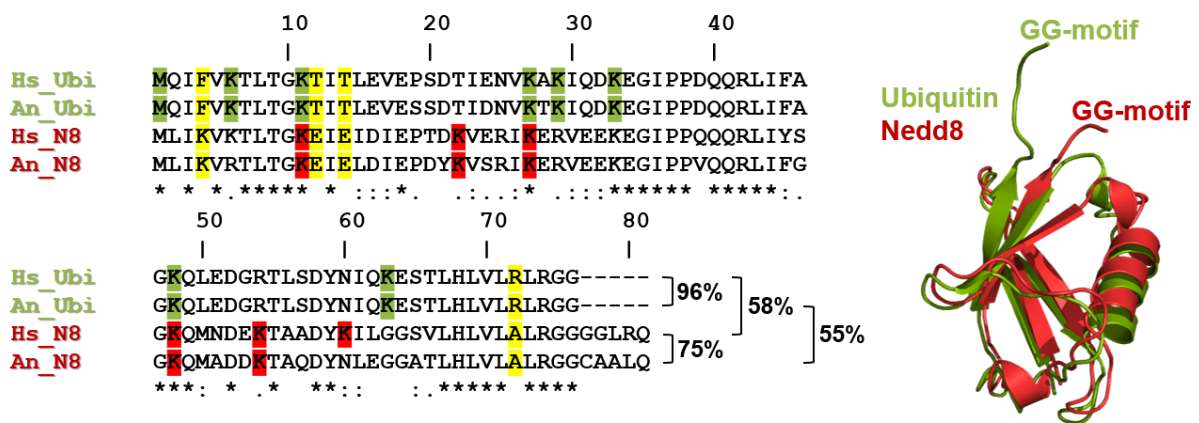


Figure 4. Comparison of ubiquitin and Nedd8. Protein sequences of Human (Hs) and *A. nidulans* (An) ubiquitin and Nedd8 (UniProt IDs: Hs_Ubi J3QS39; An_Ubi A2RVC1; Hs_N8 Q15843; An_N8 Q5AZV1) were aligned with MUSCLE multiple sequence alignment tool (Edgar, 2004). Conserved residues are indicated by an asterisk (“*”), strongly similar residues by a colon (“:”) and weakly conserved amino acids are marked by a period (“.”). Lysine residues labeled in green or red are specific cross-linkage targets for ubiquitin or Nedd8, respectively. Amino acid residues labeled in yellow are required for proteases to discriminate between both substrates. High similarity of ubiquitin and Nedd8 is also visible in the overlay of 3D structures (PDB IDs ubiquitin: 2RUG; Nedd8: 1NDD). Only the C-terminal end harboring the di-glycine (GG) motif differs in orientation. Overlay was conducted with PyMOL (The PyMOL Molecular Graphics System, Version 2.0 Schrödinger, LLC.).

The other ubiquitin linkage types, besides Lys48 linkage, have profound function in signaling, cell cycle control, DNA damage response and NF- κ B mediated immune response signaling (reviewed in Swatek and Komander, 2016b and Enchev *et al.*, 2014). Nedd8 was shown to form chains at its residues Lys11, 22, 27, 48, 54 and Lys60 (highlighted in red Figure 4) (Jones *et al.*, 2008; Jeram *et al.*, 2010), whereas Lys60 is replaced by asparagine (Asn, N) in *A. nidulans* (Figure 4). Komander and co-workers describe the complexity of ubiquitin and UBLs as the 'ubiquitin code', which comprises 'writers', 'readers' and 'erasers' (Komander and Rape, 2012; Swatek and Komander, 2016). 'Writers' are the enzymes conjugating ubiquitin, UBL or other modifications to target substrates. 'Readers' are proteins comprising ubiquitin binding domains and deubiquitinases or deneddylases are described as 'erasers', removing the modification (Komander and Rape, 2012; Swatek and Komander, 2016). All enzymes involved are highly specific for either ubiquitin or Nedd8, but can discriminate between both proteins although Nedd8 and ubiquitin sequence and tertiary structure are similar (Shen *et al.*, 2005). On a first glance, only the C-terminal ends harboring the di-glycine motif seem to be differentially orientated. However, discrimination of ubiquitin or Nedd8 specific proteases is mainly due to residues 4, 12, 14 and 72 (highlighted in yellow Figure 4) as well as due to the structural arrangement of the catalytic center of the proteases (Shen *et al.*, 2005; Shin *et al.*, 2017).

1.2.3 The E1, E2, E3 enzyme cascade – a PTM labelling apparatus

Nedd8 is translated as an inactive precursor protein with a five-amino acid C-terminal extension. This extension is processed by isopeptidases like deneddylase A (DenA) leaving the di-glycine (GG) motif at its C-terminus. In *A. nidulans* ubiquitin is synthesized as a fusion protein with the small ribosomal subunit protein S27a (AN4872) or as tetra-ubiquitin (AN2000). Ubiquitin and Nedd8 are synthesized in plants as fusion proteins (Mergner and Schwechheimer, 2014) and humans comprise even a huge ubiquitin multigene family of different fusions (Wiborg *et al.*, 1985), which need to be processed into monomers by deubiquitinating enzymes (DUBs).

The Nedd8 and ubiquitin protein monomers undergo a multistep enzymatic conjugation process for substrate modification or chain formation. The mechanisms are very similar but there are specific E1 activating, E2 conjugating and E3 ligases (Figure 5) (Metzger *et al.*, 2014; Enchev *et al.*, 2015). The E1 activating enzyme binds ATP (adenosine-triphosphate), Mg²⁺ and Nedd8 or ubiquitin at its adenylation site and thereby conjugates AMP to the di-glycine C-terminus of Nedd8/ubiquitin. In the following, the active C-terminus is attacked by a cysteine residue thiol group located in the catalytic center of the E1, releasing AMP and pyrophosphate. The E1 binds a second Nedd8 or ubiquitin molecule and thereby forms a UBC binding groove

(Huang *et al.*, 2007; Enchev *et al.*, 2015). Consequently, the catalytic active cysteine of the E2 takes over Nedd8 or ubiquitin and is released from the E1 (Enchev *et al.*, 2015).

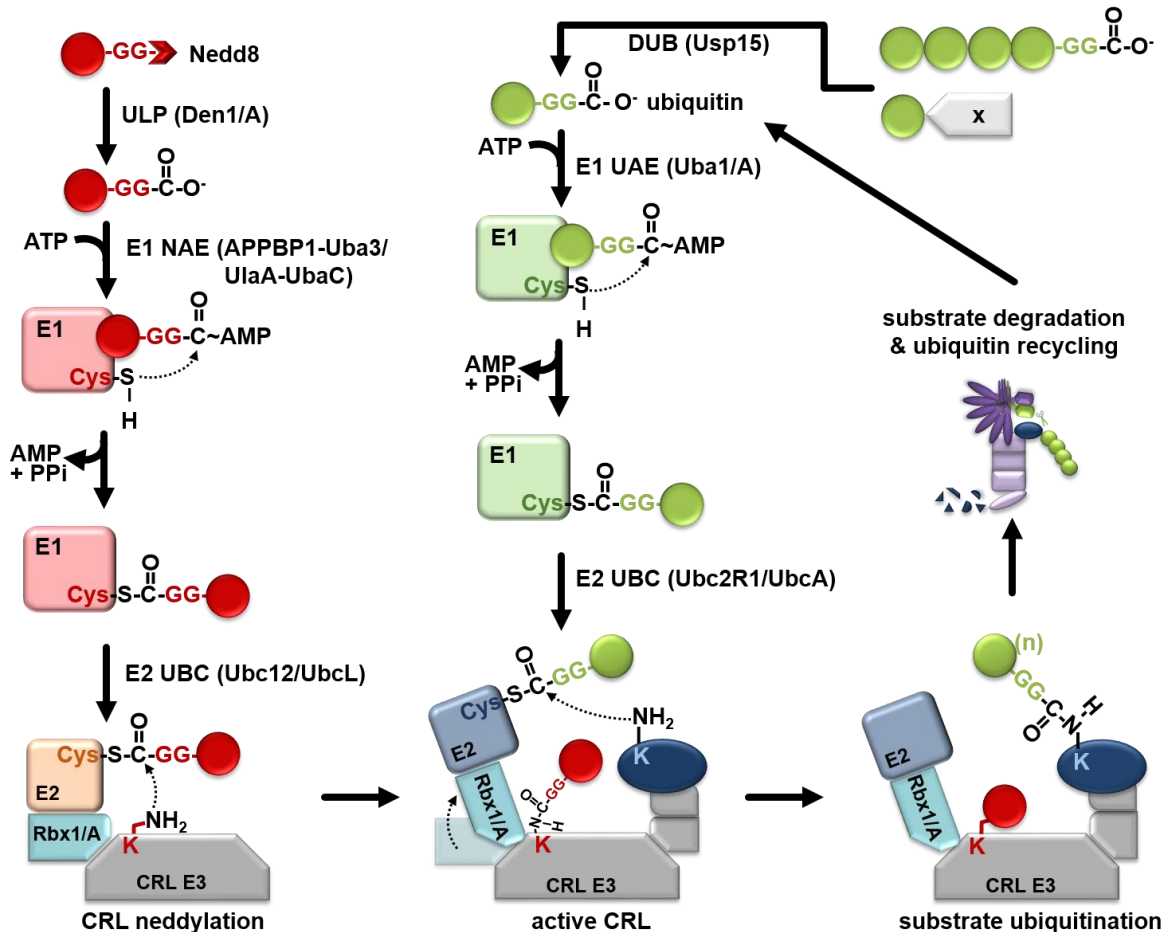


Figure 5. Neddylaton and ubiquitination cascades. Nedd8 precursor is processed by ubiquitin-like proteases (ULP) bearing the di-glycine motif at the Nedd8 C-terminal end. Nedd8 binds to the adenylation site of the heterodimeric Nedd8 E1 activating enzyme (NAE), which activates Nedd8 by adenosine monophosphate (AMP) conjugation to the Nedd8 C-terminus followed by Nedd8 C-terminal thiolation. Then Nedd8 is transferred to a cysteine residue of a E2 ubiquitin-like conjugating enzyme (UBC). The E2 binds to Rbx1/A (RING box protein) of E3 cullin RING ligases (CRL E3) and ligates the Nedd8 to the cullin lysine acceptor residue. Ubiquitin conjugates are processed by deubiquitinating enzymes (DUBs) into monomers. The activation by E1 ubiquitin activating enzyme (UAE) and transfer to E2 UBC is the same process as described for Nedd8. E2 transfer of ubiquitin to target substrates is facilitated by Rbx1/A conformational change in the CRL due to neddylaton. By this, substrates are polyubiquitinated and most often targeted for degradation in the ubiquitin proteasome system (UPS). Recycled Nedd8 and ubiquitin are processed for new rounds of E1-E2-E3 enzyme cascades. Examples for ULP and DUB, E1 NAE and UAE as well as for E2 UBC proteins from *Homo sapiens* and *A. nidulans* are indicated (modified from Mergner *et al.*, 2014 and Enchev *et al.*, 2015).

A E3 ligase is required for the ligation step of ubiquitin or Nedd8 to their target substrates. There are several different types of E3 ligases known and all of them share a basic catalytic core module but have distinct substrate-recruiting and regulatory units (Petroski and Deshaies, 2005a; Deshaies and Joazeiro, 2009; Scheffner and Kumar, 2014). In general, E3 ligases are categorized into two classes: the HECT (homologous to the E6AP carboxyl terminus)-type E3 and the RING (really interesting new gene)-type E3 ligases (Figure 6A and B) (Metzger *et al.*, 2014; Keuss *et al.*, 2016; Scott *et al.*, 2016).

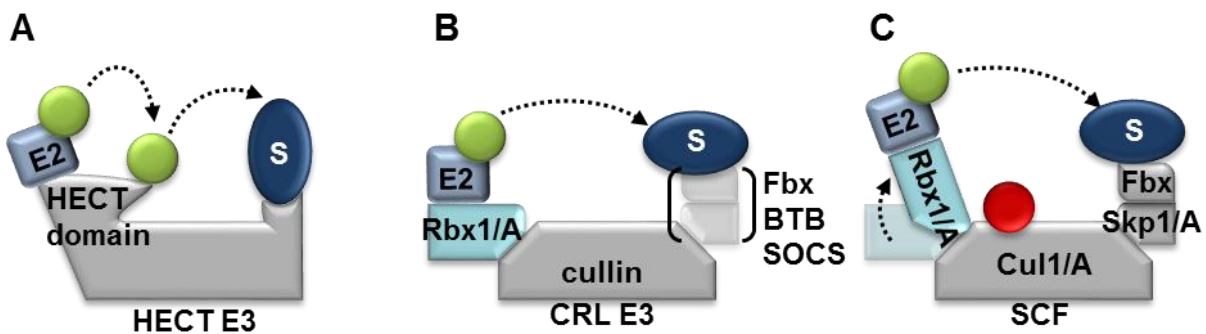


Figure 6. Types of E3 ligases. E3 ligases are classified in two main groups: HECT and RING ligases. **A** HECT ligases contain a E2 and ubiquitin binding site in the C-terminal HECT domain and an N-terminal substrate binding domain. The ubiquitination process (Ub in green) is performed in two steps. **B** RING type E3 ligases have a C-terminal bound RING domain protein (Rbx1/A), which recruits E2 enzymes. There are several different types of substrate receptors like Fbx, BTB or SOCS types. **C** The classical RING E3 ligase is the SCF complex comprised of Cul1/A-Skp1/A-Fbx that is neddylated (Nedd8 in red), providing activity for ubiquitination (modified from Deshaies and Joazeiro, 2009; Jöhnk *et al.*, 2016).

HECT ligases contain an N-terminal substrate receptor site, which varies between different HECT-type ligases. The C-terminus harbors the HECT domain, which itself is bi-lobed, meaning the N-terminal lobe is interacting with the E2, which transfers ubiquitin to the catalytic cysteine located in the C-terminal lobe. From there, ubiquitin is transferred onto the target substrate (Figure 6A) (Metzger *et al.*, 2012). This two-step ubiquitin transfer is different to the mechanism of RING-type E3 ligases, which perform a one-step ubiquitin or Nedd8 transfer (Deshaies and Joazeiro, 2009). RING-type E3 ligases are with more than 600 predicted subtypes the most common E3 ligases including the most prominent type the CRL (cullin-RING ligase) (Enchev *et al.*, 2015; Zheng and Shabek, 2017). CRLs are multi-subunit E3 ligases, in which a cullin protein builds the scaffolding core and is N-terminally connected to substrate adaptor-receptor binding proteins, e.g. Fbx (F-box), BTB (bric à brac, tramtrack, and broad

complex) or SOCS (suppressor of cytokine signaling), and C-terminally bound to a Rbx1/A/Roc1 catalytic RING finger protein (Zheng *et al.*, 2002b) (Figure 6B). Humans possess six different cullins (CUL1, 2, 3, 4A, 4B and 5) and two additional atypical cullin proteins CUL7 and PARC (parkin-like cytoplasmic protein) (Duda *et al.*, 2011). Three cullins are conserved (CulA, C, D) in *A. nidulans*, which differ in their substrate-adaptor-receptor domain (Petroski and Deshaies, 2005b; Busch *et al.*, 2007). The RING domain typically consists of cysteine and histidine residues chelating two to three zinc (Zn^{2+}) ions that form a hydrophobic surface groove for E2 binding (Deshaies and Joazeiro, 2009). In the SCF (SkpA CullinA E-box) RING-ligase substrate ubiquitination is enhanced through posttranslational modification of CulA itself with Nedd8 (Figure 6C) (Lydeard *et al.*, 2013; Keuss *et al.*, 2016). The attachment process is identical to that of ubiquitin but with Nedd8 specific E1 and E2 enzymes (Enchev *et al.*, 2015). The Nedd8-E2 binds to RbxA (RING box), which is a component of E3 CRLs and mediates the transfer of Nedd8 to lysine 720 (lysine 710 in *A. nidulans*) of Cul1/A. This ligation process was shown to be facilitated in humans by DCN (defective in cullin neddylation) proteins (Kurz *et al.*, 2005). *A. nidulans* has one DCN homolog DcnA, which has only minor contribution to cullin neddylation compared to human DCN proteins (von Zeska Kress *et al.*, 2012). Through Nedd8 binding the RbxA changes conformation, protruding out of its cullin binding pocket directing E2-bound ubiquitin into close proximity to the target substrate (Duda *et al.*, 2011).

1.2.4 The ubiquitin proteasome system

In 2004 the chemistry Nobel Prize was given to Aaron Ciechanover, Avram Hershko and Irwin Rose for their discovery of ubiquitin-mediated protein degradation in the 1980s. They found out that proteasomal protein destruction is mediated by the ubiquitin system (Figure 7), which is universally conserved in eukaryotes (Hershko and Ciechanover, 1998). The UPS is based on the regulated interplay of several macromolecular complexes including the SCF E3 ligase, the 26S proteasome, the COP9 signalosome (CSN) and the Cand1/A complex. Degradation targeted substrate proteins are bound to the CRL through substrate binding proteins or recognition sites (Skaar *et al.*, 2013). F-box proteins are responsible for substrate recruitment of SCF ligases. The amount and diversity of degradation targeted substrates requires a wide range of different receptors. Humans and *A. nidulans* possess around 70 different F-box proteins, which have different substrate recognition features (Hua and Vierstra, 2011). They can recognize substrate degron motifs, which are for example altered by post-translational modification such as phosphorylation, glycosylation or by binding of a co-factor (Skaar *et al.*, 2013). Furthermore, Fbx proteins consist of a conserved Skp1/A binding domain, which is called the F-box motif due to cyclin F, which was the first discovered protein with this motif

(Bai *et al.*, 1996; Kipreos and Pagano, 2000; Schmidt *et al.*, 2009). The Skp1/A protein serves as adaptor between the substrate bound F-box protein and Cul1/A (Zheng *et al.*, 2002b). In case a SCF is loaded with a substrate, neddylation of Cul1/A activates the E3 ubiquitin ligase (as described in chapter 1.2.3). Subsequently the substrate is polyubiquitinated with at least four ubiquitin molecules, which targets it for degradation by the 26S proteasome (Figure 7) (Meister *et al.*, 2016; Swatek and Komander, 2016).

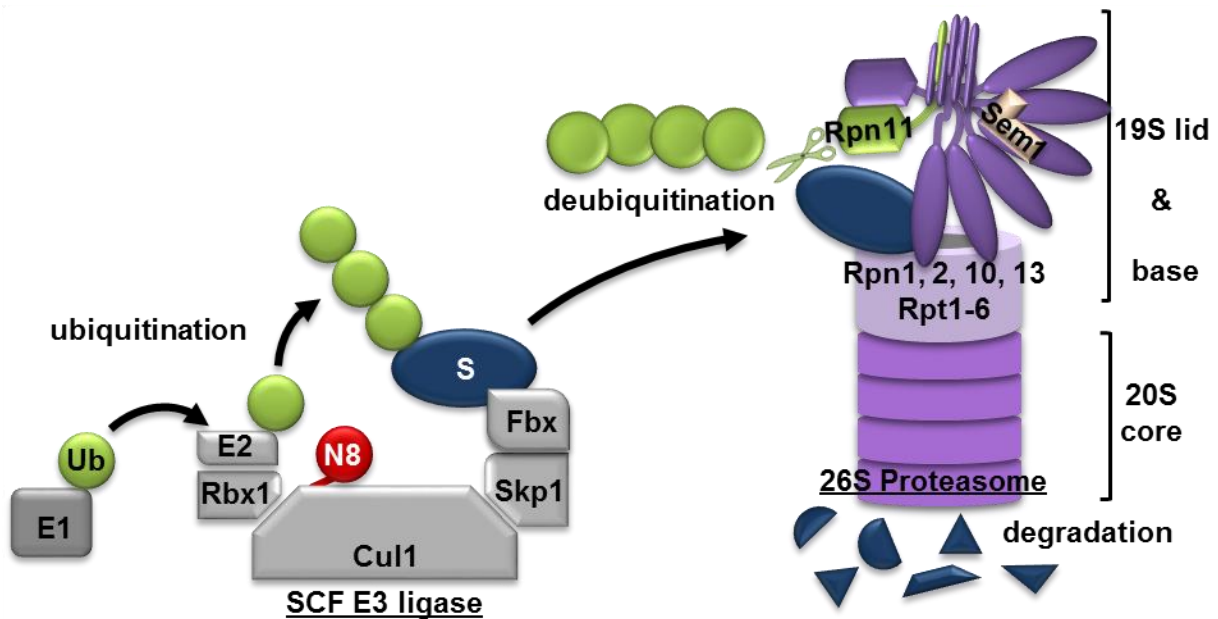


Figure 7. Ubiquitin proteasome system. Substrates (S) are poly-ubiquitinated by Nedd8 (N8) activated SCF E3 ligases and then targeted for degradation by the 26S proteasome. The proteasome consists of a 20S core particle and one or two 19S regulatory particles including lid and base. Base subunits Rpn10 and Rpn13 are ubiquitin receptors and lid subunit Rpn11 cleaves the most distal ubiquitin (Ub) allowing the substrate to enter the core particle for degradation (Meister *et al.*, 2016).

The 26S proteasome is a large 2.5 mDa multiprotein complex and described as the recycling machinery of the cell (Budenholzer *et al.*, 2017; Kolog Gulko *et al.*, 2018). It consists of a 20S core particle (CP) that is barrel shaped and contains four heptameric rings. The rings provide the substrate entry channels and proteolytic active sites. The 20S CP is capped on one or both ends with the 19S regulatory particles consisting of base and lid (Budenholzer *et al.*, 2017). The lid contains eight subunits Rpn3, 5-9, 11 and Rpn12 (regulatory particle of non-ATPase) and one additional subunit Sem1/A (Figure 7) (Kolog Gulko *et al.*, 2018). Ubiquitinated substrates are recognized by base subunits Rpn10 and Rpn13 (Schreiner *et al.*, 2008). Subsequently, the substrate is pulled into the core particle by ATP hydrolysis forces of the

AAA+ ATPase core subunits (Rabl *et al.*, 2008). Lid subunit Rpn11 is the deubiquitinating enzyme cleaving the most distal ubiquitin prior to substrate unfolding and translocation into the core particle by base subunits Rpt1-6 (regulatory particle of triple ATPase), followed by proteolysis performed by different trypsin-, chymotrypsin- and caspase-like peptidases (Verma *et al.*, 2002; Bedford *et al.*, 2010). Degradation products serve as bricks for protein synthesis and ubiquitin is recycled for new cycles of substrate ubiquitination, closing the circle of the ubiquitin proteasome system.

1.3 Regulation of the ubiquitin proteasome system

Approximately 80% of all proteins undergo the ubiquitin proteasome system for degradation (Rock *et al.*, 1994; Yen *et al.*, 2008). Therefore, this process needs tight regulation and several control checkpoints. One of the steps that need to be controlled is the labeling of substrates with ubiquitin in the CRL E3 ligase cycle. The first layer of regulation is mediated by recognition of degradation targeted substrates by F-box proteins and their subsequent recruitment to the cullin E3 ligase. Target substrates contain a degron motif, which can be of diverse nature like posttranslational modifications as phosphorylation, structural alteration or co-factor binding. These degrons are then recognized by different F-box proteins (Figure 8 I.) (Duda *et al.*, 2011; Skaar *et al.*, 2013).

The following steps of substrate labeling are controlled by SCF activation. The activation process includes covalent attachment of Nedd8 to Cul1/A of SCF complexes loaded with a substrate (Figure 8 II.) (Enchev *et al.*, 2015; Keuss *et al.*, 2016; Zhang *et al.*, 2016). Neddylation facilitates ubiquitination due to conformational change of RbxA, which positions the E2 in close proximity to the substrate (Duda *et al.*, 2008) (and chapter 1.2.3). The number and chain type of ubiquitin molecules determines if a substrate is finally targeted by the proteasome (see chapter 1.2.2 and Swatek and Komander, 2016). The ubiquitin chain is not only build and modified by E3 ligases but also cleaved by ubiquitin specific proteases (USP) (Ronau *et al.*, 2016). These proteases act against auto-ubiquitinated SCF components (most often F-box proteins) in case of depleting substrates, indicating another layer of regulation (Xu *et al.*, 2007; Gorelik and Sidhu, 2017).

Finally, Lys48/Lys11 ubiquitinated substrates are recognized by 26S proteasome subunits Rpn10 and Rpn13 (regulatory particle non-ATPase), following deubiquitination by the proteasome lid intrinsic deubiquitinase Rpn11 or associated deubiquitinating enzymes (see chapter 1.2.4 and Figure 8 III.) (Grice and Nathan, 2016; Meister *et al.*, 2016; Kolog Gulko *et al.*, 2018).

Activity of SCF E3 ligases is not only mediated by neddylation but also through the reverse process deneddylation. Nedd8 is covalently bound to CulA and peptide bond cleavage requires the catalytic activity of the deneddylating enzymes COP9 signalosome and DenA, which harbor isopeptidase activity (Cope and Deshaies, 2003; Wu *et al.*, 2003; Schinke *et al.*, 2016) (Figure 8 IV. and chapter 1.3.1). Substrate variability of E3 ligases is controlled by the exchange factor Cand1/A binding to deneddylated SCF, which results in the dissociation of Skp1/A-Fbx proteins (Figure 8 V.) (Wu *et al.*, 2013; Zemla *et al.*, 2013). The mechanism behind CandA dissociation is not completely solved yet, but putatively by binding of SkpA-Fbx complexes carrying a new substrate, which initiates a new CRL cycle (Pierce *et al.*, 2013; Straube *et al.*, 2017).

CSN and CandA show contradicting effects on CRL activity in *in vitro* compared to *in vivo* experiments, which is described as the CSN or Cand1 paradox (Dubiel, 2009). This paradox is explained by the disassembly function of CSN and Cand1/A on SCFs, which inactivates the E3 ligases *in vitro* (Zhou *et al.*, 2003). CSN can specifically recognize SCFs without substrate and protects them from autoubiquitination while it stays bound to the SCF (Dubiel, 2009; Chua *et al.*, 2011). *In vivo* disassembly is followed by assembly, because new substrate-receptor modules are available for their incorporation into the SCF complex (Cope and Deshaies, 2003; Bosu and Kipreos, 2008).

A F-box auto-ubiquitinating protective function of the CSN and Cand was described, where CSN and Cand binding to Cul1/A prevents auto-ubiquitination, explaining the paradox partially (Schmidt *et al.*, 2009; Chua *et al.*, 2011). The CSN and Cand are needed for the rapid exchange of CRL components to facilitate the labeling of diverse substrates for degradation (Mosadeghi *et al.*, 2016; Reitsma *et al.*, 2017; Straube *et al.*, 2017).

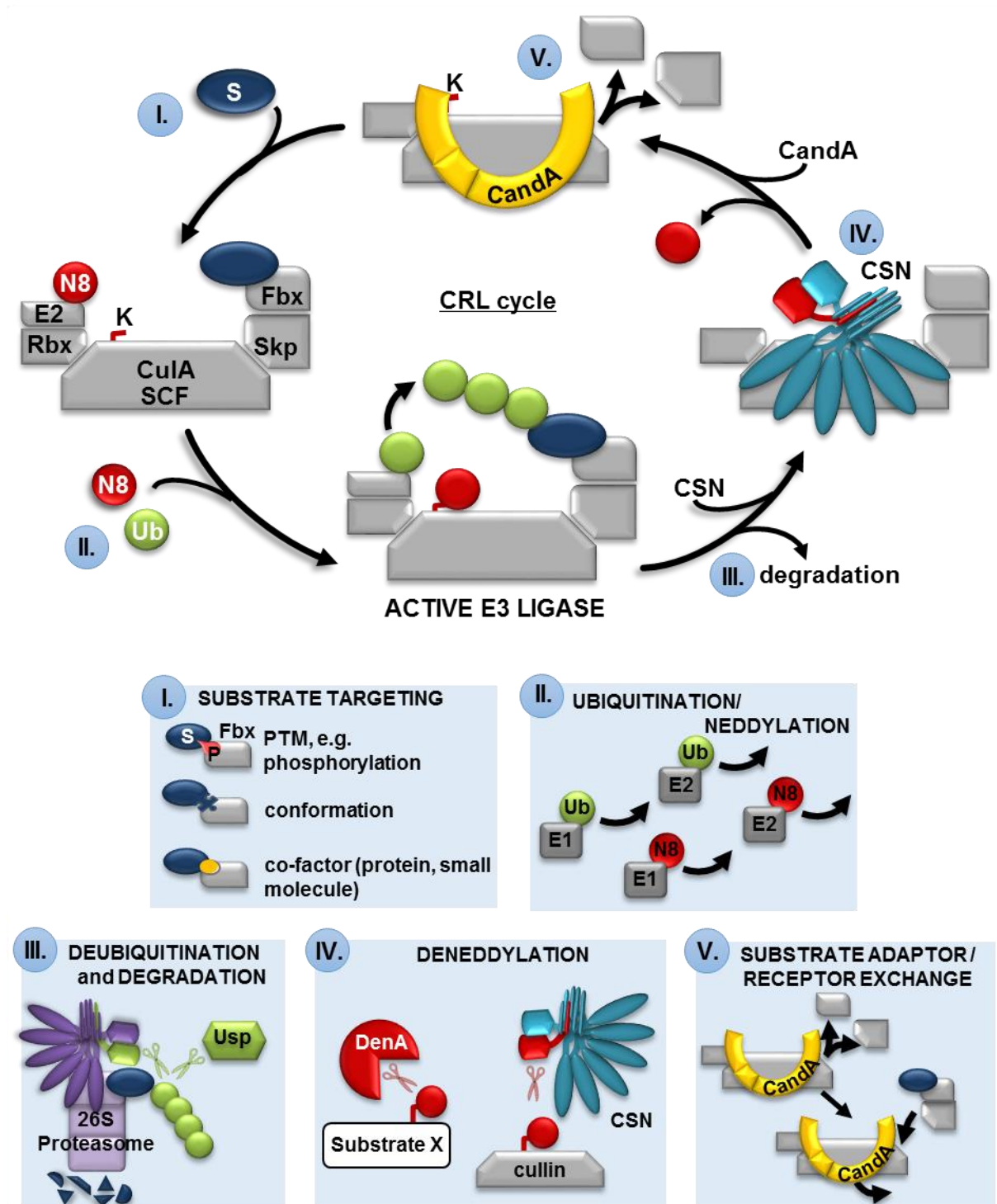


Figure 8. The CRL cycle and its regulation. Cullin RING ligases bind substrates through Skp adaptor proteins and E-box (Fbx) receptor proteins, which recognize different kinds of substrate degron motifs (I). CRLs are activated by CulaA neddylation, enhancing substrate ubiquitination (II). Poly-ubiquitinated substrates are sensed for degradation by the 26S proteasome or targeted by other ubiquitin specific proteases like UspA (III). CRLs, which are not binding substrates are recognized by CSN and inactivated by deneddylation. This is performed by the CSN intrinsic isopeptidase CsnE or DenA (IV). CandA can bind to deneddylated CRLs and releases the adaptor-receptor proteins (V), allowing new CRL assembly.

1.3.1 CSN and DenA – two deneddylating isopeptidases

The CSN is ubiquitously conserved in eukaryotes being crucial for the UPS and thereby affecting several cellular processes like cell cycle control or hormone signaling (Wei *et al.*, 2008). The CSN is a macromolecular complex of approximately 350 kDa with eight subunits named CSN1-8 in human. Like humans, *A. nidulans* has eight-subunits designated as CsnA-H (Busch *et al.*, 2003, 2007; Lingaraju *et al.*, 2014). Other fungi like *Neurospora crassa*, *Chaetomium thermophilum* or *Sordaria macrospora* have a seven-subunit CSN lacking the smallest subunit Csn8. Even smaller CSN complexes are found for example in *Schizosaccharomyces pombe*, with only six subunits and *Saccharomyces cerevisiae* has a CSN containing Csn5 as the only conserved subunit and additional subunits not found in classic CSNs (Braus *et al.*, 2010; Wang *et al.*, 2010; Yu *et al.*, 2011).

According to subunit composition and structural similarities, the CSN is classified as a member of the ZOMES (“study of large PCI complexes”), comprising two other macromolecules all involved in protein turnover (Alpi and Echalié, 2017). Those macromolecules are the lid of the 26S proteasome and the eukaryotic translation initiation factor 3 (eIF3). Lid and CSN share most similarities and have six PCI (proteasome, COP9 signalosome, eukaryotic initiation factor 3) and two MPN (Mrp1-Pad1-amino (N)-terminal) domain subunits (Figure 9) (Meister *et al.*, 2016). Three dimensional structures of the CSN revealed that the PCI domains are involved in protein-protein interactions whereby the six PCI subunits (CSN1-4, 7,8 or CsnA-D, G, H) orient in a half open ring from which the N-terminal domains protrude (Figure 9) (Enchev *et al.*, 2012; Lingaraju *et al.*, 2014). All eight subunits possess up to three C-terminal alpha helices that are connected with their core domain by large linkers. The helices assemble as a complex helical bundle, which is oriented on top of the PCI ring (Lingaraju *et al.*, 2014). The MPN subunits CSN5/E and CSN6/F are globular and sit above the helical bundle and PCI ring (Enchev *et al.*, 2012; Lingaraju *et al.*, 2014). Csn5/E or lid ubiquitin isopeptidase Rpn11 have a MPN+ domain with an intrinsic metalloprotease JAMM (JAB1/MPN/MOV34) motif (Busch *et al.*, 2007; Wauer and Komander, 2014).

It was shown that the CSN is inactive until the last subunit CSN5/CsnE is incorporated into the seven subunit pre-CSN (Beckmann *et al.*, 2015). Furthermore, since the crystal structure of the full CSN was solved, the catalytic properties could be described as an auto-inhibited inactive CSN in case it is not bound to a CRL (Figure 10) (Lingaraju *et al.*, 2014). Binding of the CSN to neddylated CRL without substrate induces conformational alterations that allow positioning of the zinc ion towards the Cul1-Nedd8 isopeptide bond (Lingaraju *et al.*, 2014; Cavadini *et al.*, 2016; Mosadeghi *et al.*, 2016).

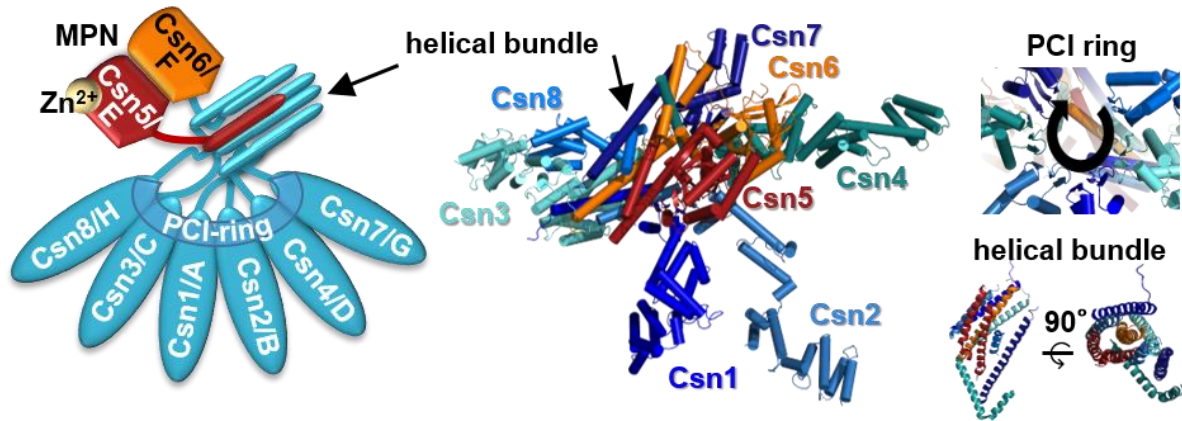


Figure 9. The COP9 signalosome subunit architecture. CSN has six PCI containing subunits (Csn1/A, 2/B, 3/C, 4/D, 7/G, 8/H), which form a ring-like structure. On top of this ring are two MPN domains containing subunits (Csn5/E, 6/F). All subunits have C-terminal alpha-helices that form a helical bundle. Csn5/E has a JAMM motif with a catalytic zinc ion for isopeptidase activity. The model (left) is based on the crystal structure (right) of human CSN and shows the organization of the PCI ring and helical bundle (Lingaraju *et al.*, 2014). 3D structure pictures (middle and right) were generated with PyMOL (The PyMOL Molecular Graphics System, Version 2.0 Schrödinger, LLC.) using PDB ID 4D10.

The catalytic mechanism is described as followed: the catalytic zinc ion is coordinated by three residues of the CSN5 active site JAMM motif His138, His140, Asp151 and one residue Glu104 of the insertion loop (Ins-1) of the MPN domain. The Ins-1 occupies the active site in a CRL unbound state (Figure 10). Another residue Glu76 coordinates a water molecule, which is not oriented towards the zinc ion in case of inactive CSN. Upon CSN-CRL interaction, CSN2/CsnB contacts the CUL1/CulA C-terminal WH-B domain and CSN3/CsnC as well as CSN8/CsnH are interacting with the substrate receptor. CSN4/CsnD senses CRL binding and thus rotates, which moves the CSN5/CsnE-CSN6/CsnF dimer towards Nedd8. Thereby the Ins-1 including Glu104 move away from the active site, allowing Glu76 to bring the water molecule close to the zinc ion, which activates the catalytic water for the nucleophilic attack of the Nedd8 isopeptide bond (Figure 10) (Lingaraju *et al.*, 2014; Cavadini *et al.*, 2016; Mosadeghi *et al.*, 2016).

CSN was shown to serve as a dynamic interaction platform for kinases, ubiquitin specific proteases and for subunits of the lid and base of the 26S proteasome as well as associated proteins (Kato and Yoneda-Kato, 2009; Fang *et al.*, 2012). *A. nidulans* CSN subunits, especially CsnG, interact with the second conserved deneddylase DEN1/DenA and DenA stability is decreased by CsnC, E, F, G and CsnH (Christmann *et al.*, 2013; Schinke *et al.*, 2016).

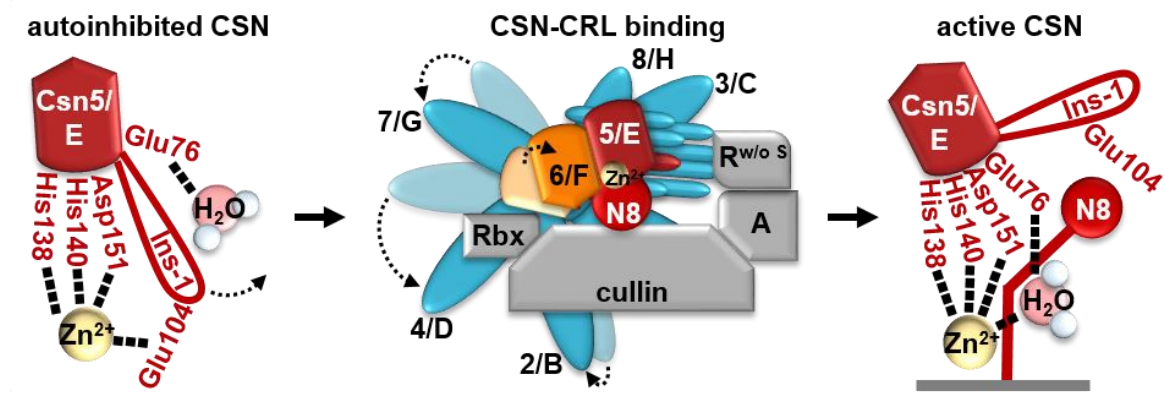


Figure 10. Csn5/E activation upon CRL binding. Left: In the unbound state, Csn5/E is autoinhibited by a glutamine residue Glu104 of the insertion loop 1 (Ins-1), which is, together with the JAMM motif residues His138, His140 and Asp151 in polar contact to the catalytic zinc ion (Zn^{2+}). Glu76 coordinates a catalytic water molecule (H_2O) but is not in proximity to the zinc ion. Middle: Upon CSN interaction to CRL with receptor without substrate ($R^{w/o S}$), CSN subunits move whereby Csn5/E is in close proximity to Nedd8 (modified from Cavadini *et al.*, 2016). Right: The rearrangement removes the Ins-1 loop away from the zinc ion and allows access of the Glu76 water to the zinc ion, which is required for the nucleophilic attack towards the isopeptide bond between cullin and Nedd8 (Lingaraju *et al.*, 2014).

Fungal DenA is a 258-amino acid protein of 29.6 kDa molecular weight. Multiple sequence alignment showed 32% sequence identity to human DEN1 (Christmann *et al.*, 2013; Schinke *et al.*, 2016). DEN1/DenA belongs to the ubiquitin-like family proteases with a catalytic triad consisting of Cys163, His102 and Asp119 in human (Reverter *et al.*, 2005) (Cys182, His123 and Asp140 in *A. nidulans*). DEN1/DenA substrate specificity differs from that of the CSN. Whereas CSN substrates are exclusively mono-neddylated CRLs, DEN1/DenA revealed specificity to poly-neddylated CRLs and other substrates that are mono-neddylated or poly-neddylated (chains or at different sites) (Enchev *et al.*, 2015; Mergner *et al.*, 2015; Schinke *et al.*, 2016). However, non-cullin targets of DEN1 are rarely known. It was reported that *Arabidopsis* DEN1 deneddylates auto-neddylated Nedd8 E1 activating enzymes as regulation for CRL neddylation (Mergner *et al.*, 2017). A second function of mammalian DEN1 is the C-terminal processing of Nedd8 (Wu *et al.*, 2003).

CSN and DenA were shown to be of importance for multicellular development of *A. nidulans* (Busch *et al.*, 2007; Christmann *et al.*, 2013; Beckmann *et al.*, 2015; Schinke *et al.*, 2016). Mutant strains which lack any of the *csn* subunits show reduced conidiospore production and impaired cleistothecia formation at the level of primordia development. Furthermore, defective *csn* leads to altered secondary metabolism as deletion strains produce red pigmented hyphae

and secrete dark red and brown metabolites into the medium (Busch *et al.*, 2003; Nahlik *et al.*, 2010; Beckmann *et al.*, 2015). DenA seems to be required for asexual development but has no impact on sexual development (Christmann *et al.*, 2013; Schinke *et al.*, 2016). In contrast, the CSN, which has higher impact on sexual development, concluding that CSN seems to be the specific Nedd8 protease in sexual development, whereas DenA is responsible for asexual development (Christmann *et al.*, 2013). The CSN is essential in mammals and plants as deletion cause embryonic lethality (Yan *et al.*, 2003; Pacurar *et al.*, 2017). The CSN was also associated to diverse malignancies as abundance of most oncogenes and tumor suppressors are regulated by the UPS (Lee *et al.*, 2011; Schlierf *et al.*, 2016; Jumpertz *et al.*, 2017). Furthermore, the CSN and Fbx15 containing SCFs play a crucial role in invasive pulmonary aspergillosis (Jöhnk *et al.*, 2016). The high conservation of CSN subunits but also other components of the UPS in the model organism *A. nidulans* and the fact that the fungus is still viable upon subunit deletions makes it a great reference organism to study the entire complexity of the UPS, which aims drug target identification.

1.3.2 CandA – a substrate adaptor-receptor exchange factor

The Cand1/A, also known as TIP120 (TATA-box binding protein (TBP) interacting protein), is a 120 kDa protein. The TIP120 function was investigated in the late 1990's when a 120 kDa protein was discovered in affinity chromatography to be associated with the TATA-box binding protein (Yogosawa *et al.*, 1996). It was shown that TIP120 enhances transcriptional activation during the preinitiation complex formation when RNA polymerase II is recruited (Makino *et al.*, 1999). These observations were actually made before Cand1 was identified to interact with cullins, which changed the name TIP120 into Cand1 (Min *et al.*, 2003).

Cand1 consists of 27 tandem HEAT repeats (Huntington, elongation factor 3, alpha-subunit of protein phosphatase 2A (PP2A), yeast PI3-kinase TOR1) (Goldenberg *et al.*, 2004). Goldenberg described that each HEAT repeat contains about 40 amino acid residues, which form a two-helix motif (A and B helix Figure 11). HEAT repeat 25 is interrupted by a β -hairpin. All HEAT repeats together form a sinuous superhelical structure resulting in a U-shaped belt. The N- and C-terminal arches (40 Å) are right- or left-handed, respectively and connected by a central arch (80 Å). Elongated molecules would fit perfectly into the cleft between the N- and C-terminal arch, which is typical for HEAT repeat proteins and allows protein-protein or protein-DNA interaction (Groves and Barford, 1999; Perry and Kleckner, 2003; Goldenberg *et al.*, 2004).

Cand1 was crystallized in complex with Cul1-Rbx1 (Figure 11) (Goldenberg *et al.*, 2004). Cand1 and Cul1 are arranged head to tail, meaning Cand1 N-terminus curls around the

globular Cul1 C-terminal domain and Cand1 C-terminus twists around Cul1 N-terminal domain. Lysine 720 (Lys 710 in *A. nidulans*) of CUL1/CulA is the target for SCF activation by modification with Nedd8. Cul1 is characterized by four repeats of a so called cullin motif that consists of two short and three long α -helices at its N-terminal domain. The C-terminus is globular and contains a four-helix bundle domain followed by a WH-A and WH-B domain that is separated by a α/β -domain (Goldenberg *et al.*, 2004). The C-terminal part interacts with Rbx1, which has a β -strand perfectly fitting into the architecture of Cul1 C-terminal β -strands.

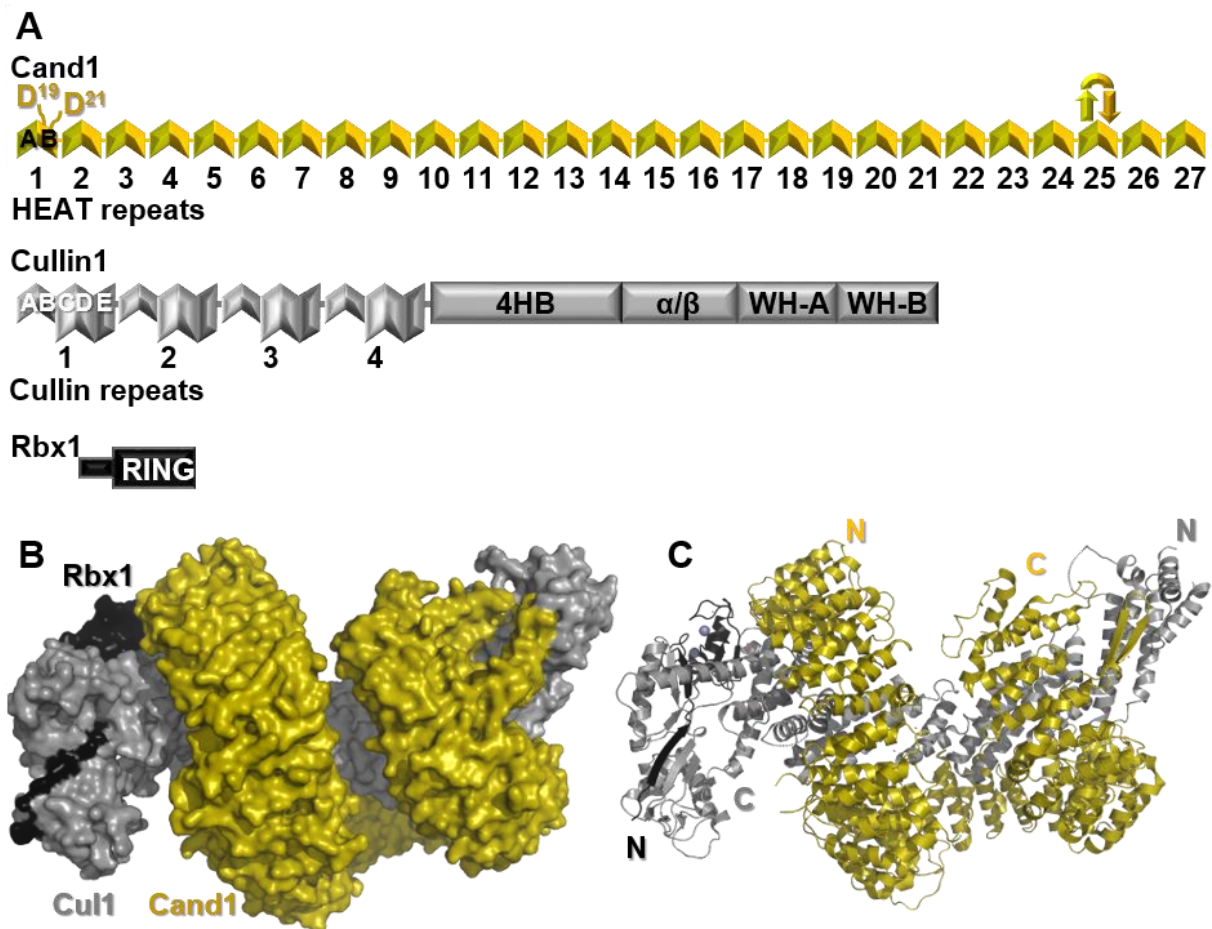


Figure 11. Domain properties and crystal structure of Cand1 in complex with Cul1-Rbx1. **A** Cand1 consists of 27 HEAT repeats, whereby each repeat is characterized by an A and B helix. HEAT repeat 25 is interrupted by a β -hairpin (Goldenberg *et al.*, 2004). Cul1 has four N-terminal cullin repeat motifs, containing two short helices (A, B) and three longer helices (C, D, E). The C-terminal domain contains a four-helix bundle domain (4HB), a α/β -domain and two winged helix domains WH-A and WH-B. Rbx1 contains an N-terminal β -sheet and a RING domain with three zinc ions. **B** Surface view of the Cand1-Cul1-Rbx1 crystal structure. Rbx1 is located at Cul1 C-terminus and Cand1 wraps around Cul1 in a head to tail orientation (Zheng *et al.*, 2002b). 3D structure figures were generated with PyMOL using PDB ID 1U6G. **C** Cartoon representation of the crystal structure in the same orientation like in B.

The catalytic center of Rbx1 is included in the C-terminal domain carrying the RING domain characterized by three cysteine residues connected to zinc ions and mediates E2 transfer enzyme binding.

Cand1/A is ubiquitously found in eukaryotes including humans, mice, plants and fungi. Whereas all higher eukaryotes, as well as fungi like the plant pathogen *Verticillium dahliae*, the unicellular *S. cerevisiae* or the saprophyte *N. crassa* possess a one-subunit Cand1 protein, CandA of *Aspergillus* species is split into at least two parts (Helmstaedt *et al.*, 2011; Sela *et al.*, 2012; Liu *et al.*, 2017b). *A. nidulans* N-terminal subunit CandA-N interacts with the C-terminal subunit CandA-C and this interaction is required for nuclear localization of CandA-N and subsequent cullin binding (Helmstaedt *et al.*, 2011). The function of Cand1 is conserved although subunit composition is different. Cand binds cullin proteins and thereby regulates the activity of CRLs (Liu *et al.*, 2002; Zheng *et al.*, 2002a; Min *et al.*, 2003; Pierce *et al.*, 2013). The crystal structure of human Cand1 elucidates that the Nedd8 binding residue Lys720 of Cul1 is almost covered by the first Cand1 HEAT repeat (Figure 12A) (Goldenberg *et al.*, 2004). The negatively charged aspartate residues Asp19 and Asp21 are in polar contact to Cul1 Lys720, preventing neddylation (Goldenberg *et al.*, 2004). A second feature of Cand1 is the interference of Skp1 binding site on Cul1 with Cand1 β -hairpin at HEAT repeat 25, resulting in the adaptor-receptor disassembly of SCFs (Figure 12B). Both SCF activity repressing features display the proposed function of Cand1 as adaptor-receptor exchange factor and furthermore, the control of Cand1 to bind only deneddylated SCFs as binding interfaces antagonize each other (Zheng *et al.*, 2002a; Chua *et al.*, 2011; Wu *et al.*, 2013).

Many studies described the function of the CSN and Cand1, however, the transition steps from CSN to Cand1 to Nedd8 attachment activating a new CRL cycle are not described so far (Enchev *et al.*, 2012; Zemla *et al.*, 2013; Dubiel *et al.*, 2015; Gummlich *et al.*, 2016; Liu *et al.*, 2018). A computational study predicts Cand1 dissociation from Cul1 dependent on higher affinities of Nedd8 and an adaptor-receptor charged substrate to Cul1 than Cand1 (Straube *et al.*, 2017). Like CSN, Cand1 malfunction is associated to many different kinds of diseases and cancers for example adipogenesis (Dubiel *et al.*, 2013; Buonanno *et al.*, 2017). CSN and Cand1 are required for tightly regulated cell cycle exit by disassembling SCFs with Skp2 carrying p27 in human cell lines. Enrichment of p27 is required for cell proliferation but increased Cand1 levels are found for instance in altered adipocyte differentiation (adipogenesis) (Dubiel *et al.*, 2013, 2015). *A. nidulans candA* deficient strains are unable to form multicellular structures (cleistothecia) in the sexual life cycle (Helmstaedt *et al.*, 2011), which is in agreement with the *csn* and *cand1* dependent defective proliferation described in other eukaryotes (Bosu *et al.*, 2010; Qian *et al.*, 2016).

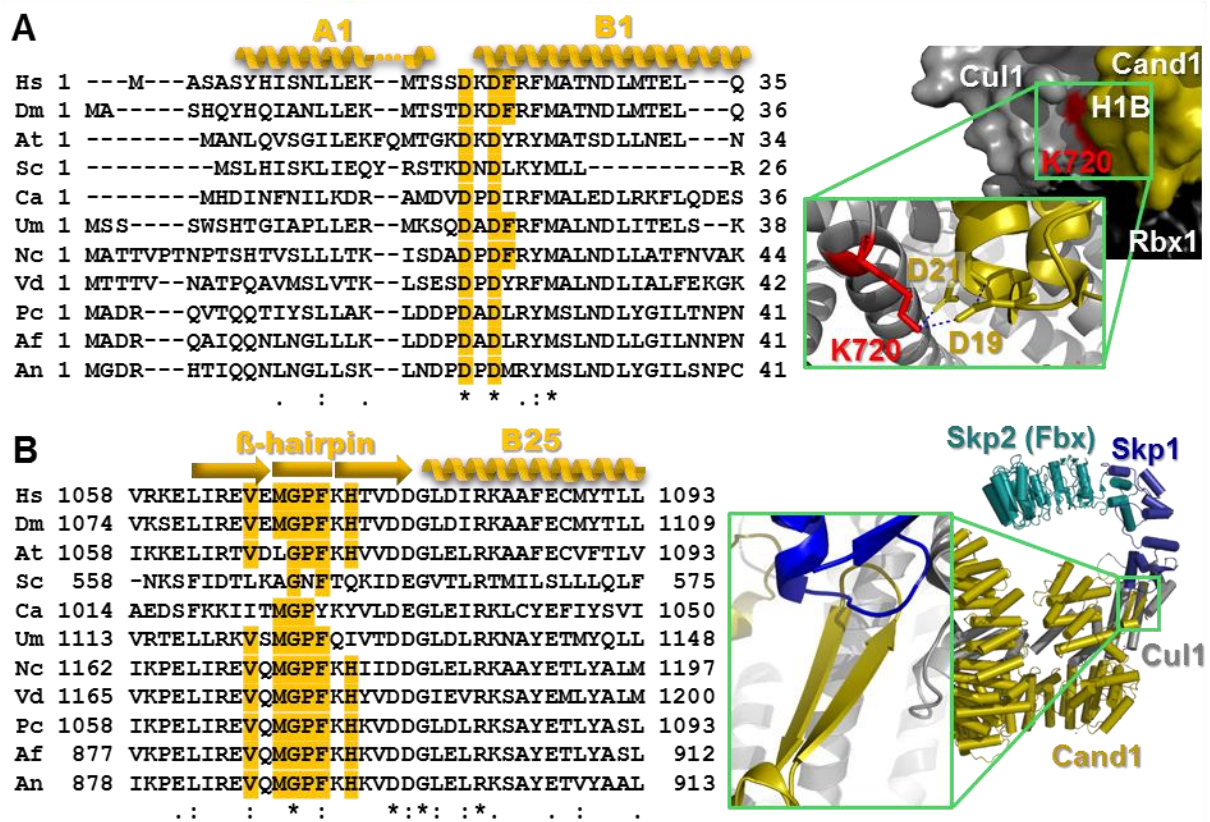


Figure 12. Cand1 has conserved Nedd8 and Skp1 blocking sites. **A** Cand1/A protein sequence alignment (Edgar, 2004) shows conservation of amino acid residues of Cand1's first HEAT repeat. Conserved residues are indicated by an asterisk ('*'), strongly similar residues by a colon (':') and weakly conserved amino acids are marked by a period ('.'). The three-dimensional structure shows that K720 is covered by HEAT repeat 1, helix B (H1B) with residues aspartate D19 and D21. Cand1 is depicted in yellow, Cul1 in grey and Rbx1 in black. **B** Cand1/A protein sequence alignment reveals the conservation of the β -hairpin between A and B helix of HEAT repeat 25. The β -hairpin competes with the Skp1 binding site on Cul1 N-terminal end. The adaptor-receptor complex Skp1-Skp2 (PDB ID: 2ASS), colored in blue and cyan, respectively, was modeled into the Cand1-Cul1 complex structure (PDB ID: 1U6G) using PyMOL and according to PDB ID: 1LDK. Cand1/A UniProt IDs: *Homo sapiens* (Hs) Q86VP6, *Drosophila melanogaster* (Dm) Q9VKY2, *Arabidopsis thaliana* (At) Q5L5Y6, *Saccharomyces cerevisiae* (Sc) Q92325, *Candida albicans* (Ca) Q5ADW3, *Ustilago maydis* (Um) A0A0D1CP07, *Neurospora crassa* (Nc) V5IKW9, *Verticillium dahliae* (Vd) G2X4I3, *Penicillium chrysogenum* (Pc) A0A161ZCA3 (N-terminal) and A0A167URG5 (C-terminal), *Aspergillus fumigatus* (Af) Q4WMC0 (N-terminal) and Q4WMC6 (C-terminal), *Aspergillus nidulans* (An) C8VP82 (N-terminal) and Q5BAH2 (C-terminal).

1.4 Aim of this work

The aim of this work was to investigate the complex *candA* genomic loci including arrangement of genes, resulting subunit composition of encoded proteins as well as their interaction partners in *A. nidulans* and *A. fumigatus*.

Cand1 is an exchange factor for substrate receptor-adaptors of cullin E3 ubiquitin ligases (Pierce *et al.*, 2013; Wu *et al.*, 2013; Zemla *et al.*, 2013). The Cand1 C-terminal domain interferes with the binding interface between cullin and the substrate adaptor-receptor subunits, which leads to dissociation of these subunits from cullin upon Cand1/A binding. The N-terminus of Cand1 covers the Nedd8 binding site and prevents thereby the activation of E3 ligases (Goldenberg *et al.*, 2004). Cand1 consists of 27 HEAT repeats that lead to a superhelical U-shaped structure, which facilitates binding of cullin E3 ubiquitin ligases that were deneddylated by the COP9 signalosome (Goldenberg *et al.*, 2004). Active ubiquitin ligases are modified with the ubiquitin-like protein Nedd8, which supports ubiquitin ligation to substrates that are targeted for degradation by the proteasome. The ubiquitin-proteasome system is the major destruction system in eukaryotic organisms for specific protein degradation. Accurate SCF ligase activity that targets the right substrates for ubiquitin-labeling is a prerequisite for multicellular development.

Aspergillus spp. are responsible for a variety of different human health risks like invasive aspergillosis and have a significant impact on agriculture by causing post-harvest food contaminations with fungal toxins. Previous studies showed, that the exchange of substrate-receptor units of cullin E3 ligases is different in *Aspergillus* spp. than in other eukaryotes. *Aspergillus* spp. require at least two CandA subunits for SCF activity regulation (Helmstaedt *et al.*, 2011). This study aimed to find the differences of the exchange mechanism performed by a multi-subunit CandA exchange factor compared to what is known about monomeric Cand1 proteins. The focus was primarily on the genetic locus of *A. nidulans candA* genes and the identification of a third CandA subunit. This newly discovered third gene of *A. nidulans* corresponds to an N-terminal extension encoded in *A. fumigatus canA*, which was used for comparison. Furthermore, the complex formation of a multi-subunit CandA was investigated and putative interacting proteins were analyzed. The cullin E3 ligase activity was investigated concerning the need of all three CandA subunits for a functional CandA complex. The impact on fungal growth, development and secondary metabolism of the single subunits was studied in *A. nidulans*. CanA impact on *A. fumigatus* asexual development was analyzed and compared to *A. nidulans candA* mutant strains.

2 Materials and Methods

2.1 Chemicals and materials

Media, buffers and other solutions were prepared with chemicals purchased from APPLICHEM GMBH (Darmstadt, Germany), BD BIOSCIENCES (Heidelberg, Germany), BIOZYME SCIENTIFIC GMBH (Hessisch Oldendorf, Germany), CARL ROTH GMBH & CO. KG (Karlsruhe, Germany), FLUKA (Neu-Ulm, Germany), INVITROGEN (Carlsbad, CA, USA), MERCK KGAA (Darmstadt, Germany), OXOID DEUTSCHLAND GMBH (Wesel, Germany), ROCHE DIAGNOSTICS GMBH (Mannheim, Germany), SIGMA-ALDRICH CHEMIE GMBH (München, Germany) and SERVA ELECTROPHORESIS GMBH (Heidelberg, Germany). Ampicillin (ROTH), chloramphenicol (APPLICHEM), pyriithiamine hydrobromide (SIGMA-ALDRICH), clonNAT nourseothricin dihydrogen sulfate (WERNER BIOAGENTS, Jena, Germany) and phleomycin (INVIVOGEN, Toulouse, France) were used for selection of microorganisms. Small-scale sterile filtration of solutions was performed with Filtropur filters with a pore size of 0.2 µm (SARSTEDT). The pH was determined with a WTW bench pH/mV Routine meter pH 526 (SIGMA-ALDRICH). Polymerases and restriction enzymes were obtained from THERMO FISHER SCIENTIFIC (Schwerte, Germany) and NEB (Frankfurt am Main, Germany). Primers were purchased from EUROFINS GENOMICS GMBH (Ebersberg, Germany). The GeneRuler 1kb DNA ladder (THERMO FISHER SCIENTIFIC, Berlin, Germany) was used for DNA *on-gel* band size determination in DNA gel-electrophoresis. The PageRuler™ Prestained Protein Ladder (26616) (THERMO FISHER SCIENTIFIC) and ProSieve Quad Color (00193837) (BIOZYME) were used for protein *on-gel* band size determination. DNA- and protein concentrations were measured with a NanoDrop ND-1000 photospectrometer from PEQLAB BIOTECHNOLOGIE GMBH (Erlangen, Germany). DNA was purified with the NucleoSpin® Plasmid Kit or NucleoSpin® Gel and PCR clean up Kit from MACHERY & NAGEL (Düren, Germany). RNA was extracted with the RNeasy Plant Mini Kit (QIAGEN, Hilden, Germany). Trypsin was used from SERVA ELECTROPHORESIS GMBH (Heidelberg, Germany). Protein pull-downs of GFP-tagged proteins were conducted with GFP-Trap®_A agarose beads from CHROMOTEK GMBH (Planegg-Martinsried, GER). Protein purification of GST-tagged proteins was performed with GSTrap FF columns and HiPep Sephacryl S-300 16/60 HR both obtained from GE HEALTHCARE (Solingen, Germany). The following named electrophoresis equipment was obtained from BIO-RAD LABORATORIES (Hercules, CA, USA): DNA agarose gel electrophoresis was performed with Mini-Sub® Cell GT chambers and the PowerPac™ 300 power supply, SDS polyacrylamide gel electrophoresis were conducted with the Mini-Protean® Tetra Cell, Mini Trans-Blot® Electrophoretic Cell and

with the PowerPac™ 3000 power supply. DNA was blotted to Amersham™ Hybond-NTM nylon membranes (GE HEALTHCARE) and Proteins were transferred from SDS-polyacrylamide gels onto Amersham™ Protran™ 0.45 µm NC nitrocellulose blotting membranes (GE HEALTHCARE). Chemiluminescence of Southern hybridization was detected by developing the Amersham™ Hyperfilm™-ECL (GE HEALTHCARE) with the Optimax X-ray Film Processor from PROTEC GMBH & CO. KG (Oberstenfeld, Germany). Western hybridization was visualized with the Fusion SL chemiluminescence detector from PEQLAB. As primary antibodies α-GFP antibody sc-9996 (SANTA CRUZ BIOTECHNOLOGY, Santa Cruz, CA, USA), α-tubulin antibody T0926 (SIGMA-ALDRICH), α-actin NB100-74340 (NOVUS BIOCHEMICALS, Abingdon, UK), α-CulA antibody, α-Nedd8 antibody (GENESCRIP, Piscataway, NJ, USA) and α-Ubiquitin 05-944 (MERCK) were used. As secondary antibodies horseradish peroxidase-coupled rabbit antibody G21234 (INVITROGEN) and mouse antibody 115-035-003 (JACKSON IMMUNORESEARCH, Newmarket, UK) were used. Nuclei were visualized in fluorescence microscopy with 4',6-Diamidin-2-phenylindol (DAPI) from ROTH and mitochondria were highlighted with MitoTracker™ Red FM (THERMO FISHER SCIENTIFIC). Pipet tips, reaction tubes, petri dishes and other plastic consumables were purchased from SARSTEDT AG & CO. (Nümbrecht, Germany), STARLAB GMBH (Hamburg, Germany) and NERBE PLUS GMBH (Winsen/Luhe, Germany). Centrifugation of 1.5 and 2 mL reaction tubes was performed with Biofuge fresco (cooled) and Heraeus™ Pico™ 17 Microcentrifuges from HERAEUS INSTRUMENTS GMBH (Hanau, Germany)/THERMO FISHER SCIENTIFIC. For centrifugation of 10, 15 and 50 ml centrifuge tubes Centrifuge 5804R from EPPENDORF AG (Hamburg, Germany) and 4K15C from SIGMA LABORZENTRIFUGEN GMBH (Osterode am Harz, Germany) were used. For bigger volumes the SorvallRC-3B Plus Refrigerated Centrifuge and Sorvall RC-5B Plus Refrigerated Centrifuge from THERMO FISHER SCIENTIFIC were used. Materials and instrumentations, which were not listed here are indicated in the following chapters.

2.2 Media and growth conditions

In general, media were prepared with deionized H₂O (dH₂O) and sterilized by autoclaving at 121°C for 20 min and 2 bar. Solutions with heat instable substances were filter-sterilized.

2.2.1 Bacterial growth

Plasmid construction and cloning was performed with *Escherichia coli* strain DH5 α TM (Hanahan *et al.*, 1991). Rosetta II *E. coli* strain (NOVAGEN[®], MERCK) was used for the recombinant expression of *A. nidulans* proteins. Genotypes of these strains are listed in Table 1. *E. coli* strains were cultivated in lysogeny broth (LB) (Bertani, 1951) medium (1 % (w/v) tryptophan, 0.5 % (w/v) yeast extract, 1 % (w/v) NaCl) on a rotary shaker at 37°C. Selection was performed with 100 mg/mL Ampicillin or 34 mg/mL chloramphenicol in a dilution of 1:1000 (v/v). For solid medium 2 % (w/v) agar was added.

Table 1. *E. coli* strains used in this study.

Strain	Genotype
DH5α	F-, Δ (<i>argF-lac</i>)169, ϕ 80d <i>lacZ</i> Δ M15, Δ <i>phoA8</i> , <i>glnX44</i> (AS), λ -, <i>deoR481</i> , <i>rfbC1</i> , <i>gyrA96</i> (NalR), <i>recA1</i> , <i>endA1</i> , <i>thiE1</i> , <i>sdR17</i>
Rosetta II	F-ompT hsdANB (rB-mB-) gal dcm (DE3) pRARE2 (Cam ^R)
One Shot[®] TOP10	F- <i>mcrA</i> , Δ (<i>mrr-hsdRMS-mcrBC</i>), ϕ 80d <i>lacZ</i> Δ M15, Δ <i>lacX74</i> , <i>recA1</i> , <i>araD139</i> , Δ (<i>araleu</i>)7697, <i>galU</i> , <i>galK</i> , <i>rpsL</i> (StrR), <i>ndA1 nupG</i>

2.2.2 Fungal growth

The *Aspergillus nidulans* and *fumigatus* strains were cultivated in liquid or solid minimal medium (MM, 1% (w/v) glucose, (for solid medium 2% (w/v) Agar and if needed 2.5 % *uracil* (ROTH)), 1x AspA (70 mM NaNO₃, 7 mM KCl, 11.2 mM KH₂PO₄, pH 5.5), 2 mM MgSO₄, 1x trace elements solution pH 6.5 (76 μ M ZnSO₄, 178 μ M H₃BO₃, 25 μ M MnCl₂, 18 μ M FeSO₄, 7.1 μ M CoCl₂, 6.4 μ M CuSO₄, 6.2 μ M Na₂MoO₄, 174 μ M EDTA). Depending on the strains different supplements like 0.1 % para-amino-bezeoacid (paba, SIGMA-ALDRICH), 0.1 % pyridoxine-HCl (SIGMA-ALDRICH), 0.1 % phleomycin (INVIVOGEN) for the *ble* marker gene, 0.07 % nourseothricin (ClonNAT, WERNER BIOAGENTS, Jena, Germany) for the *nat* resistance marker, 0.15 % pyrithiamine hydrobromide (*ptrA*, SIGMA-ALDRICH), 0.1 % uridine (ROTH) were added after autoclaving. For *A. fumigatus* spotting or western hybridization

experiments modified minimal medium (1 % (w/v) glucose, 1x Aspergillus salt solution (7 mM KCl, 4.3 mM MgSO₄, 11.2 mM KH₂PO₄), 10 mM NaNO₃, 1x trace element solution) was used. Spores were harvested in sodium-tween solution (0.5 % NaCl, 0.01 % Tween80) and stored at 4°C for further usage. For spot tests, 4 000 conidiospores were used for point inoculation of plates containing 30 ml MM paba (for *A. nidulans*) or modified MM (for *A. fumigatus*). *A. nidulans* plates were incubated at 37°C (if not indicated different) in light for asexual development favoring conditions or plates were sealed with parafilm (BEMIS, Braine L'Alleud, Belgium) and incubated in the dark for sexual development. *A. fumigatus* plates were incubated without illumination. Vegetative growth was performed with liquid MM or modified MM in baffled flasks at 37°C for 20 hours and agitation.

2.2.3 *Aspergillus fumigatus*

The *A. fumigatus* strain AfS35 (Krappmann *et al.*, 2006) was used as host for the generation of *A. fumigatus* mutant strains in this study (Table 2).

Table 2. *A. fumigatus* strains used in this study. ^P: promoter, ^T: terminator, PP: PreScission cleavage site, L: linker.

Strain	Genotype	Reference
AfS35 (FGSC#1159)	$\Delta akuA::loxP$ wild type	(Krappmann <i>et al.</i> , 2006)
AfGB76	$\Delta akuA::loxP$; $P_{gpdA}:gfp:his2a^T$, $ptrA^R$	(Lin <i>et al.</i> , 2015)
AfGB140	$\Delta akuA::loxP$, $canA^{\Delta exon1(1-596)}::six$	This study
AfGB141	$\Delta akuA::loxP$, $\Delta canA::six$	This study
AfGB142	$\Delta akuA::loxP$, $canA^{\Delta exon1(1-596)}::An_candA-C1:canA^{exon2-4(597-4078)}::six$	This study
AfGB143	$\Delta akuA::loxP$, $P_{canA}:canA:PP:L:gfp:six:canA^T$	This study
AfGB144	$\Delta akuA::loxP$, $\Delta canA-N::six$	This study
AfGB145	$\Delta akuA::loxP$, $\Delta canA^{838-4078}::six$	This study
AfGB146	$\Delta akuA::loxP$, $\Delta canA-N::six$, $\Delta canA^{838-4078}::six$	This study

2.2.4 *Aspergillus nidulans*

The *A. nidulans* strains AGB552 and AGB551 (Bayram *et al.*, 2012) were used as hosts for the generation of *A. nidulans* mutant strains in this study (Table 3).

Table 3. *A. nidulans* strains used in this study. ^P: promoter, ^T: terminator, ^R: resistance, PP: PreScission cleavage site; L: linker, *nat*^R: non-recyclable *nat* resistance, *phleo*^R: non-recyclable *phleo* resistance.

Strain	Genotype	Reference
AGB160	<i>pyrG89, pyroA4, pyr4</i> ⁺	(Busch <i>et al.</i> , 2003)
AGB316	<i>pyrG89, pyroA4, ΔdenA::pyr4</i> ⁺	(Christmann <i>et al.</i> , 2013)
AGB552	<i>ΔnkuA::argB, pabaA1, yA2, veA</i> ⁺	(Bayram <i>et al.</i> , 2012)
AGB596	<i>ΔnkuA::argB, ^PgpdA:sgfp:phleo^R; pabaA1, yA2, veA</i> ⁺	(Bayram <i>et al.</i> , 2012)
AGB989	<i>ΔnkuA::argB, pabaA1, yA2, veA</i> ⁺ , <i>^PgpdA:mrfp:h2A:hisB^T, phleo^R</i>	C. Gross, p.c.
AGB1014	<i>ΔnkuA::argB, pyrG89, pyroA4, veA</i> ⁺ , <i>^PgpdA:mrfp:h2A:hisB^T;nat^R</i>	(Thieme <i>et al.</i> , 2018)
AGB1094	<i>ΔnkuA::argB, pabaA1, yA2, veA</i> ⁺ , <i>ΔcandA-N::six</i>	This study
AGB1095	<i>ΔnkuA::argB, pabaA1, yA2, veA</i> ⁺ , <i>^PcandA-N:candA-N:six:candA-N^T</i>	This study
AGB1096	<i>ΔnkuA::argB, pabaA1, yA2, veA</i> ⁺ , <i>ΔcandA-C::six</i>	This study
AGB1097	<i>ΔnkuA::argB, pabaA1, yA2, veA</i> ⁺ , <i>^PcandA-C:candA-C:six:candA-C^T</i>	This study
AGB1098	<i>ΔnkuA::argB, pabaA1, yA2, veA</i> ⁺ , <i>ΔcandA-N::six, ΔcandA-C::six</i>	This study
AGB1099	<i>ΔnkuA::argB, pabaA1, yA2, veA</i> ⁺ , <i>ΔcandA-C1::six</i>	This study
AGB1100	<i>ΔnkuA::argB, pabaA1, yA2, veA</i> ⁺ , <i>^PcandA-C1:candA-C1:PP:L:gfp:six:candA-C1^T</i>	This study
AGB1101	<i>ΔnkuA::argB, pabaA1, yA2, veA</i> ⁺ , <i>5'fl candA-C1:^PniiA/niaD:candA-C1:PP:L:gfp:six:candA-C1^T</i>	This study
AGB1102	<i>ΔnkuA::argB, pabaA1, yA2, veA</i> ⁺ , <i>5'fl candA-C1:^PniiA/niaD:candA-C1:PP:L:gfp:six:candA-C1^T, ^PgpdA:mrfp:h2A:hisB^T;phleo^R</i>	This study
AGB1103	<i>ΔnkuA::argB, pabaA1, yA2, veA</i> ⁺ , <i>^PgpdA:mrfp:h2A:hisB^T;phleo^R, ^PcandA-N:gfp:PP:L:candA-N:^PgpdA:nat^R:candA-N^T</i>	This study
AGB1104	<i>ΔnkuA::argB, pabaA1, yA2, veA</i> ⁺ , <i>^PgpdA:mrfp:h2A:hisB^T;phleo^R, ^PcandA-C:candA-C:PP:L:gfp:^PgpdA:nat^R:candA-C^T</i>	This study
AGB1105	<i>ΔnkuA::argB, pabaA1, yA2, veA</i> ⁺ , <i>Δigr::six</i>	This study
AGB1106	<i>ΔnkuA::argB, pabaA1, yA2, veA</i> ⁺ , <i>ΔcandA-C1:igr::six</i>	This study
AGB1107	<i>ΔnkuA::argB, pabaA1, yA2, veA</i> ⁺ , <i>ΔcandA-C1::six, ^PcandA-C1:candA-C1:candA-C1^T:^PgpdA:phleo^R:trpC^T (ectopic)</i>	This study
AGB1108	<i>ΔnkuA::argB, pabaA1, yA2, veA</i> ⁺ , <i>Δ^{ATG}candA-C1::six</i>	This study
AGB1109	<i>ΔnkuA::argB, pabaA1, yA2, veA</i> ⁺ , <i>ΔcandA-C1:: ^PcandA-C1:Af_canA exon1:six:candA-C1^T</i>	This study
AGB1110	<i>ΔnkuA::argB, pabaA1, yA2, veA</i> ⁺ , <i>^PcandA-C1:candA-C1^{Δstop}:igr:^{Δstart}candA-C:PP:L:gfp:six:candA-C^T</i>	This study
AGB1111	<i>ΔnkuA::argB, pabaA1, yA2, veA</i> ⁺ , <i>ΔcsnE::six</i>	This study

Table 3 continued

Strain	Genotype	Reference
AGB1112	$\Delta nkuA::argB, pabaA1, yA2, veA^+, \Delta candA-N::six, \Delta csnE::six$	This study
AGB1113	$\Delta nkuA::argB, pabaA1, yA2, veA^+, \Delta candA-C::six, \Delta csnE::six$	This study
AGB1114	$\Delta nkuA::argB, pabaA1, yA2, veA^+, \Delta candA-N::six, \Delta candA-C::six, \Delta csnE::six$	This study
AGB1115	$\Delta nkuA::argB, pyrG89, pyroA4, veA^+; P_{gpdA}:mrfp:h2A:hisB^T; nat^R, P_{niiA}:Nyfp:niiA^T:P_{niiD}:Cyfp:candA-N:niiD^T:phleo^R$	This study
AGB1116	$\Delta nkuA::argB, pyrG89, pyroA4, veA^+; P_{gpdA}:mrfp:h2A:hisB^T; nat^R, P_{niiA}:Nyfp:niiA^T:P_{niiD}:candA-C:Cyfp:niiD^T:phleo^R$	This study
AGB1117	$\Delta nkuA::argB, pyrG89, pyroA4, veA^+; P_{gpdA}:mrfp:h2A:hisB^T; nat^R, P_{niiA}:candA-C1:Nyfp:niiA^T:P_{niiD}:candA-C:Cyfp:niiD^T:phleo^R$	This study
AGB1118	$\Delta nkuA::argB, pyrG89, pyroA4, veA^+; P_{gpdA}:mrfp:h2A:hisB^T; nat^R, P_{niiA}:candA-C1:Nyfp:niiA^T:P_{niiD}:Cyfp:candA-N:niiD^T:phleo^R$	This study
AGB1119	$\Delta nkuA::argB, pyrG89, pyroA4, veA^+; P_{gpdA}:mrfp:h2A:hisB^T; nat^R, P_{niiA}:candA-C1:Nyfp:niiA^T:P_{niiD}:Cyfp:niiD^T:phleo^R$	This study
AGB1120	$\Delta nkuA::argB, pabaA1, yA2, veA^+, \Delta csnE::six, P_{niiA}:candA-C1:Nyfp:niiA^T:P_{niiD}:candA-C:Cyfp:niiD^T:phleo^R$	This study
AGB1121	$\Delta nkuA::argB, pabaA1, yA2, veA^+, \Delta csnE::six, P_{niiA}:candA-C1:Nyfp:niiA^T:P_{niiD}:Cyfp:candA-N:niiD^T:phleo^R$	This study
AGB1122	$\Delta nkuA::argB, pabaA1, yA2, veA^+, P_{gpdA}:mrfp:h2A:hisB^T; phleo^R, P_{candA-C}:candA-C:PP:L:gfp:P_{gpdA}:nat^R:candA-C^T, \Delta candA-C1::six$	This study
AGB1123	$\Delta nkuA::argB, pabaA1, yA2, veA^+, P_{gpdA}:mrfp:h2A:hisB^T; phleo^R, P_{candA-N}:gfp:PP:L:candA-N:P_{gpdA}:nat^R:candA-N^T, \Delta candA-C1::six$	This study
AGB1124	$\Delta nkuA::argB, pabaA1, yA2, veA^+, \Delta candA-C::six, P_{candA-C}:candA-C^{\Delta NLS}:PP:L:gfp:P_{gpdA}:nat^R:candA-C^T, P_{gpdA}:mrfp:h2A:hisB^T; phleo^R$	This study
AGB1125	$\Delta nkuA::argB, pabaA1, yA2, veA^+, P_{gpdA}:mrfp:h2A:hisB^T; phleo^R, P_{candA-N}:gfp:PP:L:candA-N:P_{gpdA}:nat^R:candA-N^T, P_{candA-C}:candA-C^{\Delta NLS}:six:candA-C^T$	This study
AGB1126	$\Delta nkuA::argB, pabaA1, yA2, veA^+, P_{gpdA}:mrfp:h2A:hisB^T; phleo^R, P_{nedd8}:gfp:PP:L:nedd8^{cDNA}:P_{gpdA}:nat^R:nedd8^T, P_{candA-C}:candA-C^{\Delta NLS}:six:candA-C^T$	This study
AGB1127	$\Delta nkuA::argB, pabaA1, yA2, veA^+, 5'fl\ candA-C1:P_{niiA}/niaD:candA-C1:PP:L:gfp:six:candA-C1^T, P_{gpdA}:mrfp:h2A:hisB^T; phleo^R, candA-C^{\Delta NLS}:candA-C^T$	This study
AGB1128	$\Delta nkuA::argB, pabaA1, yA2, veA^+, \Delta candA-C::six, 5'fl\ candA-C1:P_{niiA}/niaD:candA-C1:PP:L:gfp:six:candA-C1^T$	This study
AGB1129	$\Delta nkuA::argB, pabaA1, yA2, veA^+, \Delta candA-N::six, 5'fl\ candA-C1:P_{niiA}/niaD:candA-C1:PP:L:gfp:six:candA-C1^T$	This study
AGB1130	$\Delta nkuA::argB, pabaA1, yA2, veA^+, \Delta candA-C::six, 5'fl\ candA-C1:P_{niiA}/niaD:candA-C1:PP:L:gfp:six:candA-C1^T, \Delta candA-N::six$	This study
AGB1176	$\Delta nkuA::argB, pabaA1, yA2, veA^+, P_{gpdA}:mrfp:h2A:hisB^T; bleo^R, P_{nedd8}:gfp:PP:L:nedd8^{cDNA}:P_{gpdA}:nat^R:nedd8^T$	This study
AGB1177	$\Delta nkuA::argB, pabaA1, yA2, veA^+, \Delta denA::six$	This study
AGB1178	$\Delta nkuA::argB, pabaA1, yA2, veA^+, \Delta candA-N::six, \Delta denA::six$	This study
AGB1179	$\Delta nkuA::argB, pyrG89, pyroA4, veA^+; P_{gpdA}:mrfp:h2A:hisB^T; nat^R, P_{niiA}:Nyfp:nedd8^{cDNA}:niiA^T:P_{niiD}:candA-C:Cyfp:niiD^T:phleo^R$	This study
AGB1180	$\Delta nkuA::argB, pyrG89, pyroA4, veA^+; P_{gpdA}:mrfp:h2A:hisB^T; nat^R, P_{niiA}:Nyfp:nedd8^{cDNA}:niiA^T:P_{niiD}:Cyfp:niiD^T:phleo^R$	This study

Table 3 continued

Strain	Genotype	Reference
AGB1181	$\Delta nkuA::argB$, <i>pyrG89</i> , <i>pyroA4</i> , <i>veA</i> ⁺ ; <i>PgpdA:mrfp:h2A:hisB^T;nat^R</i> , <i>Pnii::Nyfp:nedd8^{cDNA}:niiAT:PniiD:Cyfp:candA-N:niiD^T:phleo^R</i>	This study
AGB1182	$\Delta nkuA::argB$, <i>pyrG89</i> , <i>pyroA4</i> , <i>veA</i> ⁺ ; <i>PgpdA:mrfp:h2A:hisB^T;nat^R</i> , <i>PniiA::Nyfp:nedd8^{cDNA}:niiAT:PniiD:candA-C1:Cyfp:niiD^T:phleo^R</i>	This study
AGB1183	$\Delta nkuA::argB$, <i>pabaA1</i> , <i>yA2</i> , <i>veA</i> ⁺ , $\Delta csnE::six$, <i>PniiA::Nyfp:nedd8^{cDNA}:niiAT:PniiD:candA-C:Cyfp:niiD^T:phleo^R</i>	This study
AGB1184	$\Delta nkuA::argB$, <i>pabaA1</i> , <i>yA2</i> , <i>veA</i> ⁺ , $\Delta csnE::six$, <i>PniiA::Nyfp:nedd8^{cDNA}:niiAT:PniiD:Cyfp:candA-N:niiD^T:phleo^R</i>	This study
AGB1185	$\Delta nkuA::argB$, <i>pabaA1</i> , <i>yA2</i> , <i>veA</i> ⁺ , $\Delta csnE::six$, <i>PniiA::Nyfp:nedd8^{cDNA}:niiAT:PniiD:Cyfp:niiD^T:phleo^R</i>	This study
AGB1186	$\Delta nkuA::argB$, <i>pabaA1</i> , <i>yA2</i> , <i>veA</i> ⁺ , $\Delta csnE::six$, <i>PniiA::Nyfp:nedd8^{cDNA}:niiAT:PniiD:candA-C1:Cyfp:niiD^T:phleo^R</i>	This study
AGB1187	$\Delta nkuA::argB$, <i>pabaA1</i> , <i>yA2</i> , <i>veA</i> ⁺ , $\Delta candA-C::six$, <i>PcandA-C1:candA-C1^{Δstop}:Δigr:candA-C1:PP:L:gfp:PgpdA:phleo^R:trpC^T</i> (ectopic)	This study
AGB1189	$\Delta nkuA::argB$, <i>pyrG89</i> , <i>pyroA4</i> , <i>veA</i> ⁺ ; <i>PgpdA:mrfp:h2A:hisB^T;nat^R</i> , <i>PniiA::Nyfp:niiAT:PniiD:candA-C1:Cyfp:niiD^T:phleo^R</i>	This study

2.3 Computational methods

BLAST search was performed with National Center for Biotechnology Information (Geer *et al.*, 2010) tool and Joint Genome Institute – JGI MycoCosm (Grigoriev *et al.*, 2012, 2014; de Vries *et al.*, 2017). Sequences were mainly obtained from AspGD (Cerqueira *et al.*, 2014), FungiDB (Stajich *et al.*, 2012) and UniProt (The UniProt Consortium, 2017). Sequences for BLAST analysis of different *Aspergillus* species were obtained from JGI MycoCosm and alignment was performed with MUSCLE Multiple Sequence Alignment tool (EMBL) (Edgar, 2004). Maximum likelihood tree data was imported to iTOL (Letunic and Bork, 2016) to generate a phylogenetic tree. Motif prediction was performed with InterPro (Finn *et al.*, 2017). NLS prediction was conducted with cNLS mapper (Kosugi *et al.*, 2009b). Phyre² (Protein Homology/analogy Recognition Engine V 2.0) was used for secondary structure prediction (Kelley *et al.*, 2015). Figures with three-dimensional protein structures were prepared with PyMOL (The PyMOL Molecular Graphics System, Version 2.0 Schrödinger, LLC.).

2.4 Morphological methods

The number of conidiospores was determined with a Coulter Z2 particle counter (BECKMAN COULTER, Krefeld, Germany) or spore numbers were counted manually with a Thoma cell counting chamber (hemocytometer) (PAUL MARIENFELD, Lauda-Königshofen, Germany). Phenotypes were analyzed with a binocular microscope SZX12-ILLB2-200 (OLYMPUS

DEUTSCHLAND GMBH, Hamburg, Germany) and ascospores of cleistothecia were analyzed with an Axiolab light microscope (ZEISS, Oberkochen, Germany). For conidiospore amount quantification, conidia were harvested in sodium-tween solution (0.5 % NaCl, 0.01 % Tween80) and then diluted for counting. The colony diameter was determined by measuring the diameter with a ruler at the indicated time point of three independent experiments.

2.5 Nucleic acid methods

2.5.1 Isolation of fungal genomic DNA

Strains were grown in liquid cultures over night. Mycelia were harvested through Miracloth filters (MERCK MILLIPORE) and washed with 0.96 % NaCl solution. The mycelia were dried, frozen in liquid nitrogen and ground with a Mixer Mill MM 400 (RETSCH, Haan, Germany). Ground mycelia were mixed with 500 µl genomic DNA lysis buffer (200 mM Tris-HCl pH 8.5, 250 mM NaCl, 25 mM EDTA, 0.5 % (w/v) SDS) and incubated 15 min at 65°C. Mycelia solutions were mixed with 100 µl 8 M potassium acetate and centrifuged for 15 min at 13 000 rpm at room temperature (RT). The supernatant was transferred to a new test tube and mixed with 100 µl 8 M potassium acetate and centrifuged for 15 min at 13 000 rpm at RT. The supernatant was transferred into new test tubes and mixed with 300 µl isopropanol. The samples were centrifuged for 15 min at 13 000 rpm at RT. DNA pellets were washed with 100% (v/v) ethanol by centrifugation for 5 min at 13 000 rpm, RT and then dried at 42°C before resolving in dH₂O at 37°C for 60 min.

2.5.2 Isolation of fungal genomic RNA

RNA was isolated from 20 hours vegetative grown mycelium from liquid cultures. The mycelia were harvested by filtration through miracloth, washed with 0.96 % NaCl solution and then frozen in liquid nitrogen. The mycelia were ground with a Mixer Mill MM 400 (RETSCH). The protocol of the RNeasy Plant Mini Kit (QIAGEN) was followed for RNA extraction.

2.5.3 Isolation and purification of plasmid DNA, PCR products and linearized DNA fragments

Plasmid DNA was isolated from *E. coli* cultures by utilization of the NucleoSpin® Plasmid Kit (MACHEREY-NAGEL, Düren, Germany) according to manufacturer's specifications. Plasmid DNA was eluted from spin column with dH₂O. PCR amplification or enzymatic digest fragments were excised from agarose gels by employing the NucleoSpin® Gel and PCR Clean-up Kit (MACHEREY-NAGEL).

2.5.4 Polymerase chain reaction

Polymerase chain reaction (PCR) (Saiki *et al.*, 1988) was performed to amplify DNA fragments for plasmid construction and for 'colony PCR' (Bergkessel and Guthrie, 2013) to analyze the presence of a desired plasmid in *E. coli* strains after plasmid transformation. PCRs were performed in T Professional Standard 96, T Professional Trio 48 and T Professional Standard 96 Gradient thermocyclers (BIOMETRA GMBH, Göttingen, Germany) and in Primus 96 Thermal Cyclers (MWG BIOTECH AG, Ebersberg, Germany). Phusion® High-Fidelity DNA Polymerase (THERMO FISHER SCIENTIFIC), Q5® High Fidelity Polymerase (NEB), Taq DNA Polymerase (THERMO FISHER SCIENTIFIC) or Pfu Polymerase (THERMO FISHER SCIENTIFIC) were used for DNA amplification. PCR programs were designed after manufacturer's instructions and according to calculated melting temperatures of the primers.

2.5.5 Agarose gel electrophoresis

Agarose gel electrophoresis was used to separate DNA according to size. The gels contained 1 % (w/v) agarose and 0.001 mg/ml ethidium bromide in TAE buffer (40 mM Tris, 20 mM acetic acid, 1 mM EDTA). The DNA was mixed with 10x DNA loading dye (10 % (v/v) Ficoll 400, 200 mM EDTA pH 8.0, 0.2 % (w/v) bromophenol blue, 0.2 % (w/v) xylene cyanol FF) and visualized *in-gel* by exposure to UV light ($\lambda = 254$ nm) with a Gel iX20 Imager Windows Version and the *Intas GDS* gel documentation software (INTAS SCIENCE IMAGING INSTRUMENTS GMBH, Göttingen, Germany).

2.5.6 Quantitative real-time polymerase chain reaction

Transcription of *candA-C1*, *candA-C* and *candA-N* was analyzed by quantitative real-time (qRT) PCR with the primers from Table 4. Histone *h2A* served as housekeeping gene. RNA was extracted as described in chapter 2.5.2. cDNA was transcribed from 0.8 µg RNA using QuantiTect Reverse Transcription Kit (QIAGEN). Transcription levels were analyzed with a CFX Connect™ Real Time System cycler (BIORAD) using Mesa Green qPCR™ MasterMix Plus for SYBR® Assay (EUROGENTEC) and the standard protocol Table 5. Expression levels were quantified relative to the housekeeping gene (*h2A*) in $\Delta\Delta CT$ method (Livak and Schmittgen, 2001). Gene study of three independent experiments was performed using *CFX Manager™* Software version 3.1 (BIORAD).

Table 4. Oligonucleotides used for qRT-PCR. *f*: forward primer, *r*: reverse primer.

Primer	Sequence (5' to 3')	Target	Reference
MG277-RT	CGTCTTCTTCGCAAGGGAAACT	<i>h2A-f</i>	(Kolog Gulko <i>et al.</i> , 2018)
MG278-RT	CGGGTTTTCTTGTTGTCACGAG	<i>h2A-r</i>	(Kolog Gulko <i>et al.</i> , 2018)
rtAMK01	AGACGGGGCTACTGTCTACAAG	<i>candA-C1-f</i>	This study
rtAMK02	GACTTGAGCAGGCTGAGTTTTT	<i>candA-C1-r</i>	This study
rtAMK03	CTCCATTCCGTCAAGGAGTTAC	<i>candA-C-f</i>	This study
rtAMK04	CTCCCATAGCACGGTTATCTTC	<i>candA-C-r</i>	This study
rtAMK05	GTATTCTCAGCAATCCCTGCTC	<i>candA-N-f</i>	This study
rtAMK06	AGACATTTCAGTGCCTGGTTTT	<i>candA-N-r</i>	This study

Table 5. qRT-PCR program used in this study. Steps 2 to 4 were repeated 39 times.

step	Temperature [°C]	Time [min]
1	95	2:20
2	95	0:20
3	60	0:22
4	72	0:22 + plate read
go to step 2, 39x		
5	95	0:10
6	Melting curve: 65 to 95°C, increment 0.5°C for 0:05 min and plate read	
7	end	

2.5.7 cDNA amplification assay

cDNA of *candA* genes was amplified by PCR from different mutant strains to study the transcript variants of the *candA-C1/candA-C* genetic locus. Total RNA was extracted as described in chapter 2.5.2 from 20 hours vegetative mycelium. cDNA was synthesized from 0.8 µg RNA as described in chapter 2.5.6. The Phusion® High-Fidelity DNA Polymerase (THERMO FISHER SCIENTIFIC) was used according to manufacturer's instructions. 2 µl cDNA (~2 µg) were used as template for each PCR reaction with the primers indicated in Table 6 and the number of cycles was increased to 37. 2 µl 1:10 diluted gDNA served as positive control for amplifications with different primer pairs. The annealing temperature of 60°C was used for all primer combinations except for primer 1 + 4, where 67°C were used. PCR fragments were analyzed by agarose gel electrophoresis.

Table 6. Oligonucleotides used for cDNA amplification assay. Primer # indicates the primer number from Figure 18. *igr*: intergenic region, *f*: forward primer, *r*: reverse primer.

Primer #	Primer name	Sequence (5' to 3')	Target gene
1	oAMK120	ATGCATTTCAAAGAACACACCCC	<i>candA-C1-f</i>
2	oAMK121	TCACTGGAGAAAGTCGAAC	<i>candA-C1-r</i>
3	oAMK03b	ATGTCTTCCGACGCAATGTCTG	<i>candA-C-f</i>
4	oAMK04b	TTAGAACTCCGACTCGAGGTTA	<i>candA-C-r</i>
5	rtAMK07	CAACTTTTTTGATGCCAAGAGC	<i>igr-f</i>
6	rtAMK08	GCTCGAGAGCTTCAGTGTCAGT	<i>igr-r</i>
Control	oAMK01	ATGGGAGATCGACACAC	<i>candA-N-f</i>
Control	oAMK02	CTACATACCAGTAATTAGCTTTTCTTTAGGC	<i>candA-N-r</i>

2.6 Plasmid construction for genetic manipulation of *A. nidulans*, *A. fumigatus* and *E. coli*

Fragments were amplified from genomic DNA (gDNA) of the respective wild type if not indicated different. Fragments were fused by fusion PCR (Szewczyk *et al.*, 2006) and ligated with T4 DNA ligase (THERMO FISHER SCIENTIFIC) according to manufactures instructions. Fragment ligation was also performed by the usage of the GeneArt® Seamless Cloning and Assembly Kit (INVITROGEN) or the GeneArt® Seamless Cloning and Assembly Enzyme Mix (INVITROGEN). Mostly, linearized pUC19L, provided by the Seamless Cloning Kits, was used as backbone for plasmid construction if not indicated differently. The cloned cassettes were excised by *PmeI* (cutting site: GTTT/AAAC) restriction digest, as this restriction site was always included or introduced in the terminal sequence of the flanking regions for *in locus* integration.

2.6.1 Self-excising marker cassettes as selection markers

Gene targeting by homologous recombination was mostly performed with a recyclable marker cassette. This cassette contains a β -recombinase gene, which is inducible with xylose. The expressed β -recombinase recognizes and excises the marker cassette at two identical and asymmetric recognition six sites, leaving only one six site (~100 bp) after cleavage (Figure 13) (Hartmann *et al.*, 2010). In the present study different self-excisable marker cassettes were used: pME4304 (J. Gerke, p.c.) and pME4696 contain the *nat1* gene from *Streptomyces noursei*, which is resistant against nourseothricin (Kück and Hoff, 2006). pME4305 (J. Gerke, p.c.) contains the *ble* gene from *Streptoalloteichus hindustanus*, which is resistant to phleomycin (Drocourt *et al.*, 1990).

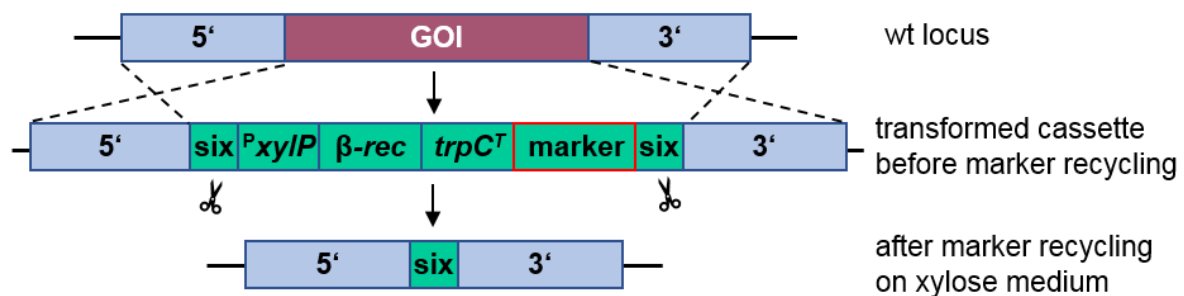


Figure 13. Scheme of *in locus* integration of a recyclable marker cassette and its recycling. A gene of interest (GOI) is replaced by homologous recombination of the 5' and 3' flanking regions integrating the recyclable marker cassette. This cassette contains a xylose promoter (P_{xyIP}), a gene encoding the β -recombinase (β -rec), a *trpC* terminator sequence ($trpC^T$) flanked by two six sites. The six sites include recognition sequences for the cleavage by the β -recombinase, which is expressed upon cultivation on 0.5 % (w/v) xylose containing media, leaving only one six site at the position of the gene of interest (adapted from Hartmann *et al.*, 2010).

pSK485 and pCHS314 (C. Sasse, p.c.) harbor the *Aspergillus oryzae ptrA* gene, which is responsible for resistance against pyrithiamine (Hartmann *et al.*, 2010). In the following, recyclable marker cassettes for *nat* are termed *nat*-RM, for *bleo phleo* *phleo*-RM and for *ptrA* *ptrA*-RM. pME4696 and pCHS314 are cloning plasmids and each six site is flanked by a *Swal* or *Pml* cloning site, respectively. The cassettes of pME4304, pME4305 and pSK485 must be excised by *Sfi*I restriction digest from the plasmid backbone prior to the cloning procedure. The self-excisable marker cassettes can be recycled by cultivation of the strains on solid minimal medium containing 0.5 % glucose and 0.5 % xylose.

2.6.2 Primer and plasmid design

Table 7 shows the primers, which were generated and used to construct the plasmids listed in Table 8. Primers and plasmids were designed using the Lasergene software package from DNA STAR INC (Madison, WI, USA). The terminal ends of the flanking regions were chosen to comprise a naturally occurring GTTT or AAAC sequence for cassette *in locus* integration by *PmeI* restriction digest of the cassette containing plasmid. The primers designed for the amplification of the terminal ends of the cassette introduce the corresponding second half of the *PmeI* restriction site. This prevents the integration of additional base pairs into the *A. nidulans* or *A. fumigatus* genome and genes, to avoid interruption of sequences. Primers used for seamless cloning reactions contain a 15 base pairs (bp) overhang, which is complementary to adjoining sequences in the way that two bordering sequences share a 15 bp homology region. All constructed plasmids were sequenced by SEQLAB SEQUENCE LABORATORIES (Göttingen, Germany).

Table 7. Oligonucleotides designed and used in this study.

Primer	Sequence (5' to 3')	Reference
AL39	ATTCGAGCTCGGTACGTTTAAACACTTACTCGTCCACAAGCTT	This study
AL40	ACCTATAGGCCTGAGTGATGATTGTCAGGTGGGGATAT	This study
AL43	ATTCGAGCTCGGTACGTTTAAACCCTTTCAAAGCCCTTGCG	This study
AL44	ACCTATAGGCCTGAGTCTTATCTGATGGTCTAATCACGA	This study
AL45	ATAATATGGCCATCTTAGTTGGCCGACCGCT	This study
AL46	GCCAAGCTTGCATGCCGTTTAAACAACGAAGTCGAAGCAG	This study
AL47	AAGTTGAGCATAATATCAGATGATGAGACGATCTATG	This study
AL48	CCAAGCTTGCATGCCGTTTAAACTGGGGACGATATGATCAG	This study
CM108	CGCTCCATCGCCACGGTGAGCAAGGGCGAGGA	Dissertation of C. Meister, 2018
EB2	CTACTTGTACAGTTCGTCCATG	E. Beckmann, p.c.
EB10	ATGGTGAGCAAGGGCGAGG	E. Beckmann, p.c.
oAMK02	CTACATACCAGTAATTAGCTTTTCTTTAGGC	This study
oAMK03b	ATGTCTTCCGACGCAATGTCTG	This study
oAMK04b	TTAGAACTCCGACTCGAGGTTA	This study
oAMK14	TCTCAGACCCTTGATTGTG	This study
oAMK21	GGTGGTGAATTCATGGGAGATCGACACACG	This study
oAMK22	GGTGGTGTGACCTACATACCAGTAATTAG	This study
oAMK23	GGTGGTGAATTCATGTCTTCCGACGCAATG	This study
oAMK24	GGTGGTGCGGCCGCTTAGAACTCCGACTCGAG	This study
oAMK61	ATTCGAGCTCGGTACGTTTAAACGGCACTAAGTACACATCC	This study
oAMK78	TCTAGCATTATTTATGGGCTGG	This study

Table 7 continued

Primer	Sequence (5' to 3')	Reference
oAMK79	CCAAGCTTGCATGCCGTTTAAACTTTTCTCACGAGCTAGGTTTC	This study
oAMK80	TAAATAAATGCTAGATCAGGGGCAGGGCATGCTC	This study
oAMK82	CTGGAAGTTCTGTTCCAGGG	This study
oAMK87	ATTCGAGCTCGGTACGTTTAAACTAATATCTCAGTCAAAGATGCATTTTC	This study
oAMK92	CCAAGCTTGCATGCCGTTTAAACTCATTGATTCTTTTATTACCC	This study
oAMK94	GCCCTTGCTCACCATCGTGAACAGAACCCCGCG	This study
oAMK95	ACCACCGCTACCACCGGG	This study
oAMK96	GGTGGTAGCGGTGGTATGGGAGATCGACACACGATC	This study
oAMK97	CCAAGCTTGCATGCCATTTAAATCTACATACCAGTAATTAGCTTTTC	This study
oAMK98	CTGGTATGTAGATTTGGCGGCTCTGAGGTGCAG	This study
oAMK100	ATGCCCTGCCCTGAGACAAGACTTTGCCATTGGATTT	This study
oAMK101	ATTCGAGCTCGGTACGTTTAAACGATTTTCTCCATAATCCAG	This study
oAMK102	GCCCTTGCTCACCATCTTGAGAATGCGATGCTCTATTC	This study
oAMK103	GGTGGTAGCGGTGGTATGTTGATCAAGGTCCGTACAC	This study
oAMK104b	CCAAGCTTGCATGCCATTTAAATCTACTGAAGGGCGGCGCAG	This study
oAMK105	AGTTCGTGCTGGTCAACCG	This study
oAMK106	CCAAGCTTGCATGCCGTTTAAACCTCGATCGTCTAAATAGAG	This study
oAMK107	CCTTCAGTAGATTTAGGCGGCTCTGAGGTGCAG	This study
oAMK108	TTGACCAGCACGAACCTCAGGGGCAGGGCATGCTC	This study
oAMK109	CCTATAGGCCTGAGTTGTGGCGGGTGAGTGAGTT	This study
oAMK110	ATAATATGGCCATCTGACAAGACTTTGCCATTGG	This study
oAMK111	CCTATAGGCCTGAGTCGTGAACAGAACCCCGCG	This study
oAMK112	ATAATATGGCCATCTTCTAGCATTATTTATGGGCTGG	This study
oAMK120	ATGCATTTCAAAGAACACACCC	This study
oAMK121	TCACTGGAGAAAGTCAAC	This study
oAMK125	GAACAGAACTTCCAGGAACCTCCGACTCGAGGTTAC	This study
oAMK126	ATTCGAGCTCGGTACGTTTAAACACACCTGCTATAGCAAGC	This study
oAMK127	CCTATAGGCCTGAGTCTTTGACTGAGATATTAAGACGAG	This study
oAMK128	ATAATATGGCCATCTTTTACCATTACTGCATTATCTTCG	This study
oAMK131	GAACAGAACTTCCAGCTGGAGAAAGTCAACAGATCA	This study
oAMK137	CCTATAGGCCTGAGTCTACATACCAGTAATTAGCTTTTC	This study
oAMK138	CCTATAGGCCTGAGTTTAGAACTCCGACTCGAGGTTA	This study
oAMK139	CCTATAGGCCTGAGTTCACTGGAGAAAGTCAAC	This study
oAMK142	ATTCGAGCTCGGTACGTTTAAACAATGACTTATCAAAGCCAGAGGC	This study
oAMK143	CCAAGCTTGCATGCCGTTTAAACTGTGGCGGGTGAGTGAGT	This study
oAMK163	ATGGTGAGCAAGGGCGAG	This study
oAMK164	CGGCGCGCCCGTGGCGATGGAGCGCATGATATAGACGTTGTGGCTG	This study
oAMK165	GCCACGGGCGCGCCGATGTTGATCAAGGTCCGTACAC	This study
oAMK166	CTACTGAAGGGCGGCGCA	This study
oAMK167	TTACTTGTACAGCTCGTCCATG	This study
oAMK168b	ATGGCCGACAAGCAGAAGAACG	This study
oAMK169b	CGGCGCGCCCGTGGCGATGGAGCGCTTGTACAGCTCGTCCATGC	This study
oAMK170	GCCACGGGCGCGCCGATGGGAGATCGACACACGATC	This study
oAMK173	CAGCCACAACGTCTATATCATGTAG	This study
oAMK197	CGTGGCGATGGAGCGCTGGAGAAAGTCGAACAGATC	This study
oAMK198	CTACATGATATAGACGTTGTGGC	This study
oAMK199	TGCGAACCCGTATTTCTACATGATATAGACGTTGTGGC	This study
oAMK200	CATACTCTCACATTTATGCATTTCAAAGAACACACCC	This study
oAMK204	CTTGACAGGCCGGGCGCTGGAGAAAGTCGAACAGATC	This study
oAMK205	TTCGACTTTCTCCAGCGCCCGGCCTGCAAGATC	This study

Table 7 continued

Primer	Sequence (5' to 3')	Reference
oAMK214	ATTCGAGCTCGGTACGTTTAAACCTTCTCAGAACAACATGAC	This study
oAMK215	CCTATAGGCCTGAGTTCACTGGAGAAAGTCGAACAGAT	This study
oAMK216	ATAATATGGCCATCTATGTCTTCCGACGCAATGTCCG	This study
oAMK217	CCAAGCTTGCATGCCGTTTAAACTCAGGGTTTCAATCTGCAG	This study
oAMK224	CGGTACATTTAAATATGCATTTCAAAGAACACACCCC	This study
oAMK225	ATCCCATACTCTCACCTTTGACTGAGATATTAAGACGAG	This study
oAMK226	ATATCTCAGTCAAAGGTGAGAGTATGGGATAGGAAAAT	This study
oAMK227	GATGGCGGGCGCGGTGAT	This study
oAMK228	ATAATATGGCCATCTTTTTACCATTACTGCATTATCTTCG	This study
oAMK229	TTCGACTTTCTCCAGTTTTACCATTACTGCATTATCTTCG	This study
oAMK230	CATTGCGTCGGAAGATGTGGCGGGTGAGTGAGTT	This study
oAMK231	CACTCACCCGCCACATCTTCCGACGCAATGTCCG	This study
oAMK232	GACAAGACTTTGCCATTGGATTT	This study
oAMK243	ATTCGAGCTCGGTACGTTTAAAC	This study
oAMK247	ATTCGAGCTCGGTACGTTTAACTTTCCGGTTGAGAGAAGC	This study
oAMK248	CCTATAGGCCTGAGTATCGTCAAAGTAAAAGGGCTGC	This study
oAMK249	ATAATATGGCCATCTGTGAGCTACCTCGGGGGC	This study
oAMK250	CCAAGCTTGCATGCCGTTTAAACCATCCAAGATAATGGGCATGTA	This study
oAMK252	TTTACTTTTGACGATATGCATTTCAAAGAACACACC	This study
oAMK253	CCTATAGGCCTGAGTTGCTGTAGAAAATCGAATAAATCAAG	This study
oAMK254	ATATCTCAGTCAAAGCATTTCAAAGAACACACCCCTC	This study
oAMK255	GTGTTCTTTGAAATGCTTTGACTGAGATATTAAGACGAG	This study
oAMK256	ATCACTGATAGGCATCTTTGACTGAGATATTAAGACGAG	This study
oAMK257	ATATCTCAGTCAAAGATGCCTATCAGTGATCATACTCC	This study
oAMK262	TTCTTTGAAATGCATATCGTCAAAGTAAAAGGGCTGC	This study
oAMK267	ATATGGCCATCTCACGCGTGCCTTTTAGACGAAAGAA	This study
oAMK268	GATAAGCTTGATCACGTTTAAACTGGAGCAACTCGGCGTGC	This study
oAMK269	AGGAATTCGATATTTGTTTAACTTACGCAACCCTCAAAGC	This study
oAMK270	GAACAGAACTTCCAGCTAGAATTCCGTCTCGAGGC	This study
oAMK271	ATAGGCCTGAGATTTTACTTGTACAGTTCGTCCATGC	This study
oAMK273	AGGAATTCGATATTTGTTTAACTTTCCGGTTGAGAGAAGC	This study
oAMK274	ATAGGCCTGAGATTTATCGTCAAAGTAAAAGGGCTGC	This study
oAMK276	GGCATCGCTATCTTGCGAGATCTTGGAACCACTAC	This study
oAMK277	GGTTCCAAGATCTCGCAAGATAGCGATGCCAGTATG	This study
oAMK278	CGAGATCTTGGAACCACTAC	This study
oAMK279	CAAGATAGCGATGCCAGTATG	This study
oAMK283	CCAAGCTTGCATGCCGTTTAAACAACGGTTAGACTGAGCACA	This study
oAMK286	GTATACCCATTGAATGACGTGTC	This study
oAMK290	AGGAATTCGATATTTGTTTAACTATTGTGCTATGTAATATATTAC	This study
oAMK291	ATAGGCCTGAGATTTGAGGACGTTGAAGTTCGAAAA	This study
oAMK295	GTTTAAACACGTGCAAAGATGGATGTG	This study
oAMK296	CTAGCTGATTGTGTTTAGACACT	This study
oAMK298	CTGGAGAAAGTCGAACAGATC	This study
oAMK299	ATCAAGCTTATCGATACCGTC	This study
ST06	CCTATAGGCCTGAGTCTACTTGTACAGTTCGTCCATG	C. Meister, p.c.

Table 8. Plasmids designed and used in this study. *A. nidulans* genes are labeled with An_geneX and *A. fumigatus* genes with Af_geneX. ^P: promoter, ^T: terminator, ^R: resistance, PP: PreScission cleavage site; L: linker, *bla*: ampicillin resistance gene, *nat*-RM: recyclable *nat* resistance cassette from pME4304 or pME4696, *phleo*-RM: recyclable *phleo* resistance cassette from pME4305, *ptrA*-RM: recyclable *ptrA* resistance cassette from pSK485 or pCHS314, p.c. = personal communication.

Plasmid	Genotype	Reference
pBluescript KSII-/+	cloning vector	FERMENTAS
pCHS314	Cloning plasmid with self-excising β - <i>rec</i> / <i>six</i> <i>ptrA</i> -RM	C. Sasse, p.c.
pCM3	Template for PCRs; contains <i>gfp</i> :L:PP: <i>csnF</i>	C. Meister, p.c.
pGEX-6P-1	Cloning plasmid for expression of GST fusion proteins,	GE Healthcare
pME3173	Plasmid for ectopic integration of <i>mrfp</i> : <i>h2A</i> : <i>natR</i> ,	(Bayram <i>et al.</i> , 2008a)
pME3281	Cloning plasmid (Q96) for ectopic integration, <i>phleo</i> ^R	Helmstaedt <i>et al.</i> , 2011
pME3741	BiFC vector, used as template	Helmstaedt <i>et al.</i> , 2011
pME3857	Plasmid for ectopic integration of <i>mrfp</i> : <i>h2A</i> : <i>phleo</i> ^R	(Bayram <i>et al.</i> , 2012)
pME3929	<i>gfp</i> : <i>natR</i> cassette, used as template for PCR	Christmann <i>et al.</i> , 2013
pME4304	Self-excising β - <i>rec</i> / <i>six</i> <i>nat</i> -RM containing vector	J. Gerke, p.c.
pME4305	Self-excising β - <i>rec</i> / <i>six</i> <i>phleo</i> -RM containing vector	J. Gerke, p.c.
pME4313	BiFC cloning plasmid	J. Gerke, p.c.
pME4649	^P <i>candA-N</i> : <i>gfp</i> :L:PP:An_ <i>candA-N</i> : ^P <i>gpdA</i> : <i>nat</i> ^R : <i>candA-N</i> ^T in pUC19, <i>bla</i>	This study
pME4650	An_ Δ <i>candA-N</i> : <i>nat</i> -RM in pUC19, <i>bla</i>	This study
pME4651	An_ Δ <i>candA-C</i> : <i>nat</i> -RM in pUC19, <i>bla</i>	This study
pME4652	^P <i>candA-C</i> :An_ <i>candA-C</i> :PP:L: <i>gfp</i> : <i>gpdA</i> : <i>nat</i> ^R : <i>candA-C</i> ^T in pUC19, <i>bla</i>	This study
pME4653	An_ Δ <i>candA-C1</i> : <i>phleo</i> -RM in pUC19	This study
pME4654	An_ Δ <i>csnE</i> : <i>phleo</i> -RM in pUC19, <i>bla</i>	This study
pME4655	Complementation: An_ <i>candA-N</i> : <i>phleo</i> -RM in pUC19, <i>bla</i>	This study
pME4656	Complementation: An_ <i>candA-C</i> : <i>phleo</i> -RM in pUC19, <i>bla</i>	This study
pME4657	An_ Δ <i>candA-C1</i> : <i>ptrA</i> -RM in pUC19, <i>bla</i>	This study
pME4658	Complementation An_ <i>candA-C1</i> : <i>nat</i> -RM in pUC19, <i>bla</i>	This study
pME4659	BiFC vector: ^T <i>NiiA</i> :An_ <i>nedd8</i> ^{cDNA} : <i>yfp</i> ^N : ^P <i>niiA</i> / <i>niaD</i> :An_ <i>candA-C</i> : <i>yfp</i> ^C : <i>NiiD</i> ^T : <i>phleo</i> ^R in pME3741, <i>bla</i>	This study
pME4660	BiFC vector: ^T <i>NiiA</i> :An_ <i>nedd8</i> ^{cDNA} : <i>yfp</i> ^N : ^P <i>niiA</i> / <i>niaD</i> : <i>NiiD</i> ^T : <i>yfp</i> ^C : <i>phleo</i> ^R in pME3741, <i>bla</i>	This study
pME4661	BiFC vector: ^T <i>NiiA</i> :An_ <i>nedd8</i> ^{cDNA} : <i>yfp</i> ^N : ^P <i>niiA</i> / <i>niaD</i> : <i>yfp</i> ^C :An_ <i>candA-N</i> : <i>NiiD</i> ^T : <i>phleo</i> ^R in pME3741, <i>bla</i>	This study
pME4662	BiFC vector: ^T <i>NiiA</i> : <i>yfp</i> ^N : ^P <i>niiA</i> / <i>niaD</i> : <i>yfp</i> ^C :An_ <i>candA-N</i> : <i>NiiD</i> ^T : <i>phleo</i> ^R in pME3741, <i>bla</i>	This study
pME4663	BiFC vector: ^T <i>NiiA</i> : <i>yfp</i> ^N : ^P <i>niiA</i> / <i>niaD</i> :An_ <i>candA-C</i> : <i>yfp</i> ^C : <i>NiiD</i> ^T : <i>phleo</i> ^R in pME3741, <i>bla</i>	This study
pME4664	BiFC vector: ^T <i>NiiA</i> : <i>yfp</i> ^N :An_ <i>candA-C1</i> : ^P <i>niiA</i> / <i>niaD</i> :An_ <i>candA-C</i> : <i>yfp</i> ^C : <i>NiiD</i> ^T : <i>phleo</i> ^R in pME3741, <i>bla</i>	This study
pME4665	BiFC vector: ^T <i>NiiA</i> : <i>yfp</i> ^N :An_ <i>candA-C1</i> : ^P <i>niiA</i> / <i>niaD</i> : <i>yfp</i> ^C :An_ <i>candA-N</i> : <i>NiiD</i> ^T : <i>phleo</i> ^R in pME3741, <i>bla</i>	This study

Table 8 continued

Plasmid	Genotype	Reference
pME4666	BiFC vector: <i>TNiiA:yfp^N:An_candA-C1:PniiA/niaD:yfp^C:NiiD^T:phleo^R</i> in pME3741, <i>bla</i>	This study
pME4667	BiFC vector: <i>TNiiA:An_nedd8^{cDNA}:yfp^N:PniiA/niaD:An_candA-C1:yfp^C:NiiD^T:phleo^R</i> in pME3741, <i>bla</i>	This study
pME4668	<i>An_Δigr:phleo</i> -RM in pUC19, <i>bla</i>	This study
pME4669	<i>An_ΔcandA-C1/igr:phleo</i> -RM in pUC19, <i>bla</i>	This study
pME4670	Overexpression <i>An_candA-C1-gfp:nat</i> -RM in pBluescriptKS(-), <i>bla</i>	This study
pME4671	Fusion of <i>An_candA-C1-candA-C:nat</i> -RM in pME4696, <i>bla</i>	This study
pME4672	<i>Af_canA^{Δexon1}:ptrA</i> -RM in pUC19, <i>bla</i>	This study
pME4673	Complementation of <i>Af_canA^{Δexon1}</i> with <i>An_candA-C1:ptrA</i> -RM in pUC19, <i>bla</i>	This study
pME4674	<i>An_candA-C1</i> start codon deletion: <i>phleo</i> -RM in pUC19, <i>bla</i>	This study
pME4675	Complementation <i>An_ΔcandA-C1</i> with <i>Af_canA^{Δexon1}:phleo</i> -RM in pUC19, <i>bla</i>	This study
pME4676	Vector for ectopic integration of <i>An_candA-C1:PcandA-C1:candA-C1:candA-C1^T:phleo</i> in Q96	This study
pME4677	<i>Af_ΔcanA:ptrA</i> -RM in pUC19, <i>bla</i>	This study
pME4678	Complementation of <i>Af_canA:ptrA</i> -RM in pUC19, <i>bla</i>	This study
pME4679	<i>An_candA-C^{ΔNLS}:ptrA</i> -RM in pCHS314, <i>bla</i>	This study
pME4680	<i>PcandA-C:An_candA-C^{Δ2151-2165(NLS)}:PP:L:gfp:gpdA:nat^R:candA-C^T</i> in pUC19, <i>bla</i>	This study
pME4681	<i>Af_ΔcanA-N:ptrA</i> -RM in pCHS314, <i>bla</i>	This study
pME4682	Vector for ectopic integration of fusion <i>An_candA-C1-candA-C:PcandA-C1:candA-C1^{Δstop}:candA-C:PP:L:gfp:candA-C^T:phleo^R</i> in Q96	This study
pME4683	<i>Af_canA^{Δ838-4078}:ptrA</i> -RM in pCHS314, <i>bla</i>	This study
pME4684	preBiFCII cloning vector: <i>TNiiA:yfp^N:PniiA/niaD:NiiD^T:phleo^R</i> in pME3741, <i>bla</i>	This study
pME4685	preBiFCIII cloning vector: <i>TNiiA:yfp^N:An_candA-C1^PniiA/niaD:NiiD^T:phleo^R</i> in pME3741, <i>bla</i>	This study
pME4696	Cloning plasmid with self-excising <i>β-rec/six nat</i> -RM	C. Meister, p.c.
pME4716	<i>Pnedd8:gfp:L:PP:An_nedd8^{cDNA}:gpdA:nat^R:nedd8^T</i> in pUC19, <i>bla</i>	This study
pME4717	<i>An_ΔdenA:nat</i> -RM in pUC19, <i>bla</i>	This study
pME4718	preBiFCI cloning vector: <i>TNiiA:An_nedd8^{cDNA}:yfp^N:PniiA/niaD:NiiD^T:phleo^R</i> in pME3741, <i>bla</i>	This study
pME4720	pGEX-6P-1 expression vector with <i>gst:PP:An_candA-C</i> , <i>bla</i>	This study
pME4721	pGEX-6P-1 expression vector with <i>gst:PP:An_candA-N</i> , <i>bla</i>	This study
pME4722	<i>PcandA-N:An_candA-N:candA-C:PP:L:gfp:gpdA:nat^R:candA-C^T</i> in pUC19, <i>bla</i> used as template for PCR amplification	This study
pSK409	Cloning plasmid with nitrate promotor: <i>PniaD:niaD^TPniiA:niiA^T; ptrA^R</i>	(Schinke <i>et al.</i> , 2016)
pSK485	Self-excising <i>β-rec/six ptrA</i> -RM containing vector	(Hartmann <i>et al.</i> , 2010)
pUC19L	Cloning vector, linearized with <i>Pst</i> I and <i>Kpn</i> I	INVITROGEN

2.6.3 Plasmid and strain construction of *A. nidulans* mutant strains

Plasmid and strain construction of the GFP-CandA-N fusion construct

For the construction of the N-terminal GFP fused CandA-N plasmid, the 5' flanking region of *candA-N* was amplified with oAMK61/94 (1772 bp). A fusion of *gfp* to a PreScission protease cleavage site (PP; sequence: LEVLFQGP) and to a linker (L; sequence: GGSGG) were amplified from pCM3 (Cindy Meister, personal communication) with EB10/oAMK95 (771 bp). *candA-N* was amplified with oAMK96/97 (1099 bp). The fragments were ligated by seamless cloning to pUC19L (linearized, provided by the kit) and transformed into DH5 α . For the second cloning step, the vector was linearized with *Swa*I, which restriction site was integrated by oAMK97. A non-recyclable marker cassette $P_{gpdA-nat}^R$ was amplified from pME3929 using oAMK98/80 (1394 bp). 3' flanking *candA-N* was amplified with oAMK78/79 (1513 bp). The fragments were ligated with the linear vector from first cloning step resulting in pME4649. The plasmid was cut with *Pme*I and the cassette (6436 bp) was transformed with AGB989 resulting in AGB1103.

Plasmid and strain construction of the CandA-C-GFP fusion construct

C-terminal GFP tagged CandA-C was constructed by amplification of 5' flanking and *candA-C* with oAMK87/125 (4121 bp). A fusion of *PP-L-gfp-gpdA-nat* was amplified from pME4722 with oAMK82/80 (2127 bp). 3' flanking *candA-C* was amplified with oAMK100/92 (552 bp). All fragments were ligated into linearized pUC19 with seamless cloning kit resulting in pME4652. The plasmid was *Pme*I digested and the cassette (6732 bp) was transformed to AGB989 resulting in AGB1104.

Plasmid and strain construction of the GFP-Nedd8 fusion construct

The 5' flanking region of *nedd8* was amplified from wt gDNA with oAMK101/102 (1941 bp). The *gfp-L-PP* fragment was amplified from pME4649 with EB10/oAMK95. Wild type cDNA was used for the amplification of *nedd8* with oAMK103/104b. The fragments were ligated to linear pUC19 with seamless cloning kit. The plasmid was digested with *Swa*I to linearize the vector. A non-recyclable marker cassette $P_{gpdA-nat}^R$ was amplified from pME3929 using oAMK107/108 (1394 bp). The 3' flanking region of *nedd8* was amplified with oAMK105/106. The fragments were ligated with the linear vector using the seamless cloning kit resulting in pME4716. The plasmid was cut with *Pme*I and the fragment of 6239 bp was transformed into AGB989 resulting in AGB1176.

Plasmid and strain construction of $\Delta candA-N$

For the *candA-N* deletion cassette, the 5' and 3' flanking regions were amplified with oAMK61/111 (1772 bp) and oAMK112/79 (1528 bp), respectively. The fragments and the *nat*-RM were ligated with seamless cloning into linearized pUC19 provided by the kit. The resulting plasmid pME4650 was *PmeI* digested and the cassette (7905 bp) was transformed to AGB552. Marker recycling resulted in AGB1094.

Plasmid and strain construction of $\Delta candA-C$

The *candA-C* deletion cassette was constructed by amplification of the 5' and 3' flanking regions using oAMK87/109 (870 bp) and oAMK110/92 (552 bp), respectively. The fragments and the *nat*-RM were ligated with seamless cloning into linear pUC19 resulting in pME4651, which was then transformed into DH5 α . The plasmid was *PmeI* digested and the cassette (6027 bp) was transformed to AGB552 and AGB1094. Marker recycling resulted in AGB1096 and AGB1098.

Plasmid and strain construction of *candA-N* and *candA-C* complementation

Complementation of *candA-N* was achieved by designing a flipper cassette containing the 5' flanking region with *candA-N* amplified by oAMK61/137 (2852 bp) and an oAMK112/79 (1528 bp) amplified 3' flanking region. For *candA-C* complementation plasmid, 5' flanking region and *candA-C* were amplified using oAMK87/138 (4124 bp) and the 3' flanking region with oAMK110/92 (552 bp). The fragments for both complementation plasmids were ligated with the *phleo*-RM into pUC19 resulting in pME4655 and pME4656, respectively. Both were *PmeI* digested and the cassettes *candA-N* (9198 bp) and *candA-C* (9494 bp) were transformed to AGB1094 resulting in AGB1095 and to AGB1096 resulting in AGB1097 after marker recycling.

Plasmid and strain construction of $\Delta candA-C1$

Two different deletion cassettes for *candA-C1* were constructed, differing in the marker. For both the 5' flanking region was amplified with oAMK142/127 (425 bp) and 3' flanking regions with oAMK128/143 (307 bp). The fragments were ligated with either the *phleo*-RM or *ptrA*-RM into linearized pUC19 resulting in pME4653 and pME4657, respectively. *PmeI* restriction digest of pME4653 resulted in a 5553 bp deletion cassette, which was transformed to AGB552 leading to AGB1099 after marker recycling. *PmeI* digestion of pME4657 resulted in a deletion

cassette of 5966 bp, which was transformed with AGB1103 and AGB1104 resulting in AGB1122 and AGB1123, respectively.

Plasmid and strain construction of *candA-C1* complementation

To complement *candA-C1*, a *gfp* fusion construct was designed. Therefore, *candA-C1* was amplified with its 5' flanking region using oAMK126/131 (3400 bp), the *PP-L-gfp* fragment was amplified using oAMK82/ST06 (773 bp) and the 3' flanking region with oAMK128/143 (307 bp). The fragments were ligated with *nat*-RM to linear pUC19 resulting in pME4658. The *PmeI* excised cassette with a size of 9070 bp was transformed to AGB1099 resulting in AGB1100 after marker recycling.

Plasmid and strain construction of overexpression *candA-C-gfp*

An overexpression *candA-C1* with C-terminal *gfp* fusion was achieved by amplification of *candA-C1* fused to *PP-L-gfp*, *nat*-RM and 3' flanking region from pME4658 with Q5 polymerase (NEB) using oAMK224/143 (6280 bp). The fragment was ligated to pBluescript KS(+). The plasmid was linearized with *SwaI*, which restriction site was integrated within oAMK224. The 5' flanking region of *candA-C1* was amplified by oAMK126/225 (2857 bp) and the nitrate promoter was amplified from pME4662 using oAMK226/227 (1281 bp). Both fragments were combined by fusion PCR using oAMK126/227 (4108 bp) and then ligated to the linearized plasmid resulting in pME4670. The cassette was excised with *PmeI* and AGB552, AGB1094 and AGB1096 were transformed with the fragment of 10340 bp resulting in AGB1101, AGB1129 and AGB1128 after marker recycling. To visualize nuclei in this strain, AGB1101 was transformed with pME3857 resulting in AGB1102. AGB1128 was transformed with the Δ *candA-N* flipper cassette obtained from pME4650 resulting in AGB1130 after marker recycling.

Plasmid and strain construction of Δ *igr*

To delete the *intergenic region (igr)* between *candA-C1* and *candA-C* open reading frames a deletion flipper cassette was designed. The 5' flanking region was amplified with oAMK214/215 (879 bp) and the 3' flanking region using oAMK216/217 (1005 bp). Both fragments were ligated together with a *nat*-RM into pUC19 producing the plasmid pME4668. AGB552 was transformed with the *PmeI* excised cassette of 6489 bp resulting in AGB1105 after marker recycling.

Plasmid and strain construction of $\Delta candA-C1/igr$

To generate a *candA-C1/igr* double deletion cassette, the 5' flanking was amplified with oAMK142/127 (428 bp) and the 3' flanking region with oAMK216/217 (1005 bp). Both fragments were ligated together with a *nat*-RM into pUC19 giving the plasmid pME4669. AGB552 was transformed with the *PmeI* excised cassette of 6038 bp resulting in AGB1106 after marker recycling.

Plasmid and strain construction of ectopic expressed *candA-C1*

For ectopic integration of *candA-C1* the gene was amplified together with its 5' and 3' flanking regions using oAMK126/143 (3680 bp). The resulting PCR product was ligated to *Eco32I* linearized pME3281 (Q96). AGB1099 was transformed with the resulting plasmid pME4676 giving AGB1107.

Plasmid and strain construction of a *candA-C1~igr~candA-C-gfp* fusion construct

The *candA-C* 3' flanking region was amplified using oAMK232/92 (537 bp). This fragment was ligated to *SwaI* linearized pME4696. oAMK243/228 were used for amplification of 5' flanking region together with *candA-C1* (971 bp), deleting its stop codon. The *igr* was amplified using oAMK229/230 (299 bp). Both fragments were fused using oAMK243/230 (1240 bp). *candA-C* was amplified without its first ATG start codon together with *PP-L-gfp* from pME4652 using oAMK231/EB2 (4022 bp). This fragment was fused to the PCR product of oAMK243/230 giving a product of 5232 bp. This fragment was then ligated to the *PmlI* digested plasmid containing the *candA-C* 3' flanking region. The resulting plasmid was pME4671. AGB1096 was transformed with the *PmeI* digested fragment (10434 bp) resulting in AGB1110 after marker recycling.

Plasmid and strain construction of a *candA-C1~candA-C-gfp* fusion construct

The plasmid backbone and 5' flanking region of *candA-C1* and *candA-C1* were amplified from pME4676 with oAMK298/299 generating a fragment of 7955 bp. *candA-C-PP-L-gfp* (cDNA) was amplified from pME4671 using oAMK03/EB2 resulting in a fragment of 3882 bp. The 3' flanking region of *candA-C* was amplified using oAMK300/92 giving a 537 bp fragment. The oAMK03/EB2 fragment was fused with the oAMK300/92 fragment by PCR using oAMK03/92 resulting in a 4419 bp fusion product. This fragment was then ligated with the oAMK298/299

fragment resulting in pME4682. The plasmid was ectopically integrated into AGB1096 resulting in AGB1187.

Plasmid and strain construction of *candA-C* with Δ ATG

To analyze if *candA-C1* translation is dependent on its predicted start codon, a Δ ATG deletion cassette was designed. The 5' flanking region was amplified using oAMK142/255 (390 bp) and *candA-C1* was amplified without the first ATG using oAMK254/139 (543 bp). Both fragments were fused using oAMK142/139 (971 bp). The 3' flanking region was amplified using oAMK128/143 (269 bp). All fragments were ligated with the *phleo*-RM into linear pUC19 resulting in the plasmid pME4674. AGB552 was transformed with *PmeI* excised cassette (6096 bp) resulting in AGB1108 after marker recycling.

Plasmid and strain construction of *candA-C* NLS deletion strains

The 3' flanking region of *candA-C* was amplified with oAMK232/92 (537 bp) and ligated to *PmlI* linearized pCHS314. The 5' flanking region was amplified together with one part of *candA-C* using oAMK87/276 (1461 bp) and the second half oAMK277/04b (2663 bp). Fusion of both fragments deleted the nuclear localization signal (NLS) sequence and the resulting fragment was ligated to *Swal* linearized vector from the first cloning step resulting in pME4679. The *PmeI* excised cassette (9901 bp) was used for transformation with AGB1103 and AGB1102 and marker recycling resulted in AGB1125 and AGB1127, respectively.

To study *CandA-C* localization without NLS the pME4652 plasmid was amplified with oAMK278/279 (9384 bp), deleting the NLS. Ligation resulted in pME4680. AGB1096 was transformed with *PmeI* cleaved cassette (6717 bp) and pME3173 for observing RFP fluorescence in the nuclei resulting in AGB1124.

Plasmid and strain construction of *A. nidulans* Δ *candA-C1* complementation with *A. fumigatus* *canA* exon 1

To analyze whether *A. fumigatus* *canA*^{exon1} would complement *candA-C1* deletion a complementation cassette was designed. The 5' flanking *candA-C1* was amplified by oAMK142/256 (390 bp) and then fused to the PCR product of oAMK257/253, which is *Af_canA*^{exon1} (596 bp). The 3' flanking region of *candA-C1* was amplified with oAMK128/143 (269 bp). Both fragments were ligated with the *phleo*-RM flipper cassette to linear pUC19 resulting in pME4675. AGB552 was transformed with *PmeI* excised cassette (6149 bp) resulting in AGB1109 after marker recycling.

Plasmid and strain construction of $\Delta csnE$

The 5' flanking region was amplified using AL39/40 (903 bp) and the 3' flanking region with AL47/48 (1295 bp). Ligation of flanking regions with the *phleo*-RM into pUC19 resulted in pME4654. The *PmeI* digested plasmid was a cassette of 7015 bp that was transformed to AGB552 creating AGB1111 after marker recycling. For double deletions with *candA-N* and *candA-C*, as well as a triple deletion with *candA-N/A-C*, AGB1094, AGB1096 and AGB1098 were transformed with the cassette resulting from pME4654 giving strains AGB1112, AGB1113 and AGB1114, respectively.

Plasmid and strain construction of $\Delta denA$

The 5' flanking region was amplified using AL43/44 (1017 bp) and the 3' flanking region with AL45/46 (1115 bp). Ligation of flanking regions with the *nat*-RM into linear pUC19 resulted in pME4717. The *PmeI* digested plasmid resulted in a cassette of 6713 bp and was transformed to AGB552 and AGB1094 creating AGB1177 and AGB1178, respectively after marker recycling.

Plasmid and strain construction of BiFC constructs

Interaction of CandA proteins was studied by bimolecular fluorescence complementation experiments. Therefore, a BiFC cloning plasmid was used (pME4313) with bidirectional nitrate promoter. Either *SwaI* and *PmeI* restriction sites between each promoter and terminator allow insertion of two fragments fused to either *yfp^N*, which expresses the N-terminal half of YFP or fused to *yfp^C* expressing the C-terminal half of YFP.

To generate the preBiFCI cloning plasmid *nedd8* was amplified from wild type cDNA using oAMK166/165 (261 bp) and *yfp^N-L* was amplified from pME3741 with oAMK164/163 (486 bp) introducing a linker (RSIATGAP). Both fragments were fused using oAMK166/163 which resulted in a 731 bp fusion fragment. This fragment was ligated to *SwaI* linearized pME4313 resulting in pME4718.

To generate the preBiFCII plasmid (pME4684) *yfp^N* was amplified from pME3741 with oAMK173/163 (465 bp) and ligated to *SwaI* linearized pME4313 resulting in pME4684.

To generate preBiFCIII cloning plasmid containing *candA-C1-L-yfp^N*, *yfp^N-L* (linker: RSIAT) was amplified using oAMK198/CM108 and *candA-C1* using oAMK197/120. Both fragments were fused using oAMK199/200 for ligation to *SwaI* linearized pME4313 resulting in pME4685.

Plasmid and strain construction of *candA-N*, *candA-C* and *candA-C1* BiFC control plasmids

oAMK168b/169b were used to amplify *yfp^C-L* (linker: RSIATGAP) from pME3741 and oAMK170/02 for *candA-N*. Both fragments were fused (1362 bp). Primers oAMK03b/167 were used to amplify *candA-C-L-yfp^C* (3441 bp) from pME3741. pME4684 was linearized with *PmeI* and used for ligation with *yfp^C-L-candA-N* or *candA-C-L-yfp^C* resulting in pME4662 and pME4663, respectively. *yfp^C* was amplified from pME3741 with oAMK168b/167 and ligated to *PmeI* linearized pME4685 resulting in pME4666. Transformation of AGB1014 with pME4662 resulted in AGB1115, with pME4663 in AGB1116 and with pME4666 resulting in AGB1119. *candA-C1* was amplified with oAMK120/204 producing a fragment of 558 bp. *yfp^C* was amplified with oAMK205/167 from pME3741, which resulted in a fragment of 333 bp. Both fragments were fused by fusion PCR using oAMK120/167 giving a fragment of 861 bp. This fragment was ligated into *Pml* linearized pME4684 resulting in pME4719. AGB1014 was transformed with pME4719 resulting in AGB1189

Plasmid and strain construction of *CandA-C1* BiFC with *CandA-N* or *CandA-C*

For interaction studies of *CandA-C1* with *CandA-N* and *CandA-C*, PCR fragments of oAMK03b/167 (*candA-C-L-yfp^C*) and oAMK168b/02 (*yfp^C-L-candA-N*) were ligated in *PmeI* linearized pME4685 resulting in pME4664 and pME4665, respectively. AGB1014 was transformed with pME4664 resulting in AGB1117 and with pME4665 in resulting in AGB1118. For BiFC experiments in a *csnE* deletion strain AGB1111 was transformed with pME4664 and pME4665 resulting in AGB1120 and AGB1121, respectively.

Plasmid and strain construction of the *nedd8* BiFC control plasmid

yfp^C was amplified from pME3741 with oAMK168b/167 and ligated to *PmeI* linearized pME4781 resulting in pME4660, which was transformed to AGB1014 giving AGB1180. For BiFC interaction studies of *Nedd8* in a *csnE* deletion background AGB1111 was transformed with pME4660 resulting in AGB1184.

Plasmid and strain construction of *Nedd8* BiFC with *CandA-N*, *CandA-C1* and *CandA-C*

For interaction studies of *Nedd8* with *CandA-N*, *CandA-C1* and *CandA-C*, *PmeI* linearized pME4718 was ligated with PCR fragments of oAMK168b/02 (*yfp^C-L-candA-N*), oAMK120/167 (*candA-C1-L-yfp^C*) and oAMK03b/167 (*candA-C-L-yfp^C*) resulting in pME4661, pME4667 and

pME4659, respectively. AGB1014 was transformed with pME4661 giving AGB1181, with pME4667 giving AGB1182 and with pME4659 giving AGB1179.

For BiFC interaction studies of Nedd8 with CandA proteins in a *csnE* deletion background AGB1111 was transformed with pME4661 giving AGB1185, with pME4667 giving AGB1186 and with pME4659 giving 1183.

2.6.4 Plasmid and strain construction of *A. fumigatus* mutant strains

Plasmid and strain construction of *A. fumigatus canA*^{Δ*exon1*} complementation with *A. nidulans candA-C1*

For complementing *canA*^{Δ*exon1*} with *A. nidulans candA-C1* the 5' flanking region of *canA* was amplified with oAMK247/262 (2147 bp) and fused to *candA-C1*, amplified with oAMK252/139 (576 bp). The resulting fragment (2693 bp) was ligated with 3' flanking region (oAMK249/250) and *ptrA*-RM to pUC19 resulting in pME4673. AfS35 was transformed with the *PmeI* excised cassette (10360 bp) resulting in AfGB142 after recycling the marker.

Plasmid and strain construction of a *canA*^{Δ*exon1*} deletion

The 5' flanking region was amplified using oAMK247/248 (2147 bp) and the 3' flanking region of *canA*^{Δ*exon1*} using oAMK249/250 (2429 bp). Both fragments were ligated with the *ptrA*-RM into linear pUC19 resulting in pME4672. AfS35 was transformed with the *PmeI* excised cassette (9814 bp) resulting in AfGB140 after recycling the marker.

Plasmid and strain construction of Δ*canA*

For full gene deletion of *canA* the 3' flanking region was amplified with oAMK267/268 (781 bp) and ligated to *PmlI* linearized pCHS314. The plasmid was re-linearized with *SwaI* and ligated with the 5' flanking region of *canA*, which was amplified with oAMK273/274 (2147 bp). The resulting plasmid pME4677 was cleaved with *PmeI* and the cassette (8168 bp) was used for transformation with AfS35 resulting in AfGB141 after marker recycling.

Plasmid and strain construction of Δ*canA-N*

The 3' flanking region was amplified by oAMK286/283 (945 bp), which was ligated to *PmlI* linearized pCHS314. This plasmid was linearized with *SwaI* for ligation with the 5' flanking

region, which was amplified using oAMK290/291 (1492 bp) resulting in pME4681. AfS35 was transformed with the *PmeI* digested cassette (7692 bp) resulting in AfGB144 after marker recycling.

Plasmid and strain construction of *canA*^{Δ838-4078}

To delete only the *canA* base pairs 838-4078 which are homolog to *A. nidulans candA-C*, the 5' flanking region was amplified with oAMK295/296 (1203 bp) and ligated to the *SwaI* linearized plasmid containing the 3' flanking region (oAMK267/268) resulting in pME4683. AfS35 and AfGB144 were transformed with *PmeI* digested cassette (7254 bp) resulting in AfGB145 and AfGB146, respectively after marker recycling.

Plasmid and strain construction of CanA-GFP fusion construct

The 5' flanking region of *canA* was amplified together with *canA* using oAMK269/270 (4595 bp). The PP-L-*gfp* fragment was amplified from pME4652 using oAMK82/271 (773 bp) and then both fragments were ligated to *SwaI* linearized plasmid containing the 3' flanking region of *canA*. The generated plasmid pME4678 was digested with *PmeI* and the cassette (11374 bp) was used for transformation with AfS35, which resulted in AfGB143 after marker recycling.

2.6.5 Plasmid construction for protein expression in *E. coli*

Plasmid and strain construction of GST-CandA-N

candA-N was amplified from wild type cDNA using oAMK21/22 introducing an *EcoRI* and a *SaII* restriction site, respectively. pGEX-6P-1 and the oAMK21/22 fragment were digested with *EcoRI* and *SaII* and then ligated. Rosetta II were transformed with the resulting plasmid pME4721.

Plasmid and strain construction of GST-CandA-N

candA-C was amplified from wild type cDNA using oAMK23/24 introducing an *EcoRI* and a *NotI* restriction site, respectively. pGEX-6P-1 and the oAMK21/22 fragment were digested with *EcoRI* and *NotI* and then ligated. Rosetta II were transformed with the resulting plasmid pME4720.

2.7 Genetic manipulation of microorganisms

2.7.1 Transformation of *E. coli*

Transformation of *E. coli* was performed as described by Inoue *et al.*, 1990; Hanahan *et al.*, 1991. Chemical competent *E. coli* were incubated with plasmid DNA for 30 min on ice. Then a heat shock at 42°C for 60 seconds was performed. Afterwards, the *E. coli* cells were chilled on ice for one to two minutes. 800 µl LB was added and the cells were incubated under constant agitation for up to one hour at 37°C. The cells were centrifuged, resuspended in ~150 µl remaining medium and inoculated on solid LB plates, which were supplemented with ampicillin (1:1000 v/v) or for *Rosetta II* with *chloramphenicol* (1:1000 v/v). The plates were incubated over night and the clones were tested by colony PCR concerning plasmid uptake.

2.7.2 Transformation of *A. nidulans* and *A. fumigatus*

Transformation of *A. nidulans* and *A. fumigatus* was performed according to the polyethylene glycol-mediated protoplast fusion method (Punt and van den Hondel, 1992). AGB552, AGB551 and their derivatives served as transformation hosts for *A. nidulans* mutant strains and AfS35 for *A. fumigatus* mutant strains. These wild type strains have a $\Delta nkuA$ and $\Delta akuA$ mutation, respectively. Loss of these orthologous genes increases homologous recombination during the transformation (Krappmann *et al.*, 2006; Nayak *et al.*, 2006). The appropriate *Aspergillus* strains were grown overnight in submerged cultures at 37°C with agitation. All working steps were conducted under sterile conditions. The mycelium was filtered through a sterile miracloth (Calbiochem, Merck, D) and washed with citrate buffer (150 mM potassium chloride, 580 mM NaCl, 50 mM natrium citrate). The mycelium was transferred to a sterile flask without chicane and carefully mixed with filter-sterilized 30 mg/ml Vinoflow[®] Max or Vinotaste[®] Pro (NOVOZYMES, Bagsvaerd, Denmark) and 15 mg/ml lysozyme (SERVA, only added to transformations with *A. nidulans*). The mycel-enzyme mix was incubated at 30°C for 100-120 min to dissolve the cell wall leaving protoplasts. The protoplasts were filtered through a sterile miracloth filter into a pre-cooled 50 ml falcon that was then filled up with cold STC buffer (1.2 M Sorbitol, 0.1 M Tris-HCl pH 7.0, 10 MM CaCl₂). The protoplasts were centrifuged twice for 15 min at 2 500 rpm and 4°C, the supernatant was discarded in between, and the protoplasts were resuspended in the remaining buffer. The protoplasts were then distributed to two 15 ml falcon tubes. One of the tubes was mixed with at least 10 µg of the DNA cloning cassettes or of whole plasmid DNA in case of ectopic integration. The other tube served as control. This mixture was incubated in ice for 25 min. Then 1.35 ml polyethyleneglycol (PEG)

solution (10 mM Tris pH 7.5, 50 mM CaCl₂, 60 % (v/v) PEG4000) was added successively followed by incubation above ice for 20 min. The mixture was centrifuged again and the protoplasts were resuspended in the remaining buffer. Selective MM (pyrithiamine 1:1000, nourseothricin 0.7:1000, phleomycin 1:1000) containing 1.2 M sorbitol was inoculated with different amounts of protoplasts mixed with top agar (0.7 % agar, 1 % glucose, 1.2 M sorbitol). The transformation plates were incubated at 37°C for several days. The clones were individualized on selective MM plates and then verified by a Southern hybridization. The positive clones were cultivated on MM xylose/glucose, which contained instead of 1 % (w/v) glucose 0.5 % (w/v) xylose and 0.5 % (w/v) glucose for the recycling of the self-excising marker cassette. Successful recycling was analyzed by Southern hybridization.

2.8 Southern hybridization

Southern hybridization was used to confirm successful mutagenesis of target genes (Southern, 1975). Restriction enzymes (THERMO FISHER SCIENTIFIC) were selected to highlight specific sequences of interest, which were compared to wild type or the transformation host strain. At least one restriction site was outside of the integrated construct to confirm *in-locus* integration. Genomic DNA (for extraction protocol see chapter 2.5.1) was digested overnight and separated by agarose gel electrophoresis. The gels were washed for 10 min in wash buffer 1 (0.25 M HCl), followed by washing with buffer 2 for denaturation (0.5 M NaOH, 1.5 M NaCl) for 25 min and 30 min in buffer 3 (0.5 M Tris, 1.5 M NaCl, pH 7.4) for neutralizing. All washing steps were performed under agitation at room temperature. DNA was transferred onto Amersham™ Hybond™-Nylon membranes (GE HEALTHCARE) by dry blotting for 2 h at room temperature. The membranes were baked at 75°C for 10 min and then the DNA was cross-linked to the membrane by exposure to UV light ($\lambda = 254$ nm) for 3 min per side of the membrane. Pre-hybridization of the membranes was performed with hybridization solution from the Amersham™ Gene Images AlkPhos Direct Labelling and Detection System (GE HEALTHCARE, prepared after manufacturer's instructions) for 30 min at 55°C in a HERA hybrid R hybridization oven (HERAEUS INSTRUMENTS). Then the probe was added for overnight incubation in the oven. Membranes were washed twice with post-hybridization buffer I (1 mM MgCl₂, 3.5 mM SDS, 50 mM sodium phosphate buffer, 150 mM NaCl, 2 M Urea, 0.2% (w/v) blocking reagents) for 10 min at 55°C and twice with post-hybridization buffer II (2 mM MgCl₂, 50 mM Tris, 100 mM NaCl, pH 10) for 5 min at room temperature under constant agitation. DNA detection was then performed with CDP-Star (GE HEALTHCARE), which was applied to the membranes, and then exposed to Amersham™ Hyperfilm™ ECL (GE HEALTHCARE).

2.9 Protein methods

2.9.1 Protein extraction from *A. nidulans*

Protein crude extracts for western hybridization or pull-down experiments were obtained from liquid cultures grown at 37°C for 20 hours in MM paba (for *A. nidulans*) or in modified MM (for *A. fumigatus*). Mycelium was frozen in liquid nitrogen and then ground by mortar and pestle or using a Mixer Mill MM 400 (RETSCH). The mycelium was mixed with B* buffer (300 mM NaCl, 10 mM Tris pH 7.5, 0.5 mM EDTA, 10% (v/v) Glycerol, 0.02% (v/v) NP40), freshly supplemented with 1 mM PMSF, 2 mM DTT and 10 µl/ml (v/v) Protease inhibitor cocktail mix (ROCHE) (stock solution: 1.5 tablets in 1 ml B* buffer). The wet mycelium was mixed. For western hybridization, crude extracts were centrifuged for 30 min at 4°C and 13 000 rpm. The supernatant was transferred to a new test tube and centrifuged again. The protein concentration was determined with Nanodrop ND-1000 photo spectrometer from PEQLAB.

2.9.2 *In vitro* protein pull-down

Mycelia for pull-down experiments was obtained from 1 l submerged cultures inoculated with 2×10^9 spores for 20 hours at 37°C on a rotary shaker. The crude extracts were prepared as described in 2.9.1. The B* buffer mixed mycelium was centrifuged for 1 hour at 4°C and 15 000 rpm in a Sorvall RC-5B Plus superspeed centrifuge (GMI). The supernatant was filtered through miracloth (MILLIPORE) into a polyprep column (BIORAD) containing 80 µL GFP-Trap® beads (CHROMOTEK) pre-equilibrated with B* buffer. After incubation of the supernatant with GFP beads on a rotary shaker for 2 hours at 4°C the beads were washed with 6 ml washing buffer W300 (300 mM NaCl, 10 mM Tris pH 7.5, 0.5 mM EDTA) and W500 (500 mM NaCl, 10 mM Tris pH 7.5, 0.5 mM EDTA). Elution of GFP-trap beads bound proteins was performed three times by adding 0.2 mM glycine pH 2.5 for 25 seconds and then neutralization with 1 M Tris pH 10.4. Elution samples were mixed with protein sample buffer (250 mM Tris-HCl pH 6.8, 15% (v/v) 2-Mercaptoethanol, 30% (v/v) Glycerol, 7% (w/v) SDS, 0.3% (w/v) Bromphenolblue) and then boiled at 95°C for 5 min for SDS page analysis.

8 M urea was added to all buffers used for pulldowns performed with GFP-Nedd8 (AGB1176) and the control strain AGB596 under denaturing conditions to select for covalent Nedd8 binding partners.

2.9.3 SDS-PAGE

Proteins were separated according to their molecular weight by sodium dodecyl sulfate polyacrylamide gel electrophoresis (SDS-PAGE) (Smith, 1984). SDS supplements proteins with negative charges, correlating to their molecular weight. This allows the proteins to migrate through an electric field, which is applied across the gel, from the negative electrode (cathode) towards the positive electrode (the anode). Each protein runs differently depending on its size whereas small molecules can fit easier through the gel pores than larger ones. Proteins were mixed with protein sample buffer (250 mM Tris-HCl pH 6.8, 15% (v/v) 2-Mercaptoethanol, 30% (v/v) Glycerol, 7% (w/v) SDS, 0.3% (w/v) Bromphenolblue) and boiled at 95°C for 5 min.

SDS PAGE was performed with 12 % acrylamide gels (resolving gel: 2.5 ml 2 x resolving buffer (1 M Tris-HCl pH 8.8, 10 % SDS), 2 ml 30 % acryl amide, 0.5 ml H₂O, 75 µl 10 % APS, 7.5 µl TEMED; stacking gel: 1 ml 2x stacking buffer (1 M Tris-HCl pH 6.8, 10 % SDS), 0.25 ml 30 % acryl amide, 0.75 ml H₂O, 30 µl 10 % APS, 3.75 µl TEMED). SDS PAGE was performed in SDS running buffer (25 mM Tris, 0.25 M Glycine, 0.1 % SDS) at 200 V. Gels were either stained or prepared for western hybridization. For detailed protocol of SDS PAGE and western hybridization see also (Köhler *et al.*, 2016). For staining the SDS gels, the gel was incubated in fixation solution (40 % ethanol, 10% acetic acid) for one hour prior to colloidal Coomassie staining (0.1 % (w/v) Coomassie Brilliant Blue G250, 5 % (w/v) aluminum sulfate-14-18-hydrate, 10 % (v/v) methanol, 2 % (v/v) ortho-phosphoric acid) over night.

2.9.4 Western hybridization

Western blot hybridization was performed by wet electroblotting in transfer buffer (25mM Tris, 192mM glycine, 10% methanol, 0.5 % SDS) to an Amersham™ Protran™ 0.45 µm NC nitrocellulose membranes (GE HEALTHCARE) overnight at room temperature or for 1 hour with cooled buffers. The membrane was stained with ponceau solution (0.2 % Ponceau S, 3 % TCA) which served as loading control. The membrane was blocked in blocking solution (5 % (w/v) milk powder (Sucofin skimmed milk powder, TSI GmbH), TBST buffer (Tris-Buffered Saline Tween 20: 100 mM Tris-HCl pH 8.0, 1.5 M NaCl, 0.5 % Tween-20) for 1 hour. Primary antibodies (α-GFP (B-2: sc-9996, SANTA CRUZ), α-CulA, α-Nedd8 (both GENESCRIP), α-Ubiquitin 05-944 (MERCK), α-tubulin antibody T0926 (SIGMA-ALDRICH), were incubated one hour to overnight. After washing the membrane three times with TBST buffer for 10 min, the membrane was incubated with the respective secondary antibody (α-goat mouse (115-035-003, JACKSON IMMUNO RESEARCH) or α-goat rabbit (G21234, INVITROGEN). The membrane was washed again three times 10 min with TBST buffer. Detection was performed by incubating the membrane with detection solutions A and B (solution A: 2.5 mM luminol,

0.4 mM paracoumarat, 100 mM Tris pH 8.5; solution B: 5.4 mM H₂O₂, 100 mM Tris pH 8.5) for two minutes. Signals were detected with Fusion System (PEQLAB). Pixel densities of signals were measured with *BIO1D Software* (PEQLAB). Membranes were striped in 0.2 mM NaOH for 8 min. Signals were quantified against the loading control (tubulin, actin or ponceau) and wild type served as control. Error bars display the standard error of the mean (SEM) and the significance was determined using the Oneway Anova test from *SISA* (Simple Interactive Statistical Analysis) tool (<http://www.quantitativeskills.com/sisa/statistics/oneway.htm>).

The *in vitro* deneddylation assay protocol is published in (Köhler *et al.*, 2016).

2.9.5 Heterologous protein overexpression in *E. coli* and purification

Recombinant proteins of *Aspergillus nidulans* were transgenically overexpressed in *E. coli* using the IPTG induction system. LB pre-cultures, supplemented with ampicillin and chloramphenicol (both 1:1000) were inoculated with 5 µL of a glycerol stock containing transformed *E. coli* Rosetta II cells carrying plasmids pME4720 or pME4721. Cultures were incubated overnight at 37°C on a rotary shaker. The pre-cultures were used to inoculate the expression cultures. 1 L LB was incubated at 37°C and 220 rpm for 2-3 hours until the OD₆₀₀ of 0.6-0.8 was reached. Protein expression was induced by adding 1 mM IPTG (1:1000 v/v) (Roth, Karlsruhe, D). Proteins were overexpressed at 20°C at 180 rpm for 20 hours. Before harvesting the cultures, an “induction” sample was collected to analyze overexpression by SDS PAGE. Cells were collected by centrifugation at 4 000 rpm for 30 min and 4°C. The supernatant was discarded, and the pellets were resuspended in ice cold buffer A (50 mM Tris pH 8.0, 500 mM NaCl). The resuspended *E. coli* cells were transferred into 50 mL Falcon tubes (SARSTEDT) and centrifuged at 4 000 rpm for 30 min at 4°C. Again, the supernatant was discarded, and the pellet was stored at -80°C until further usage.

2.9.6 Lysis of *E. coli* cell material

To get access to recombinant overexpressed proteins, the cells must be destroyed. This process is called cell lysis. A cell pellet was first thawed on ice and then resuspended in three-times the amount (v/v) of lysis buffer (500 mM NaCl, 50 mM Tris pH 8.0, 10 mM PMSF, 1:10 (v/v)) compared to the volume of cell pellet. Subsequently, the cells were destroyed by pouring the suspension 4-5 times through the Fluidizer (Microfluidics, Westwood, USA). A Fluidizer uses high pressure (80 psi), which produces strong mechanical forces whereby the *E. coli* cells

burst. Afterwards the cell suspension was centrifuged at 20 000 rpm, 4°C for 30 min to separate the protein (in the supernatant) from cell material (pellet).

2.9.7 Affinity purification via GSTrap

Chromatography purification steps were performed with a manual pump or Äkta Explorer 10 purification system (GE HEALTHCARE) at 4°C. Columns were washed with three column volumes ddH₂O followed by equilibration with the respective buffer. All buffers, ddH₂O and 20 % ethanol were filtered and degassed (SARTORIUS, Göttingen, D).

The affinity chromatography column GSTrap FF (GE HEALTHCARE) was equilibrated with three column volumes of Buffer A (500 mM NaCl, 50 mM Tris pH 8.0) to immobilize the GST (Glutathione-S-Transferase)-tagged protein of interest to the column glutathione Sepharose[®] matrix during affinity purification. After loading the protein to the column with a manual pump (GE HEALTHCARE), the column was connected to the Äkta system. The target protein can be eluted by washing the column in a gradient of 0-50 % elution buffer B (500 mM NaCl, 50 mM Tris pH 8.0, 20 mM glutathione). Afterwards the columns were recovered with 100 % Buffer B and then washed with three column volumes ddH₂O and with 20 % ethanol for storage.

2.9.8 Dialysis and GST-tag cleavage

Dialysis was used to exchange buffer conditions of a protein sample. Dialysis is based on the exchange of small particles by passive diffusion through a semi-permeable membrane (Lee, 2017). The protein sample was transferred into a pretreated dialysis tube (Serva, Heidelberg, D). The dialysis was performed overnight at 4°C in 5 L Dialysis Buffer (120 mM NaCl, 20 mM Tris pH 8.0, 1 mM EDTA, 1 mM DTT, 5 % glycerol). During dialysis the GST-tag was cleaved off by adding 150 µM per ml sample (w/v) PreScission Protease (E. Beckmann, p.c.). The free GST was washed out by another affinity purification. The sample was concentrated with Amicons (MERCK) (10 kDa molecular weight cut off (MWCO) for CandA-N and 50 kDa MWCO for CandA-C).

2.9.9 Size-exclusion chromatography

Proteins were separated according to molecular weight by size-exclusion chromatography (SEC), also known as gel filtration chromatography. Proteins with a high molecular weight are passing faster through the bead matrix than low molecular weight proteins. Therefore, this

method can be of use to separate mono- or polymeric forms of the target protein. HiPrep Sephacryl S-300 16/60 HR (GE HEALTHCARE) was equilibrated with three volumes of size exclusion buffer (120 mM NaCl, 20 mM Tris pH 8.0, 1 mM EDTA, 1 mM DTT, 5 % glycerol). The protein sample was centrifuged for 10 min at 13 000 rpm at 4°C and up to 5 ml of the supernatant was injected via 2 or 5 ml sample loops or 50 ml super loop (GE HEALTHCARE). Samples of peak fractions were analyzed by SDS PAGE. The theoretical protein molecular weight was calculated from calibration curves, derived from standard proteins with known elution volume according to manufactures instructions.

2.10 Microscopy

Strain morphology was analyzed using a stereo microscope SZX12 (OLYMPUS, Hamburg, Germany) and Axiolab light microscope (ZEISS). For fluorescence microscopy 300 ml MM (supplemented as desired by strains) was inoculated with 500 spores per well in an 8 well microscopy chamber (IBIDI, Martinsried, Germany) for 18-24 hours at 37°C. Microscopy was performed using a confocal Zeiss Observer Z1 microscope (ZEISS) including a CSU-X1 A1 confocal scanner unit (YOKOGAWA, Ratingen, Germany), QuantEM:512SC digital camera (PHOTOMETRICS, Tucson, AZ, USA) and *SlideBook 6.0* software package (INTELLIGENT IMAGING INNOVATIONS, Göttingen, Germany). Pictures were taken with Plan-Neofluar 100x/1.4 oil objective (ZEISS). 100 ms exposure was used for GFP and BiFC signals and 50-100 ms exposure time for RFP signals. Nuclei were visualized with ectopically integrated *rfp:h2A* or stained with 0.1 % (v/v) 4',6-diamidino-2-phenylindole (DAPI) and observed with 50 ms exposure time. Mitochondria were stained with 50 nM MitoTracker® Red (INVITROGEN).

2.11 Secondary metabolite extraction

Secondary metabolite extraction was performed as described previously by (Gerke *et al.*, 2012). MM paba plates were inoculated with 500 µl of 2×10^6 spores/ml and incubated at 37°C and light for 7 days. Spores and mycelia were removed from the plates to extract extracellular secondary metabolites from the agar. The agar was cut into pieces and incubated with 200 ml ethyl acetate for 30 min at 150 rpm and 25°C. Then the solution was incubated in an ultrasonic bath Bandelin Sonorex™ Digital 10P from BANDELIN ELECTRONIC GMBH & CO.KG

(Berlin, Germany) at highest level for 20 min. The liquid was filtered through miracloth into round bottom flasks and the extraction from the agar pieces with ethyl acetate was repeated. The solvent was evaporated. For high-performance liquid chromatography (HPLC) measurements the metabolites were dissolved in 750 μ l methanol and centrifuged to remove particles. Analytical HPLC/UV-DAD/ELSD measurements were performed by Dr. Jennifer Gerke (Department of Molecular Microbiology and Genetics, Georg-August University Göttingen, Germany) using the following system: HPLC pump 420, SA 360 autosampler, Celeno UV-DAD HPLC detector, ELSD-Sedex 85 evaporative light-scattering detector (ERC)) with a Nucleodur 100-5 C18 end-capped (ec) column (250 mm x 3 mm) and the solvent system: A = H₂O + 0.1% (v/v) trifluoroacetic acid (TFA), B = acetonitrile + 0.1% (v/v) TFA (from GOEBEL INSTRUMENTELLE ANALYTIK GMBH, Au/Hallertau, Germany). 20 μ l of the dissolved metabolites were analyzed under gradient conditions (20% B to 100% B in 20 minutes) with a flow rate of 0.5 ml/min. HPLC data was analyzed with the Geminix III software from GOEBEL INSTRUMENTELLE ANALYTIK GMBH (Au/Hallertau, Germany).

2.12 Bottom-up protein analysis with mass spectrometry after pull-down experiments

2.12.1 *In-gel* digest of proteins with trypsin

For the analysis of proteins with LC-MS, samples were subjected to SDS-PAGE and only short-term separated within the resolving gel. The gel was stained as described in chapter 2.9.3. The gel was cut into pieces of approximately 2 mm² in size, and transferred to *Protein LoBind* tubes (EPPENDORF, Hamburg, Germany) for *in-gel* digestion with trypsin according to the protocol of Shevchenko *et al.*, 1996. The gel pieces were covered with acetonitrile and incubated at room temperature for 10 min with agitation. The acetonitrile was then removed, and the gel pieces were dried using the SpeedVac (Savant SPD 111V, THERMO SCIENTIFIC) for 10 min at 55°C. Afterwards, the gel pieces were incubated with 150 μ l 10 mM DTT solved in 100 mM ammonium bicarbonate (NH₄HCO₃) for 1 h at 56°C on a heating block (LIEBISCH, Bielefeld, Germany). After removal of the DTT solution 150 μ l of a 55 mM iodoacetamide solution was added for cysteine alkylation at room temperature for 1 h in the dark. The iodoacetamide solution was then replaced by 150 μ l of a 100 mM NH₄HCO₃ solution for another 10 min of incubation at room temperature. 150 μ l of acetonitrile were added for another 10 min of incubation and subsequently removed. The steps with ammonium bicarbonate and acetonitrile were repeated one more time and the supernatants removed after every incubation step. The gel pieces were then dried in the SpeedVac for 10 min at 55°C and the trypsin

(SERVA) solution was added for an incubation period of 45 min on ice. The supernatant was discarded, and the pieces were incubated in 30 μ l 25 mM NH_4HCO_3 at 37°C over-night. At the next day, the supernatants of all following steps were collected in a *Protein LoBind* tube. The gel pieces were covered with 20 mM NH_4HCO_3 and incubated for 10 min at room temperature with agitation to preferentially extract acidic peptides. Afterwards, the gel pieces were incubated with a 50 % acetonitrile, 5 % formic acid solution for 20 min at room temperature and with agitation. This step was repeated three times and after each incubation step the samples were centrifuged for 1 min at 13.000 rpm to separate and collect the supernatant within the collection tubes. Finally, the collected supernatants were dried completely in the SpeedVac. The dried samples were stored at room temperature until further processing or immediately resolved in a resuspension buffer (98 % H_2O , 2% (v/v) acetonitrile, 0.1 % (v/v) formic acid) for the following *StageTip* protocol.

2.12.2 Sample clean-up of peptide samples with *C18 StageTips*

Prior to LC-MS analysis, dried peptide pellets were resolved in (2% acetonitrile 0.1% formic acid) and purified to remove salts and hydrophobic organic components by employing the *C18 StageTip* method (Rappsilber *et al.*, 2007). For all steps vinyl gloves and *Protein LoBind* tubes (EPPENDORF) were used. For preparation of reverse-phase *C18 StageTips*, 200 μ L pipette tips were stuffed with two plugs of *C18* material. *StageTips* were equilibrated with 100 μ l 0.1 % (v/v) formic acid in HPLC grade methanol, followed by 100 μ l 0.1 % (v/v) formic acid in 70 % (v/v) acetonitrile and 100 μ l 0.1 % (v/v) formic acid in dH_2O . This step was repeated once. The resolved peptides were loaded onto the equilibrated *StageTips* and centrifuged at 3.500 rpm for 5 min. The flow-through was re-loaded and the bound peptides washed twice with 100 μ L 0.1 % (v/v) formic acid through centrifugation at 10.000 rpm for 2 min. Peptides were eluted with 60 μ L elution buffer (70 % (v/v) acetonitrile, 0.1 % (v/v) formic acid) through 5 min of incubation followed by centrifugation at 4.000 rpm. The eluate was subsequently dried completely in a SpeedVac at 50°C. Finally, peptides were resolved in 20 μ l sample buffer (2% acetonitrile 0.1% formic acid) within an ultrasonic bath at maximum power for 3 min at 35°C.

2.12.3 Peptide analysis with LC-MS

Peptide samples were analyzed with mass spectrometry coupled to liquid chromatography (LC-MS). Therefore, an Orbitrap Velos ProTM mass spectrometer and an Ultimate 3000TM liquid chromatography system (both THERMO FISHER SCIENTIFIC) were used. Peptides were separated at nano-flow rates (300 nl/min) using Acclaim PepMap RSLCTM columns (THERMO

FISHER SCIENTIFIC) through the application of a water-acetonitrile gradient. Chromatographically separated peptides were on-line ionized by an electrospray (nESI) using the Nanospray Flex Ion Source™ (THERMO FISHER SCIENTIFIC) at 2.4 kV, and continuously transferred into the mass spectrometer. Full scans within the mass range of 300-1850 were recorded with the Orbitrap-FT analyzer at a resolution of 30,000. In parallel data-dependent top-ten fragmentation spectra (MS2) were acquired by collision-induced dissociation (CID) in the LTQ Velos Pro™ linear ion trap. The *XCalibur 2.2™* software (THERMO FISHER SCIENTIFIC) was applied for LC-MS method programming and data acquisition. MS/MS2 data processing for protein analysis and identification was carried out with the *MaxQuant (Version)* software and *Perseus 1.6.1.1* software (Cox and Mann, 2008; Tyanova *et al.*, 2016) or the *Proteome Discoverer 1.4™* software (THERMO FISHER SCIENTIFIC) employing the *SequestHT™* and *Mascot™* search engines. As protein database an *A. nidulans*- and an *A. fumigatus*-specific database with common contaminants were used.

Peptides of 1 µl sample solution were loaded with 0.07% TFA on an Acclaim® PepMap 100 pre-column (100 µm x 2 cm, C18, 3 µm, 100 Å, Thermo Scientific) at a flow rate of 20 µl/min for 3 min. Analytical peptide separation by reverse phase chromatography was performed at a flow rate of 300 nl/min on an Acclaim® PepMap RSLC column (75 µm x 50 cm, C18, 3 µm, 100 Å, Thermo Scientific). A gradient from 98% solvent A (0.1% formic acid) and 2% solvent B (80% acetonitrile, 0.1% formic acid) to 55% B was applied within 30 min and was followed by 90% B for 4 min (Optima® LC-MS solvents and acids were purchased from Fisher Chemical). Nano ESI mass spectrometry – Q Exactive HF (Thermo Scientific): Chromatographically eluting peptides were on-line ionized by nano-electrospray (nESI) using the Nanospray Flex Ion Source (Thermo Scientific) at 1.5 kV (liquid junction) and continuously transferred into the mass spectrometer. Full scans within the mass range of 300-1,800 m/z were taken from the Orbitrap-FT analyzer at a resolution of 30,000 with parallel data-dependent top 10 MS2-fragmentation (HCD). The resolution was set to 60,000 for tSIM scans and to 15,000 for dd-MS2 scans. The maximum ion time was 100 ms for tSIM scans (AGC target 1e6) and 2,000 ms for dd-MS2 (AGC target 1e5). The loop count equaled the number of m/z values on the inclusion list. LCMS method programming and data acquisition was performed with the software *XCalibur 4.0* (Thermo Scientific).

3 Results

3.1 Organization of *canA/canda* genes in Aspergilli

3.1.1 *A. fumigatus* carries an N-terminal extension of the CanA protein

Cand1/A serves as substrate-receptor exchange factor for cullin-RING ligases and is conserved in eukaryotes (Helmstaedt *et al.*, 2011). Cand1 is encoded as a single gene in higher eukaryotes. In contrast, *Aspergillus* spp. possess at least two genes encoding two subunits like in *A. nidulans* CandA-N (1055 bp, 313 aa, 33 kDa) and CandA-C (3254 bp, 1041 aa, 114 kDa) (Figure 14) (Helmstaedt *et al.*, 2011). The CandA-N subunit corresponds to the N-terminal domain and the CandA-C subunit to the middle and C-terminal parts of monomeric Cand1 from higher eukaryotes (Helmstaedt *et al.*, 2011). This split CandA protein was exclusively found in *Aspergillus* spp. and other fungi like *Verticillium dahliae* have a monomeric Cand1 protein as reported for higher eukaryotes.

CandA-C is the orthologous protein to *A. fumigatus* CanA (4078 bp, 1240 aa, 135 kDa) and BLAST (Basic Local Alignment Search Tool) search analysis revealed that CandA-N of *A. nidulans* corresponds in *A. fumigatus* to Afu6g10440 that was named CanA-N (973 bp, 304 aa, 33 kDa). Both N-terminal orthologs share 77% identity on protein level and have an Armadillo-type fold, which is typically found in HEAT repeat proteins (Fournier *et al.*, 2013; Gul *et al.*, 2017). The C-terminal subunit of *A. nidulans* consists of the same Armadillo-type fold and has a monopartite nuclear localization signal (NLS) sequences (RKRRR) in the N-terminal region. A TATA-box binding domain was predicted for the C-terminal end. The same features could be identified also for *A. fumigatus* CanA, but it has an N-terminal extension (NTE).

BLAST search and protein alignments revealed, that the additional sequence corresponds to the *A. nidulans* gene AN12234 (546 bp, 181 aa, 19 kDa), which is located only 269 bp upstream of *candA-C* and was not considered to encode a CandA subunit so far. The AN12234 gene product was named CandA-C1 (Figure 14). It has an N-terminal RNase P Rpr2/Rpp21 domain motif and its C-terminus is predicted to be disordered. The same features could be identified for the corresponding *A. fumigatus* CanA NTE, indicating that *A. fumigatus* CanA consists of two proteins, whereas *A. nidulans* has three CandA subunits.

This genome comparison suggests that *A. fumigatus* CanA corresponds to a fusion protein of orthologous sequences to two *A. nidulans* separately encoded CandA-C1 and CandA-C proteins. The *intergenic region (igr)* between these genes of *A. nidulans* includes the presumed promoter and terminator signals of transcription and corresponds to an intron in the fused genes of *A. fumigatus*. The initial examined question was whether an *A. nidulans* three-subunit

and an *A. fumigatus* two-subunit CandA complex encoded by three or two genes could be verified.

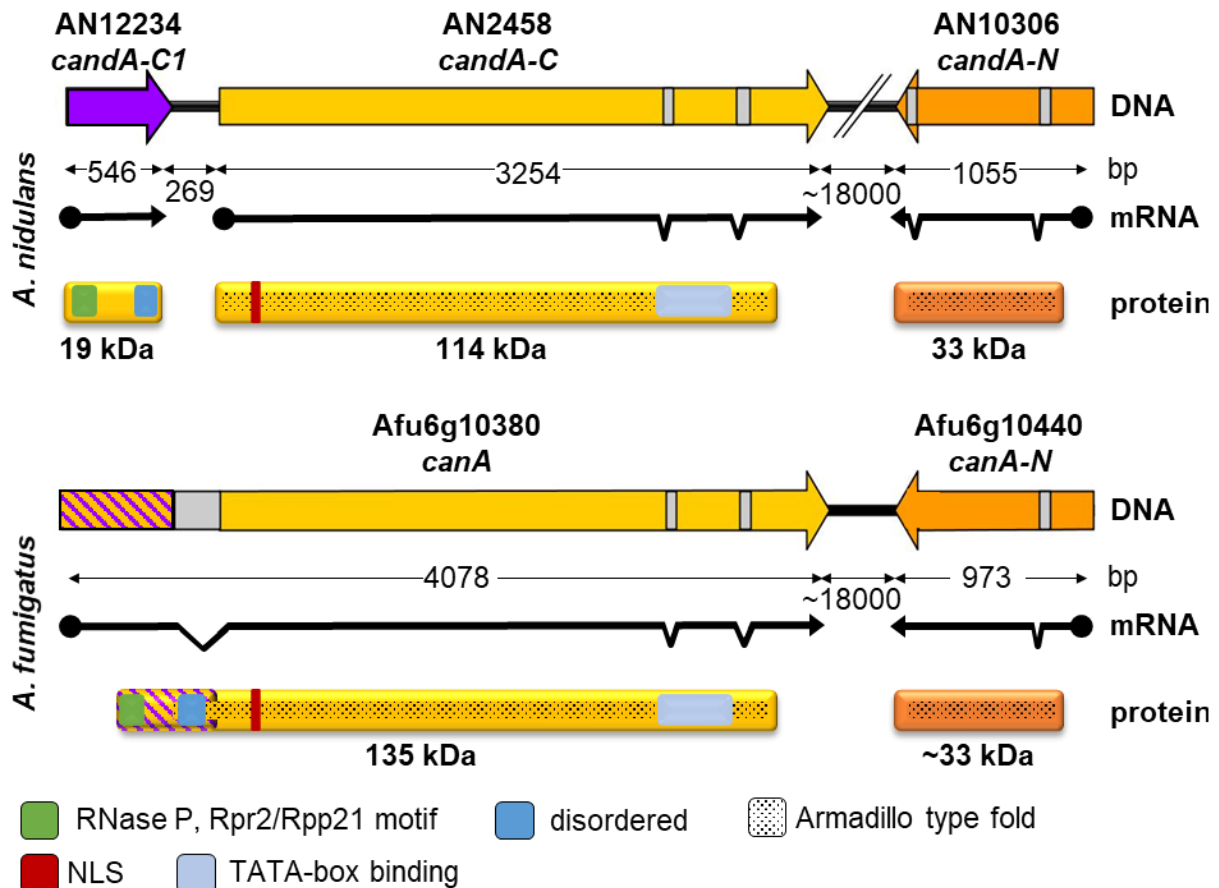


Figure 14. *A. nidulans* CandA has three genes coding for three subunits and *A. fumigatus* CanA has two genes coding for two CanA proteins. *A. nidulans candA-C1* and *candA-C* correspond to a fused *A. fumigatus canA*; *A. nidulans candA-N* corresponds to *A. fumigatus canA-N*. CandA-C1 and the N-terminus of CanA (striped) are predicted to share a Rpr2/Rpp21 subunit motif (green box), which is found in the protein complex RNase P, a protein complex involved in RNA binding and modification. The C-terminal end of CandA-C1 and the corresponding sequence of CanA are predicted as disordered (blue box). Both CandA and CanA show an Armadillo-type fold (dotted box) and TATA-box binding protein domain (light blue box). CandA-C and CanA have an NLS (RKRRR) (red box). Introns are indicated as grey boxes in the DNA. *A. fumigatus canA-N* has only one intron, different than its ortholog *candA-N*. Length of genes is indicated in base pairs (bp) and molecular weight of proteins in kDa. Motif prediction is based on InterPro Scan search (Finn *et al.*, 2017).

3.1.2 *A. nidulans* carries an additional separate gene *candA-C1* corresponding to *A. fumigatus* N-terminal extension of CanA

BLAST search and multiple sequence alignments were performed to investigate whether CandA-C1 exists in other *Aspergillus* species as a fusion or separate protein (JGI MycoCosm); (de Vries *et al.*, 2017). CandA-C1 is not conserved in other fungi like *V. dahliae* or higher eukaryotes like human (Figure 15). Amino acid sequence alignments with CandA-C1 show 59 % identity to the N-terminal extension (NTE, exon 1) of *A. fumigatus* CanA. CandA-C shows 79 % identity to full length CanA (Figure 16). The human Cand1 protein sequence lacks most of the sequence parts that would correspond to CandA-C1 or the CanA NTE sequence. Protein sequence alignments of 15 different *Aspergillus* spp. revealed that a majority of 12 species carry two separated adjacent genes that encode similar proteins as in *A. nidulans* including the fungal-specific CandA-C1 and CandA-C. Only *A. fumigatus*, *A. clavatus* and *A. aculeatus* encode deduced fusion proteins with similar lengths and intron distributions as *A. nidulans* CandA-C with more than 50 % amino acid identity in the N-terminal CandA-C1 and more than 70 % identity in the C-terminal CandA-C corresponding domains (Figure 16). In addition, the *A. niger* strain NRRL3 is annotated to contain an orthologous gene but a *candA-C1* ortholog is not annotated in an industrial strain for citric acid production CBS513.88. These results show that CandA-C1 is an *Aspergillus* specific third subunit of the CandA protein family, which is part of the CandA-C N-terminal domain in some *Aspergillus* spp. but the majority contains a trimeric CandA complex.

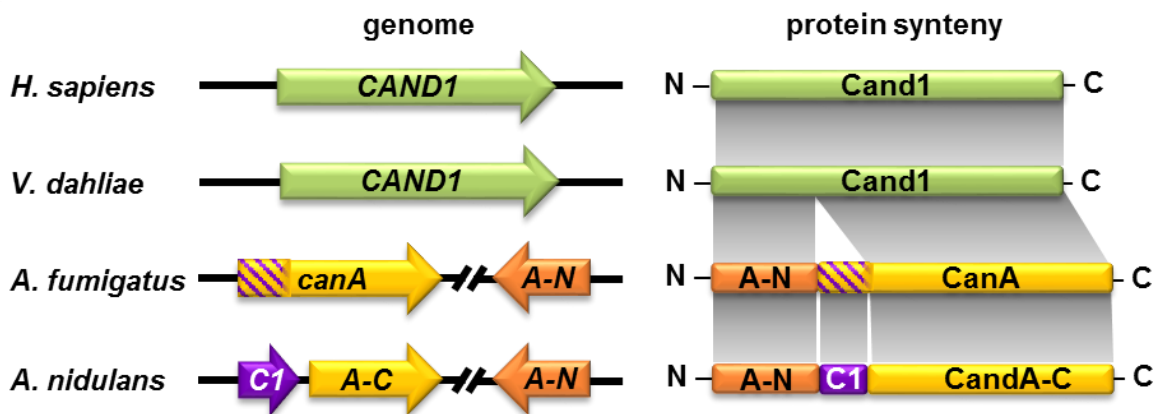


Figure 15. Comparison of single and split Cand proteins in human and fungi. Human (*Homo sapiens*) as well as numerous fungi like *Verticillium dahliae* have one Cand1 gene which encodes a single Cand1 polypeptide. The counterpart of human Cand1 is split in Aspergilli in an N-terminal (CandA-N: A-N) and C-terminal (CandA-C) part encoded by separate genes. Aspergilli require an additional Cand polypeptide CandA-C1 (C1), which is not present in humans or *V. dahliae*. The CandA-C1 polypeptide represents the N-terminal part of the CanA protein of *A. fumigatus* (striped) but is encoded by a separate *candA-C1* gene in *A. nidulans*, which is located next and upstream to *candA-C*.

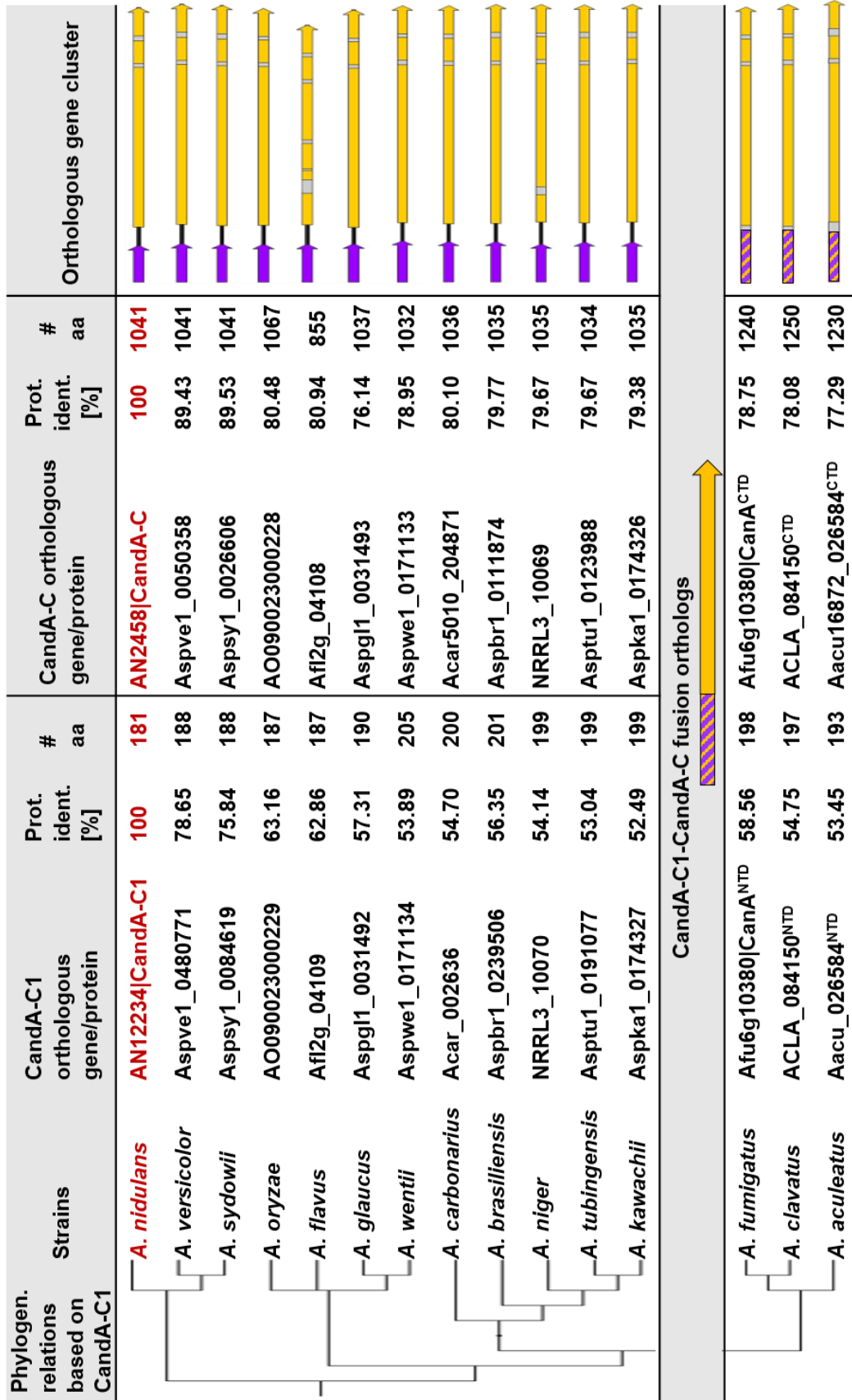


Figure 16. For description see next page.

Figure 16. Comparative analysis of CandA-C1 and CandA-C orthologs in different *Aspergillus* spp. Protein sequence of *A. nidulans* CandA-C1 (AN12234), highlighted in red, was compared to deduced polypeptides of genomes of different *Aspergillus* spp. by BLASTp search in the JGI MycoCosm genome portal (Grigoriev *et al.*, 2012, 2014; de Vries *et al.*, 2017). Genomic clusters of orthologs of separated *candA-C1* (purple) followed by intergenic regions (*igr.* black line) and downstream located *candA-C* (yellow) genes are depicted on the right (IBS software; Liu *et al.*, 2015). Three corresponding fused *candA-C1~candA-C* genes of *A. fumigatus*, *A. clavatus*, *A. acuelatus* encoding the CandA-C1- like domain marked in purple-yellow striped followed by an intron (grey) instead of the *intergenic region* are depicted in the bottom. Phylogenetic relations are based on protein identities of the CandA-C1 orthologs in the genus *Aspergillus* similar to relations described by de Vries *et al.*, 2017. Protein identities in percentage (%) are in relation to *A. nidulans* CandA-C1 and CandA-C. Amino acid (aa) numbers indicate the protein length.

Aspergillus candA genes presumably encountered a DNA rearrangement, which resulted in separation of the *candA* genomic locus. The synteny of the afore analyzed strains was investigated using the synteny tool of FungiDB.org (Stajich *et al.*, 2012). In half of the analyzed *Aspergillus* species *candA-C* and *candA-N* are separated by five conserved open reading frames, as observed for *A. nidulans* (Figure 17): AN2459 is coding for a protein involved in the septation initiation network (SepK, Kim *et al.*, 2009), AN2460 is uncharacterized, AN12235 is coding for a putative ubiquitin E3 RING ligase involved in histone ubiquitination (*S. cerevisiae* homolog Pep5/Vps11 (Singh *et al.*, 2012)), AN12236 is uncharacterized and AN10309 encodes a putative chitin deacetylase. From 13 analyzed *Aspergillus* genomes, ten species have putatively similar genes between the *candA* loci (Figure 17). The six species *A. nidulans*, *A. versicolor*, *A. sydowii*, *A. fumigatus*, *A. clavatus* and *A. acuelatus* possess the same five genes between the *candA* genes, whereas *A. wentii*, *A. carbonarius*, *A. brasiliensis* and *A. tubingensis* carry one additional or miss one of the five genes according to annotations. *A. oryzae*, *A. flavus* and *A. glaucus* carry more than one additional small open reading frame or miss genes and sequence parts, which could also be due to yet incomplete annotations. The conserved position of homologous genes indicates a common ancestor of all *Aspergillus* spp., which had encountered a specific rearrangement of *candA* genes and which has not yet been found in other fungi.

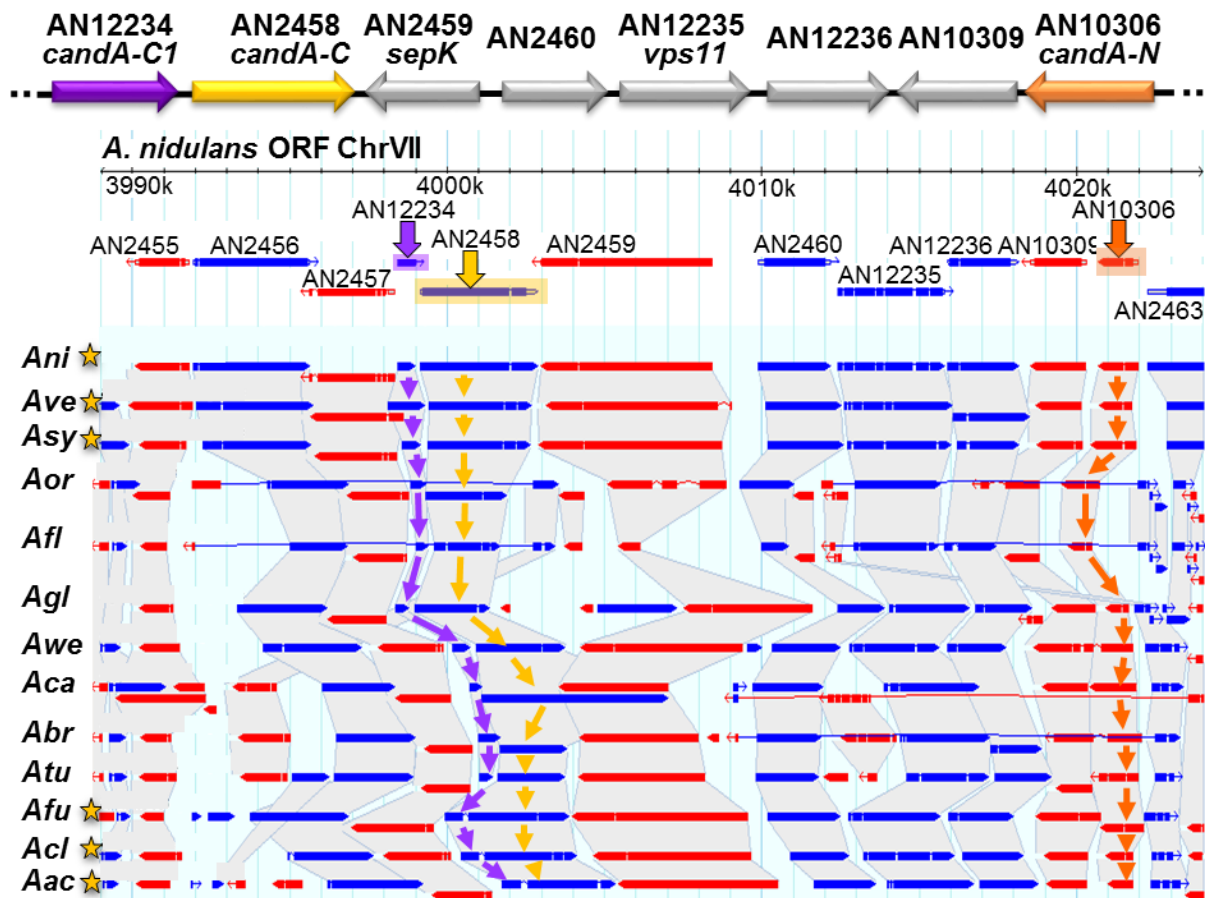


Figure 17. The genomic environment of the *candA* genes within *Aspergilli*. Cartoon representation of the genetic region of *candA* genes of *A. nidulans*. The FungiDB synteny tool (Stajich *et al.*, 2012) was used for the analysis of *candA* localization in different *Aspergillus* species. The *A. nidulans* *candA* genomic locus was used as basis for this search and the localization of *candA-C1* is indicated with purple arrows, *candA-C* with yellow arrows and *candA-N* with orange arrows. Orthologous genes can also be tracked by continuous shading. Genes on the sense strand are depicted in blue and of the antisense strand in red. Species with a star indicate that they are annotated with five conserved open reading frames between *candA-C* and *candA-N* gene loci. (*Ani*: *A. nidulans*, *Ave*: *A. versicolor*, *Asy*: *A. sydowii*, *Aor*: *A. oryzae*, *Afl*: *A. flavus*, *Agl*: *A. glaucus*, *Awe*: *A. wentii*, *Aca*: *A. carbonarius*, *Abr*: *A. brasiliensis*, *Atu*: *A. tubingensis*, *Afu*: *A. fumigatus*, *Acl*: *A. clavatus*, *Aac*: *A. acuelatus*).

3.1.3 *A. nidulans candA-C1* and *candA-C* express different transcripts

Annotation revealed for *A. fumigatus* an extension of the CanA N-terminus correspondingly to the highly similar *A. nidulans* CandA-C1 protein. The existence of a putative CandA-C1~CandA-C fusion transcript as predicted for *A. fumigatus* CanA was examined by employment of a complementary DNA (cDNA) amplification assay. Different sets of primer pairs were used to amplify *candA-C1*, *candA-C*, a putative fusion transcript as well as variants of *candA-C1* and *candA-C* RNAs with the putative *intergenic region* from wild type genomic DNA (gDNA), cDNA and different mutant strain cDNA samples (Figure 18A).

Specific PCR products for *candA-C1* (primer 1+2) could be obtained from both wild type samples, Δ *candA-C* and Δ *igr* strains, which was expected (Figure 18B). Analysis of gene expression levels revealed that *candA-C1* RNA amounts are around two-fold increased when *candA-C* is deleted suggesting that the CandA-C might negatively regulate *candA-C1* expression (Figure 18C). Prominent signals in the expected size of *candA-C* (primer 3+4) were observed from PCRs on wild type genomic and cDNA samples and from cDNA of a *candA-C1* deletion strain. When the *intergenic region* was deleted a very faint signal of a *candA-C* PCR product was found, which might correspond to a *candA-C1* read-through into *candA-C* due to a weak terminator sequence. This suggests that the *intergenic region* includes the terminator sequence for *candA-C1* and the promoter sequence for *candA-C*.

The transcription of a long read-through transcript or alternatively an antisense RNA (or a combination of both) was analyzed by amplification of *candA-C1* together with the *intergenic region* and *candA-C* (primer 1+4). Putative read-through or antisense transcripts could be observed in wild type samples and were visible as a faint band in the Δ *igr* strain (Figure 18B). These findings support an additional combined transcript corresponding to read-through and/or antisense of *candA-C1* and *candA-C*.

The PCR reaction with primer 1+4 also resulted in a ~1.6 kb small product when cDNAs of Δ *candA-C1*, Δ *igr* or Δ *candA-C1/igr* were used as template. This fragment was sequenced and identified as a region in the 3' end of *candA-C* with partially complementary sequence to primer 1, which resulted in unspecific binding of primer 1 in the *candA-C* sequence. Parts of primer 1 are similar to several sequence patches of *candA-C* and it shows highest similarity to the region of base pairs 1454 to 1484 where it putatively anneals with 13 nucleotides that have an annealing temperature of approximately 42°C. PCR reactions using primers 4+5 and 1+6 further support a possible read-through and/or antisense RNA connecting both genes (Figure 18B). These data suggest that *candA-C1* and *candA-C* are encoding two distinct transcripts and the *intergenic region* contains the *candA-C1* terminator and the *candA-C* promoter. The situation is more complicated, because there is also an additional transcript combining both

genes, which could be either a read-through or an antisense transcript and might be part of a transcriptional control.

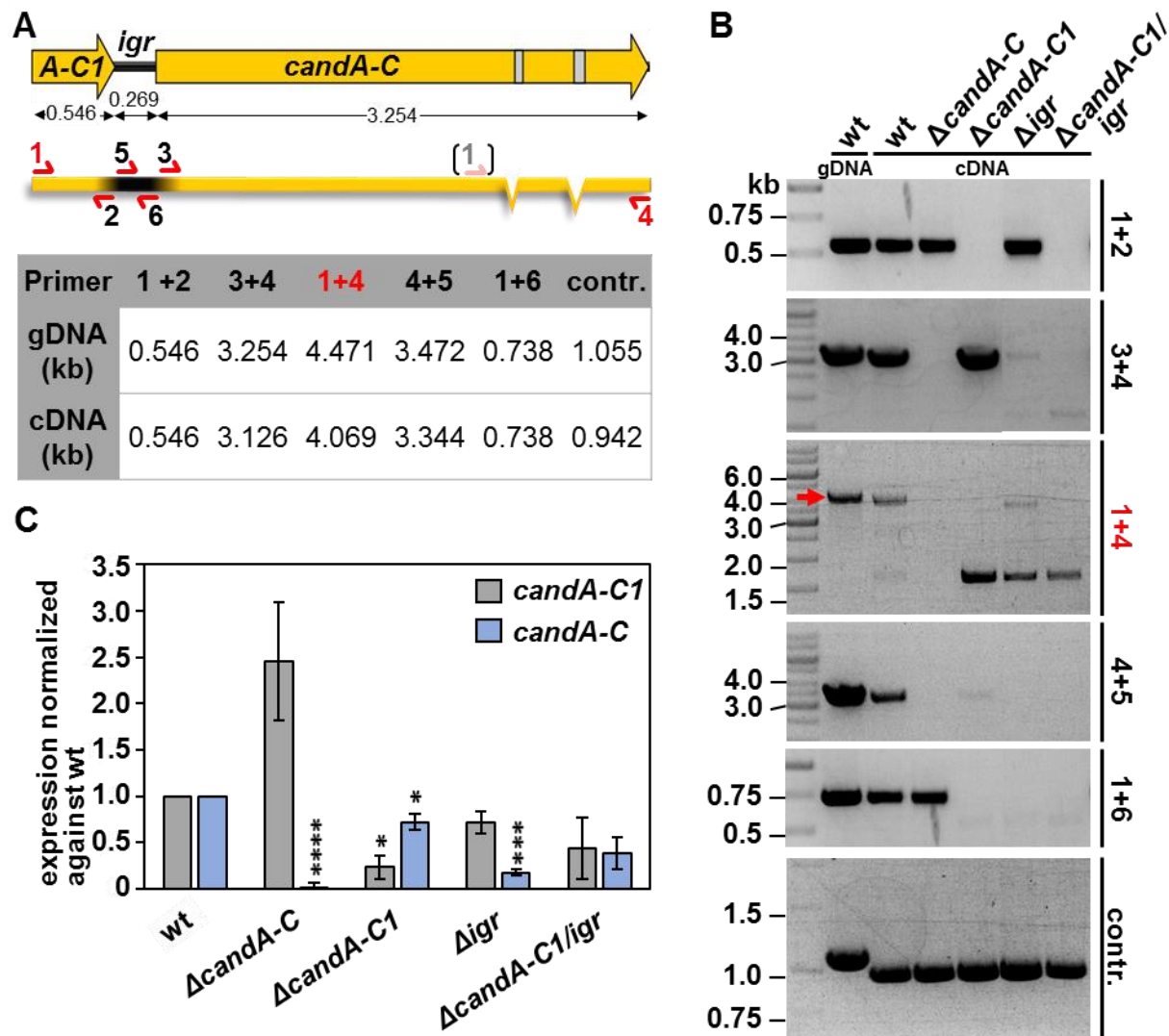


Figure 18. *A. nidulans candA-C1* and *candA-C* have a shared transcript and the intergenic region promotes *candA-C* transcription. **A** Overview of different PCR setups used to amplify *candA-C1* (primer 1+2), *candA-C* (primer 3+4), *candA-C1-candA-C* (primer 1+4, red), *igr-candA-C* (primer 4+5) and *candA-C1-igr* (primer 1+6). Expected sizes in kilo base pairs (kb) from genomic DNA (gDNA) or complementary DNA (cDNA) are depicted in the table. Amplification of *candA-N*, which contains two introns was used as control to exclude gDNA contamination in cDNA samples (shaded primer 1 in brackets putative unspecific binding of primer 1). **B** PCR amplified signals are depicted, and sizes are indicated. Respective primer pairs are given on the right. The amplified fused transcript is marked with a red arrow. **C** qRT-PCR experiments show the expression levels after 20 hours vegetative growth of *candA-C1* and *candA-C* in wild type compared to *candA-C*, *candA-C1* and *igr* deletion mutants. Expression of *candA-C* is significantly downregulated when *igr* is deleted. (n=3 except of Δ *candA-C1/igr* n=2; p-values: *: $p \leq 0.05$, ***: $p \leq 0.001$, ****: $p \leq 0.0001$).

The RNA amount of both *candA-C* genes was investigated to analyze whether the expression of *candA-C* is dependent on *candA-C1*. The transcription levels of *candA-C1*, *candA-C* and *candA-N* in wild type and a strain overexpressing *candA-C1:gfp* under the nitrate promoter (OE *candA-C1:gfp*) were compared in qRT-PCR measurements. Whereas *candA-C1* was significantly (fifty -times) overexpressed in the overexpression *candA-C1:gfp* strain compared to wild type expression used as reference, expression levels of *candA-C* and *candA-N* did not change in the overexpression strain (Figure 19A). This supports that *candA-C1* has its own promoter and terminator and is thereby primarily independent of *candA-C* and the shared transcript. The shared transcript might represent an additional control layer for *candA-C1* and *candA-C* expression. Consequently, overexpression of *candA-C1* does not influence expression of *candA-C*, which was underlined by the wild type-like phenotype of the overexpression mutant strain (Figure 19B).

Investigations on the genomic localization of *candA-C1* were conducted to analyze if *candA-C1* is necessarily upstream of *candA-C*. Ectopic integration of *candA-C1* under its native promoter into the Δ *candA-C1* strain resulted in a wild type-like strain in asexual development (Figure 19B). In summary, the *intergenic region* contains primarily the terminator sequence for *candA-C1* and the promoter sequence for the *candA-C* gene.

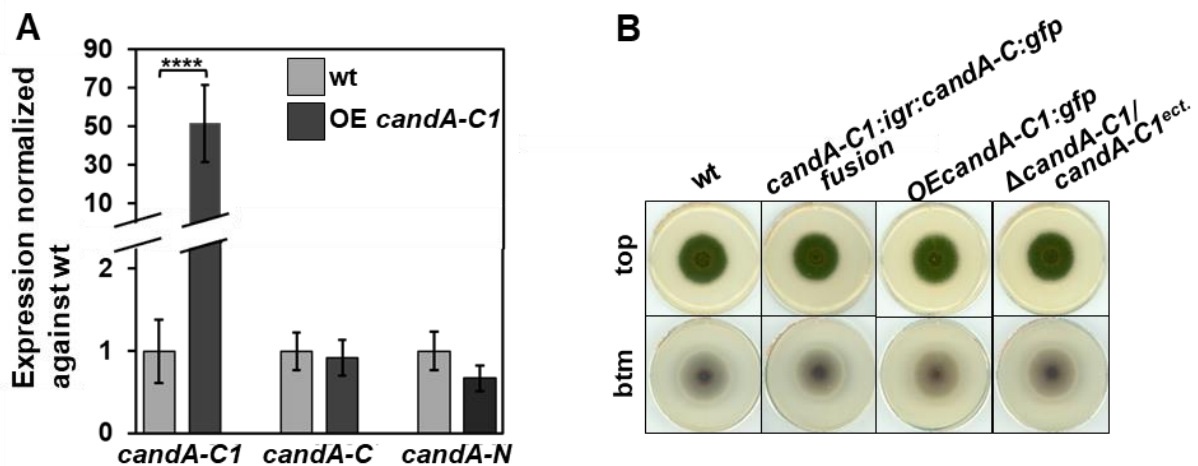


Figure 19. Expression of *candA-C* is independent from *candA-C1* expression. **A** Quantitative real-time PCR (qRT-PCR) measurements show gene expression of *candA-C1*, *candA-C* and *candA-N* in wild type (wt) compared to the overexpression *candA-C1:gfp* strain. *candA-C1:gfp* is significantly overexpressed compared to wild type expression (****: p -value ≤ 0.0001). Histone encoding *h2A* served as housekeeping gene ($n=3$). **B** Phenotypes of 5 days old asexually developed *A. nidulans* wild type compared to *candA-C1-A-C:gfp* fusion strain, overexpression (OE) *candA-C1:gfp* and Δ *candA-C1* strain expressing ectopic integrated *candA-C1*. All mutant strains show wild type-like asexual development.

3.1.4 *A. fumigatus* expresses a CanA protein corresponding to the combined molecular weight of *A. nidulans* CandA-C1 with CandA-C

The finding of an additional shared transcript of *candA-C1* and *candA-C* was followed by investigation of a possible fusion protein in *A. nidulans* as annotated for *A. fumigatus* CanA. In this case, splicing would be necessary to keep the reading frame for protein synthesis. Splice site prediction revealed a 182 bp long intron with low probability, spanning from base pair 434 of *candA-C1* to base pair 69 of the *intergenic region*. *A. fumigatus* has a putative intron separating the N-terminal extension from the CanA C-terminal domain.

Western hybridization with CandA-C-GFP showed only one band at the expected size of 141.7 kDa and no additional signal for a CandA-C1~CandA-C-GFP fusion protein at 164.1 kDa (Figure 20A, B). A *candA-C1~igr~candA-C:gfp* fusion construct was designed, which is missing the stop codon of *candA-C1* and start codon of *candA-C* (Figure 20A). The *intergenic region* of 269 bp was included between both ORFs. The splicing of the afore mentioned low putative intron would be necessary to keep the reading frame for the synthesis of a putative fusion protein. The fusion construct was integrated ectopically into the *candA-C* deletion strain and complemented the phenotype (Figure 19B).

Western hybridization with α -GFP antibody showed for the fusion protein a signal of the size of a single protein at ~141 kDa (Figure 20B), that was most likely translated from the sixth codon after the deleted annotated translation start, which is a methionine serving as an alternative start codon. These observations indicate, that splicing of the putative intron was not performed, instead *candA-C* was expressed separately from the alternative start codon.

Another fusion construct was generated, which was missing the *intergenic region* (Figure 20A). Western hybridization showed two different protein bands migrating at the size of the fusion protein (161.3 kDa) and the CandA-C-GFP single protein (141.7 kDa) (Figure 20C). This suggests that the higher migrating signal is indeed a fusion protein resulting from ectopic expressed *candA-C1~candA-C:gfp^{ect.}* and the lower migrating protein is CandA-C-GFP alone. Comparison of C-terminal GFP-tagged Af_CanA-GFP and An_CandA-C-GFP by western hybridization experiments showed that *A. fumigatus* CanA-GFP (163 kDa) migrated at higher molecular weight than *A. nidulans* CandA-C-GFP (142 kDa) (Figure 20A, D). The *A. fumigatus* CanA corresponds to combined polypeptide sequences of *A. nidulans* CandA-C1 and CandA-C that are encoded by separate genes in *A. nidulans*. The N-terminal domain of *A. fumigatus* CanA (CanA NTE) corresponds to *A. nidulans* CandA-C1 and the C-terminal domain of *A. fumigatus* CanA (CanA CTD) corresponds to *A. nidulans* CandA-C.

A

Protein	kDa	aa	Gen locus		
			A-C1 igr	candA-C/canA	gfp
An_CandA-C-GFP ✧	141.7	1293			
An_CandA-C1~igr~CandA-C-GFP	164.1	1504			
An_CandA-C1~CandA-C-GFP †	161.3	1474			
Af_CanA-GFP	163.4	1492			
Af_CanA ^{CTD} -GFP	141.7	1292			

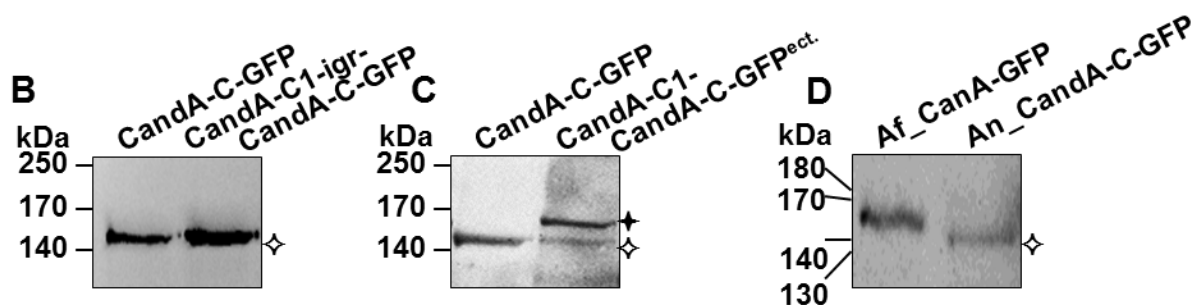


Figure 20. A synthetic fusion protein of *A. nidulans* CandA-C migrates at similar molecular weight like the *A. fumigatus* CanA. A The table depicts analyzed GFP-tagged fusion proteins and their expected sizes of *A. nidulans* CandA-C1 and CandA-C and *A. fumigatus* CanA. Molecular weights were calculated from ProtParam tool ExPASy portal (Gasteiger *et al.*, 2005). The gen locus of the analyzed constructs is indicated (TGA: stop codon, ATG: start codon). **B** Western hybridization of CandA-C-GFP and a fusion construct of CandA-C1~igr~CandA-C-GFP (*candA-C1_Δstop/igr/Δstart_candA-C*) probed with α -GFP show the same size compared to a single CandA-C-GFP protein (142 kDa). **C** A synthetic fusion protein of CandA-C1~CandA-C-GFP, derived from ectopic expression of *candA-C1_Δstop/Δigr/candA-C:gfp*, was detected at around 160 kDa (†) and another signal of CandA-C-GFP at approximately 140 kDa (✧). **D** Comparison of *A. fumigatus* CanA-GFP to *A. nidulans* CandA-GFP in a western hybridization experiment.

3.2 Cellular CanA/CandA functions

3.2.1 *A. nidulans* CandA proteins are mainly localized in the nucleus

CandA-C1 and CandA-C are separate proteins in *A. nidulans* but correspond to a combined protein CanA in *A. fumigatus*. Localization of GFP-tagged CandA proteins was examined as prerequisite to study CandA-C1 complex formation with CandA-N and CandA-C.

Functional GFP-CandA-N and CandA-C-GFP are mainly localized in nuclei (co-localization with RFP-tagged histone H2A, Figure 21). Weak signals could also be observed in the cytosol. CandA-C1-GFP is localized to nuclei, cytosol and mitochondria (co-localization with MitoTracker red (MT)). CandA-C1-GFP was also localized to certain areas in the nuclei that are not stained with RFP-H2A. These areas are most likely nucleoli. Concluding from the microscopy observations, all three CandA subunits have the same localization in the nuclei and are partially also present in the cytoplasm.

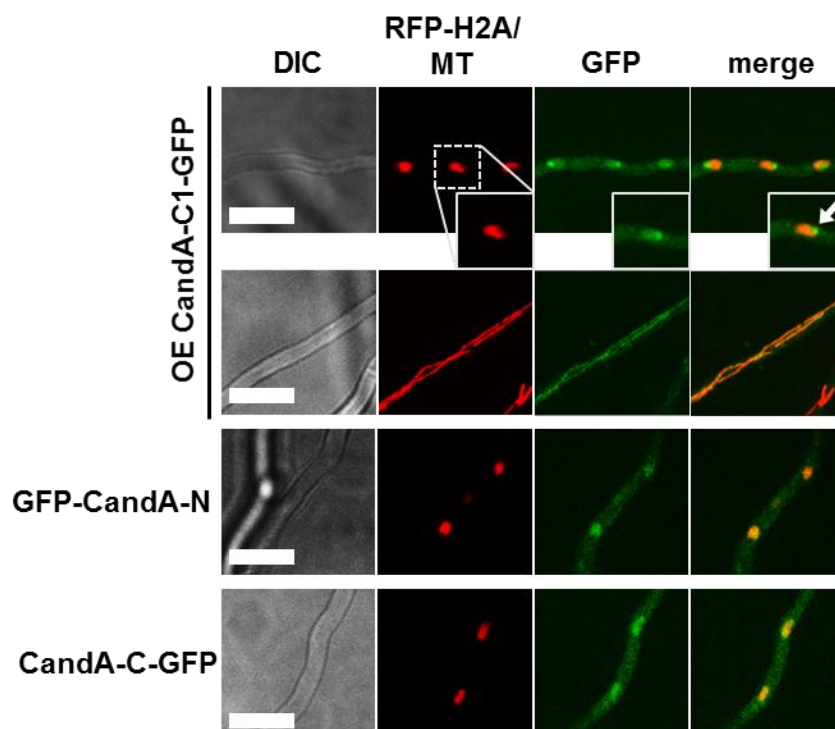


Figure 21. *A. nidulans* CandA proteins are localized in nuclei. Localization of overexpression (OE) CandA-C1-GFP, and native GFP-CandA-N and CandA-C-GFP. All three CandA proteins co-localize with mRFP-tagged histone H2A (RFP-H2A). CandA-C1-GFP is also localized to nucleoli (white arrow) and co-localizes with MitoTracker Red (MT) that stains mitochondria (size bars: 10 μ m).

Earlier experiments showed that nuclear localization of CandA-N depends on the CandA-C NLS with a RKRRR motif at amino acid position 138 to 142 (Helmstaedt *et al.*, 2011). A classic monopartite NLS could not be identified in the sequence of CandA-C1. The localization of CandA-C1 was analyzed in respect to putative dependence on the CandA-C NLS (Figure 22).

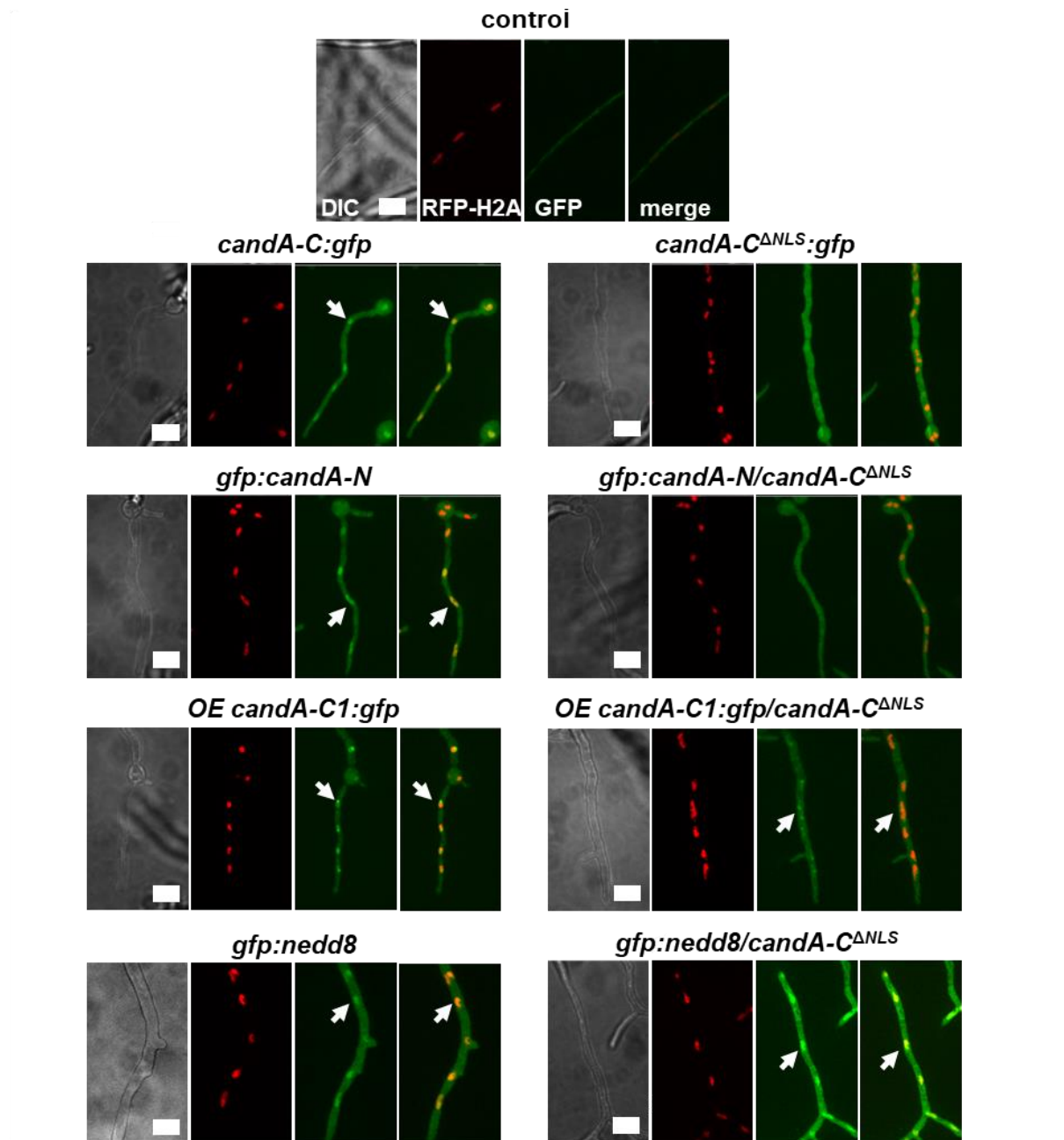


Figure 22. CandA-C1 and Nedd8 nuclear localization are independent from the CandA-C NLS in *A. nidulans*. Fluorescence images of 20 hours vegetative hyphae show that nuclear localization of CandA-C and CandA-N is dependent on CandA-C NLS sequence RKRRR as signals for both CandA proteins are absent from RFP-H2A stained nuclei when NLS is deleted. OE CandA-C1-GFP and GFP-Nedd8 are still localized to nuclei in *candA-C^{ΔNLS}* background strains. White arrows indicate nuclear localization (size bars: 10 μ m).

The CandA-C NLS was deleted in wild type background strain expressing a CandA-C^{ΔNLS}-GFP protein. In GFP-CandA-N, OE CandA-C1-GFP and GFP-Nedd8 strains a CandA-C^{ΔNLS} was expressed. Fluorescence microscopy showed CandA-C1-GFP localizing to nuclei, whereas CandA-N and CandA-C without NLS were absent from nuclei (Figure 22). Therefore, the CandA-C1 nuclear protein population is independent from the NLS of CandA-C.

Besides the impact of CandA-C NLS on the other CandA subunits the nuclear localization of Nedd8 was also studied. GFP-Nedd8 colocalizes to nuclei and cytoplasm like CandA (Figure 22). Nedd8 cellular localization was not altered in a *candA-C^{ΔNLS}* strain. In summary, only the nuclear transport of CandA-N relies on the CandA-C NLS, whereas the nuclear transport of CandA-C1 and Nedd8 are independent of CandA-C.

It was analyzed whether CandA-C1 needs CandA-N for nuclear import or if the full CandA-C protein is required for CandA-C1 nuclear localization. Inspection of CandA-C1-GFP in *ΔcandA-N*, *ΔcandA-C* or *ΔcandA-N/C* strains showed CandA-C1 localized to nuclei (Figure 23A), indicating CandA-C1 nuclear import must be independent from both other CandA proteins. The question of localization dependence was inversed, and the localization of CandA-N and CandA-C in a *ΔcandA-C1* strain was examined. In the absence of CandA-C1 both other CandA subunits still localized to nuclei (Figure 23B). All localization mutants showed that neither CandA-C1 nuclear localization is dependent on CandA-N or CandA-C, nor CandA-N nor CandA-C localization changes in the absence of CandA-C1. The nuclear localization of Nedd8 is also independent from CandA-C. This supposes that Nedd8, CandA-C1 and CandA-C travel independently into the nucleus and only the nuclear transport of CandA-N is dependent on CandA-C.

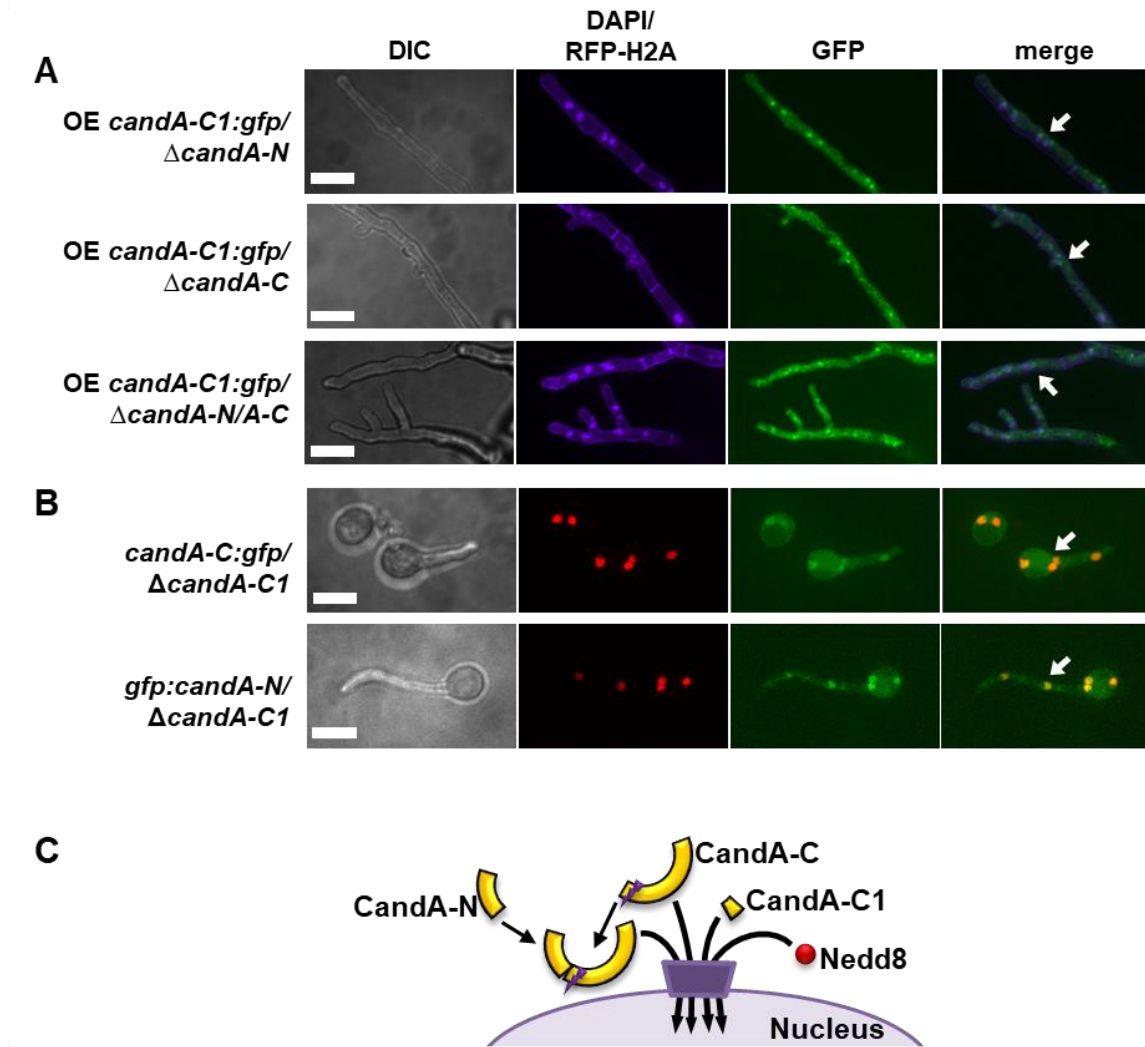


Figure 23. CandA-C1 is found in nuclei independent of CandA-N and CandA-C and vice versa. **A** Overexpression (OE) CandA-C1-GFP is localized to nuclei and nucleoli in Δ *candA-N*, Δ *candA-C* and Δ *candA-N/A-C* strains. Nuclei are stained with DAPI. **B** CandA-N and CandA-C are localized to nuclei in Δ *candA-C1* strain. Nuclei are highlighted by expression of RFP-H2A. White arrows indicate co-localization to nuclei (size bars: 10 μ m). **C** Model of nuclear import. Nedd8 and CandA-C1 are independent from the CandA-C NLS. CandA-N is co-transported with CandA-C.

3.2.2 *A. nidulans* CandA-N, CandA-C1 and CandA-C can physically interact and presumably form a trimeric complex

Bimolecular fluorescence complementation (BiFC) were conducted to examine *A. nidulans* CandA protein interactions *in vivo*. For these experiments strains were constructed, which ectopically express CandA-C1 C-terminally tagged to one half of yellow fluorescent protein (YFP) and the other half of YFP to either the N-terminus of CandA-N or to the C-terminus of CandA-C under the control of a bidirectional nitrate promoter. The control strains expressed only one protein tagged to one half of YFP leaving the other half of YFP un-tagged and did not show any fluorescent signals (Figure 24). Strains with YFP-tagged CandA-C1 and either CandA-N or CandA-C showed signals in the nuclei indicating protein interaction (Figure 24). Furthermore, BiFC signals were sometimes co-localized to long filamentous structures. Staining the hyphae with MitoTracker Red showed that the BiFC signal is co-localized to mitochondria (Figure 24).

The CSN deneddylase inactivates CRLs by an isopeptide bond cleavage between cullin and Nedd8. The catalytic active subunit of the CSN is CsnE but for activity all eight subunits are required. CandA is proposed to bind only to deneddylated cullins. It was examined if the CandA subunits interact with each other without binding to cullins in strains with an inactive CSN complex. BiFC microscopy with CandA subunits in *csnE* deletion background strains showed signals in the nuclei (Figure 24), indicating that the CandA complex is also formed when CRLs are not deneddylated. The observations of the interaction of CandA-C1 with CandA-N and CandA-C in nuclei and at mitochondria match with the observed localization of the single subunits and thereby support the *in vivo* formation of a trimeric CandA complex in *A. nidulans*.

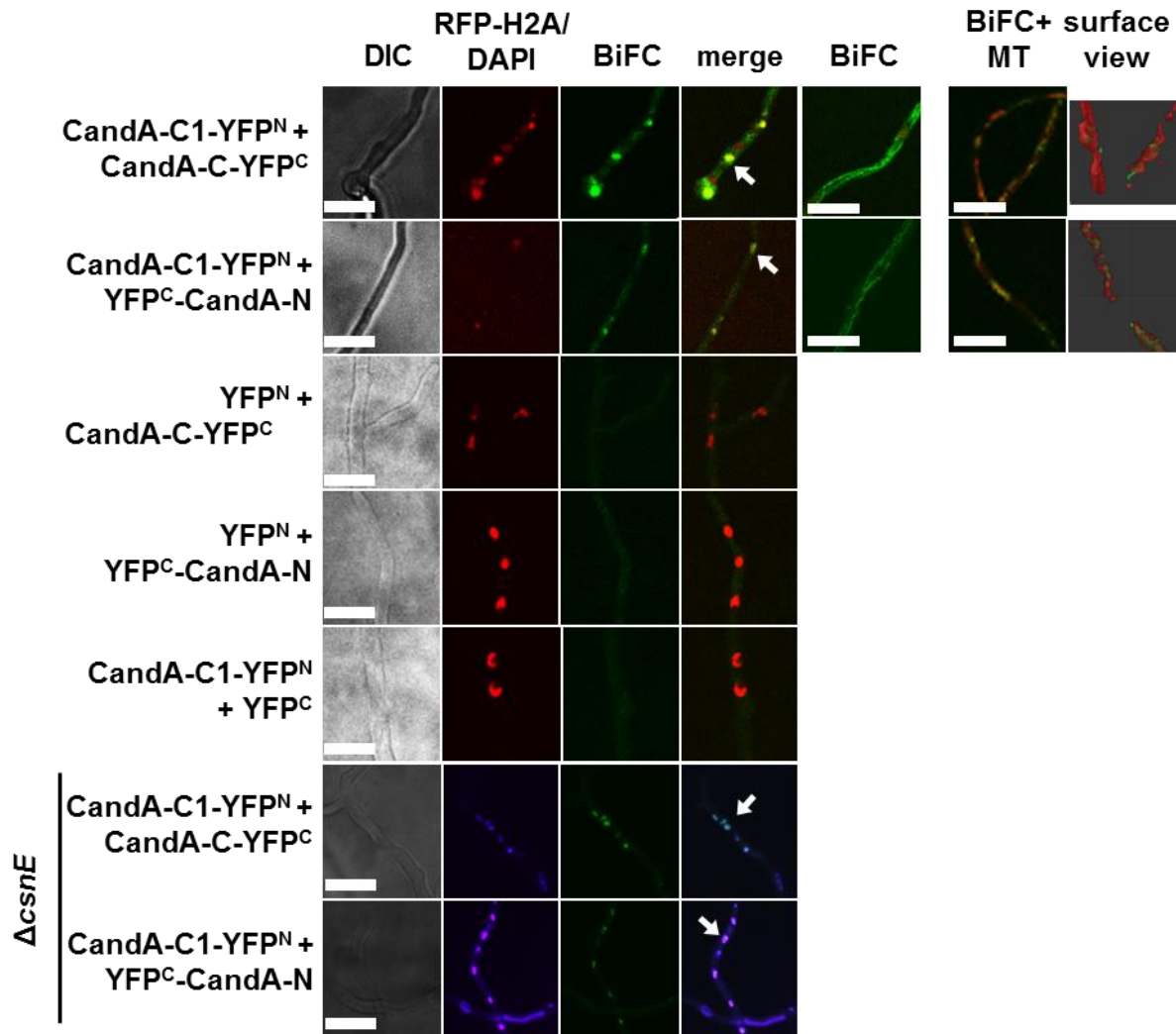


Figure 24. CandA-C1 interacts with CandA-C and CandA-N. Bimolecular fluorescence complementation (BiFC) microscopy experiments of CandA-C1-YFP^N with CandA-C-YFP^C and YFP^C-CandA-N in wild type background as well as in a *csnE* deletion strain. BiFC signals are visible in green and localized to nuclei (white arrows), which are stained with H2A-RFP or 4',6-Diamidin-2-phenylindol (DAPI). BiFC signals of CandA proteins could also be observed co-localized to mitochondria, stained with MitoTracker red. Three-dimensional surface views highlight the co-localization of BiFC and MitoTracker signals (size bars: 10 μm).

3.2.3 *A. nidulans* CandA interacts exclusively with cullin-1 (CulA)

The trimeric CandA physical interaction suggested by the BiFC interaction experiments was analyzed by pull-down experiments from fungal cell extracts. Pull-downs of *A. nidulans* strains expressing functional GFP-CandA-N and CandA-C-GFP (native promoter) and CandA-C1-GFP (overexpression) were performed from vegetative mycelium. Strains overexpressing GFP were used as controls.

The pull-down samples of GFP-tagged bait proteins were first investigated by SDS PAGE and western hybridization. The bait proteins could be observed on colloidal Coomassie stained SDS PAGE and on western hybridization with α -GFP antibody at expected sizes: (1) GFP-CandA-N: 58.6 kDa, (2) free GFP: 27 kDa, (3) CandA-C-GFP: 138.5 kDa, (4) CandA-C1-GFP: 47.8 kDa (Figure 25). Samples were digested with trypsin and peptides were analyzed by mass spectrometry. LC-MS data were processed with *MaxQuant* and *Perseus* and a work flow for the identification of specifically interacting proteins was established (Figure 26). All pulldowns together included approximately 2 000 identified proteins. Filtering to the final 51 putative interaction partners was performed by following the commands (blue boxes Figure 26) from the main menu and selecting the respective criteria as described on the right next to the commands.

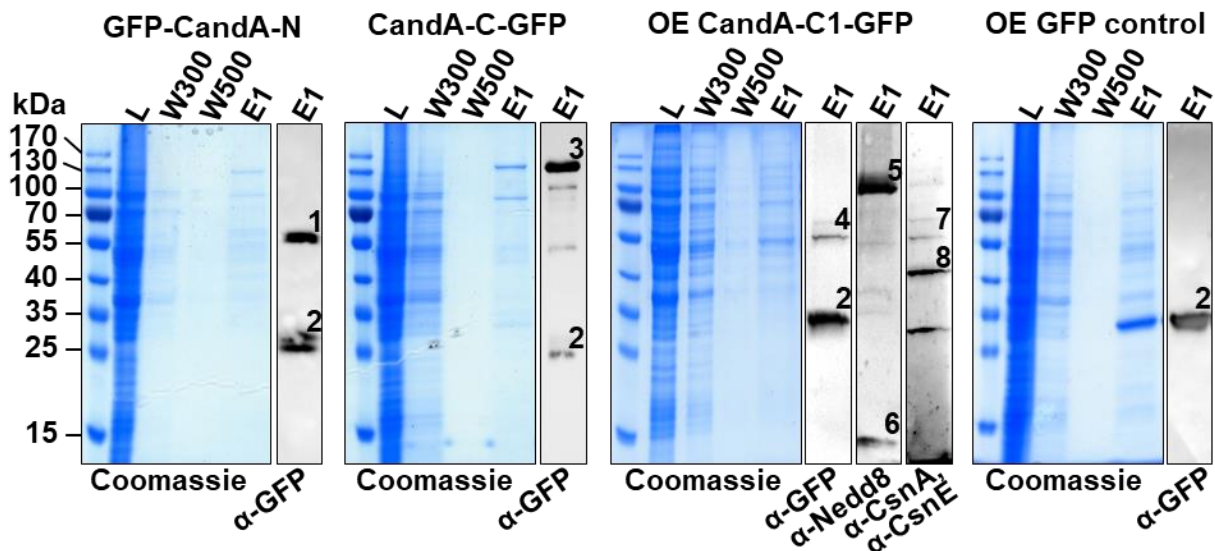


Figure 25. *A. nidulans* CandA-C1 pulls Nedd8, CulA and CSN subunits as components of SCF regulation. Colloidal Coomassie stained 12% SDS gels of load (L), washing steps (W300 and W500) and first elution (E1) samples are depicted. Western hybridization of E1 with α -GFP highlights the respective bait protein and free GFP (1: GFP-CandA-N, 2: free GFP, 3: CandA-C-GFP, 4: CandA-C1-GFP). E1 of CandA-C1-GFP pull-down was also probed with α -Nedd8 as well as with α -CsnA and α -CsnE showing signals as indicated (5: CulA-Nedd8, 6: Nedd8, 7: CsnA, 8: CsnE).

Results

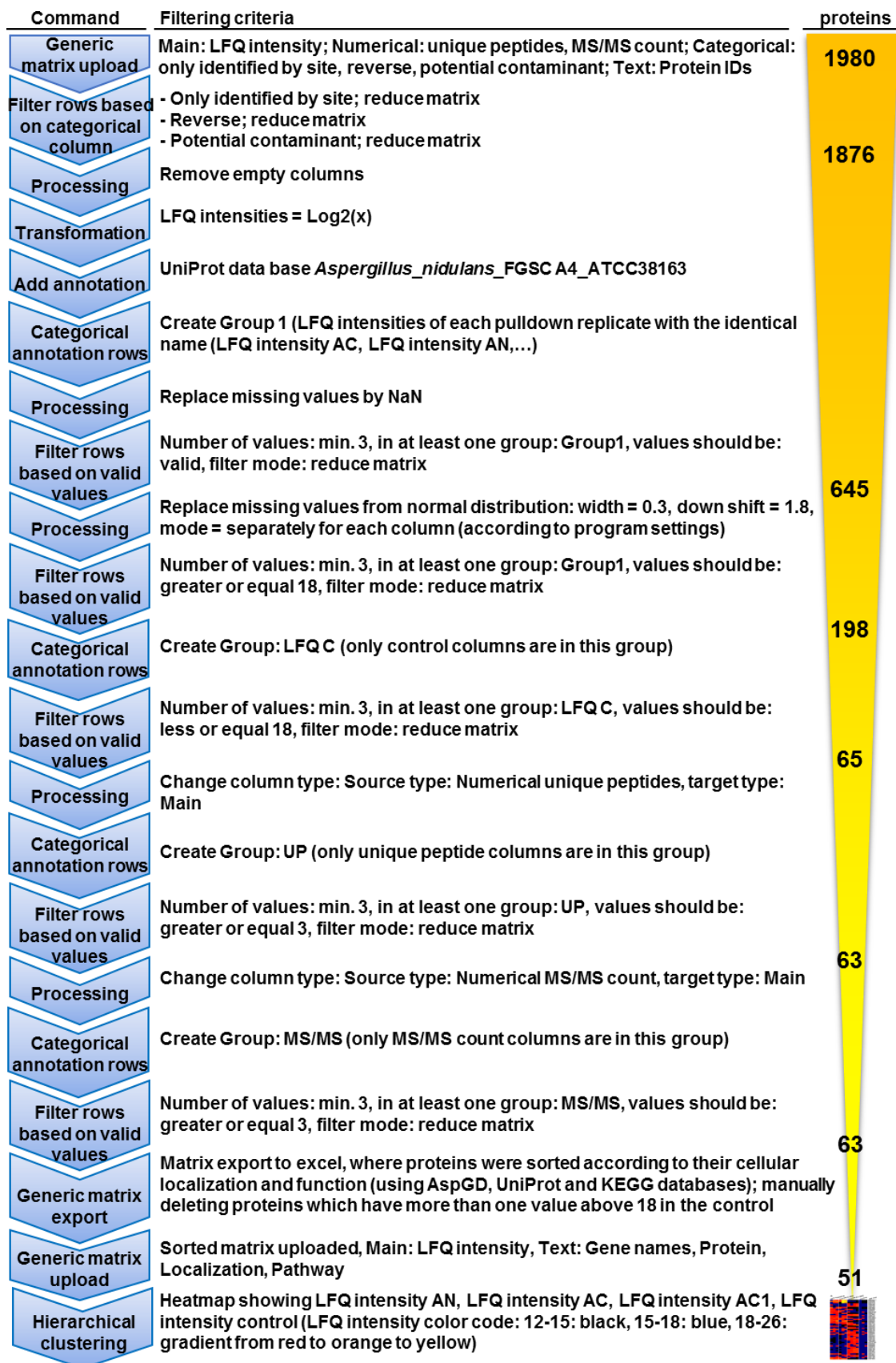


Figure 26. Perseus workflow. Step-by-step statistical LC-MS2 data analysis with *Perseus* version 1.6.0.7. The blue boxes contain commands of the *Perseus* main menu and the description on their right includes chosen criteria of the commands for filtering from 1 980 identified proteins to 51 proteins, which are depicted in the heat map of Figure 27.

The interaction partners of GFP-CandA-N, CandA-C-GFP and CandA-C1-GFP proteins were compared. Identified putative interacting proteins are depicted with label free quantification intensities (LFQ) in a heat map (Figure 27A) and with detailed protein description in Table 9. CandA-N and CandA-C were identified with highest LFQ intensities in pull-downs with CandA-C and CandA-N as bait proteins, respectively. CulA could be identified among the best hits, but never CulC or CulD. This indicates that CandA is specific for CulA-containing CRLs. CulC- or CulD- containing CRLs might be regulated differently. Cullin proteins were not identified by LC-MS of CandA-C1 pull-down samples. Western hybridization of the elution fraction showed a band of neddylated cullins and free Nedd8 when probed with α -Nedd8 antibody (Figure 25). It was of interest whether CandA-C1 also interacts with CSN subunits. Probing the western membrane with α -CsnA and α -CsnE antibodies revealed signals for both proteins in the elution fraction of CandA-C1-GFP (Figure 25). LC-MS identified CandA-N and CandA-C as the only CRL associated proteins but with low LFQ intensities.

LC-MS analyses of CandA-C1-GFP pull-down samples poorly identified CandA-C1 itself although it was enriched through the pull-down procedure as visible by western hybridization. Using chymotrypsin instead of trypsin for *in-gel* digest or using *in-solution* tryptic digest did never result in increased numbers of identified peptides. Several different peptides of CandA-C1 could be identified by LC-MS analysis of GST-tagged CandA-C1 recombinantly expressed in *Escherichia coli* leading to a sequence coverage of 60%. This indicated that the detection of CandA-C1 peptides is generally possible. These identified peptides were then used as templates for a specific scanning LC-MS run (tSIM) on CandA-C1-GFP pull-down elution fractions but still not more than one peptide could be found although CandA-C1-GFP was specifically identified by western hybridization. CandA-C1 was not identified as putative interaction partner of CandA-C-GFP and GFP-CandA-N in LC-MS analysis of pull-down samples. These results indicate that CandA-C1 peptides from fungal extracts are not good targets to be captured by LC-MS or are modified when expressed in *A. nidulans* and the modification was not yet identified. These results also suggest that the addition of CandA-C1 to the dimeric CandA-N/C complex might be highly dynamic.

In total ten nucleus (nucleolus) localized proteins (green), 14 mitochondrial proteins (red), 25 cytosolic proteins (light yellow), one extracellular protein (light blue) and one membrane associated protein (light grey) were identified as putative interaction partners of CandA proteins. Among the nucleus specific proteins, there are three importins: KapA, KapB and KapJ, whereby KapJ is predicted to be a nucleolar importer (Markina-Iñarrairaegui *et al.*, 2011). All three proteins have high LFQ intensities in CandA-C1 pull-downs, supposing that they act as cargos for CandA-C1. Except of one protein, all mitochondrial proteins that are putative interaction partners of CandA proteins are involved in primary or secondary metabolism. Within the cytosolic group there are metabolism- and transport- associated proteins.

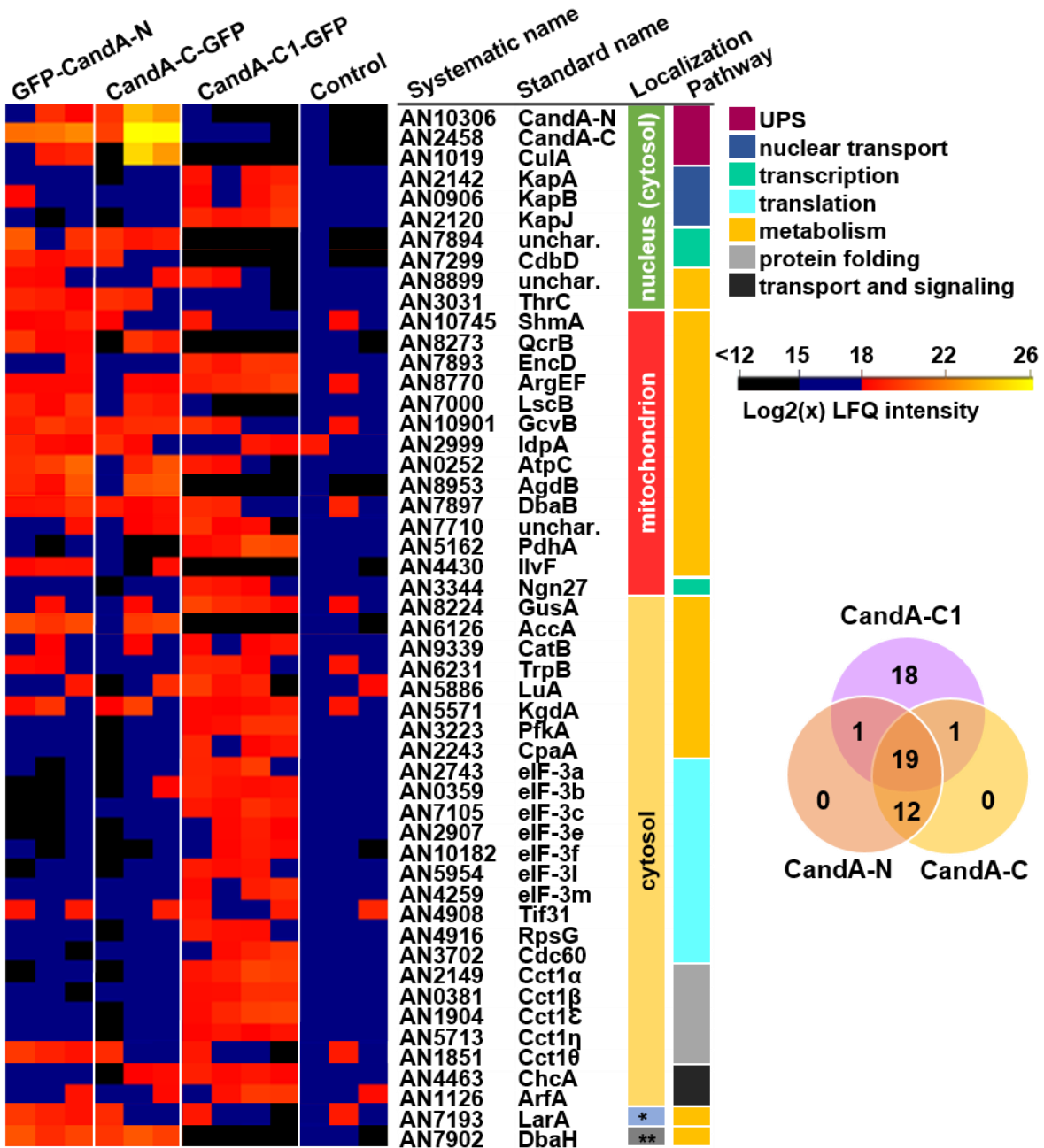


Figure 27. Pull-downs coupled to LC-MS of CandA-N, CandA-C and CandA-C1 support the existence of a trimeric CandA complex in *A. nidulans*. **A** Comparison of putative interaction partners of CandA-C and CandA-N with CandA-C1 from pull-down experiments. The heat map, generated with Perseus depicts the $\log_2(x)$ label free quantification (LFQ) intensities of three biological replicates of GFP control, CandA-N, CandA-C and four replicates of CandA-C1. CandA-C1 was never identified in LC-MS analysis. Data were processed as described in Figure 26. Colored bars indicate cellular localization, based on KEGG and UniProt databases (nucleus: green, mitochondrion: red, cytosol: light yellow, extracellular *: grey-blue, membrane **: light grey) and the pathway where the putative interaction partners are predicted to be involved in ubiquitin proteasome system (UPS, berry), nuclear transport (dark blue), transcription (cyan), translation (light blue), metabolism (yellow), protein folding (grey), transport (dark grey). LFQ intensities range from 12-15: black: not considered as identified, 15-18: blue: low intensity and 18-26: gradient from red to orange to yellow: low to high LFQ intensities. For detailed protein description see Table 9. The Venn diagram depicts distribution of identified interaction partners with LFQ threshold of 18.

Seven out of thirteen eIF3 subunits (eIF3a, b, c, e, f, l, and m) were found, which is a member of the ZOMEs. Other proteins of the ZOMEs from CSN or proteasomal lid were not among the identified proteins. The list of cytosolic proteins includes five subunits of the chaperonin containing *t*-complex (TCP1 or CCT), which is involved in protein folding. Both, eIF3 and TCP1 complex proteins had higher LFQ intensities in CandA-C1 than in CandA-N and CandA-C pull-down samples. CandA-N and CandA-C showed a putative interaction with the oxygenase DbpA of the *dba* secondary metabolite gene cluster. DbpA is involved in the production of yellow pigments by oxidation of 2,4-dihydroxy-3-methyl-6-(2-oxopropyl)benzaldehyde (DHMBA) and plays an important role in sexual development (Dissertation of Jennifer Gerke, 2012 and Gerke *et al.*, 2012). These data support the existence of a putative trimeric CandA complex in *A. nidulans* that binds CulA containing SCF complexes and shares different additional interaction partners.

Table 9. Identified proteins in CandA-N, CandA-C and CandA-C1 pull-downs. Detailed information about identified proteins from the heat map in Figure 27 according to UniProt and AspGD (Cerqueira *et al.*, 2014; The UniProt Consortium, 2017).

Systematic name	Standard name	Description
Nucleus (cytosol)		
AN10306	CandA-N	Cullin-associated NEDD8-dissociated protein 1, N-terminal part
AN2458	CandA-C	Cullin-associated NEDD8-dissociated protein 1, C-terminal part
AN1019	CulA	SCF ubiquitin ligase complex subunit CulA
AN2142	KapA	Importin subunit alpha
AN0906	KapB	Importin subunit beta1
AN2120	KapJ	Importin subunit beta-4
AN7894	-	Uncharacterized protein, alpha-beta barrel and YCII domain predict enzymatic function
AN7299	Arx1	Uncharacterized protein; curved DNA-binding protein, aminopeptidase activity, nuclear export
AN2343	HbnA	Uncharacterized protein; nitroreductase family protein
AN8899	-	Putative 1-aminocyclopropane-1-carboxylate deaminase
AN3031	ThrC	Threonine synthase
Mitochondrion		
AN10745	ShmA	Serine hydroxy methyltransferase
AN8273	QcrB	Ubiquinol-cytochrome c reductase complex core protein 2
AN7893	EncD	Uncharacterized protein; oxidoreductase with Fe ligand

Table 9 continued

Systematic name	Standard name	Description
AN8770	ArgEF	Acetylglutamate kinase
AN7000	LscB	Succinyl-CoA synthetase beta subunit,
AN10901	GcvB	Uncharacterized protein; glycine cleavage system P protein
AN2999	IdpA	Isocitrate dehydrogenase
AN1923	AltA	Alanine transaminase
AN10296	FrdA	Putative FAD dependent oxidoreductase
AN9403	PdhC	Pyruvate dehydrogenase E1 component, beta subunit
AN0252	AtpC	ATP synthase subunit gamma
AN8953	AgdB	Uncharacterized protein; glycosidase and hydrolase activity
AN6246	CycA	Cytochrome C
AN7897	DbxB	FAD binding domain protein of the <i>dba</i> secondary metabolite gene cluster
AN7895	CipB	Zinc-binding alcohol dehydrogenase domain-containing protein, concanamycin-induced protein B
AN7710	-	Uncharacterized protein; HAD-superfamily hydrolase
AN7169	FhbA	Uncharacterized protein; expressed flavohemoprotein
AN5162	PdhA	Pyruvate dehydrogenase E1 component subunit alpha
AN4430	-	Uncharacterized protein; acetolactate synthase activity, role in branched-chain amino acid biosynthetic process
AN3344	Ngn27	Uncharacterized protein; acetyltransferase activity
Cytosol		
AN8224	GusA	Glutamyl-tRNA synthetase
AN6126	AccA	Uncharacterized protein; acetyl-CoA carboxylase activity
AN2286	AlcC	Alcohol dehydrogenase 3 (ADH III)
AN9339	CatB	Catalase B
AN4888	PdcA	Pyruvate decarboxylase
AN6231	TrpB	Bifunctional tryptophan synthase TRPB
AN5886	LuA	3-isopropylmalate dehydratase (Alpha-IPM isomerase)
AN5571	KgdA	Uncharacterized protein; Oxoglutarate dehydrogenase (Succinyl-transferring)
AN3223	PfkA	6-phosphofructokinase
AN2243	CpaA	Carbamoyl-phosphate synthase arginine-specific small chain (CPS-A)
AN2743	eIF-3a	Eukaryotic translation initiation factor 3 subunit A (eIF3a)
AN0359	eIF-3b	Putative eIF3b subunit of translation initiation factor 3 (eIF3), required for conidial germination
AN7105	eIF-3c	Eukaryotic translation initiation factor 3 subunit C (eIF3c)
AN2907	eIF-3e	Eukaryotic translation initiation factor 3 subunit E (eIF3e)
AN10182	eIF-3f	Eukaryotic translation initiation factor 3 subunit F (eIF3f)
AN5954	eIF-3l	Eukaryotic translation initiation factor 3 subunit L (eIF3l)
AN4259	eIF-3m	Eukaryotic translation initiation factor 3 subunit M (eIF3m)
AN4908	Tif31	Clustered mitochondria protein homolog

Table 9 continued

Systematic name	Standard name	Description
AN4916	RpsG	40S ribosomal protein S7
AN3702	Cdc60	Uncharacterized protein; Leucyl-tRNA synthetase
AN2149	Cct1 α	T-complex protein 1 subunit alpha, protein folding
AN0381	Cct1 β	T-complex protein 1, beta subunit, protein folding
AN1904	Cct1 ϵ	T-complex protein 1, epsilon subunit, protein folding
AN5713	Cct1 η	T-complex protein 1, eta subunit, protein folding
AN1851	Cct1 θ	T-complex protein 1, theta subunit, protein folding
AN6688	SepB	Septin B
AN4463	ChcA	Clathrin heavy chain
AN1126	ArfA	ADP-ribosylation factor
AN6004	VipA	Actin cytoskeleton protein (VIP1)
AN0285	PglA	Uncharacterized protein; 6-phosphogluconolactonase
AN7193	LarA	Uncharacterized protein; D-xylose reductases
Extracellular		
AN6048	AatB	Uncharacterized protein; Aspartate transaminase
Membrane		
AN7902	DbaH	Uncharacterized protein; FAD binding monooxygenase of <i>dba</i> secondary metabolite gene cluster

3.2.4 *A. fumigatus* CanA interacts with CulA and CulC

Interaction partners of the *A. fumigatus* CanA complex were investigated for comparison with the results obtained in *A. nidulans*. Pull-down experiments of functional CanA-GFP, expressed under its native promoter were conducted. SDS PAGE and western hybridization with α -GFP antibody show the GFP-tagged bait protein at its expected size of 163 kDa and putative degradation products at lower molecular weight (Figure 28A). The degradation signals were verified to be CanA-GFP truncations by LC-MS analyses from samples of excised single bands. The control strain shows a signal for free GFP. LC-MS analyses identified seven specific interacting proteins and the bait protein itself with highest LFQ intensity (Figure 28B). Compared to pull-down results from *A. nidulans* the number of identified proteins is smaller because only one bait protein was considered in this study. Among those proteins are CanA-N and CulA, which were also identified in *A. nidulans* pull-downs. CulC and RbxA were found as putative interaction partners of *A. fumigatus* CanA but were not identified in *A. nidulans* CanA pull-downs above the used thresholds. Besides those CRL proteins that have mainly nuclear

localization, a ribonuclease T2-like family protein RnyA was identified. Furthermore, peptides for either ArfA or ArfB were found, which are ADP ribosylation factors involved in signaling. As the identified peptides are identical due to high protein identities, it could not be discriminated whether only one or both factors are putative interaction partners of CanA.

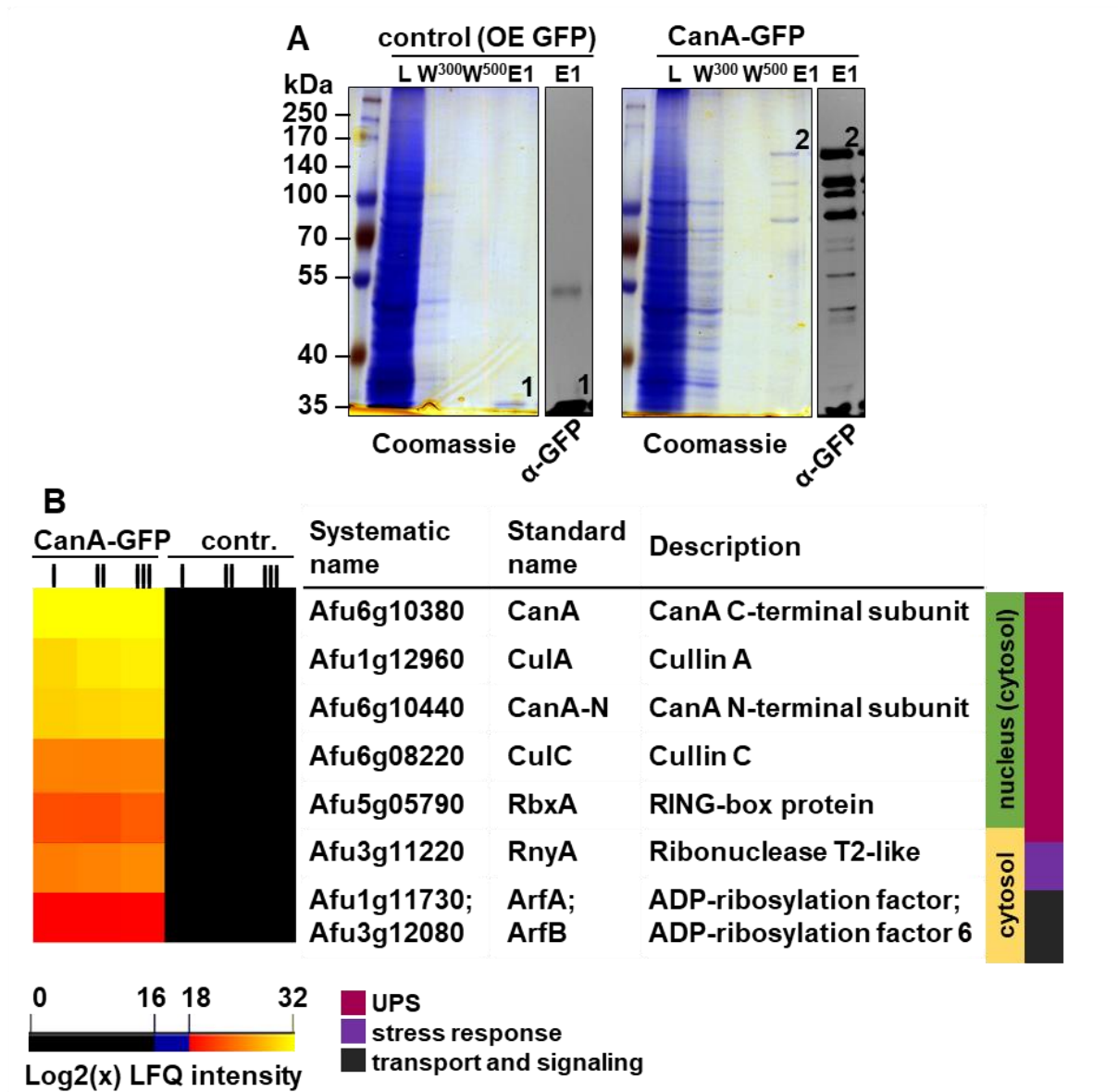


Figure 28. *A. fumigatus* CanA pulls CulA and CulC. **A** Colloidal Coomassie stained SDS PAGE and western hybridization with α -GFP antibody show pull-down samples load (L), washing samples (W300 and W500) and the first elution sample (E1) of the control strain overexpressing GFP (left) and the CanA-GFP bait expressing strain (right). Free GFP (1) has a molecular weight of 27 kDa and CanA-GFP full length protein (2) of 163.4 kDa. **B** Heat map generated with Perseus after filtering for specific CanA interacting proteins shows log₂(x) label free quantification intensities (LFQ) where black (0-16) means not identified and gradient from red to yellow (18-22) increasing intensity of identified proteins. Three biological replicates were performed indicated with roman numbers.

Comparison with *A. nidulans* pull-downs showed that ArfA was also identified as putative interaction partner of CandA-N, CandA-C and CandA-C1 (Figure 27). These data showed that different to *A. nidulans* CandA, the *A. fumigatus* CanA complex binds CulA and CulC containing SCFs. CulD was not identified to interact with either CandA/CanA from *A. nidulans* or *A. fumigatus*. Both orthologous CanA/CandA complexes share an additional non-CRL cycle associated protein, which is the essential ADP ribosylation factor ArfA, involved in signaling and required for hyphal growth (Lee and Shaw, 2008).

3.2.5 *A. nidulans* CandA subunits but not recombinant CandA-N and CandA-C proteins activate CULA SCFs

Deneddylation assays were originally developed to analyze the COP9 signalosome deneddylation activity towards CRLs in *A. nidulans* *csn* deletion mutants (Köhler *et al.*, 2016). With this assay coupled to western hybridization of *A. nidulans* crude extracts probed with α -CulA antibody it is possible to visualize inactive deneddylated CulA (~96 kDa) as lower migrating signal and a higher migrating signal for active neddylated CulA (~106 kDa). Our group could previously show, that all subunits of the COP9 signalosome are required for deneddylation of CRLs and that only the addition of the deneddylase subunit CsnE to a seven subunit pre-CSN confers activity towards cullins (Beckmann *et al.*, 2015). The exact events after CRL inactivation by the COP9 signalosome are still not well known. The other regulator of CRL's is CandA. CandA is known to exchange the substrate receptor-adaptor complex to allow the assembly of various adaptor-receptor bound CRLs what contributes to high substrate variability. Pull-downs showed that a trimeric CandA complex binds to CulA containing SCFs. To test if CandA has impact on the activity of these SCFs, the neddylation status of CulA in *candA* deletion strains was investigated.

Accumulation of significantly higher amounts of deneddylated CulA compared to wild type were visible in Δ *candA-C*, Δ *candA-N* as well as in double deletion Δ *candA-C/N* strains (Figure 29A). CandA-N seems to be important for CulA neddylation as a *candA-N* deletion strain showed two-fold higher amounts of deneddylated CulA than the Δ *candA-C* strain. Double and triple deletion strains with *candA* and *csnE* were generated to examine the order of CRL inactivation and adaptor-receptor exchange. These mutant strains accumulated neddylated CulA like a Δ *csnE* single deletion strain, but contrary to *candA* deletion strains (Figure 29A). These observations suggest that CRLs are first deneddylated by the CSN as defective *csn* causes accumulation of neddylated cullins. The following steps include CandA binding and CRL complex disassembly, required for a new cycle of complex assembly and cullin neddylation as

without CandA an increased amount of inactive CulA was observed. CulA is impaired or even unable to initiate new cycles of neddylation when CandA subunits are absent.

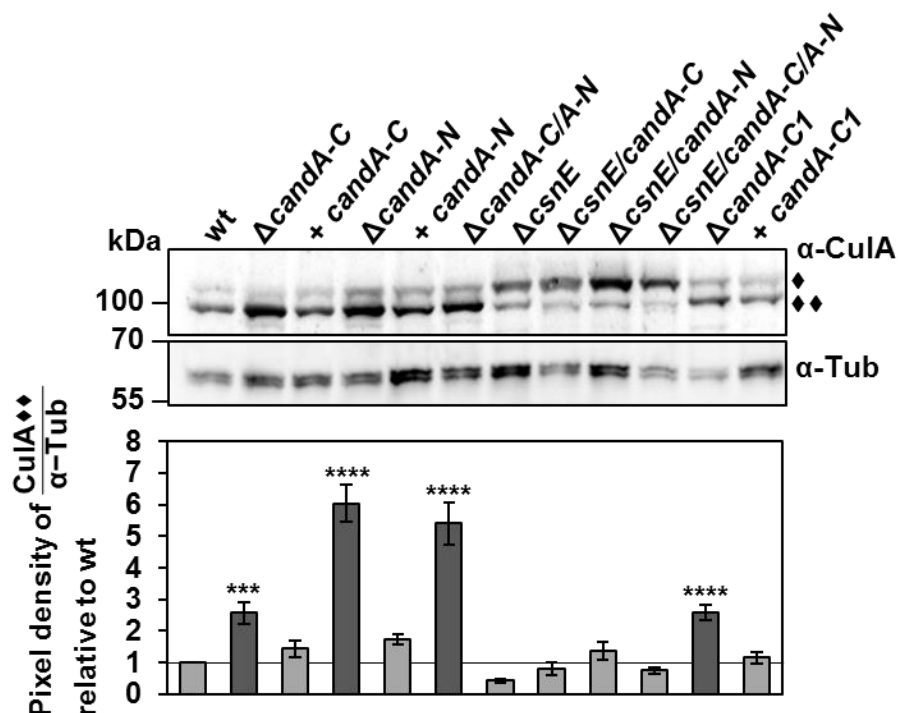


Figure 29. CandA is required for CulA neddylation in *A. nidulans*. Western hybridization was performed with *A. nidulans* crude extracts from vegetative mycelium grown for 20 hours. Western hybridization probed with α-CulA antibody showed neddylated and deneddylated CulA. In wild type most CulA is deneddylated (♦♦). This is different to a ΔcsnE strain, which is defective in cullin deneddylation whereby neddylated CulA accumulates (♦). Deneddylated CulA accumulates in ΔcandA as well as in ΔcandA-C1 deletion strains. Double and triple deletions of csnE, candA-C and/or candA-N show accumulation of neddylated CulA as observed for ΔcsnE. This is convenient with the quantification of pixel density measurements using the *BIO1D software* (PEQLAB) of 12 replicates (three biological with each four technical replicates). Tubulin served as loading control. Dark grey bars show candA deletion strains with increased deneddylated CulA, light grey bars show wild type or increased neddylated CulA; error bars represent the standard error of the mean, *p*-values of candA deletion strains relative to wild type control (***: *p* ≤ 0.001, **** *p* ≤ 0.0001).

Western hybridization showed accumulation of inactive CulA in *candA* deletion strains. In turn, it was tested if recombinant expressed CandA-N and CandA-C are sufficient to restore cullin activity to wild type levels as seen for the *in vitro* deneddylation assay with recombinant CsnE (Beckmann *et al.*, 2015; Köhler *et al.*, 2016). CandA-N and CandA-C were expressed in *E. coli* with N-terminal GST-tag for purification with the aim to produce high amounts of CandA proteins. CandA-C1 purification was not successful due to protein stability issues and low expression levels. Affinity chromatography (GSTrap) was conducted to enrich and clean both CandA proteins from full *E. coli* cell extracts. The SDS PAGE shows high amounts of GST-CandA-N (~55 kDa) and GST-CandA-C (~140 kDa) in the respective peak elution fractions (Figure 30A and B). The GST-tag was cleaved off and both proteins were mixed in a 1:1 ratio for size exclusion chromatography with the aim to analyze complex formation of both subunits. Three clearly separated peaks could be observed from the size exclusion chromatogram, where the first peak included probably degraded and aggregated proteins and the last peak included surplus of CandA-N as samples of this peak show bands of the expected size of CandA-N in SDS PAGE analysis (Figure 30C). Recalculation of the predicted molecular weight from the elution volume resulted in a protein with the size of ~50 kDa, which would approximately correspond to a CandA-N dimer. The difference of calculated to actual molecular weight might be due to its elongated secondary structure that changes migration through the column matrix compared to globular proteins. The middle peak had an elution volume of 58 mL, which corresponds to a protein of approximately 138 kDa. SDS-PAGE analysis confirmed that both proteins are found in this peak, suggesting that they eluted as heterodimeric complex (Figure 30C).

The heterodimeric complex of CandA-N and CandA-C as well as the single proteins obtained by chromatography were then used for *in vitro* deneddylation assays. Crude extracts of *candA-N*, *candA-C* single and *candA-N/A-C* double deletion strains were mixed with purified proteins to test whether excess of CandA single proteins or the CandA-N/A-C complex can reduce the amount of deneddylated CulA. Western hybridization depicts higher amount of deneddylated CulA in deletion strains than in wild type in the buffer control samples as well as when CandA-N, CandA-C or both proteins were added (Figure 31). Complementation strains showed less deneddylated CulA as also seen in Figure 29. The addition of recombinant CandA-N and CandA-C could not reduce the amount of deneddylated CulA but rather increased the levels (Figure 31). The increase in deneddylated CulA signal and the smear visible in the signal when recombinant CandA-N was added to the crude extract might be due to the excess of recombinant CandA-N and/or its instability. These results demonstrate that recombinant CandA proteins are not sufficient for CRL activation.

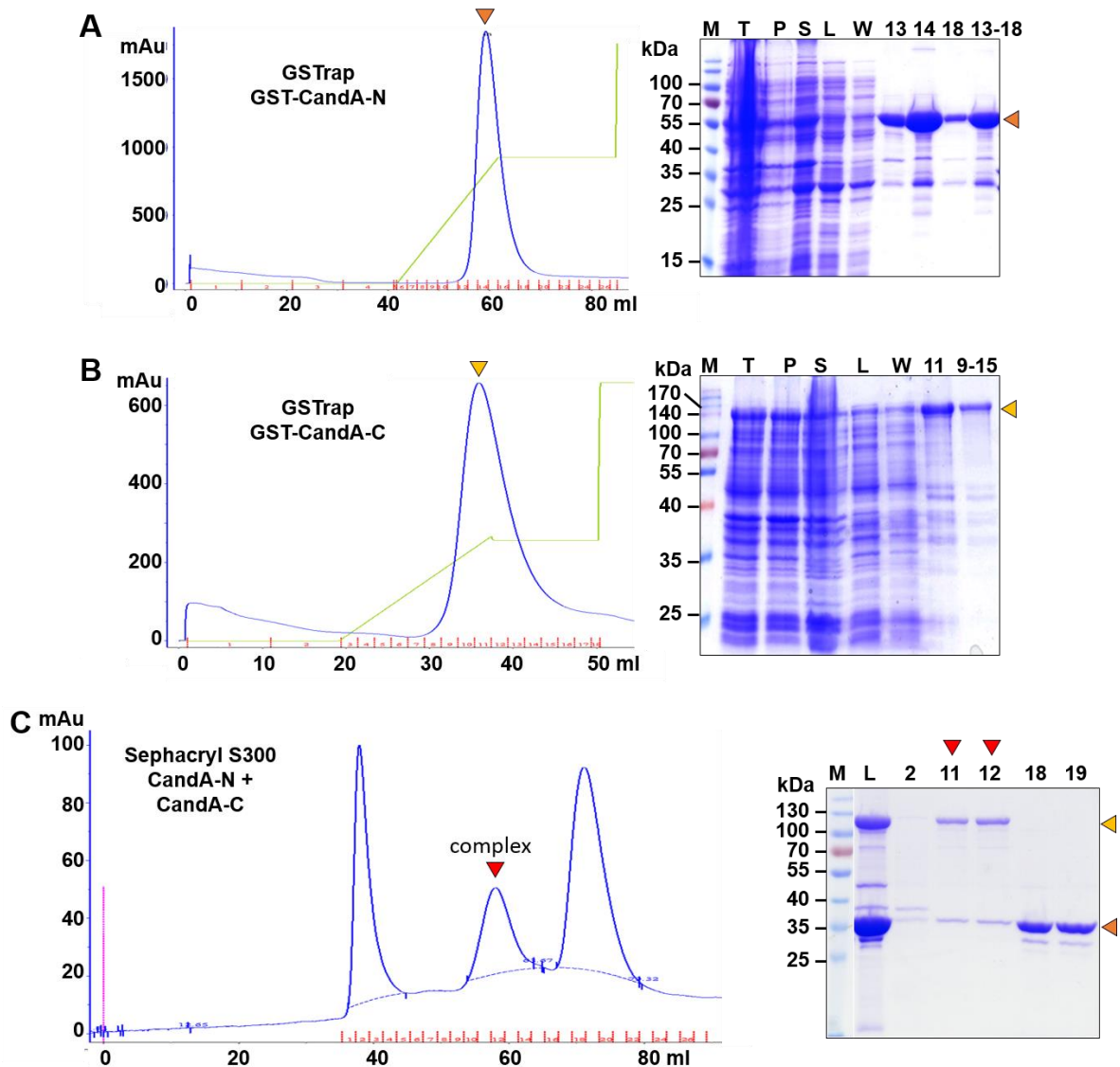


Figure 30. Recombinant CandA-N and CandA-C form a complex. **A** GST-CandA-N was expressed in *E. coli* and total cell extract (T) was prepared. After centrifugation the pellet (P) was discarded and only the supernatant (S) was subjected to purification with a GSTrap FF affinity column. The chromatogram shows a peak of ~1700 mAu absorption at 280 nm at a glutathione concentration of ~5.8 mM. SDS PAGE shows the samples T, P, S, L (flow-through of the loaded sample), W (washing phase between loading and elution) and samples of the peak fractions. Peak samples contain high amounts of a protein at ~55 kDa corresponding to GST-CandA-N (orange arrow). **B** GST-CandA-C was purified following the same protocol resulting in GST-CandA-C elution from the column beads at ~4.6 mM glutathione, and the peak fraction showed a protein of ~140 kDa in SDS PAGE analysis corresponding to GST-CandA-C (yellow arrow). **C** After GST-tag cleavage proteins were mixed in a ratio of 1:1 (w/w) and then loaded on a Sephacryl S300 HR size exclusion chromatography column. The chromatogram shows three peaks. SDS PAGE analysis of peak fractions indicates that the middle peak (red arrow) contains proteins of ~35 kDa (CandA-N, orange arrow) and ~120 kDa (CandA-C, yellow arrow).

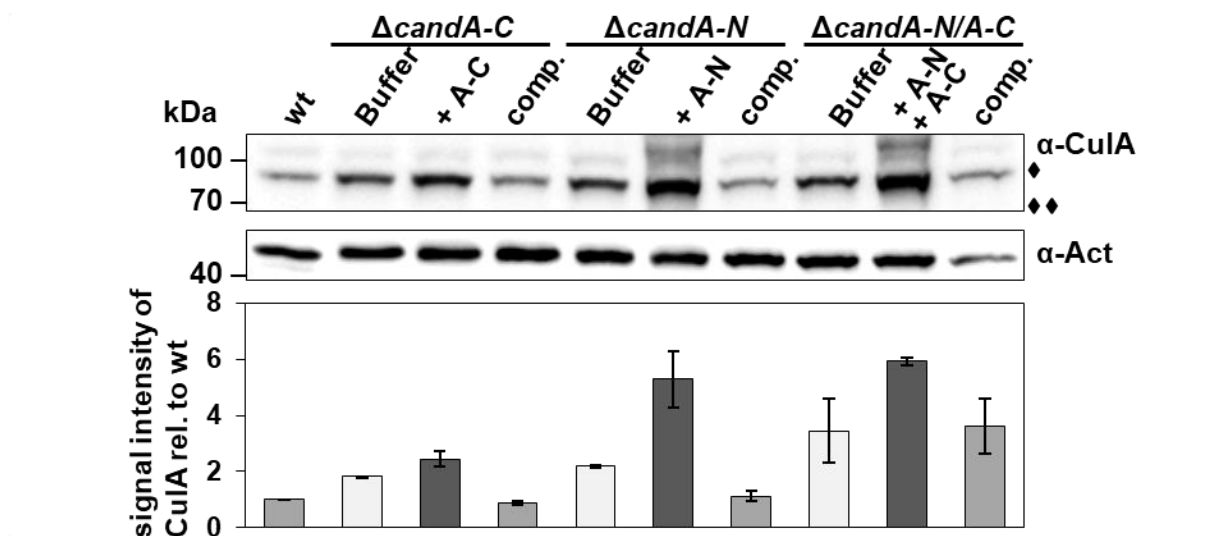


Figure 31. Recombinantly expressed CandA-N and CandA-C are not sufficient to reduce accumulated unneddylated CuIA in *candA* deletion strains. *A. nidulans* crude extracts of $\Delta candA-C$, $\Delta candA-N$ or $\Delta candA-N/A-C$ strains were incubated with recombinantly expressed and purified CandA-N, CandA-C or with both subunits together. Only buffer was added to crude extracts as additional control to wild type and complementation strains. Samples were subjected to SDS PAGE and western hybridization using α -CuIA antibody shows accumulation of a deneddylated CuIA signal at ~100 kDa (\blacklozenge ; neddylated CuIA is indicated with \blacklozenge). Unneddylated CuIA signal intensity was quantified against the actin loading control relative to wild type signal and from two biological replicates. Error bars represent the standard error of the mean.

3.2.6 CandA-C1 contributes to SCF activation

In this study CandA-C1 was identified as additional subunit of the *A. nidulans* CandA complex. The function of CandA-C1 in the CulA neddylation cycle was analyzed. CandA-C and CandA-N are required for CulA neddylation meaning its activation for new cycles of substrate ubiquitination. Defects in CandA result in accumulation of deneddylated CulA. The same deneddylation assay was performed as described above with a *candA-C1* deletion and complementation strain. The result showed accumulation of deneddylated CulA in the *candA-C1* deletion strain like observed for Δ *candA-C*. The complementation could restore the ratio of deneddylated CulA amounts to wild type level (Figure 29A).

As CulA neddylation status is dependent on CandA proteins and the COP9 signalosome, it was analyzed whether the total neddylated cullin amount and total ubiquitin levels are altered in *candA* deletion strains. Western hybridization showed no changes of total neddylated cullins for Δ *candA-N* and Δ *candA-C* strains (Figure 32). This observation fits to the findings of CulA being the only cullin protein that interacts with the CandA complex. The Δ *candA-C1* strain showed slightly increased levels of neddylated cullin compared to Δ *candA-N* or Δ *candA-C* strains. Levels of total ubiquitin were lower in all deletion strains, especially in the Δ *candA-N* strain, which showed higher levels of deneddylated CulA. These findings support that all CandA subunits contribute to the accurate ratio of CRL assembly with neddylated CulA complexes relative to deneddylated CulA disassembly within the fungal cell.

The *in vitro* deneddylation assay was performed with crude extracts of the *candA-C1* overexpression strain in wild type background as well as in *candA* deletion background strains to investigate the effects of CandA-C1 on SCF activity. Western hybridization membranes probed with α -CulA antibody showed that the amount of deneddylated CulA in *OE candA-C1/* Δ *candA-N* strain was similarly increased like in the Δ *candA-N* strain, indicating that elevated amounts of CandA-C1 cannot complement Δ *candA-N* for CulA neddylation (Figure 32). Overexpression of *candA-C1* decreased the amount of deneddylated CulA back to wild type levels in Δ *candA-C* and Δ *candA-N/A-C* background strains. *OE candA-C1* in wild type background did not show any effect on deneddylated CulA. These data show that CandA-C1 overexpression can overcome defects in CulA neddylation cycle caused by the absence of CandA-C.

The total amount of neddylated cullins was analyzed in the afore-mentioned strains. Western hybridization with α -Nedd8 antibody displays cullin neddylation levels comparable to wild type for overexpression *candA-C1* in wild type background strains. Overexpression of *candA-C1* in Δ *candA-N/A-C* deletion background strains significantly increased the total number of neddylated cullins. The total amount of ubiquitinated proteins is dependent on active neddylated SCF ligases. All strains overexpressing *candA-C1* showed significantly lower

amounts of total ubiquitinated proteins compared to wild type. Taken together, the total number of deneddylated cullins is lower in strains with *candA-C* deletion and simultaneous *candA-C1* overexpression, but does not activate the SCF ligases for protein ubiquitination similar as observed in *csn* deficient strains (Figure 29A and Beckmann *et al.*, 2015). Therefore, the CRL activity is not only dependent on a functional CSN but also on a CandA-C1, CandA-C and CandA-N.

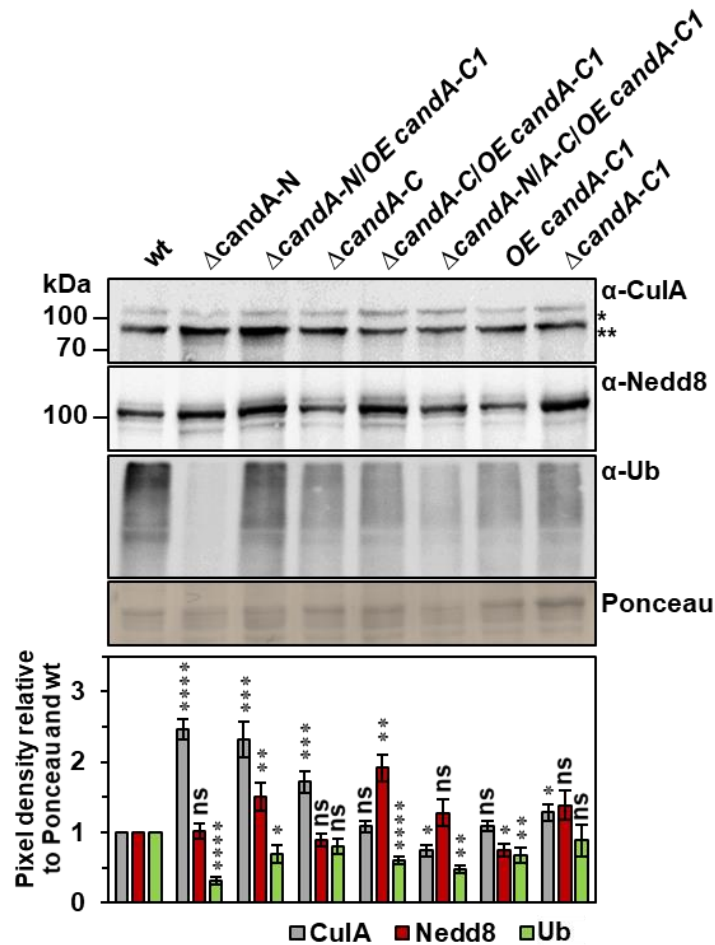


Figure 32. CandA-C1 supports the reduction of deneddylated CulA accumulation in *candA-C* deletion strains of *A. nidulans*. Western hybridization probed with α-CulA (grey), α-Nedd8 (red) and α-Ubiquitin (green) antibodies. Ponceau served as loading control. Δ*candA* strains were compared to *candA-N* and *candA-C* deletion strains overexpressing *candA-C1*. Pixel density ratio was determined with *BIO 1D software* (PEQLAB), quantified against Ponceau and normalized to wild type signals. ♦ CulA-Nedd8, ♦♦ deneddylated CulA; CulA, Ub: 3 biological with each 3 technical replicates, Nedd8: 4 biological with each 3 technical replicates; error bars represent the standard error of the mean, *p*-value of mutant strains relative to wild type control (ns: $p > 0.05$, *: $p \leq 0.05$, **: $p \leq 0.01$, ***: $p \leq 0.001$, ****: $p \leq 0.0001$).

3.2.7 CandA-C and CandA-N predominantly interact with each other and with Nedd8

The *in vitro* deneddylation assay revealed that CandA proteins are required for efficient CulA neddylation. Investigations of a possible CandA-Nedd8 interaction had the aim to show whether CandA directly mediates Nedd8 shuffling to CulA and if CandA itself is neddylated as it was reported for the *Saccharomyces cerevisiae* CandA ortholog Lag2 (Siergiejuk *et al.*, 2009). Nedd8 was detected by western hybridization in the elution fraction of the CandA-C1-GFP pull-down. LC-MS analyses could never identify Nedd8 in any of the CandA pull-downs. This might be due to the small size of Nedd8, where tryptic digestion results only in a few peptides suited for LC-MS detection.

Pull-downs were performed with GFP-Nedd8 as bait to enrich Nedd8 and its putative interaction partners. GFP-trap pulled proteins were detected by LC-MS and compared to CandA-N and CandA-C pull-downs. GFP-Nedd8 pulled around 600 interaction partners and this high number of interacting proteins was expected from a protein modifier. The list of identified proteins was applied to the *Perseus* software to filter for a minimum $\log_2(x)$ LFQ intensity of 16 in the samples and maximum in controls to specify putative interaction partners. Further filtering included a maximum of one allowed identification in the control replicate samples. Proteins identified as putative interaction partners of GFP-Nedd8 must be identified in at least two out of three independent replicates.

The resulting list included 46 putative interaction partners of Nedd8 depicted in the heat map in Figure 33. A detailed protein description is given in Table 10. 18 of the 46 proteins have nuclear, 16 have mitochondrial, 7 have cytosolic and 5 proteins have other or unknown localizations (Figure 33). UlaA and UbaC, subunits of the ubiquitin-like activating heterodimeric enzyme were identified with the highest LFQ intensities followed by CulA, CulC, CulD and three F-box proteins Fbx22, Fbx28 and Fbx33 of the UPS. The ubiquitin-like protein SumO (AN1191), an uncharacterized WD40 (motif of 40 amino acids with a tryptophan (W), aspartic acid (D) dipeptide) protein (AN4800) with 32 % similarity to the transcriptional co-repressor TupA/RcoA (AN6505), the nuclear pore proteins Ntf2 (AN10977) and Pom33 (AN6689) and the mitochondrial import receptor TOM20 (AN0559) were among all identified proteins.

CandA-N and CandA-C were found as putative interaction partners of GFP-Nedd8. CandA-C and Nedd8 share 17 of the identified interaction partners and 13 of these were also identified for CandA-N (Figure 33). CandA-C1 was not identified by LC-MS in GFP-Nedd8 pulldowns, probably because of post-translational modifications, low abundance, insufficient peptides for LC-MS or highly dynamic interactions as also described before (3.2.3, p. 84).

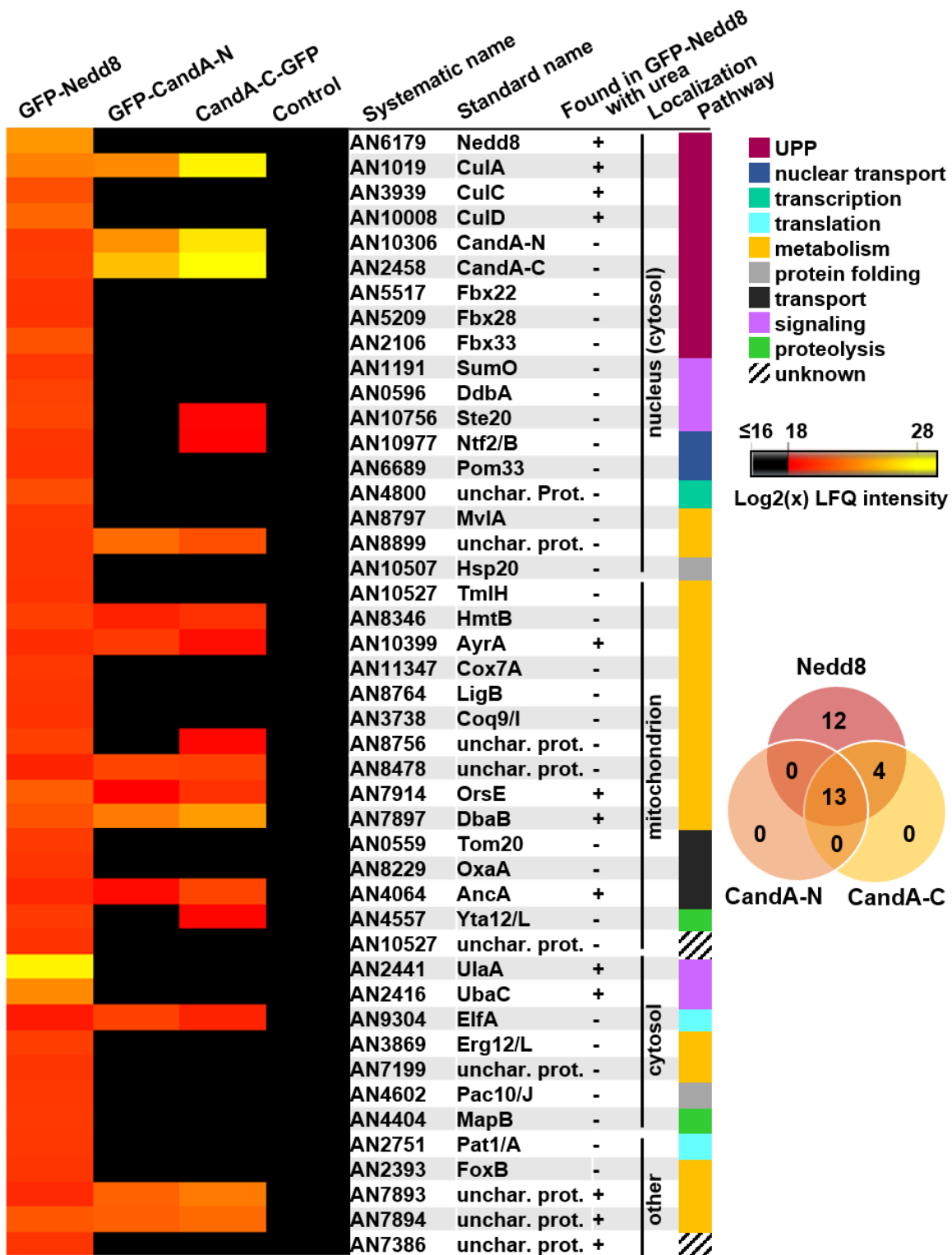


Figure 33. Nedd8 pulls CandA-N and CandA-C but not CandA-C1 under native buffer conditions. Pull-downs were performed with *A. nidulans* strains expressing GFP-Nedd8, GFP-CandA-N, CandA-C-GFP and the control strain overexpressing GFP. Samples of elution fractions were prepared for *in gel* tryptic digestion for LC-MS2 analysis. Data analysis was performed with *MaxQuant* and *Perseus* to filter proteins by minimal $\log_2(x)$ label free quantification (LFQ) intensity value of 16 for samples and maximal LFQ of 16 for controls. The heat map shows the mean value of two biological replicates of $\log_2(x)$ LFQ intensities (≤ 16 -18

not identified (black), 18-28 identified (gradient red to yellow)). Accession numbers, protein names and cellular localization are depicted right to each heat map row. Colored bars indicate the pathway where the putative interaction partners are predicted to be involved in (berry: ubiquitin proteasome system (UPS), dark blue: nuclear transport, cyan: transcription, light blue: translation, orange: metabolism, grey: protein folding, black: transport, purple: signaling, ice blue: proteolysis, black-white striped: unknown). Pull-downs of GFP-Nedd8 and the control strain were also performed in triplicates using denaturing buffers containing 8 M urea. The list of proteins was compared to GFP-Nedd8 interaction partners found under native buffer conditions. In total twelve proteins plus Nedd8 itself were identified as putative neddylated proteins marked with a plus (+, not identified in urea pull-down: -). Venn diagram depicts distribution of exclusively identified interaction partners.

Table 10. Identified proteins of Nedd8 pull-downs. Detailed information about identified proteins from the heat map (Figure 33) according to UniProt and AspGD (Cerqueira *et al.*, 2014; The UniProt Consortium, 2017) (+:found in GFP-Nedd8 pull-down with 8 M urea; - not found in GFP-Nedd8 pull-down with 8 M urea; unchar.: uncharacterized).

Systematic name	Found with urea	Standard name	Description
Nucleus (cytosol)			
AN6179	+	Nedd8	Nedd8
AN1019	+	CulA	SCF ubiquitin ligase complex subunit CulA
AN03939	+	CulC	SCF ubiquitin ligase subunit CulC
AN10008	+	CulD	Ubiquitin ligase subunit CulD
AN10306	-	CandA-N	Cullin-associated NEDD8-dissociated protein 1, N-terminal part
AN2458	-	CandA-C	Cullin-associated NEDD8-dissociated protein 1, C-terminal part
AN5517	-	Fbx22/Cdc4	F-box domain protein; cell division control protein
AN5209	-	Fbx28	Uncharacterized protein; F-box domain protein
AN2106	-	Fbx33	Uncharacterized protein; F-box domain protein
AN1191	-	SumO	Small ubiquitin-like modifier
AN0596	-	DdbA	Damaged DNA binding protein, associated to Nedd8
AN10756	-	Ste20	TORC2 signaling
AN10977	-	Ntf2/B	Uncharacterized protein; nuclear transport factor
AN6689	-	Pom33	Uncharacterized protein; nuclear pore entry
AN4800	-	Unchar.	Uncharacterized protein; WD repeat protein 32% similarity to RcoA
AN8797	-	MvIA	modulator of VeA loss

Table 10 continued

Systematic name	Found with urea	Standard name	Description
AN8899	-	Unchar.	putative 1-aminocyclopropane-1-carboxylate deaminase
AN10507	-	Hsp20	Heat shock protein Hsp20/Hsp26
Mitochondrion			
AN10527	-	TmlH,	Uncharacterized protein; trimethyllysine dioxygenase
AN8346	-	HmtB	Uncharacterized protein; oxidoreductase FAD/NAD binding
AN10399	+	AyrA	Uncharacterized protein; short-chain dehydrogenase/reductase
AN11347	-	Cox7A	Cytochrome C oxidase subunit 7A
AN8764	-	LigB	Uncharacterized protein; aromatic ring-opening dioxygenase subunit
AN3738	-	Coq9/I	Uncharacterized protein; ubiquinone biosynthetic process
AN8756	-	Unchar.	Uncharacterized protein; phenol monooxygenase
AN8478	-	Unchar.	Uncharacterized protein; zinc binding dehydrogenase
AN7914	+	OrsE	Uncharacterized protein; oxidoreductase activity, orsellinic acid secondary metabolite gene cluster
AN7897	+	DbxB	FAD binding domain protein of the <i>dba</i> secondary metabolite gene cluster
AN0559	-	Tom20	Mitochondrial import receptor subunit (Tom20)
AN08229	-	OxaA	Mitochondrial export translocase
AN4064	+	AncA	ADP, ATP carrier protein/translocator
AN4557	-	Yta12/L	Mitochondrial inner membrane AAA protease Yta12
AN10527	-	Unchar.	Uncharacterized protein; trimethyllysine dioxygenase activity, role in carnitine biosynthetic process
Cytosol			
AN2441	+	UlaA	Ubiquitin-like activating enzyme subunit
AN2416	+	UbaC	NEDD8 activating enzyme subunit
AN9304	+	ElfA	Translation elongation factor eEF-1B gamma subunit
AN3869	-	Erg12/L	Uncharacterized protein; mevalonate kinase
AN7199	-	Unchar.	Uncharacterized protein; oxidoreductase activity
AN4602	-	Pac10/J	Uncharacterized protein; prefoldin subunit 3
AN4404	-	MapB	Methionine aminopeptidase 2-1 (Peptidase M)
Other			
AN2751	-	Pat1/A	Topoisomerase II associated protein

Table 10 continued

Systematic name	Found with urea	Standard name	Description
AN2393	-	FoxB	Uncharacterized protein; short chain oxidoreductase/dehydrogenase
AN7893	+	Unchar.	Uncharacterized protein; oxidoreductase with iron
AN7894	+	Unchar.	Uncharacterized protein; alpha-beta barrel and YCII domain predict enzymatic function
AN7386	+	Unchar.	Uncharacterized protein; putative transmembrane domain protein

The CandA-Nedd8 interaction was further analyzed as *in vitro* pull-down experiments showed that Nedd8 binds CandA-C and CandA-N. The aim was to examine whether the CandA and Nedd8 interaction is due to covalent binding, a non-covalent protein-protein interaction or if the interface is dependent on other interacting proteins, for example through CulA. The localization of GFP-Nedd8 was investigated and fluorescence signals of the GFP-Nedd8 fusion protein were observed in nuclei and cytoplasm (Figure 34A) like for CandA proteins (Figure 21). BiFC assays with *A. nidulans* strains expressing CandA-N, CandA-C or CandA-C1 tagged to one half of YFP and Nedd8 carrying the other half of YFP were conducted to identify a direct protein-protein interaction. CandA-N, CandA-C and CandA-C1 together with Nedd8 emitted a signal mainly localized to the nuclei and partly in the cytoplasm, different to controls with only one half of YFP tagged to the protein of interest (Figure 34B, C). Comparison of BiFC fluorescence from CandA-N, CandA-C and CandA-C1 with Nedd8 suggest similar nuclear localization signals.

In vitro pull-downs and BiFC experiments showed an interaction of CandA with Nedd8. In a possible model CandA bound to CulA interacts with Nedd8 either through neddylation or protein-protein interaction to keep the Nedd8 close to CulA for the next cycle of neddylation. Microscopy of strains expressing BiFC constructs and carrying a *csnE* deletion, which leads to deneddylation deficiency was performed to prove this hypothesis (Beckmann *et al.*, 2015). For these strains fluorescence signals could be detected in nuclei (Figure 34D). These observations show that CandA interacts with Nedd8 independent from CandA-CulA binding as CandA cannot bind to neddylated CulA. This underlines the finding that CandA is required for CulA neddylation in a way that CandA might bind Nedd8 or is itself neddylated to recycle Nedd8 to CulA. This mechanism would then ensure the activity of CRL for labeling substrates with ubiquitin for degradation by the 26S proteasome.

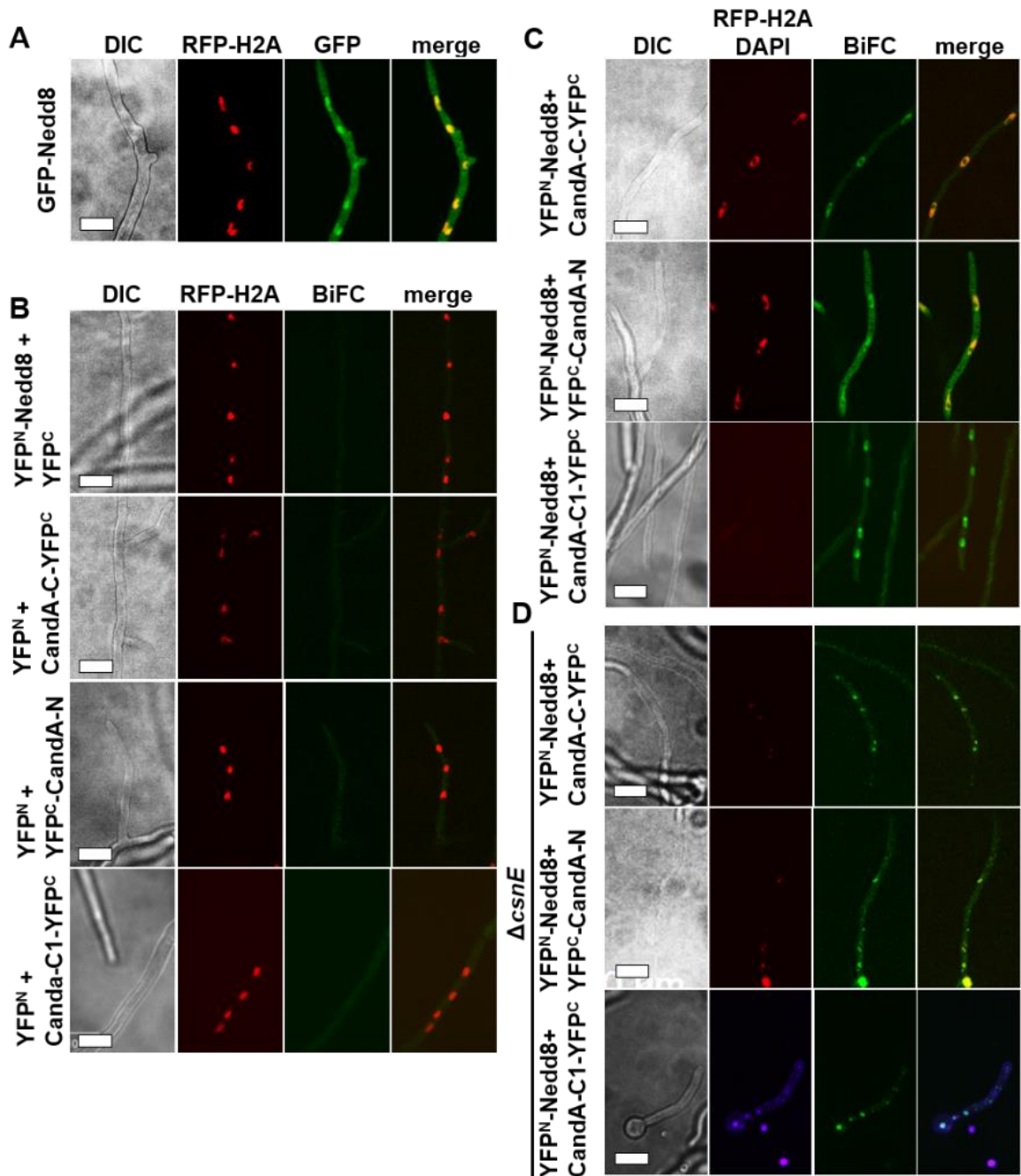


Figure 34. Nedd8 interacts with CandA-N, CandA-C and CandA-C1 in nuclei and cytoplasm. **A** GFP-Nedd8 is localized in nuclei and cytoplasm of 20 hours old hyphae as GFP signals co-localize with RFP-H2A. **B** Interaction of Nedd8 with CandA-C and CandA-N was analyzed by bimolecular fluorescence complementation (BiFC). The control strains expressing only one half of YFP fused to Nedd8, CandA-C, CandA-N or CandA-C1 and the other half of YFP was expressed as single protein did not show signals. **C** Signals of Nedd8 interacting with CandA-C or CandA-C1 were detected mainly in the nuclei whereas Nedd8-CandA-N interaction was found in nuclei and cytoplasm. **D** Similar interaction could be observed in BiFC strains deleted in *csnE* (RFP-H2A or DAPI were used to stain nuclei; size bars: 10 μ m).

Cullins are the best-known targets for the post-translational modification with Nedd8 and not much is known so far about other neddylation targets. Western hybridization of protein crude extracts with Nedd8 antibody showed several bands of putative neddylated proteins (Schinke *et al.*, 2016). So far, no other neddylation target could be identified in *A. nidulans*. Due to the observed interaction of CandA with Nedd8 it was analyzed whether CandA itself is neddylated. CandA-N has a putative neddylation targeted lysine residue in its first HEAT repeat, which is blocking the Nedd8 binding site of cullins.

Pull-downs were performed under denaturing conditions applying 8 M urea to the buffers used during pull-down experiments to dissect between covalent and non-covalent protein interactions. Samples were measured with LC-MS and compared to samples generated under native buffer conditions. Under denaturing conditions CandA subunits could not be identified as interaction partners of Nedd8 (Figure 33), suggesting that CandA is not covalently neddylated. In total twelve proteins pulled under native conditions were also identified in the pull-downs with urea. From the UPS pathway CulA, CulC, CulD, UlaA and UbaC were identified when urea buffers were used, which was expected as they are known to be covalently attached to Nedd8. Furthermore, the secondary metabolite gene cluster encoded proteins DbaB and OrsE, a putative short chain dehydrogenase/reductase AyrA and ADP/ATP carrier protein AncA of the mitochondrion were identified as putatively covalently bound to Nedd8. There were also three uncharacterized proteins found: AN7893 (putative oxidoreductase with iron ligand), AN7894 (putative alpha-beta barrel and YCII domain protein) and AN7386 (no conserved domains found). These results show, that CandA and Nedd8 interact by a non-covalent protein-protein interface. This interaction is independent from CandA binding to CulA and the observed interaction is also not due to CandA-C NLS mediated nuclear import. The consequence of the observed CandA~Nedd8 interaction needs to be analyzed to investigate whether the interaction might be required for the next cullin-neddylation cycle. Besides the known cullin and Nedd8 activating enzyme targets the pull-down performed under denaturing conditions could identify putative covalently neddylated proteins of secondary and primary metabolism.

3.3 The CandA-complex and fungal growth, development and secondary metabolism

3.3.1 CandA promotes spore germination

A. fumigatus is very robust and adaptable to many stressors and can cope with different gene deletions without showing altered phenotype (Gsaller *et al.*, 2016; Jöhnk *et al.*, 2016; Hagiwara *et al.*, 2017; Paulussen *et al.*, 2017). The question was addressed whether *A. fumigatus* $\Delta canA$ mutant strains show growth and developmental defects. For an overview of similarities and differences between *A. fumigatus canA* and *A. nidulans candA* mutants, both species were compared with each other. The *canA* deletion mutant strain showed delayed germination, growth and development. A hyphal network with a diameter of ~4 mm was only observed after three days of incubation on solid medium at 37°C (Figure 35A). This colony grew slowly and after seven days the diameter was around 6 mm and the beginning of conidia formation could be observed (Figure 35A). After 14 days of incubation the colony had approximately the size of a 3 days old wild type colony (Figure 36). The same phenotype could be observed for *canA* ^{$\Delta exon1$} strain, which is only missing the sequence part encoding the N-terminal extension, corresponding to *A. nidulans* CandA-C1. (Figure 35A).

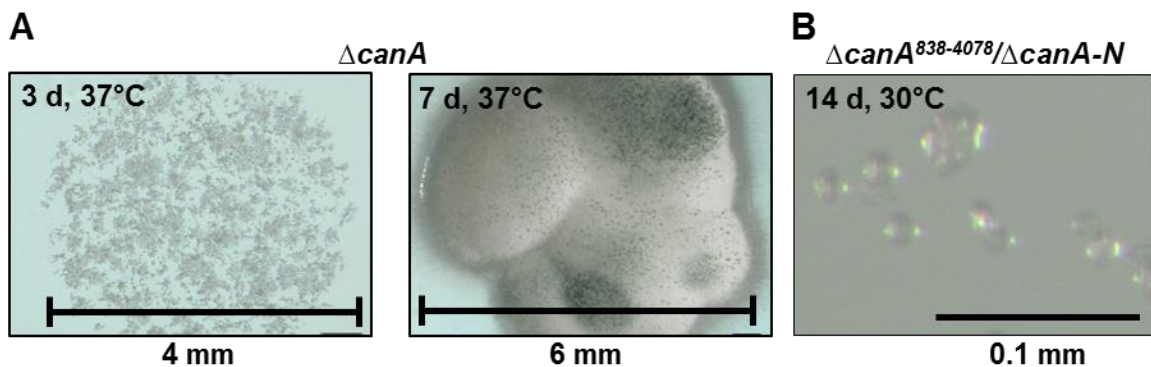


Figure 35. *A. fumigatus canA* mutants are delayed in development. A Micrographs of spots of the $\Delta canA$ strain after three and seven days of growth at 37°C show reduced growth. The formation of a hyphal network starts after three days with a colony diameter of around 4 mm. After seven days the colony diameter reached 6 mm and conidiospore and aerial hyphae production was initiated. **B** Micrograph of $\Delta canA^{838-4078}/\Delta canA-N$ shows colorless conidiospores, which did not germinate after 14 days of incubation on solid medium at 30°C.

Furthermore, we investigated the phenotypes of knockout strains of $\Delta canA^{838-4078}$ (C-terminal domain corresponds to An_*canA*-C) and $\Delta canA$ -N. Deletion of *canA*⁸³⁸⁻⁴⁰⁷⁸ resulted in different phenotype than the *canA* ^{$\Delta exon1$} or $\Delta canA$ full gene deletions. Single and double deletion of $\Delta canA^{838-4078}$ and $\Delta canA$ -N were delayed in conidiospore production as the colonies have a white halo of aerial hyphae and immature white conidiospores when the strains were incubated at 37°C (Figure 36). After 7 days wild type showed a dark green halo in the colony, which was not observed for $\Delta canA^{838-4078}$ and $\Delta canA^{838-4078}/canA$ -N strains, supposing that CanA⁸³⁸⁻⁴⁰⁷⁸ and CanA-N are required for appropriate conidiospore production.

Growth of *A. fumigatus* is slower at temperatures below its optimum of 37°C (Krijgsheld *et al.*, 2013; Kwon-Chung and Sugui, 2013). Subsequently, it is convenient to follow the different phenotypes caused by delayed development at lower temperature (30°C) and higher temperature (42°C). At both temperatures the wild type had reduced colony size compared to cultivation at its temperature optimum (Figure 36). Strains deleted in *canA* ^{$\Delta exon1$} and *canA* show the same growth defect at 30°C as observed at 37°C. Surprisingly, deletion strains $\Delta canA^{838-4078}$, $\Delta canA$ -N and $\Delta canA$ -N/ $\Delta canA^{838-4078}$, which grow similarly to wild type at 37°C, did not form colonies after three days of incubation at 30°C. Increased incubation time of up to seven days resulted in colony formation of both single deletion strains, but not for the double deletion strain (Figure 36). This mutant was still unable to germinate after 14 days of incubation at 30°C (Figure 35B and Figure 36). The same strains were also incubated at 42°C for three and five days. Longer incubation was not possible due to condensed water that accumulated on the lid of the petri dish and resulted in secondary colonies when water drops with spores fell on the agar plate. At 42°C *canA* ^{$\Delta exon1$} and $\Delta canA$ did not germinate even after five days of incubation, whereas $\Delta canA^{838-4078}$, $\Delta canA$ -N and $\Delta canA$ -N/ $\Delta canA^{838-4078}$ strains showed wild type-like growth (Figure 36). These data show, that the N-terminal domain of CanA is required for vegetative growth and conidia formation. Asexual spore germination at 30°C is dependent on the CanA C-terminal domain together with CanA-N. The CanA N-terminal insertion is required for germination at 42°C.

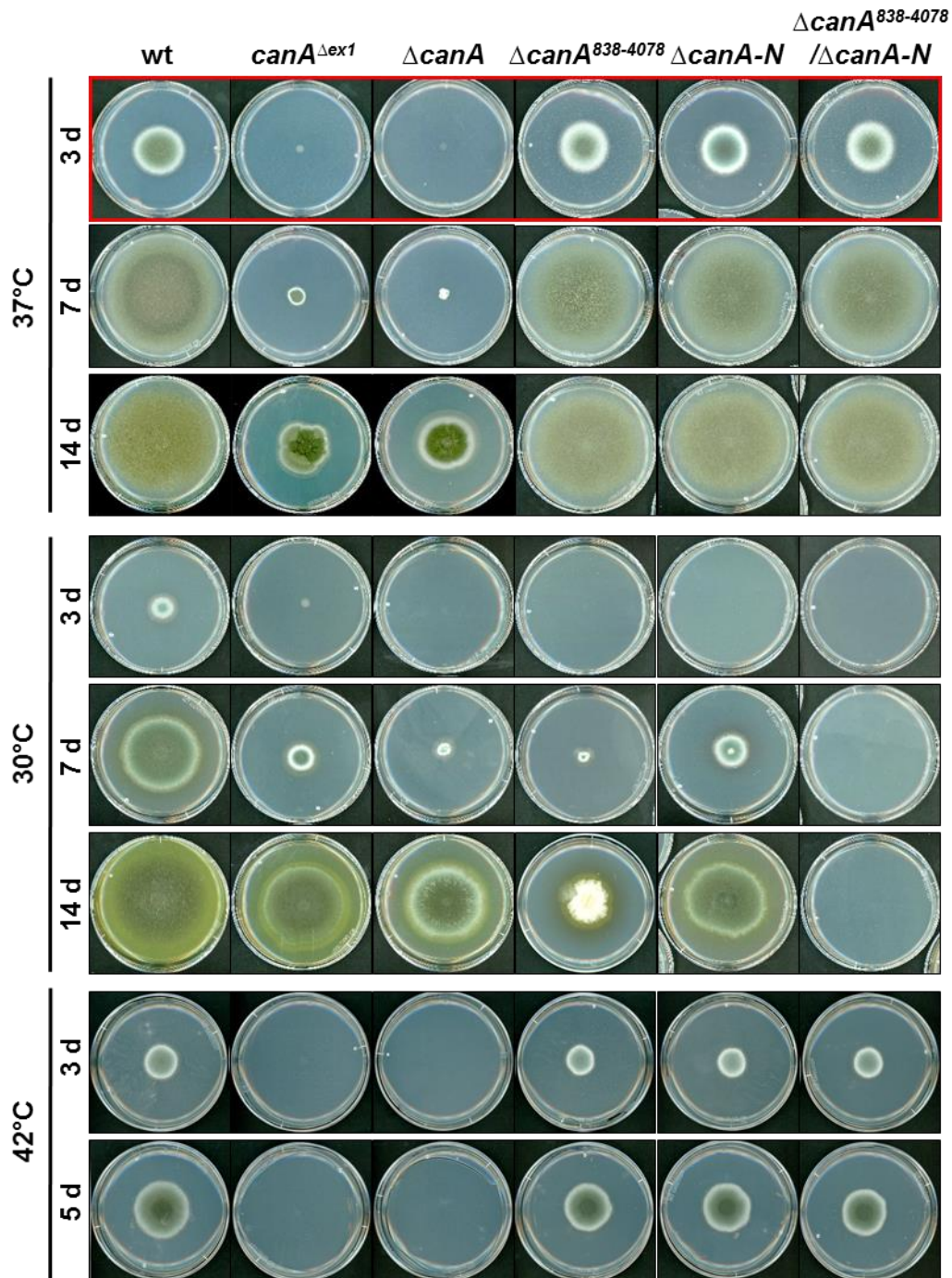


Figure 36. *A. fumigatus* CanA proteins are required for germination of asexual spores at different temperatures. *A. fumigatus* wild type and *canA* mutant strains were incubated at 30°C and 37°C for 3, 7 and 14 days and at 42°C for 3 and 5 days. Deletion of *canA* exon1 (corresponding to An_*candA*-C1) or full *canA* gene deletion result in reduced growth at 30 and 37°C and abolished growth at 42°C. Deletion of *canA*⁸³⁸⁻⁴⁰⁷⁸ (corresponding to An_*candA*-C), *canA*-N or the double deletion Δ*canA*⁸³⁸⁻⁴⁰⁷⁸/Δ*canA*-N have slightly delayed conidiospore production at 37°C and reduced growth at 30°C. The double deletion could not germinate at 30°C. These mutants grew like wild type at 42°C. Plate pictures from 3 days at 37°C are highlighted in red as standard observation conditions.

A. nidulans candA mutant strains were incubated at the same temperatures to compare growth and development of *A. fumigatus canA* with *A. nidulans candA* phenotypes. Figure 37 shows *A. nidulans* phenotypes of five days asexual and seven and fourteen days sexual development. The *candA-C1* deletion strain showed similar growth defects as observed for the corresponding *A. fumigatus canA^{Δexon1}* mutant. $\Delta candA-N$, $\Delta candA-C$ and the double deletion $\Delta candA-N/A-C$ never showed germination defects different to their corresponding *A. fumigatus* mutants. Deletion strains of $\Delta candA-C1$ and $\Delta candA-C1/igr$ were impaired in conidia germination at 42°C, similar as observed for the *A. fumigatus canA^{Δexon1}* mutant strain.

In asexual and sexual development, the *candA-C1* deletion strain had improved growth at 30°C when compared to 37°C. All other strains had smaller colonies at 30 and 42°C than at 37°C (Figure 37). Secondary metabolite production of *candA-N*, *candA-C* and the double deletion was similar at 30 and 37°C but at higher temperature the colony secreted metabolites that colored the agar yellow after 14 days. These three mutant strains also developed increased production of aerial hyphae, which accumulated pinkish pigments in the center of the colony whereas the outer ring was rather grey. Together with the dark brown color of the agar direct beneath the hyphal network, the colony had a colorful phenotype. These data show that *CandA-C1* is required for properly timed conidia germination at temperatures above the 37°C. *CandA-N* and *CandA-C* have stronger impact on secondary metabolism control at 42°C than at 30 and 37°C.

Concluding from this data the *A. fumigatus* *CanA* N-terminal extension and the *A. nidulans* *CandA-C1* protein have conserved functions in conidia germination as both are essential for germination at 42°C and show slower germination, growth and development at 37°C. *CanA/CandA-C1* impact on asexual conidiospore development is more severe in *A. fumigatus* than in *A. nidulans*. *CandA-N*, *CandA-C* as well as their orthologs *CanA* and *CanA-N* support conidia formation. The *A. fumigatus* dimeric *CanA* complex is necessary for conidia germination at 30°C, indicating that *A. nidulans* can cope better with lower temperatures than its relative *A. fumigatus*.

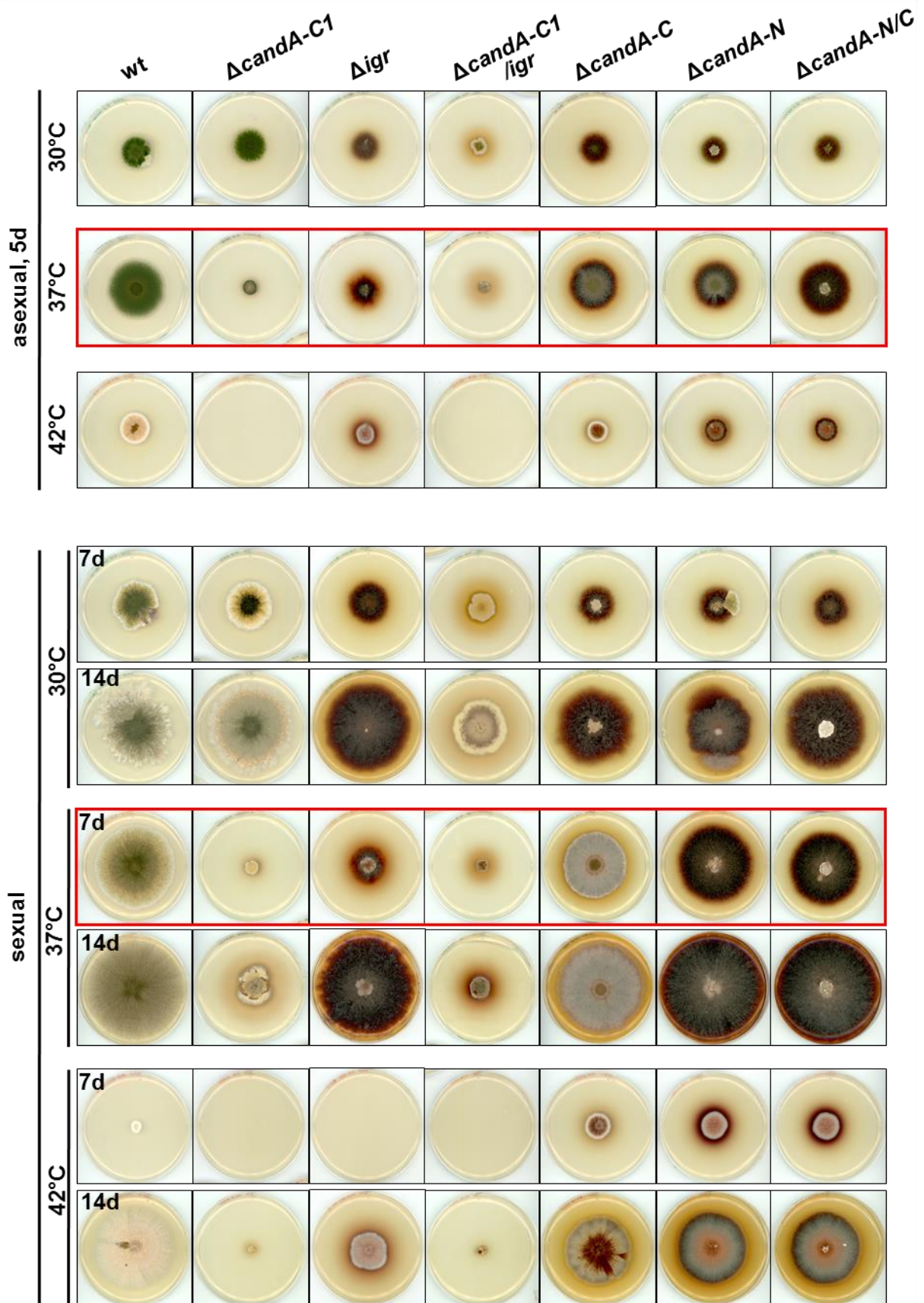


Figure 37. For description, see next page.

Figure 37. *A. nidulans* CandA-C1 is required for spore germination at 42°C. *A. nidulans* wild type and *candA* mutant strains were incubated for 5 days under asexual and 7 and 14 days under sexual promoting conditions at 30, 37 and 42°C. Colonies at 30 and 42°C appeared smaller than at 37°C except for $\Delta candA-C1$ which was growing better at 30°C than at 37°C but *candA-C1* and *igr* mutants were unable to germinate at 42°C. Increased secondary metabolism and aerial hyphae production can be observed for *candA-C*, *candA-N* and the double deletion strain when incubated at 42°C. Plate pictures from 5 days at 37°C, asexual and 7 days at 37°C, sexual are highlighted in red as standard observation conditions.

3.3.2 CandA-C1 specifically promotes vegetative growth and can be exchanged between *A. nidulans* and *A. fumigatus*

Deletion of *A. nidulans candA-C1* resulted in a strain with small colony growth (Figure 37 and Figure 38). The growth defective phenotype of *candA-C1* was then compared to a strain with deleted start codon of *candA-C1* ORF ($\Delta^{ATG}candA-C1$) and to a mutant, which carries a deletion of the 269 bp *intergenic region* (Figure 38A). The resulting phenotype of the $\Delta^{ATG}candA-C1$ mutant strain was similar to $\Delta candA-C1$ full gene deletion (Figure 38B). This result indicates that the translation of CandA-C1 depends on the predicted ATG start codon.

The open reading frames of *candA-C1* and *candA-C* are separated by an *intergenic region*. It was of interest if the *intergenic region* is required for development of *A. nidulans* in a *candA* dependent manner. Therefore, an *igr* deletion strain was generated which was lacking the 269 bp from the first nucleotide after the TGA stop codon of *candA-C1* to the last nucleotide before the ATG start codon of *candA-C* (Figure 38A). Additionally, a double deletion strain of $\Delta candA-C1/igr$ was generated. Both deletion strains showed similar growth defects compared to *candA-C1* single deletion strain in asexual development (Figure 38B). The phenotype of Δigr is similar to $\Delta candA-C$ and $\Delta candA-C1/igr$ resembles a $\Delta candA-C1$ single deletion phenotype at different temperatures (Figure 37).

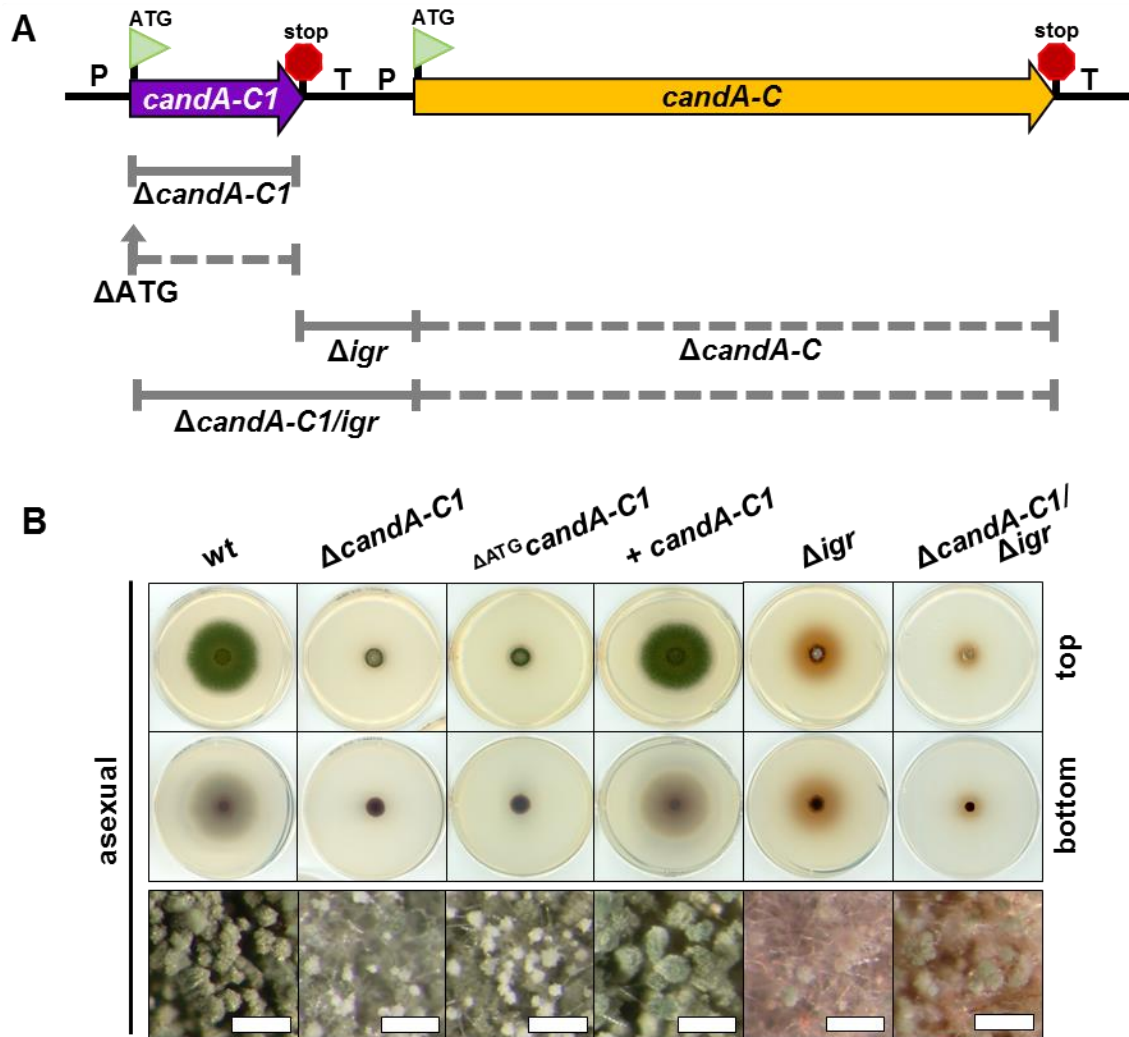


Figure 38. *candA-C1* and *igr* are required for growth and sexual development and the *igr* is possibly the promoter for *candA-C*. **A** Schema of *candA-C1* and *candA-C* gene loci with putative promoter (P) and terminator (T) regions, start codons (green flag with ATG) and stop codons (red stop sign). Deleted sequences are indicated with grey solid lines and broken lines indicate putative expression defects by promoter region deletion. **B** Strains were point inoculated and incubated under asexual development promoting conditions at 37°C for five days, respectively. The $\Delta ATG candA-C1$, *candA-C1*, *igr* and *candA-C1/igr* deletion strains exhibit similar growth defects. The *igr* and *candA-C1/igr* deletion mutant strains show only few conidia but accumulate red and brown secondary metabolites in different amounts (size bars: 100 μ m).

The impact of *A. nidulans* *CandA-C1* on vegetative growth was compared to the phenotypes of *candA-N* and *candA-C* deletion strains. In contrast to wild type, Δ *candA-N* and Δ *candA-C*, the deletion of *candA-C1* shows significantly reduced colony size with only 1 cm in diameter (Figure 39A, B).

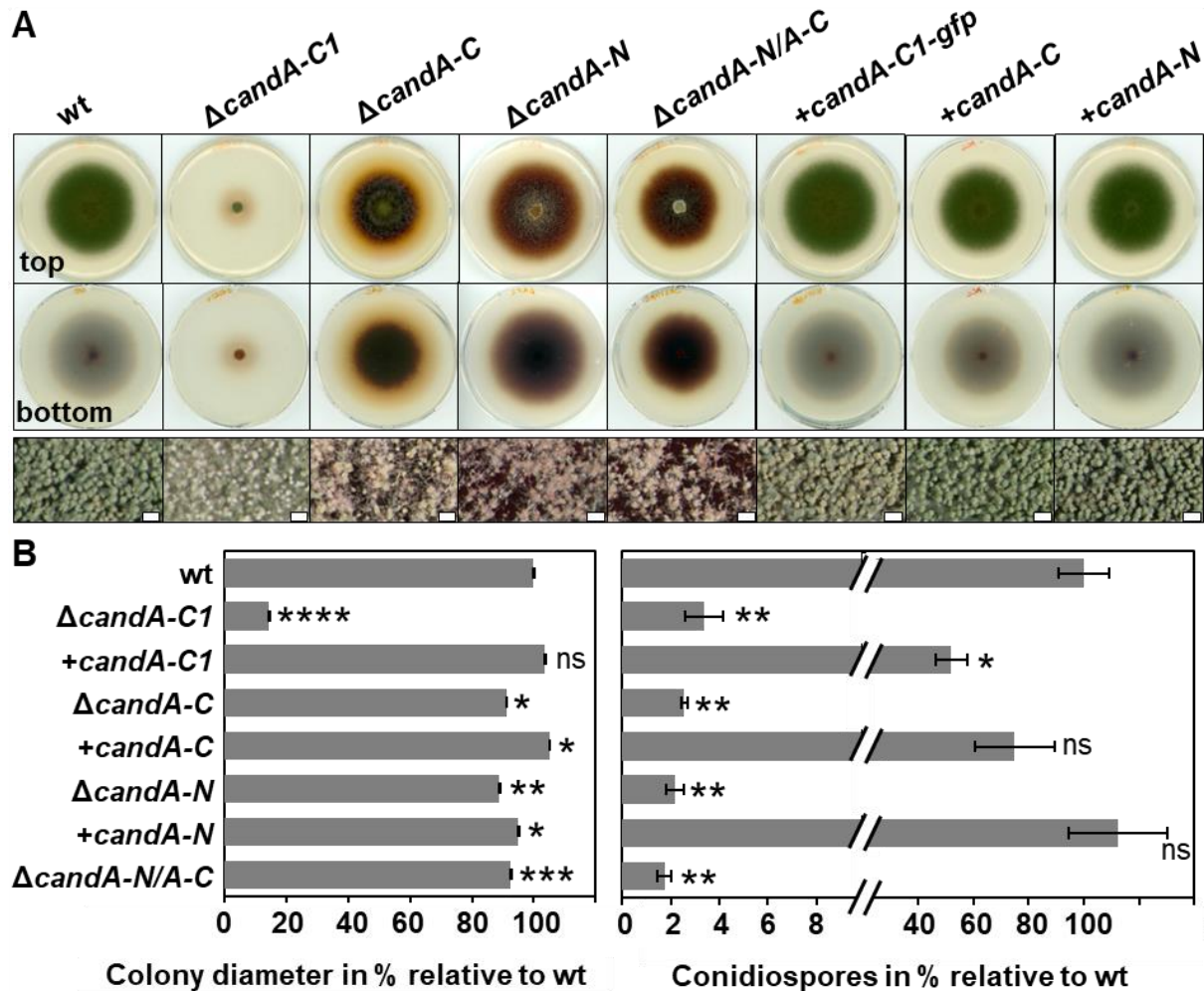


Figure 39. Asexual development is dependent on *candA-C1*. **A** Strains were point inoculated and incubated at 37°C in light for 5 days. A reduced colony radius of *candA-C1* deletion strain compared to *candA-C*, *candA-N* or double *candA-N/A-C* deletion strains, wild type and complementation strains is shown. Deletion strain of *candA-C1* forms many green and white conidia different to almost diminished conidia production in *candA-N/A-C* mutants. Conidia of Δ *candA-N*, Δ *candA-C* and Δ *candA-N/A-C* had a red pigmentation. A brownish secondary metabolite secreted in the agar was more prominent in Δ *candA-N* and Δ *candA-C* strains than in Δ *candA-C1*. (size bars: 100 μ m). **B** Quantification of colony diameter and conidia amount after 5 days of asexual growth in percentage (%) relative to wild type. Error bars represent the standard error of the mean (SEM) (n=3), *p*-values: ns: *p* > 0.05, *: *p* \leq 0.05, **: *p* \leq 0.01, ***: *p* \leq 0.001, ****: *p* \leq 0.0001.

candA-N and *candA-C* single as well as the double deletion strains had the same colony diameter as wild type. *CandA* deletion strains were complemented with *in locus* integration of the respective genes. All three strains could be complemented as the respective strains showed wild type like development. *candA-C1* deletion strain was complemented *in locus* with a natively expressed C-terminal *gfp* fusion (*candA-C1-gfp*) restoring the phenotype to wild type like growth and development.

CandA-C1 is important in germination and vegetative growth different to *CandA-N* and *CandA-C*, which deletion phenotypes have wild type-like vegetative growth. Comparison of asexual development of the *candA-C1*, *candA-C* and *candA-N* mutant strains showed that *candA-N* and *candA-C* mutants have visibly less asexual conidiospores than the *candA-C1* mutant (Figure 39A). Microscopic examination of the colony of Δ *candA-N* and Δ *candA-C* strains revealed only a few conidia, which are partially colored with a red secondary metabolite (Figure 39A). The *candA-C1* deletion strain showed next to green mature conidia also white colored immature conidia. Asexual spore quantification revealed that the total amount of spores in a five-day old asexually developed colony of *candA-C1* deletion strain had only marginally more conidia than *candA-N*, *candA-C* or *candA-N/A-C*. All these deletion strains had approximately 30 times less conidiospores than wild type and complementation strains (Figure 39B).

Comparison of conidia formation of the *candA-C1* deletion strain with the *igr* and *candA-C1/igr* double deletion strains revealed that the deletion of *igr* in combination with *candA-C1* appeared to produce less conidia than Δ *candA-C1* alone but more than the single deletion of *igr* (Figure 38B). These results showed that *CandA-N* and *CandA-C* are required for conidiophore production. *CandA-C1* is also necessary for sufficient conidia production but by supporting vegetative growth that then allows higher biomass and in turn increased generation of conidiophores. Furthermore, *CandA-C1* controls conidia coloring. The *igr* seems to contain the promoter sequence for *candA-C* expression and putatively also the terminator region of *candA-C1* which can be explained by the observed growth defect of the *igr* deletion mutant.

Vegetative growth was analyzed in a strain, which expressed *candA-C1:gfp in locus* with a nitrate promoter. This overexpression *candA-C1:gfp* strain had wild type-like growth and development (Figure 40A). It was examined, which effect the overexpression of *candA-C1:gfp* has on growth and development in strains lacking *candA-N* and *candA-C*. Gene expression levels of overexpression *candA-C1:gfp* in *candA-N* and *candA-C* single deletion strains were like overexpression *candA-C1:gfp* in wild type background (around 40-60 times upregulated; Figure 40B). The colony radius of Δ *candA-N/OE candA-C1* was not altered and like observed in the Δ *candA-N* strain (Figure 40A, C). The colony radius was reduced in a Δ *candA-C* strain overexpressing *candA-C1:gfp*. Double deletion of both *candA-N/A-C* subunits and simultaneous overexpression of *candA-C1:gfp* resulted in the same growth reduction as

observed for $\Delta candA-C/OE candA-C1:gfp$ (Figure 40A, C). These data suggest that an appropriate amount of CandA-C1 and the presence of CandA-C are required for vegetative growth.

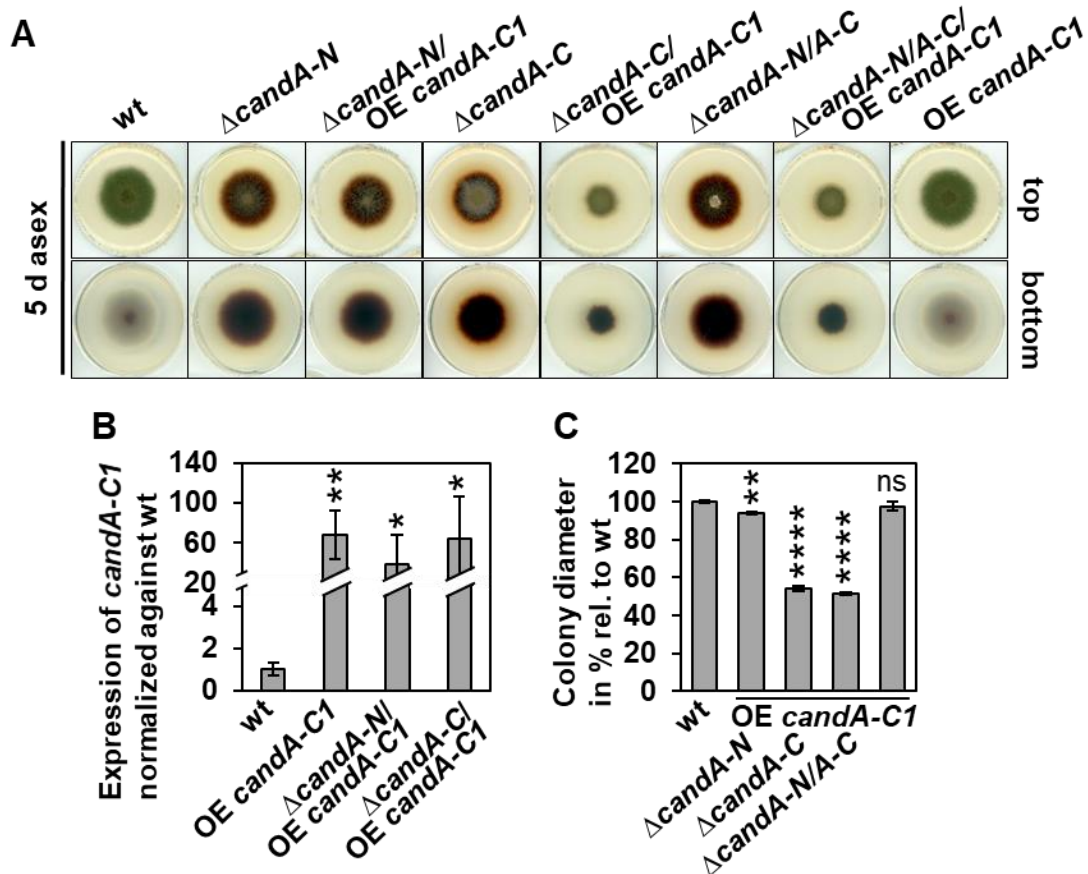


Figure 40. Overexpression of *candA-C1* reduces the colony growth of *candA-C* defective mutants. **A** Asexual colony growth was analyzed after 5 days of incubation at 37°C in light. Overexpression *candA-C1:gfp* does not alter the phenotype in wild type background neither in a $\Delta candA-N$ background strain. Deletion of *candA-C* with overexpression of *candA-C1:gfp* shows reduced growth but green conidiospores compared to the overexpression *candA-C1:gfp* in a *candA-N* deletion background strain which has mostly red colored hyphae. **B** Expression levels of *candA-C1* in wild type and *candA-N* as well as *candA-C* deletion background were analyzed by qRT-PCR relative to wild type *candA-C1* expression. *h2A* served as housekeeping gene. Overexpression levels of *candA-C1* are around 50-times higher in mutant strains compared to wild type. (n=2) **C** Measurement of colony diameter after 5 days of asexual development (n=3). Error bars represent the standard error of the mean (SEM) and significance was calculated relative to wild type with *p*-values: ns: $p > 0.05$, *: $p \leq 0.05$, **: $p \leq 0.01$ ****: $p \leq 0.0001$.

The two separate *A. nidulans* *candA-C* genes are fused into a single gene in *A. fumigatus*, which encodes a single polypeptide with a CandA-C1-like 200 amino acids long N-terminal extension (NTE, encoded in the first exon) followed by an CandA-C-like C-terminal domain (CanA^{CTD}) (Figure 41A). The cellular function of CandA-C1 as separate protein or as domain within a fused protein was analyzed by deleting the corresponding gene loci in *A. fumigatus* as well as *A. nidulans* and by exchanging both genomic sequences with their respective orthologous DNA sequences.

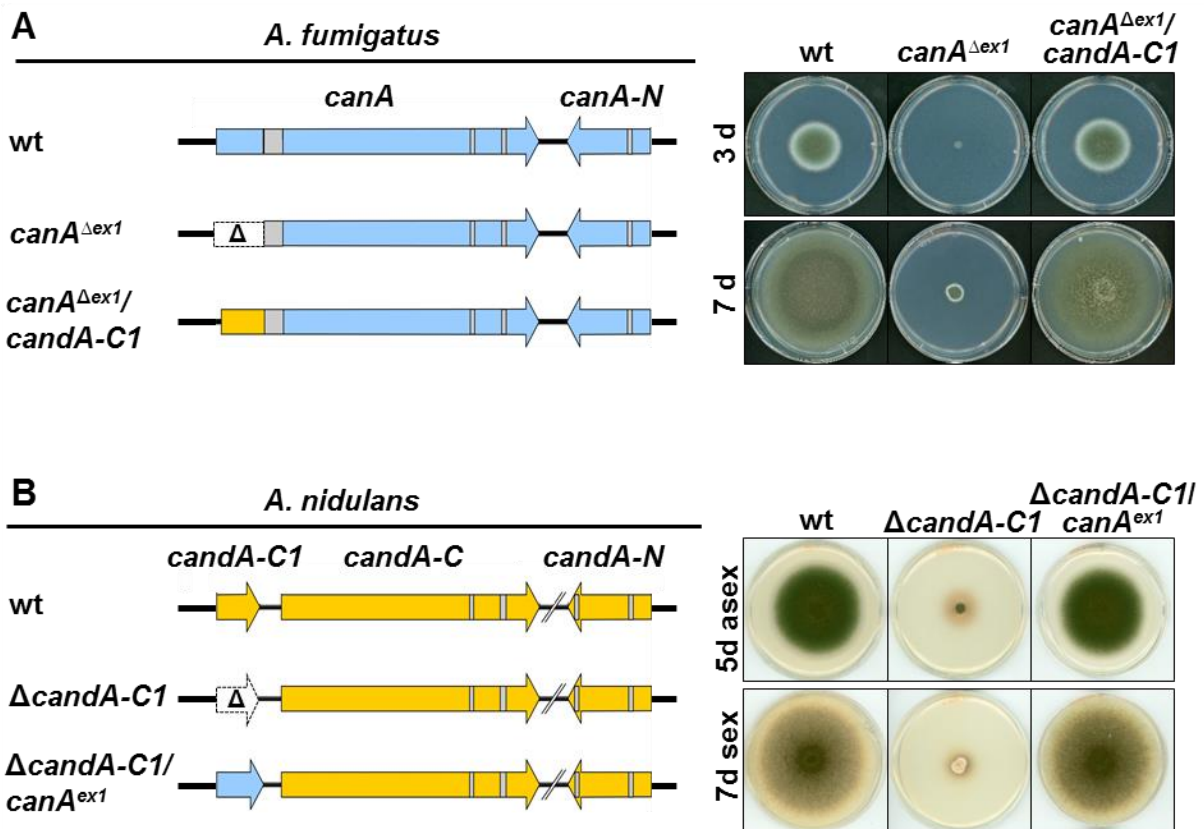


Figure 41. *A. fumigatus* and *A. nidulans* gene orthologs for *candA-C1* complement each other. **A** Genome map of *A. fumigatus* wild type *canA* and *canA-N* (blue) as well as deletion of *exon 1* mutant and replacement of *exon 1* with *A. nidulans candA-C1* sequence (yellow). Introns are colored in grey. For asexual phenotypal analysis *A. fumigatus* wild type and mutant strains were incubated for 3 or 7 days at 37°C. Deletion of *canA^{ex1}* causes drastic growth defects. Introduction of the *A. nidulans candA-C1* sequence into the locus of *A. fumigatus canA^{ex1}* resulted in a wild type like phenotype. **B** Genome map of *A. nidulans candA-C1*, *candA-C* and *candA-N* (yellow) in wild type, *candA-C1* deletion construct and *candA-C1* replacement with *A. fumigatus canA exon1* (blue). Plates were incubated at 37°C for 5 days and asexual development inducing conditions or for 7 days sexual development inducing conditions. Mutant strain deleted in *candA-C1* has similar growth defects as observed for corresponding deletion in *A. fumigatus*. Replacement of *candA-C1* with *A. fumigatus canA^{ex1}* sequence resulted in wild type like asexual and sexual development.

Deletion of the first exon of *Af_canA* revealed significant reduction in colony growth, which can be observed after three and seven days at 37°C (Figure 41A). A similar growth defect was observed when the *candA-C1* ORF was deleted in *A. nidulans* (Figure 41B).

It was then further tested if the genomic sequence of *candA-C1* and *exon1* of *Af_canA* are convertible as their protein identity is 58%. Therefore, an *A. fumigatus* strain in which *candA-C1* was integrated into the genomic locus of *Af_canA exon1*, and an *A. nidulans* strain, where *Af_canA exon1* was introduced into the genomic locus of *candA-C1* were generated (Figure 41A, B). Both mutant strains had wild type-like appearance (Figure 41A, B). Therefore, both sequences are interchangeable due to their similarity, indicating that they functionally complement each other.

3.3.3 CsnE and CandA are required for vegetative growth and development in *A. nidulans*

The effect of growth and development was also analyzed in strains, which are completely deficient in CRL regulation due to inactive CSN and missing CandA. CSN mutant strains were previously characterized (Busch *et al.*, 2003, 2007; Beckmann *et al.*, 2015). A marker recycled *csnE* deletion strain was constructed for this study and had similar phenotype as reported for *csnE* deletions in other wild type background strains. It shows reduced conidia formation, accumulation of dark brown secondary metabolites and cannot reproduce sexually (Figure 42). However, the marker free *csnE* deletion strain from this study never showed production of primordia as observed for Δ *candA* strains. Primordia were observed in a Δ *csnE* strain with *pyrG* marker, encoding a gene for *uridine/uracil* synthesis. In this strain *csnE* was only partially deleted (Busch *et al.*, 2003). This strain can develop one step further in the sexual cycle than observed for *candA* or the marker recycled *csnE* deletion strains.

Double deletion of *csnE* subunit and *candA-N* elucidates a *candA-N* single deletion phenotype with additional growth defect as the colony appears to be smaller than that of wild type or Δ *csnE* when incubated at asexual development inducing conditions (Figure 42). The *csnE* double deletion strain with *candA-C* looks different compared to both single deletions. It produces a complex network of aerial hyphae and forms greenish colored conidia in the center of the colony after five days of incubation under asexual development promoting conditions (Figure 42). A triple deletion strain Δ *csnE/candA-N/C* only formed a small colony during asexual development, which did not grow bigger after seven days of sexual development promoting conditions. Both double deletion strains depict aerial hyphae but rarely any structures of sexual development. The color of secondary metabolites secreted by Δ *csnE/candA-C* is more yellowish than observed for Δ *csnE/candA-N* or single mutants. Together these observations on *csnE/candA* deletion strain phenotypes can be described as

similar but *CandA* has an even stronger impact on development than *CsnE*. All in all, these results underline the functional dependence and close relation of both complexes in the CRL cycle.

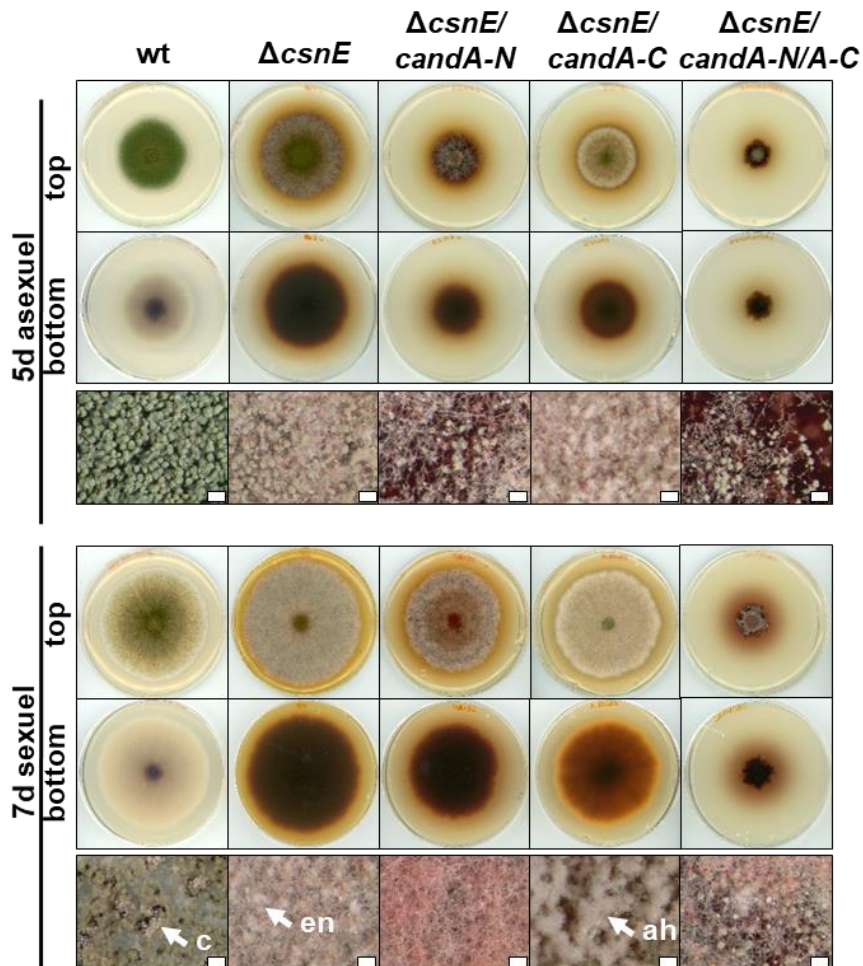


Figure 42. *CandA* and *CsnE* together are required for growth, development and coordinated secondary metabolism. Strains were incubated at 37°C for five days in light and oxygen was available to promote asexual development or for seven days in dark with limited oxygen for sexual development. Micrographs give a detailed view of colony morphology and depict conidia, aerial hyphae (ah), early nests (en) or cleistothecia (c). All deletion strains have reduced asexual conidia formation and produce dark brown colored secondary metabolites. In sexual development cleistothecia (c) formation is impaired by the mutant strains, which form only aerial hyphae and early nests (en) (size bars: 100 μ m).

3.3.4 *A. nidulans* CandA promotes accurate mitochondria development

Phenotypical characterization of *candA* deletion strains indicated reduced growth and conidiospore development as well as altered secondary metabolism. Appropriate growth and development are directly linked with energy consumption and energy supply is dependent on optimal mitochondrial activity that relies on intact long filamentous structures. Therefore, the mitochondrial structures of wild type and mutant strains were investigated.

Fluorescence microscopy was performed with MitoTracker stained hyphae 10 and 24 hours after inoculation. Wild type and the overexpression CandA-C1 strain formed long mitochondrial filaments. Deletion of *candA-C1* and *candA-N* resulted in fragmented mitochondria at both time points whereas in Δ *candA-C* mitochondrial fragmentation was observed in 24-hour old hyphae (Figure 43). These results show that CandA proteins are required for intact mitochondria and especially the importance of CandA-C1 in hyphal growth seems to be connected to mitochondrial integrity.

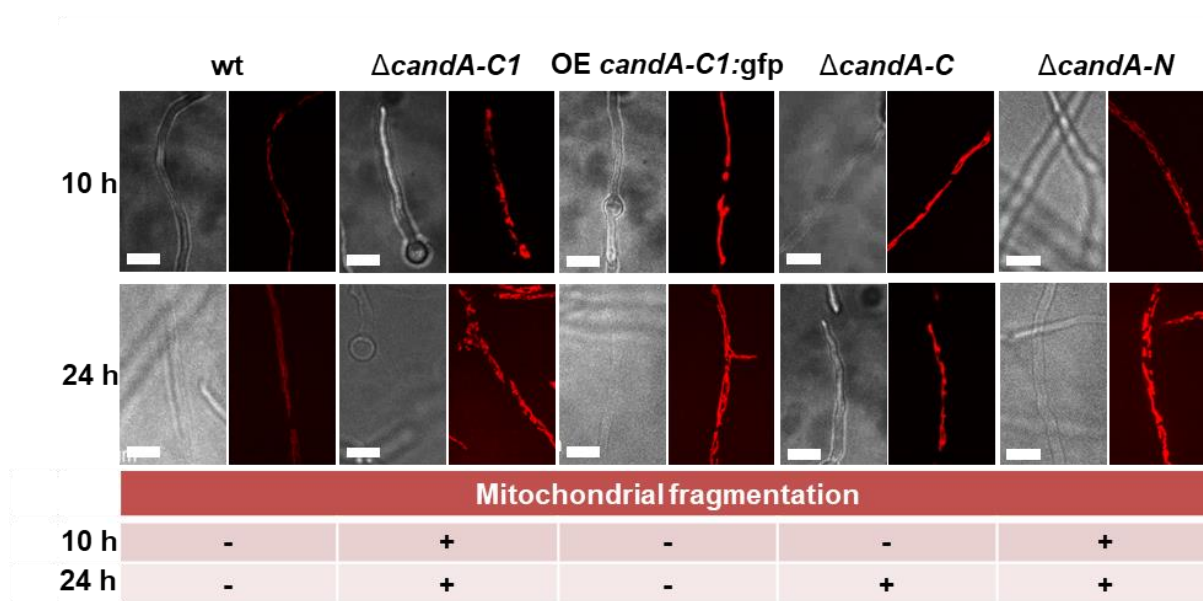


Figure 43. Mitochondria of Δ *candA* deletion strains are fragmented. Confocal fluorescence microscopy was performed with wild type, *candA* deletion strains and overexpression *candA-C1:gfp* strain after 10 and 24 hours (h) of incubation in liquid medium at 37°C. Hyphae were stained with MitoTracker Red. Pictures were taken with differential interference contrast (DIC) and red fluorescent protein (RFP) channel. Whereas wild type and OE strain show long mitochondrial filaments, Δ *candA-C1* has fragmented mitochondria already after 10 hours. Δ *candA-C* and Δ *candA-N* show less fragmentation which increases over time (size bars: 10 μ m; -: no fragmentation; + fragmentation).

3.3.5 *A. nidulans* CandA-C1 promotes conidia formation

The developmental phenotypes influenced by CandA-N and CandA-C are stronger than by CandA-C1, which has an impact on asexual spore maturation, germination and growth. It was examined whether overexpression *candA-C1* would complement conidiation defects of $\Delta\text{candA-N}$, $\Delta\text{candA-C}$ or the $\Delta\text{candA-N/A-C}$ strains. The phenotypes of *candA-N*, *candA-C* and *candA-N/A-C* deletion strains with and without overexpression *candA-C1:gfp* were compared to each other and to wild type and the overexpression *candA-C1:gfp* strain in respect to asexual spore production and sexual development (Figure 44). Whereas the developmental phenotype of $\Delta\text{candA-N/OE candA-C1:gfp}$ did not change in comparison to the *candA-N* deletion strain, the $\Delta\text{candA-C/OE candA-C1:gfp}$ strain phenotype was altered (Figure 44A). The amount of conidiospores produced by the $\Delta\text{candA-C/OE candA-C1:gfp}$ strain was around 4-times higher than the number of conidiospores counted from the $\Delta\text{candA-N/OE candA-C1:gfp}$ strain. The same was observed when both *candA-N* and *candA-C* were deleted in a *candA-C1:gfp* overexpression strain. These results suggest a promoting function of CandA-C1 in the absence of CandA-C and might result from a rescuing function of CandA-C1 for CandA-C. However, the same strains display reduced colony radius, described in Figure 40, which suggests that a certain amount of *candA-C1* transcript or CandA-C1 protein is required for wild type-like growth and development. Elevated amounts of CandA-C1 are not sufficient to rescue the impairment in cleistothecia formation and CandA-C1 does not complement any defect caused by $\Delta\text{candA-N}$.

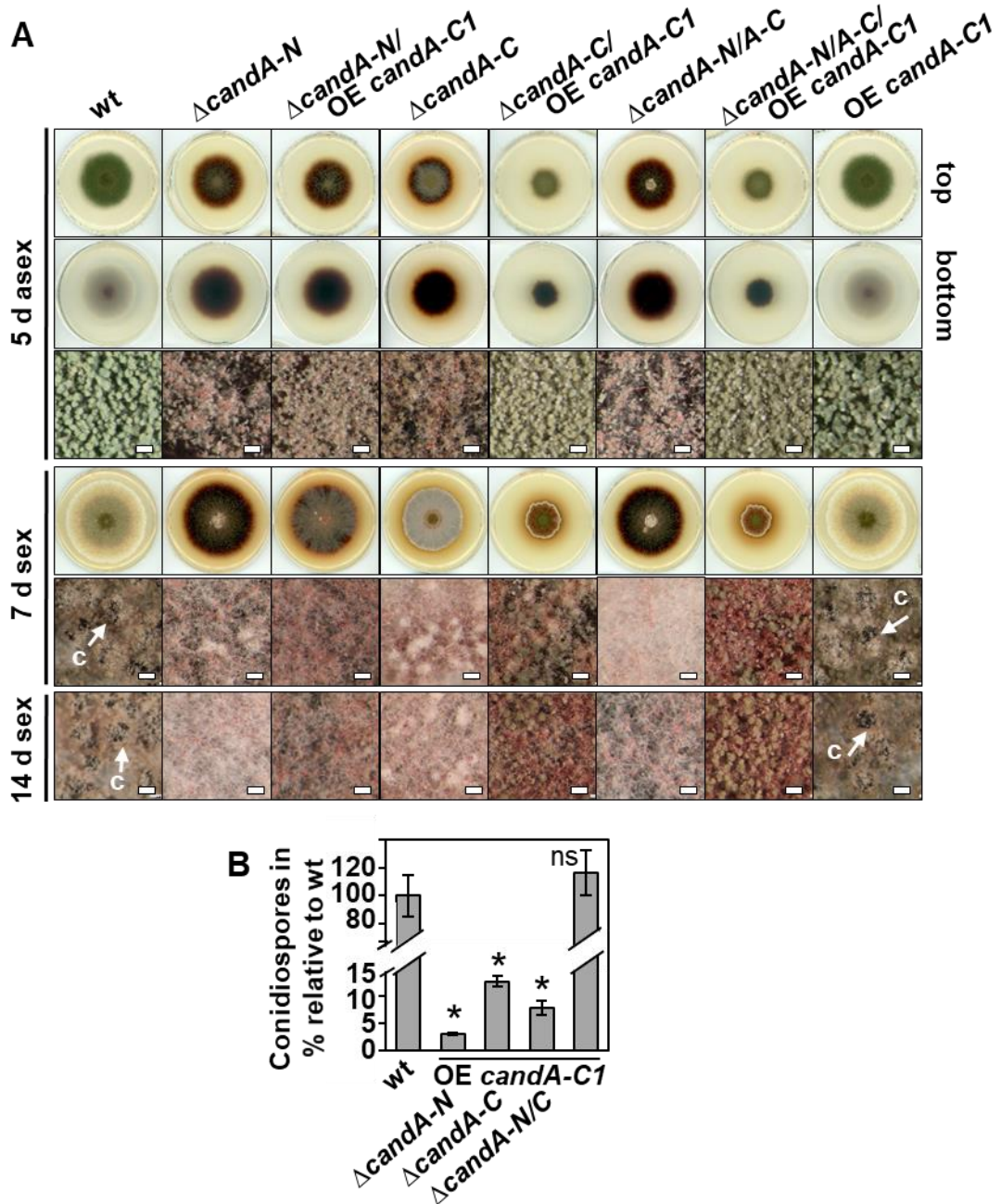


Figure 44. Overexpression *candA-C1* increases conidiospore production of strains defective in *candA-C* and *candA-N/A-C*. **A** Asexual development was analyzed after 5 days incubation at 37°C in light. Overexpression *candA-C1* support conidia production of *candA-C* and *candA-N/A-C* deletion strains but not in Δ *candA-N* neither in wild type. Plates were incubated in the dark and with limited oxygen supply for 7 and 14 days for sexual development. *candA* deletion mutants with overexpressed *candA-C1* are unable to form cleistothecia whereas the overexpression in wild type background shows wild type-like cleistothecia production. (size bars: 100 μ m, c= cleistothecia) **B** Quantification of asexual conidiospores after 5 days (n=3). Error bars represent the standard error of the mean (SEM) and significance was calculated relative to wild type with *p*-values: ns: >0.05, * \leq 0.05.

3.3.6 CandA-N and CandA-C promote early phase of sexual development and repress SM-production of orcinol derivatives, whereas CandA-C1 and DenA support later phases of cleistothecia formation

The formation of multicellular sexual fruiting bodies is a very complex developmental program, which requires the interplay of many different factors at different stages of development (Busch and Braus, 2007; Pöggeler *et al.*, 2018). As shown by Helmstaedt and co-workers CandA-N and CandA-C are required for primordia formation (Helmstaedt *et al.*, 2011). The developmental phenotypes of *candA* mutants were investigated in more detail to figure out if CandA-C1 has a similar role in the sexual cycle as CandA-N and CandA-C. The $\Delta candA-C1$ strain produced mainly Hülle cells resulting in the formation of many nests that lead to the yellow colored appearance of the colony (Figure 45A, B).

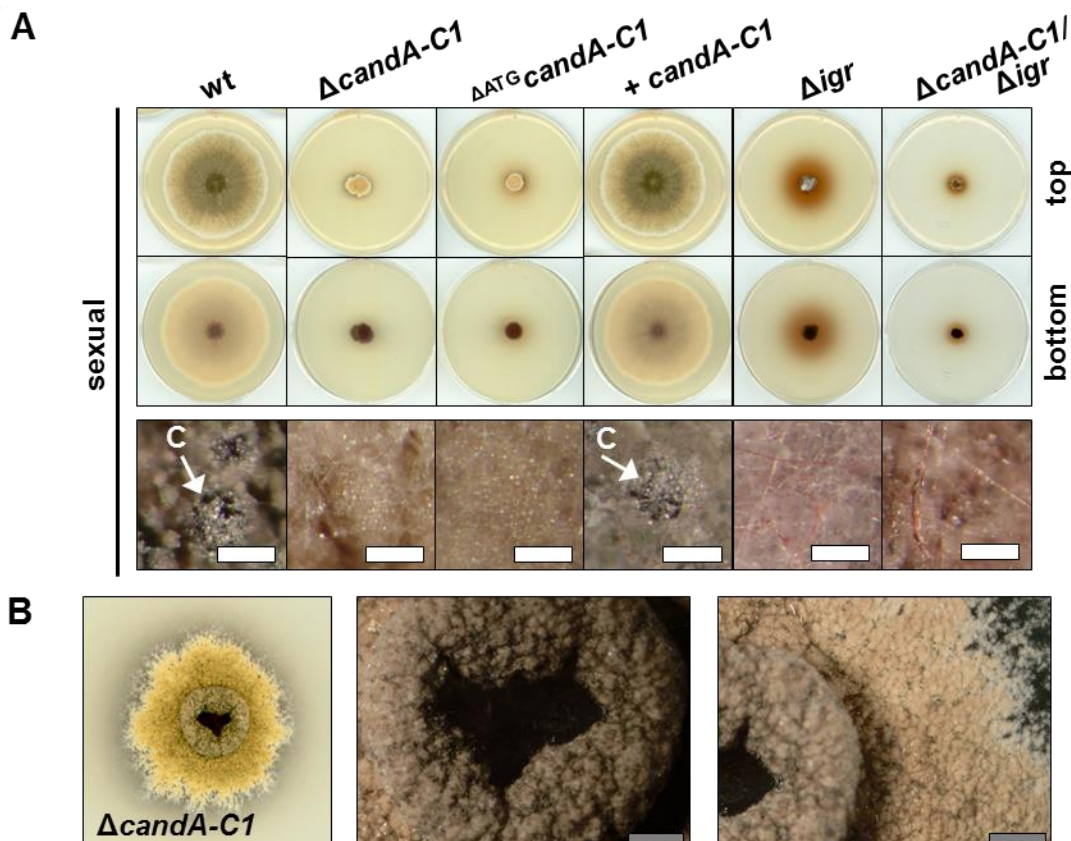


Figure 45. Colony of $\Delta candA-C1$ has a volcano-like growth in sexual development. A Strains were incubated for 7 days at 37°C and limited oxygen supply for sexual development. Deletion strains of *candA-C1* and $\Delta ATG candA-C1$ produce many Hülle cells but no mature cleistothecia after 7 days. The deletion strains of *igr* and *candA-C1/igr* produce less Hülle less but red colored aerial hyphae (c: cleistothecia, white size bars: 100 μ m). **B** Picture of a $\Delta candA-C1$ colony (left) and zoom into the colony using a binocular (middle and right). The colony grows vertically and forms a hole in the middle under sexual development promoting growth conditions. Nest structures are found all over the colony (grey size bars: 1 000 μ m).

The same phenotype was observed for the *candA-C1* strain with deleted ATG start codon. The *in locus* complemented strain shows wild type-like cleistothecia formation. The *igr* and *candA-C1/igr* deletion strains appear to have less Hülle cells than Δ *candA-C1* but increased formation of aerial hyphae which contain red pigments due to increased secondary metabolite production (Figure 45A). Detailed observation of the colony showed that it grows vertically forming a 'volcano-like' structure, which is covered with many nests and has a hole in the middle of the colony (Figure 45B).

The colony radius of the *candA-C1* deletion strain in the sexual culture was reduced as observed in asexual reproduction and different to the other *candA* deletion strains (Figure 46A). Deletion of *candA-N* and *candA-C* genes resulted in strains that are blocked in sexual development at the stadium of early nest production (Figure 46A, B). The cleistothecia of the *candA-C1* mutant strain were examined by clearing the fruiting bodies from attached Hülle cells. Most nests of the Δ *candA-C1* strain were empty or just contained primordia in early stages. Cleistothecia were only found after 14 days of incubation under sexual development promoting conditions (Figure 46C). The wall of cleistothecia from Δ *candA-C1* was moderately soft and fragile as the needle used to clean cleistothecia caused dents into the cleistothecia surface (red arrows in Figure 46C). Wild type and complementation strain cleistothecia contained mature ascospores already after 7 days (Figure 46D). Cleistothecia of the deletion strain did not contain any ascospores. They rather included a complex network of hyphae after 14 days of incubation (Figure 46D). Plating of squeezed cleistothecia on agar plates never resulted in colonies for the *candA-C1* deletion strain.

The observations on sexual development of *candA* deletion strains showed that the phenotype of *candA-C1* differs in its appearance from *candA-N* and *candA-C* deletion strains and from wild type. Cleistothecia are formed in the absence of *candA-C1*, but the decisive step for successful sexual reproduction - the ascospore production - is missing in the *candA-C1* mutant, indicating that all three CandA proteins are necessary in the process of cleistothecia formation and maturation.

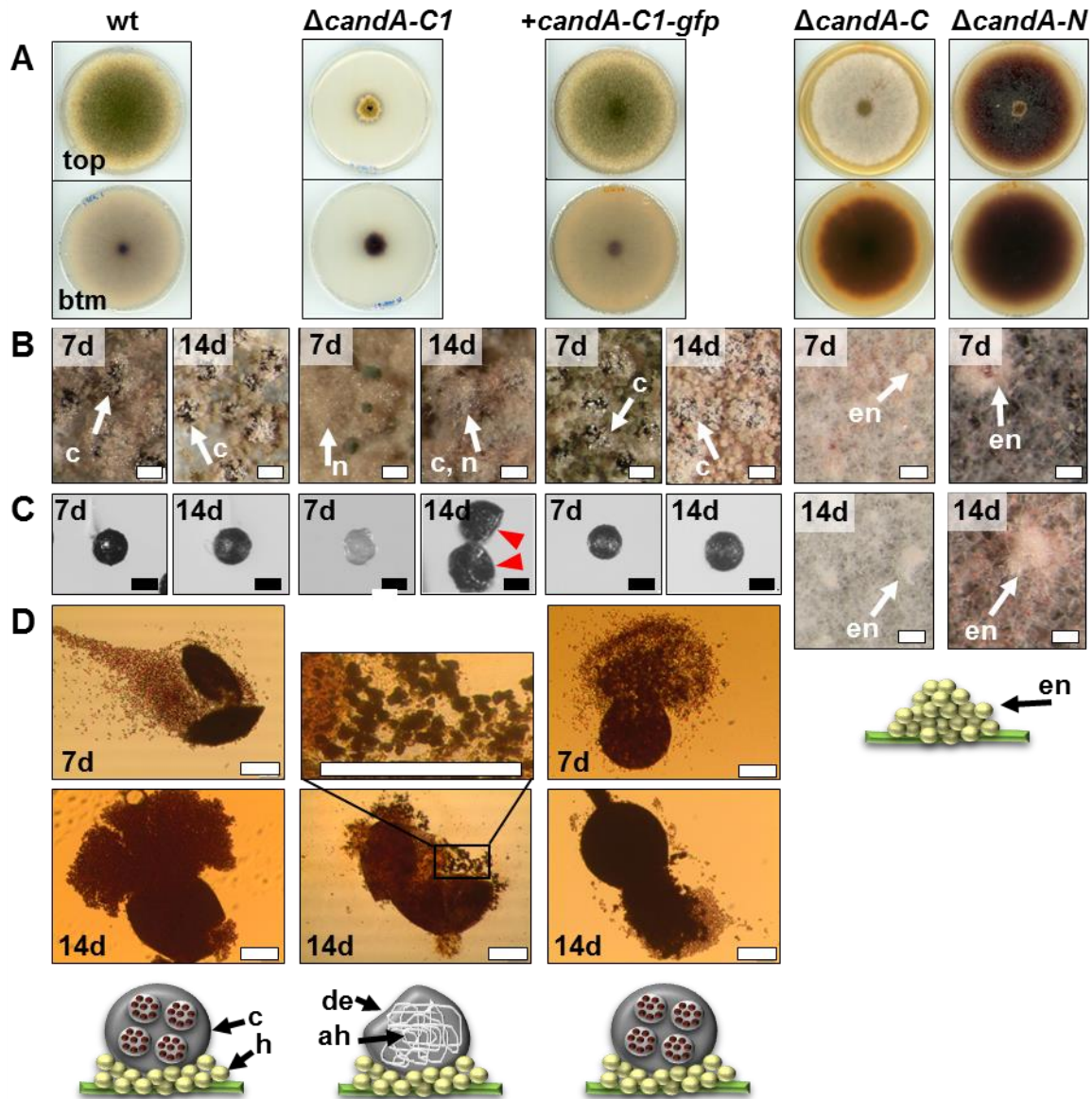


Figure 46. Ascospore formation is dependent on *candA-C1*. Strains were incubated in the dark and with limited oxygen supply for 7 and 14 days. **A** Deletion of *candA-C1* shows reduced colony radius similar to asexual development and yellow colony color due to presence of Hülle cells. **B** Micrograph pictures show cleistothecia covered by Hülle cells for wild type (wt), *candA-C1* deletion and complementation strain. *candA-C* and *candA-N* deletion strains only produce early nests but cannot undergo a complete sexual life cycle. **C** Deletion of *candA-C1* produces cleistothecia like wild type and complementation but cleistothecia were soft and had dents, indicated with red arrows. **D** Microscopic pictures of squeezed cleistothecia never showed any mature ascospores for *candA-C1* deletion strain but rather hyphae-like structures, different to wild type and complementation (size bars: 100 μ m, d, days, c: cleistothecia, h: Hülle cells, en: early nests, n: nest, de: dent, ah: ascogenous hyphae).

With the knowledge that *CandA* and *CSN* contribute greatly to *A. nidulans* sexual development, the impact of *DenA* alone and in combination with *CandA* on asexual and sexual development was investigated. *DenA* was previously characterized in a *uridine/uracil* auxotrophic background strain using a *pyrG* marker (AGB152) (Christmann *et al.*, 2013) and it was described to have reduced growth and conidia but increased production of aerial hyphae. Different to the *CSN* deneddylase *csnE* deletion strain, a $\Delta denA$ mutant was described to be blind to light as cleistothecia were observed in dark as well as in light (Christmann *et al.*, 2013). For double deletion with *candA*, first a *denA* single deletion strain was prepared in a different background wild type strain (AGB552: $\Delta nkuA::argB$, *pabaA1*, *yA2*, *veA*⁺) using the recyclable marker cassette. The resulting strain has a wild type like appearance forming green colored conidia under asexual development promoting conditions (Figure 47A). Cleistothecia were not observed in light. This is the opposite compared to the described $\Delta denA$ phenotype in AGB152 (Figure 47B). A combination of the used background strain with *uridine/uracil/pyridoxin* auxotrophy, the *pyr4* marker gene, which was used to select for a *denA* deletion and the *denA* deletion itself seemed to influence the phenotype. These observations showed, that the $\Delta denA$ phenotype in AGB152 is a synthetic phenotype due to the auxotrophies and markers used in strain design.

Double deletion of $\Delta denA/candA-N$ shows immature whitish as well as greenish conidia and aerial hyphae when incubated for five days in light and with oxygen supply at 37°C. This phenotype was different to $\Delta candA-N$ single deletion strain which appears to have less spores. The bottom view of the plates depicts different color of secondary metabolites produced by the strain deleted in both genes compared to *candA-N* single deletion strain.

Sexual development was investigated after 7 and 14 days of incubation at 37°C with oxygen limiting conditions and darkness. The $\Delta denA$ strain exhibited asexual appearance producing mostly green conidia, different to wild type which produces more Hülle cells that give the colony a yellow color. Nests were formed either below conidia or also as aerial nests at same height of conidia containing mainly immature cleistothecia with lighter color compared to wild type and contained only few ascospores and many ascogenous hyphae (Figure 47C). After 14 days cleistothecia looked like those of wild type but still contained less ascospores than a wild type cleistothecium (Figure 47C). Observations on the phenotype of *candA-N/denA* double deletion strains compared to *denA* and *candA-N* single deletion mutants showed increased production of aerial hyphae and different color of accumulated secondary metabolites. Early nests could be observed after 7 days, which could not develop further into cleistothecia after 14 days of incubation. In summary, *DenA* is required for sexual development and not for asexual conidia formation. These observations are contradicting to the phenotype of the *denA* deletion mutant strain in a wild type strain with *pyrG* marker.

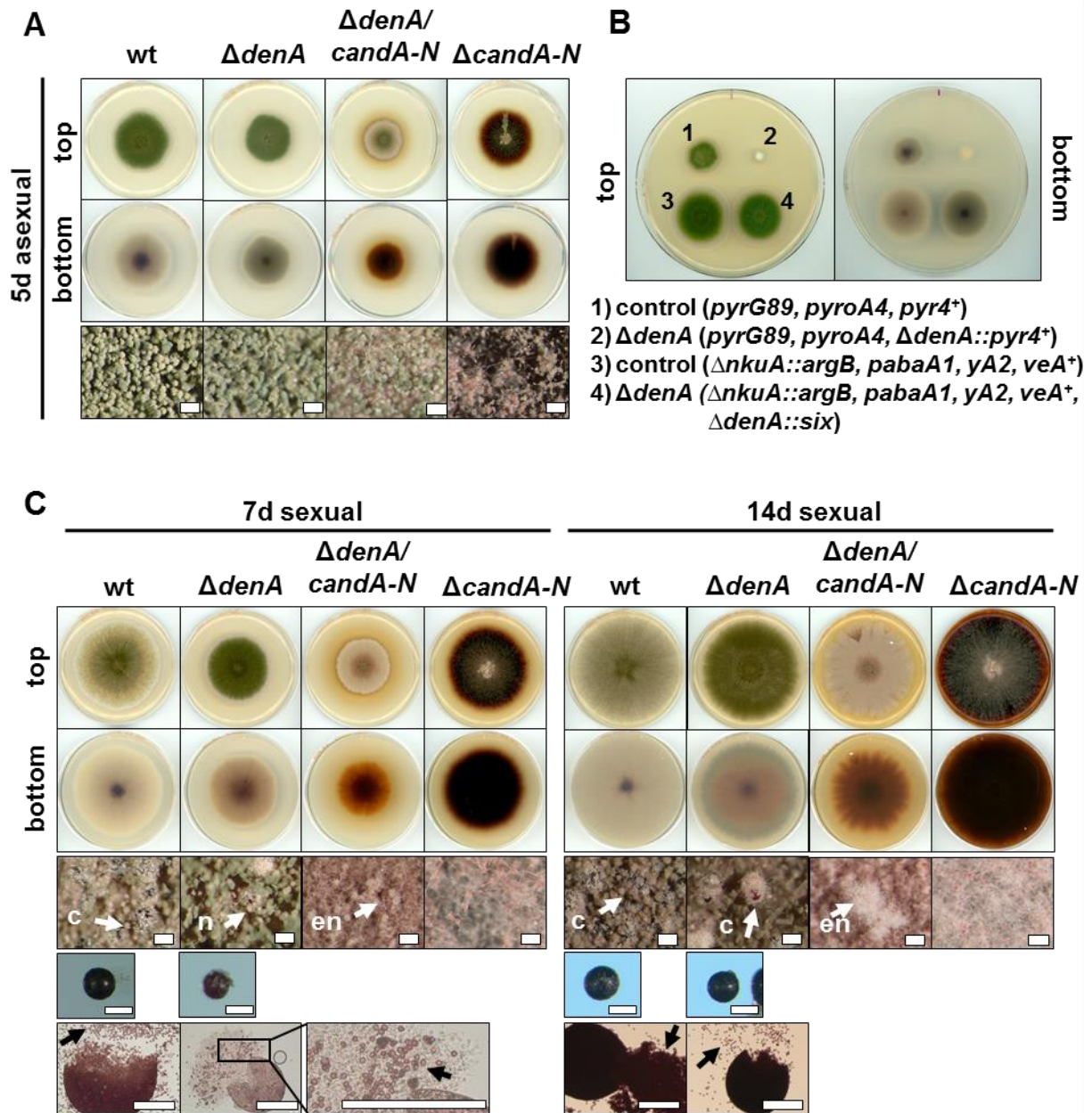


Figure 47. CandA and DenA are required for sexual development. **A** After five days of asexual development the *denA* deletion strain appears like wild type but the *denA/candA-N* double deletion has reduced conidia formation and shows accumulation of brown colored secondary metabolites similar as observed for $\Delta candA-N$. **B** Comparison of $\Delta denA$ strains in different genetic background strains with their respective control strains: 1) control AGB160 *uridine/uracil* auxotrophic control for 2) $\Delta denA$ in AGB152 and 3) control AGB552 for 4) $\Delta denA$ in AGB552 (genotypes are indicated). The *denA* deletion strain with *pyrG* marker has white aerial hyphae. **C** Sexual development was analyzed after plates were incubated seven or fourteen days in dark with limited oxygen supply. Micrographs give a detailed view of colony morphology and depict early nests (en), nests (n) or cleistothecia (c). The *denA* deletion strain has many green colored conidia and the colony shows less yellow colored Hülle cells compared to wild type. The *denA/candA-N* double deletions strain forms aerial hyphae and early nests. Cleistothecia of the *denA* deletion strain are immature after seven days with only a few ascospores (black arrows) and contain still less ascospores than wild type after 14 days of incubation (size bars: 100 μ m).

DenA seems to play an important role in nest positioning and Hülle cell formation, which then ensures cleistothecia maturation. Asexual development is not dependent on DenA. DenA and CandA-C1 seem to have similar roles in sexual development as both are required for properly timed cleistothecia formation and ascospore development.

Examination of asexual and sexual development of the *candA* mutants showed the production of red-brownish colored secondary metabolites. Secondary metabolism is highly connected to development as mutants with altered secondary metabolism often have developmental defects as shown previously for CandA-N and CandA-C (Helmstaedt *et al.*, 2011). It was shown that deletion strains of *candA-N* and *candA-C* secrete different secondary metabolite derivatives produced by the orsellinic acid secondary metabolite gene cluster. These metabolites accumulate as red pigment in the hyphae and the medium visible as dark brown colored agar (Helmstaedt *et al.*, 2011). The same colored hyphae and agar was observed in the marker free deletion strains, generated for this thesis (Figure 39A). A deletion strain of the newly identified *candA-C1* gene showed altered color of the colony and surrounding medium but less prominent than observed in the Δ *candA-N* and Δ *candA-C* strains (Figure 39A). Subsequently the role of CandA-C1 in secondary metabolism was investigated. Therefore, extracellular secondary metabolites of wild type, Δ *candA-C* and Δ *candA-C1* strains from plates incubated for seven days under asexual development favoring conditions were extracted. The obtained metabolites of Δ *candA-C* and Δ *candA-C1* had a similar orange color when dissolved in methanol (Figure 48A). The wild type had a lighter yellow color. High-performance liquid chromatography (HPLC) was performed and evaporative light scattering detector (ELSD) plot showed high amounts of different orsellinic acid derivatives for the *candA-C* deletion strain (Figure 48B). The deletion strain of *candA-C1* did not show any of these metabolites. The secondary metabolite levels of austinol and dehydroaustinol were higher in Δ *candA-C1* than in Δ *candA-C* but lower than in wild type. This corroborates with the amount of asexual conidiospores as dehydroaustinol is a marker for conidiospore production (Lo *et al.*, 2012). These results support that CandA-N and CandA-C but not CandA-C1 are required for the repression of orsellinic acid derivative production under asexual development conditions. This might be an indirect effect caused by an impaired specific protein degradation activity in the absence of the two CandA-N and CandA-C proteins. The metabolite(s) produced by the *candA-C1* mutant need to be identified in future.

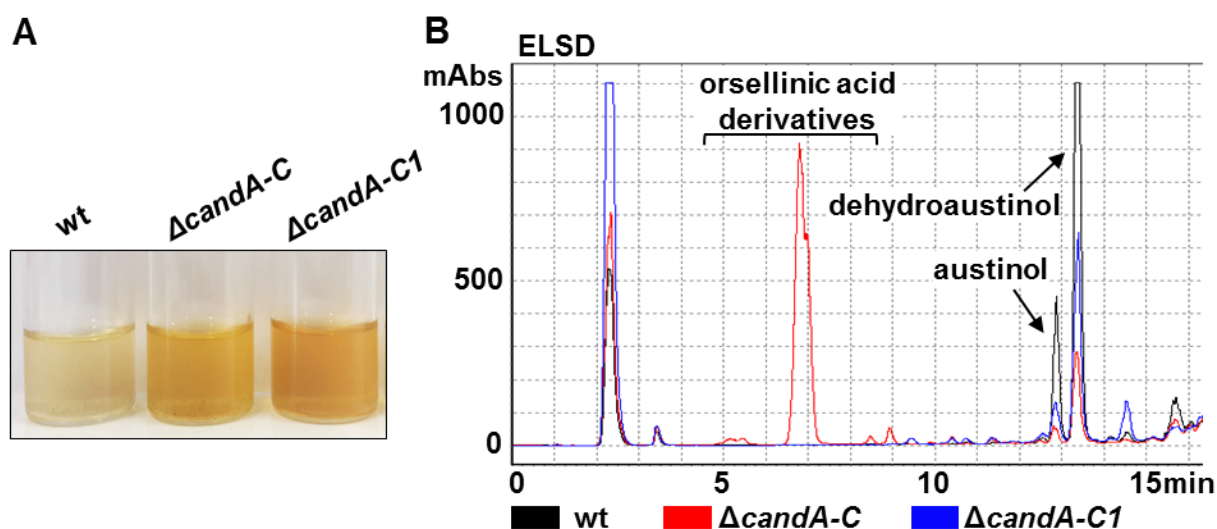


Figure 48. Orsellinic acid derivative production is independent of CandA-C1. For secondary metabolite extraction MM paba plates were inoculated with 1×10^6 spores and incubated for 7 days at 37°C and light conditions. Extracellular secondary metabolites were extracted with ethyl acetate and dissolved in methanol. **A** Dissolved metabolites of wild type (wt) show a lighter yellow color compared to $\Delta\text{candA-C}$, which is also slightly different to $\Delta\text{candA-C1}$. **B** Secondary metabolite analysis by high-performance liquid chromatography (HPLC) measurements show in an ELSD (evaporative light scattering detector) spectrum different identified metabolites. *candA-C* (red) produces different derivatives of orsellinic acid which could not be identified for the *candA-C1* deletion strain (blue) neither for the wild type (black). Less production of austinol and dehydroaustinol were recorded for $\Delta\text{candA-C}$ than for $\Delta\text{candA-C1}$ and for wild type the highest levels were measured.

This PhD thesis demonstrates that the subunit composition of CandA is changed in different organisms. Even the close relatives *A. fumigatus* and *A. nidulans* have a different number of subunits: dimeric versus trimeric CandA complex, respectively. The genetic information of both *Aspergillus* CandA proteins is very similar conserved. This work showed that *A. nidulans* CandA-C1 and CandA-C have next to separate transcripts also a shared transcript that might be the result of a RNA polymerase read-through or serves as a regulatory RNA, which might have impact on the complex stoichiometry of CandA subunits. All three CandA subunits interact with each other primarily in the nucleus. The *A. nidulans* CandA complex is required for CRL activity by interaction with Nedd8 and CulA containing SCFs. *A. fumigatus* CanA can interact with CulA and CulC containing SCFs. CandA and CSN are similarly important for functional SCFs. *A. nidulans* CandA-C1 and *A. fumigatus* CanA N-terminal extension have great impact on germination and vegetative growth. CandA-N, CandA-C and CandA-C1 support conidia formation and play important roles in sexual reproduction. CSN, CandA-N and CandA-C are similarly required to produce primordia in sexual development whereas

CandA-C1 and DenA are required for cleistothecia formation and ascospore development. *A. fumigatus* CanA C-terminal domain and CanA-N support asexual conidia production and are required for germination at low temperature. Furthermore, CandA-C1 overexpression promotes conidia formation and wild type-like levels of cullin neddylation in *candA-C* deletion strains, suggesting rescue effects of CandA-C1 for *candA-C* loss. CandA-C1 is not involved in the orsellinic acid derivative secondary metabolite production under asexual development conditions different to CandA-N and CandA-C.

4 Discussion

4.1 The subunit composition of the CandA complex differs between eukaryotes

4.1.1 CandA-C1 is a separate protein in *A. nidulans* but an N-terminally extension of CanA C-terminal subunit in *A. fumigatus*

Evolution is accompanied by genetic alterations in all living organisms. Changing external and internal conditions force adaptation. The major cellular pathways and principles are conserved in eukaryotes as for example the ubiquitin proteasome system, which maintains protein homeostasis by combining post-translational protein modification and degradation systems (Ciechanover, 1998; Hershko and Ciechanover, 1998). The ubiquitin proteasome system includes the dynamic interplay of single proteins as deubiquitinating proteins (Hetfeld *et al.*, 2005), or the substrate-receptor exchange factor CandA and three macromolecular multiprotein complexes: SkpA-CulA-Fbx (SCF) E3 RING ligase, the COP9 signalosome (CSN) and the 26S proteasome. The CSN and the proteasomal lid share a similar subunit composition and structural orientation of subunits and are therefore summarized as ZOMES ('study of large PCI complexes') (Pick and Pintard, 2009; Meister *et al.*, 2016). The eukaryotic translation initiation factor (eIF3) is also a member of this protein family and has an eight subunit ZOMES core (Alpi and Echali er, 2017). The biological relation of these three complexes in structural aspects as well as in their function in protein synthesis and degradation suggests that they might have evolved from a common ancestor (Enchev *et al.*, 2010; Barth *et al.*, 2016; Meister *et al.*, 2016). A detailed comparison of eukaryotic CSN complexes revealed that most of them contain six PCI and two MPN domain subunits, but some species miss single subunits like *N. crassa*, lacking Csn8 (Braus *et al.*, 2010; Adhvaryu *et al.*, 2015; Meister *et al.*, 2016). *S. cerevisiae* has evolved an alternative CSN having only Csn5 as conserved subunit and lid subunits are found as CSN interaction partners, which fill the gaps of missing CSN subunits (Yu *et al.*, 2011). Other eukaryotic CSN complexes have variable intron and exon insertions or different splice variants indicating evolutionary species specific adaptations (Barth *et al.*, 2016).

This work demonstrates that the subunit composition of the Cand1/A complex can be different between eukaryotic species. BLAST search analysis revealed that humans and the plant pathogenic fungus *Verticillium dahliae* as well as most other fungi have a one-subunit Cand1. *A. fumigatus* has two CandA proteins named CanA-N and CanA C-terminal subunit, which form a heterodimeric complex corresponding to a one-subunit Cand1. The C-terminal subunit CanA has an N-terminal extension, which is specific for *Aspergillus* spp. and as known so far

not conserved in humans or fungi besides the class of *Eurotiomycetes*. This N-terminal extension is the single protein CandA-C1 in *A. nidulans*. CandA-C1 is encoded by a separate gene directly upstream of the *candA-C* gene, which encodes the C-terminal subunit of *A. nidulans* CandA. CandA-C1 has different as well as overlapping functions compared to CandA-C and CandA-N, which probably leads to dimeric CandA-N/A-C but also trimeric CandA-N/A-C/A-C1 complexes.

4.1.2 CandA-C1 and CanA N-terminally extension share the same sequence features in *A. nidulans* and *A. fumigatus*

Motif prediction tools displayed that all eukaryotic Cand1/A proteins contain conserved structural features and domains independent of Cand1/A being one protein or split into two or three subunits (Figure 15, p. 69). An Armadillo-like helical fold is characterized by alpha-helical HEAT repeats (A and B helix form one HEAT repeat) and Cand1/A proteins contain 27 HEAT repeats distributed from the N- to the C-terminus (Goldenberg *et al.*, 2004; Fournier *et al.*, 2013; Gul *et al.*, 2017). Secondary structure prediction of CandA-N and CandA-C compared to the crystal structure of human Cand1 (PDB ID 1U6G) revealed that *A. nidulans* CandA-N contains HEAT repeat helices A1 to A7 and CandA-C contains HEAT repeat helices B7 to B27 (Figure 49A) (Kelley *et al.*, 2015). According to the sequence of the *A. fumigatus* CanA N-terminal extension, it is likely that the CandA-C1 protein is in between CandA-N and CandA-C. The Armadillo-like helical superfamily fold was predicted for CandA-C1 when a CandA-C1~CandA-C fusion sequence was subjected to InterPro Scan protein sequence analysis and classification server (Figure 50) (Finn *et al.*, 2017). *A. fumigatus* CanA has an Armadillo-like helical fold from amino acid 141 to 1 233 including sequence parts of the N-terminal extension. This indicates that the additional CanA N-terminal extension and CandA-C1 of both *Aspergillus* species fit and integrate into the overall helical structure of the CanA/CandA complex. The *A. nidulans* CandA complex has additional HEAT repeats due to the extra peptide sequence of CandA-C1 compared to Cand1 from human (Figure 49A). Secondary structure prediction of the CandA-C1 protein sequence without the other CandA proteins suggested similar folding to amino acids 17 to 107 of *PhoRpp21*, which is a subunit of the archaeal ribonuclease P from *Pyrococcus horikoshii* (Kakuta *et al.*, 2005; Honda *et al.*, 2008) (Figure 49B).

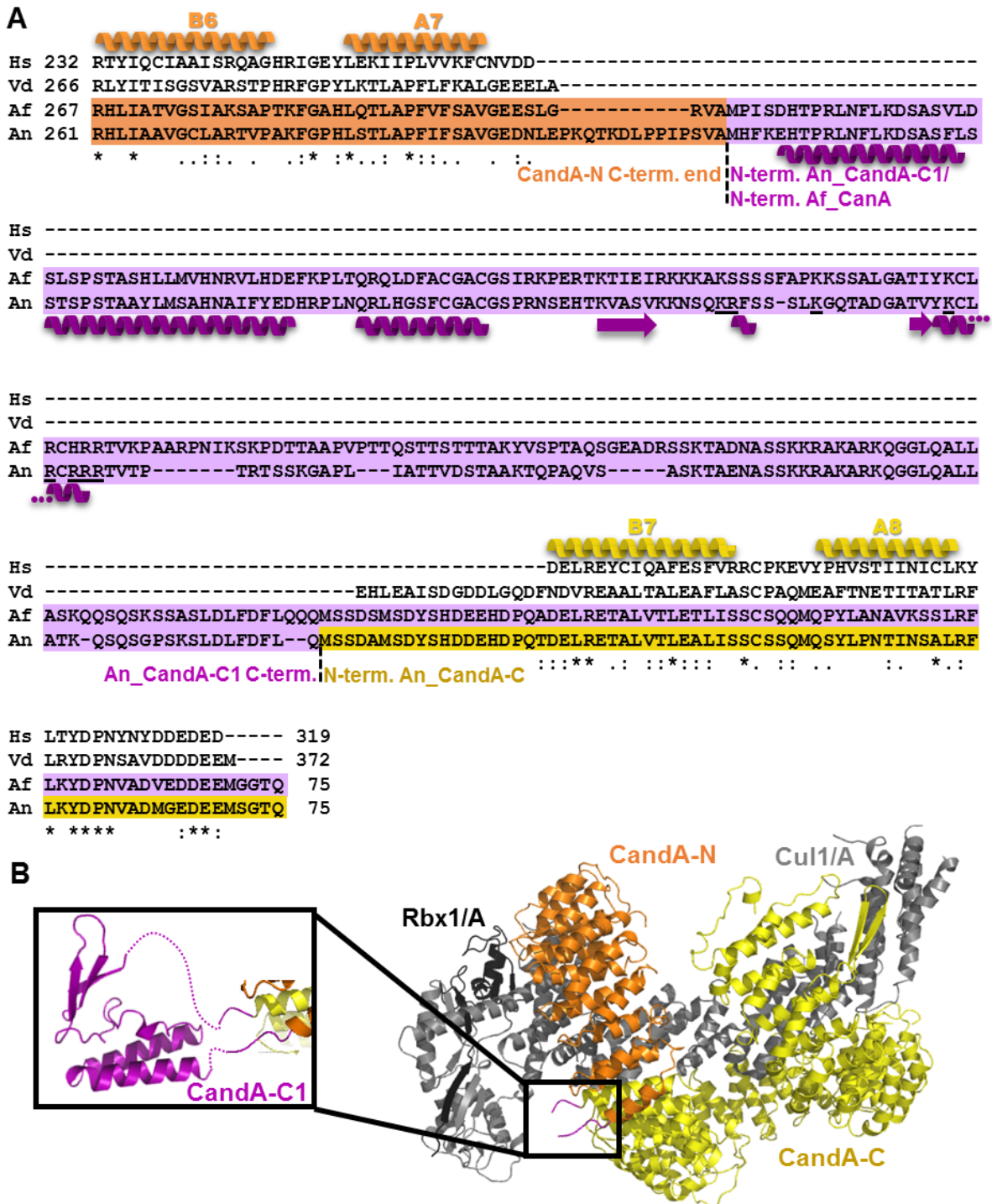


Figure 49. 3D structure prediction of *A. nidulans* CandA-C1 shows similarities to Rpr2/Rpp21. **A** MUSCLE protein alignment of Cand1 from *Homo sapiens* (Hs), *V. dahliae* (Vd), *A. fumigatus* (Af) and *A. nidulans* (An) (Edgar, 2004) showing CandA-C1 (purple) flanked by CandA-N C-terminal end (HEAT repeat helix A7, orange) and CandA-C N-terminal amino acids (HEAT repeat helix B7, yellow). The predicted secondary structure of CandA-C1 shows helices and arrows indicate β -sheets. (Conserved residue: asterisk ('*'), strongly similar residue: colon (':'), weakly conserved amino acid: period ('.')). Underlined letters indicate a putative bipartite NLS predicted for An_CandA-C1 (see also Figure 56). **B** Three-dimensional structure prediction based on CandA-C1 (purple) applied to Phyre² web portal for protein modeling, prediction and analysis (Kelley *et al.*, 2015) (PDB ID 2ZAE and 1U6G).

The TATA-box binding protein (TBP) interacting protein domain (TIP120) is also conserved in humans and *Verticillium*. The TIP120 domain is responsible for the initial name of Cand1, which was first named TIP120A and only re-named after Cand1 was found to be a cullin binding protein (Yogosawa *et al.*, 1996; Zheng *et al.*, 2002a; Min *et al.*, 2003). Reports showed that Cand1 can interact with TATA box binding proteins and thereby enhances transcription by RNA polymerases I, II and III (Yogosawa *et al.*, 1996; Makino *et al.*, 1999). The monopartite NLS is only found in the fungal Cand variants and is in the N-terminal half of the CandA-C/CanA proteins. In summary, *A. nidulans* CandA-C1 and CandA-C share all their sequence motifs and predicted secondary structure features with CanA from *A. fumigatus*. Investigations of the CandA-C1 position in the CandA superhelical complex are required for a better understanding of the function of the additional Cand subunit and for the holocomplex.

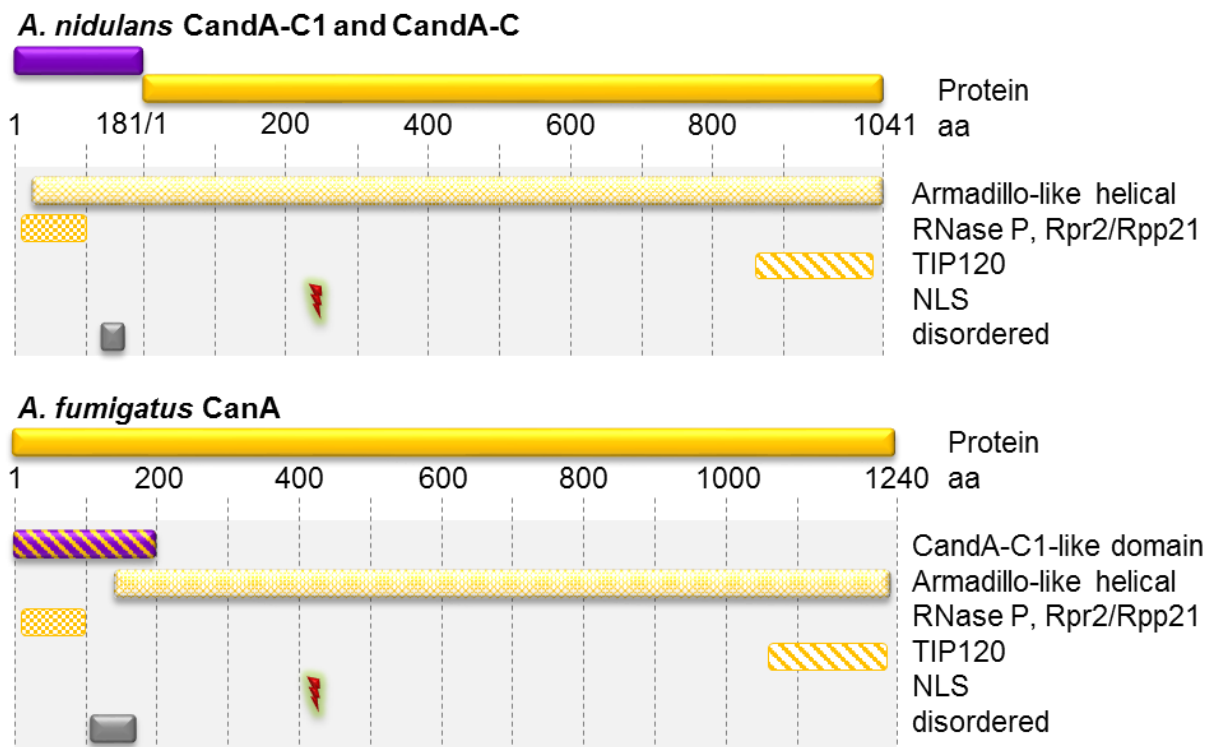


Figure 50. *A. nidulans* CandA-C and *A. fumigatus* CanA C-terminal proteins have the same sequence features. *A. nidulans* CandA-C1 (purple) together with CandA-C (yellow) and *A. fumigatus* CanA (yellow) were analyzed by InterPro protein sequence analysis and classification tool (Finn *et al.*, 2017). The nuclear localization sequences (NLS) were predicted with cNLS Mapper (Kosugi *et al.*, 2009a). Both share the same features: Armadillo-like helical superfamily fold (light yellow), an RNase P Rpr2/Rpp21 subunit motif (squarred box), a TATA box binding protein (TBP) interacting protein domain (TIP120) (striped box), a monopartite NLS sequence (RKRRR, red blizzard) and a disordered sequence part (grey box). *A. fumigatus* has a CandA-C1-like domain (purple-yellow striped box).

4.1.3 CandA-C1 and the N-terminal CanA extension are conserved in *Aspergillus* and *Penicillium* spp. and might be bifunctional

CandA-C1 is predicted to consist of helices that are related to the HEAT repeat family and its protein sequence has a motif corresponding to the RNase P subunit Rpr2/Rpp21. The CandA-C1 three-dimensional structure was predicted to be most related to *RhoRpp21* with 16 % sequence identity. *RhoRpp21* is a subunit of the *Pyrococcus horikoshii* RNase P complex, which is involved in RNA maturation. The crystal structure of *RhoRpp21* was solved in complex with *RhoRpp29* (PDB ID 2ZAE) (Kakuta *et al.*, 2005). *RhoRpp21* is a 120 amino acid protein of 14.6 kDa and thereby smaller than the 19 kDa *A. nidulans* CandA-C1 protein with 181 amino acids or the 200 amino acid long N-terminal extension of *A. fumigatus* CanA (Kakuta *et al.*, 2005). The additional sequence of CandA-C1 and CanA compared to the *RhoRpp21* protein might explain the CandA dependent function.

Ribonuclease P (RNase P) cleaves the 5' precursor of transfer RNAs (tRNA, Frank and Pace, 1998; Honda *et al.*, 2008). The RNase P complex exists in different composition of proteins and RNA (ribonucleoproteins) specified for different organelles or substrates as its close relevant the RNase MRP, which is mainly involved in nucleolar ribosome biogenesis (Hartmann and Hartmann, 2003; Walker and Engelke, 2006; Hipp *et al.*, 2012). RNase P complexes are conserved throughout all domains of life (Hartmann and Hartmann, 2003; Walker and Engelke, 2006; Esakova and Krasilnikov, 2010). Humans have ten and yeasts have nine different protein subunits and two RNAs. *A. nidulans* has one nuclear and one mitochondrial RNA and seven putative protein subunits, whereas CandA-C1 (AN12234) might be one of them (Figure 51A) (Jun Han *et al.*, 1998; Walker and Engelke, 2006). The conservation of Rpr2/Rpp21 domain family proteins was investigated in several fungal species and most of them encode a protein with this motif (Walker and Engelke, 2006). So far as analyzed in this study, a *candA-C1* homologous gene with location directly upstream of the *candA-C* gene is restricted to members of *Eurotiomycetes* like *Aspergillus* spp. as well as some *Penicillium* spp. like *P. chrysogenum*, *P. oxalicum*, *P. rubens* and *P. naegiovense*. According to JGI MycoCosm *Eurotiomycetes* are a class of ascomycetes and count mainly *Aspergillus* and *Penicillium* spp. (Grigoriev *et al.*, 2012, 2014; de Vries *et al.*, 2017). The afore mentioned *Penicillium* spp. are annotated to carry the CandA-C1-like domain as N-terminal extension of the C-terminal CandA subunit like shown here for *A. fumigatus* CanA. Comparative genomics revealed that around 20 % of all genes identified in *Aspergillus* spp. do not have orthologous genes in other fungal species (de Vries *et al.*, 2017). CandA-C1 might be among these *Aspergillus* specific genes with some exceptions in the closely-related *Penicillium* spp.

Affinity capture-MS experiments performed by Bennett and co-workers showed that human TAP-tagged Cand1 and TAP-tagged Cul3 interact with Rpp30, which is a direct interaction partner of Rpp21, the CandA-C1 homolog (Figure 51B) (Bennett *et al.*, 2010). The nature of this interaction is unclear so far and needs to be investigated in more detail.

A

<i>S. cerevisiae</i>		<i>H. sapiens</i>		<i>A. nidulans</i>			
RNase P	RNase MRP	RNase P	RNase MRP	RNase P	RNase MRP	subunit type	size
Rpr1/Rnh1	-	H1	-	AN5188 ?	-	RNA	1389 bp
-	Rpm1	-	7-2	-	AN20050 Mpr1	RNA	232 bp
Pop1	Pop1	Pop1	Pop1	AN8691	AN8691	Protein	101.9 kDa
Pop3	Pop3	-	-	-	-	Protein	-
Pop4	Pop4	Rpp29	Rpp29	AN0189	AN0189	Protein	31.1 kDa
Pop5	Pop5	Rpp14	Rpp14	AN2437	AN2437	Protein	23.6 kDa
Pop6	Pop6	-	-	-	-	Protein	-
Pop7	Pop7	Rpp20	Rpp20	AN4631	AN4631	Protein	31.1 kDa
Pop8	Pop8	-	-	-	-	Protein	-
Rpp1	Rpp1	Rpp30	Rpp30	AN1486	?	Protein	33.3 kDa
Rpr2	Rpr2	Rpp21	Rpp21	CandA-C1	?	Protein	19.6 kDa
-	-	Rpp25	Rpp25	-	-	Protein	-
-	-	Rpp14	Rpp14	-	-	Protein	-
-	-	Rpp38	Rpp38	-	-	Protein	-
-	-	Rpp40	Rpp40	AN3652	?	Protein	43.0 kDa

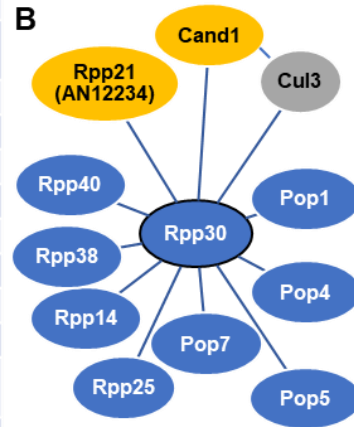


Figure 51. Overview of RNase P/RNase MRP subunits. **A** Comparison of subunits of RNase P and RNase MRP from *S. cerevisiae* (green), *H. sapiens* (blue) and *A. nidulans* (purple) (Jun Han *et al.*, 1998; Walker and Engelke, 2006). **B** Interaction of RNase P subunits, Cul3 and Cand1 based on affinity capture-MS [BioGRID <https://thebiogrid.org/>] (Bennett *et al.*, 2010).

Based on the sequence motif and secondary structure prediction as well as the observations of *A. nidulans* CandA-C1 supporting cullin neddylation, CandA-C1 could be a 'moonlighting' protein meaning that it has a dual function in ribosome-/amino acid synthesis and CRL cycle. Involvement of CandA-C1 in tRNA maturation would connect it to protein biogenesis. The generation of new polypeptides is essential in all different stages of life and allows adaptation to changing conditions. Defects in the fundamental steps of tRNA maturation, which support the ribosome with amino acid units, might explain the growth defective phenotype. This is in accordance with interaction partners of CandA-C1 identified in LC-MS measurements, which are involved in amino acid and tRNA biogenesis, as for example a threonine synthase (ThrC, AN3031) or Glutamyl-tRNA synthetase (GusA, AN8224). GFP pull downs of *A. fumigatus*

CanA revealed a putative interaction with a ribonuclease T2-like protein homolog RnyA (ribonuclease from yeast), which is involved in tRNA cleavage upon oxidative stress (Thompson and Parker, 2009).

These data show, that *A. nidulans* CandA-C1 or the N-terminal extension of *A. fumigatus* CanA carry a conserved Rpr2/Rpp21 family domain in their N-terminus, which is also conserved in most other eukaryotes. A CandA-C1-like protein with genetic connection to the gene encoding the *candA-C* subunit is specific for *Aspergillus* and some *Penicillium* species.

4.1.4 The *candA* genes encountered a DNA rearrangement in a common ancestor of *Aspergillus* spp.

Cand1/A proteins have different subunit compositions in eukaryotes but conserved features and functions, what proposes a common ancestor. The putative ancestor of all *Aspergillus* spp. might have had one *candA* gene encoding a single subunit CandA protein with N- and C-terminal domains corresponding to human Cand1 (Figure 52). The *candA-C1* gene was presumably a separate gene, which encoded a putative RNase P subunit as known for other eukaryotes. A DNA double strand break might be responsible for the rearrangement of the *candA* genes. DNA rearrangements create genomic diversity and induce speciation to allow evolution dependent adaptation in many fungal species (Braumann *et al.*, 2008). These genome alterations must be beneficial for the fitness to become the canonical sequence (Stukenbrock, 2013).

The genome rearrangement in the *Aspergillus* ancestor changed the position of the C-terminal domain encoding sequence part of the *candA* gene to a position downstream of *candA-C1*. Whether CandA-C1 was functionally linked to the CandA ancestor protein before the rearrangement or whether the reordering of genes added a CandA-function to the *candA-C1* gene product is unknown.

In *A. nidulans* the *candA* genes *candA-C1*, *candA-C* and *candA-N* were expressed separately as consequence of the rearrangement. An observed common transcript might be a terminator read-through or a regulatory RNA that controls the expression of both *candA-C* genes. In other *Aspergillus* spp. like *A. fumigatus* the rearranged *candA* C-terminal sequence must have fused with the upstream *candA-C1* gene, which resulted in a *canA* gene encoding a CanA protein with N-terminal extension and a separate *canA-N* gene (Figure 52).

Indications of further functions of CandA subunits e.g. as TATA-box binding protein regulating transcription (Yogosawa *et al.*, 1996; Makino *et al.*, 1999) support the scenario of splitting the gene to express single specialized proteins. The *A. fumigatus* *canA* gene includes the information for the *candA-C1*-like domain in the first exon, probably as adaptation in

consequence of stress response. *A. fumigatus* is exposed to various stressors that cause selection pressure as for example temperature- or oxidative stress (Paulussen *et al.*, 2017), heavy metal stress (Leiter *et al.*, 2016; de Vries *et al.*, 2017; Bakti *et al.*, 2018) and sterol-biosynthesis-inhibiting triazole fungicides (Zhang *et al.*, 2017). The production of the C-terminal subunit CanA with the N-terminal extension, which is or became important for the CanA function probably results in a more stable protein or is less energy consuming than producing equal amounts of separate subunits that must be folded and find each other for active complex formation (Williams and Dichtl, 2018). In summary, *Aspergillus* spp. presumably had a common ancestor, which expressed a one subunit CandA with N- and C-terminal domains and a separate CandA-C1 protein with a function in the RNase P complex. A DNA rearrangement resulted in the separation of CandA-C from CandA-N as either third CandA protein (*A. nidulans*) or as second CandA subunit with N-terminal extension (*A. fumigatus*).

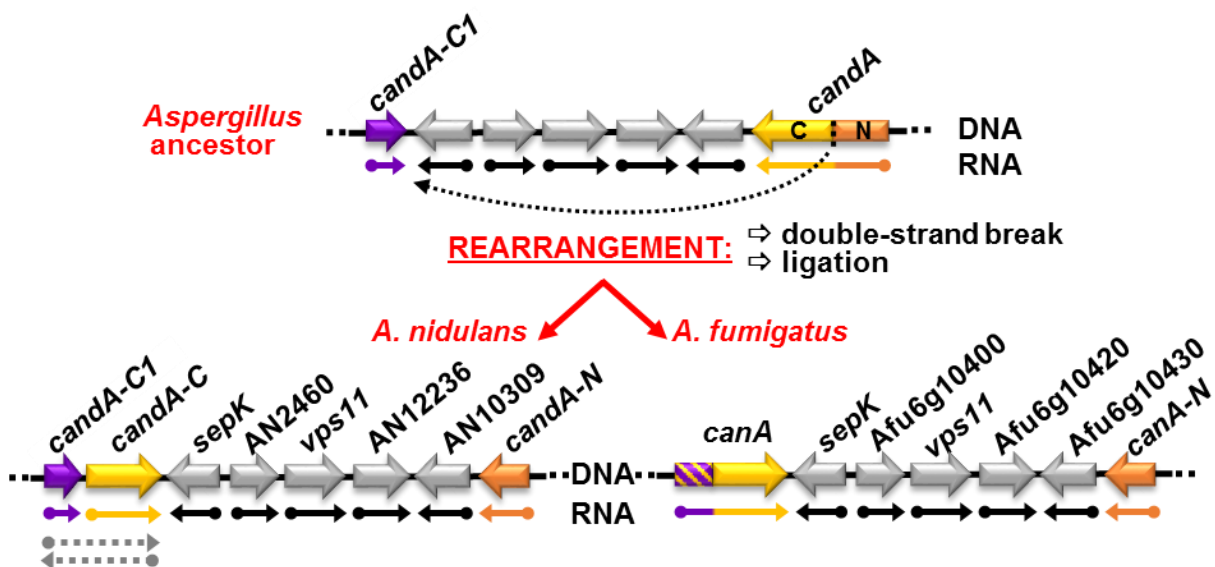


Figure 52. Scheme of a putative *Aspergillus* ancestor and DNA rearrangement of the *candA* loci. The ancestor of all *Aspergillus* spp. presumably had one gene containing sequence information of *candA-N* and *candA-C*. A DNA double strand break, followed by ligation has changed the position of *candA-C* five open reading frames upstream of *candA-N* and directly downstream of *candA-C1* in *A. nidulans*. In *A. fumigatus* the *candA-C1*-like sequence fused to the rearranged *canA*.

4.1.5 CandA-C1 and CandA-C are expressed from separate transcripts in *A. nidulans*

This study showed, that *A. nidulans candA-C1* and *candA-C* have primarily separate transcripts whereby the *intergenic region* contains the terminator signal for *candA-C1* and the promoter sequence for *candA-C* expression. PCR amplification of cDNA showed that *candA-C* and *candA-C1* additionally share one transcript (Figure 18, p. 74). This shared transcript might be either an antisense RNA for control of gene expression or a terminator read-through transcript, which is possibly translated into two proteins (Figure 53). The expression of *candA-C* was not affected when *candA-C1* was overexpressed. This observation suggests that *candA-C1* has either a strong terminator, which would exclude the read-through theory or both genes have primarily separate transcripts. Translation of CandA-C from a read-through transcript would presuppose an internal ribosomal entry site (IRES) upstream of *candA-C*. IRES prediction tools could not identify an IRES in the sequence of the long *candA-C1~candA-C* transcript. Therefore, the common transcript seems not to be the coding transcript. Whether this common transcript has a physiological function, for example as antisense transcript, is not clear so far.

Natural antisense transcripts (NATs) are RNAs that are complementary to the sense transcript, e.g. complementary to the 5' region (head-to-head) or 3' region (tail-to-tail) (Makalowska *et al.*, 2005; Smith *et al.*, 2008). The diversity of NATs is huge, bearing a broad functional range in biological processes but are typically produced to control transcription or translation (Faghihi and Wahlestedt, 2009; Werner and Swan, 2010; Wight and Werner, 2013). NATs are found in eukaryotes and exist in fungi like *N. crassa* where NATs have different expression levels dependent on external stimuli as temperature and circadian rhythm (Arthanari *et al.*, 2014). NATs were also reported in Aspergilli and it was shown that they are profuse in conidia where they influence conidiation and germination (Smith *et al.*, 2008; Tuch *et al.*, 2010; Novodvorska *et al.*, 2013; Tsujii *et al.*, 2016). *A. flavus* expresses some NATs in a temperature dependent manner and it was reported that two aflatoxin gene cluster genes have tail-to-tail associated NATs (Smith *et al.*, 2008).

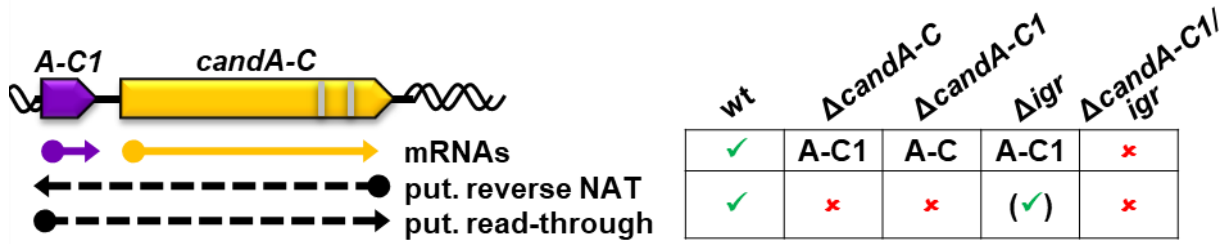


Figure 53. CandA-C1 and CandA-C have a shared transcript. Transcription of *candA-C1* (purple) and *candA-C* (yellow) open reading frames results in separate transcripts and a shared transcript, which might be the result of a *candA-C1* terminator read-through or an antisense transcript that regulates gene expression.

A. nidulans CandA-C and CandA-C1 were detected as separate proteins in contrast to *A. fumigatus* CanA, which harbors both sequences in one protein. The size difference, visible by western hybridization using GFP-tagged proteins, correlates to the predicted molecular weight of single CandA-C and CanA with N-terminal extension. The molecular weight of a CandA-C1~CandA-C fusion protein would be nearly identical to *A. fumigatus* CanA. The expression of a fusion protein was possible in *A. nidulans* when *candA-C1* was directly fused to *candA-C* without the *intergenic region*. The expression of this fusion complements the Δ *candA-C* phenotype. The functionality of the synthetic fusion could not be verified as CandA-C was also synthesized alone from its alternative translation initiation methionine encoded by the sixth codon post translational start. The expression of a shortened CandA-C must be prevented for example by mutation of the methionine residues to confirm the functionality of the CandA-C1~CandA-C fusion.

The *intergenic region* seems to be the terminator for *candA-C1* expression and the promoter for *candA-C* expression as full length *candA-C* could not be amplified in amounts comparable to wild type when the *intergenic region* was deleted (Figure 53).

In summary, *A. fumigatus* has a CanA protein with a CandA-C1-like domain in the N-terminus. In *A. nidulans* CandA-C1 and CandA-C are individual proteins translated from separate genes. Future investigations are needed to test whether the long transcript is a read-through or a natural antisense transcript and if so, whether it might be required to regulate the production of CandA-C1 and CandA-C for a stable hetero dimeric CandA-C/A-C1 complex.

4.2 CandA proteins are required for growth and development in *A. nidulans* and *A. fumigatus* and the *A. nidulans* CandA complex is connected to secondary metabolism

4.2.1 CandA-N and CandA-C but not CandA-C1 repress the production of orsellinic acid derivatives in *A. nidulans*

Developmental processes of filamentous fungi are connected to the production of secondary metabolites that can have supportive effects on developmental control under changing environmental conditions (Gerke and Braus, 2014). *A. nidulans* strains with single or double deletion of *candA-N* and *candA-C* have a characteristic dark brown color when incubated on solid medium under both, asexual and sexual development inducing conditions (Figure 39, p. 113, Figure 46, p. 124). This correlates with the already described phenotype by Helmstaedt *et al.*, 2011 and is most likely due to the production of orsellinic acid and its derivatives orcinol, diorcinol, cordyol C, violaceol I and violaceol II (Helmstaedt *et al.*, 2011). Orsellinic acid is a benzoic acid-type compound with substitution of two hydroxy groups and one methyl group. It is the product of the multidomain iterative orsellinic acid polyketide synthase OSAS encoded by the orsellinic acid gene cluster (AN7909-AN7914, *orsA-E*) (Schroeckh *et al.*, 2009; Sanchez *et al.*, 2010). These metabolites were not observed in wild type or in a strain with *candA-C1* deletion under the tested conditions (Figure 48, p. 128) indicating that CandA-C1 has no impact on this secondary metabolite gene cluster during asexual development, different than CandA-N and CandA-C. HPLC measurements showed different amounts of diorcinol and dehydroaustinol in the tested strains. The combination of both compounds was reported to induce sporulation of the conidiophore defective mutant $\Delta fluG$ (Rodríguez-Urra *et al.*, 2012). The amount of both metabolites correlated with the ability of conidiation, meaning that the highest amount of diorcinol and dehydroaustinol were measured in wild type, followed by the $\Delta candA-C1$ mutant. In the $\Delta candA-C$ strain the least amount of these metabolites was detected correlating to the low number of counted conidia (Figure 39, p. 113 and Figure 48, p. 128).

A strain deleted in the velvet-like *velB* gene has the same brownish phenotypical appearance like *candA* deletion strains (Sarikaya Bayram *et al.*, 2010; Park *et al.*, 2012) and the metabolites were identified to be orsellinic acid, F-9775B and F-9775A (Dissertation of Sabine Thieme, 2018). VelB is one of four known velvet family protein transcription factors that form different complexes of homo- or heteromers and thereby playing key roles in spore viability, development and secondary metabolism (Bayram *et al.*, 2008a; Bayram and Braus, 2012). It is likely that the stability of velvet proteins is dependent on CandA controlled SCFs (Braus *et al.*, 2010), thus phenotypical similarity can be explained. CandA-C1 might not be part of this control and therefore the orcinol secondary metabolism is not altered upon *candA-C1* deletion.

4.2.2 *Aspergillus* CandA is required for development

This work showed that a deletion strain of *canA-N* in *A. fumigatus* results in a reduced conidiospore production but vegetative growth was like wild type. The same was observed when the sequence encoding the C-terminal subunit corresponding to *A. nidulans candA-C* was deleted (*canA^{CTD}*), indicating that the N- and C-terminal subunits support conidia production (Figure 54). CanA-N and CanA^{CTD} were required for germination of conidia at 30°C, which is below the optimal growth condition at 37°C (Abad *et al.*, 2010; Krijgsheld *et al.*, 2013; Hagiwara *et al.*, 2017). In contrast, the *A. nidulans candA-N* and *candA-C* deletion strains had no germination defect of conidia but their secondary metabolism and development alterations were visibly stronger. Besides the altered secondary metabolism, decreased conidia formation and impairment of ongoing sexual development after early nest formation was observed (Figure 54), similar to the *csn* deletion strains (Busch *et al.*, 2007; Beckmann *et al.*, 2015).

A. nidulans candA-N and *candA-C* single or double deletion mutants do not alter vegetative growth but when *csn* and *candA* are defective, the colony growth is reduced possibly due to complete loss of SCF activity control. The second deneddylase DenA is also important for sexual development, as it is required for properly timed cleistothecia formation and ascospore production. These functions of DenA are different to the described impact on conidiation by Christmann *et al.*, 2013 and Schinke *et al.*, 2016. The different phenotypes of the previously described *denA* deletion strain can be explained by a combinatory effect of the used background strain AGB152 (*pyrG89*, *pyroA4*), the marker *pyr4*, which was used to introduce the *denA* deletion and the deletion of *denA* itself.

CSN complexes of other fungi are similarly important for growth and development. Csn5/E of *N. crassa*, but not Cand1, is required for hyphal growth, conidia formation and circadian rhythm (Wang *et al.*, 2010; Zhou *et al.*, 2012) *Aspergillus* is still able to propagate without the CSN and CandA, different to most higher eukaryotes that show embryonic lethality when *csn* and *cand1* were deleted (Yan *et al.*, 2003; Busch *et al.*, 2007; Gusmaroli *et al.*, 2007; Wei *et al.*, 2008; Beckmann *et al.*, 2015; Pacurar *et al.*, 2017). *Arabidopsis* seedlings deficient in *csn* are able to germinate but stop growth at early stages of root and shoot apex development due to defects in stem cell maintainance (Franciosini *et al.*, 2015; Jin *et al.*, 2018). CSN embryonic lethality in other eukaryotes is based on similar stem cell defects as shown for *Drosophila melanogaster* (Qian *et al.*, 2015) but also on misregulated cell cycle and defective DNA damage response (Brockway *et al.*, 2014; Chung *et al.*, 2015; Dubois *et al.*, 2016; Jumpertz *et al.*, 2017). Mammalian *cand1* suppressed cells show increased degradation of p27, which blocks cell cycle exit and subsequently cell differentiation and proliferation does not take place (Gummlich *et al.*, 2016; Zhang *et al.*, 2016). This is in accordance with the differentiation of LiSa-2 adipocyte cells that depend on functional Cand1 (Dubiel *et al.*, 2013, 2015). These

results correlate with impaired multicellular cleistothecia formation as observed for *A. nidulans* *csn* and *candA* deletion strains.

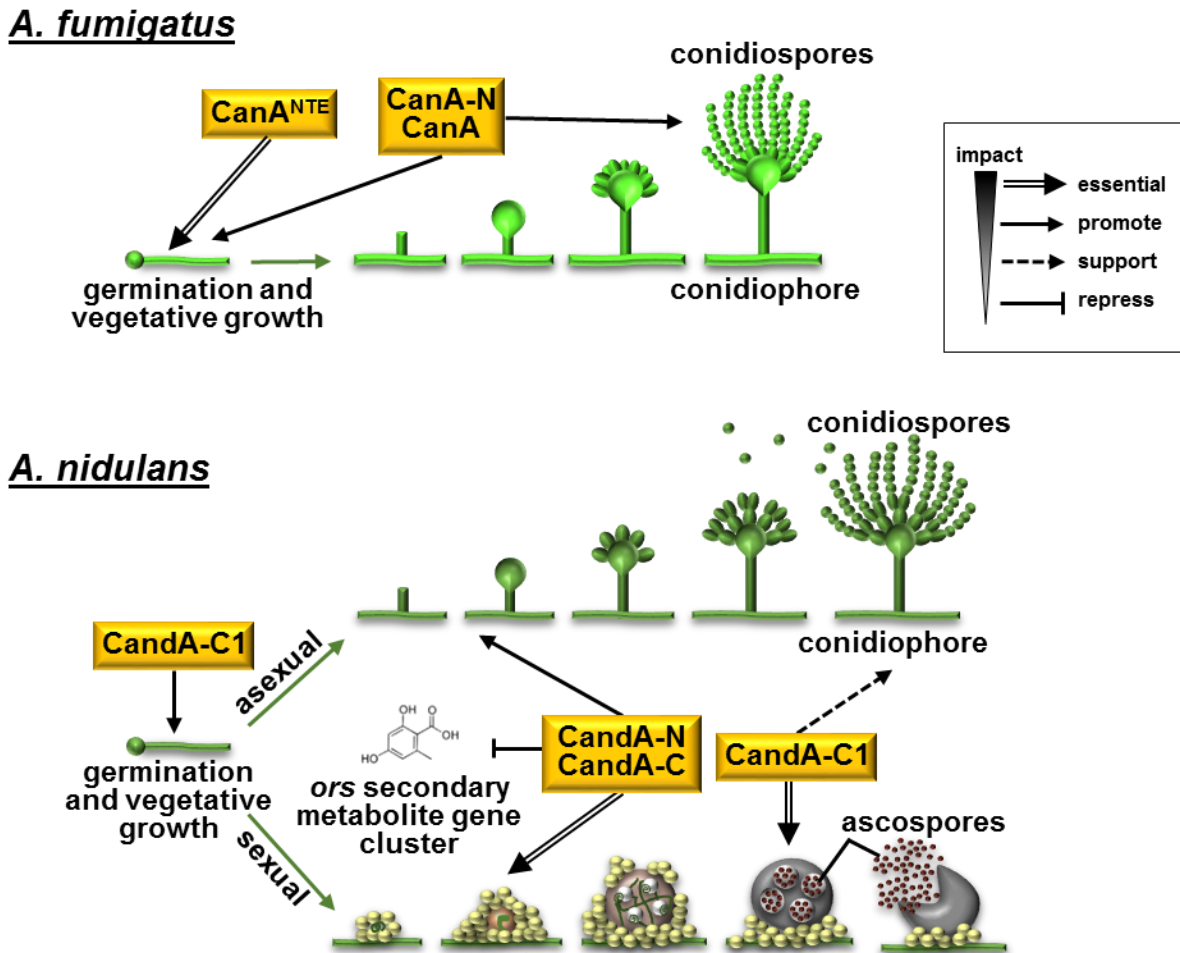


Figure 54. CandA/CanA are required for growth and development of *Aspergillus* spp. **Upper panel:** *A. fumigatus* CanA N-terminal extension is essential for properly timed spore germination and vegetative growth. CanA and CanA-N promote germination and vegetative growth during low temperature stress and promote conidiophore development. **Lower panel:** *A. nidulans* germination and vegetative growth is promoted by CandA-C1. CandA-C1 also supports conidia formation during the asexual life cycle. In the sexual cycle CandA-C1 is required for properly timed cleistothecia formation and is essential for the development of ascospores. CandA-N and CandA-C promote asexual conidiophore development and are essential for multicellular sexual fruiting bodies from the stage of early nest formation. CandA-N and CandA-C repress the orsellinic acid derivative production.

The drastic phenotypical alterations of *A. nidulans* *candA-N* and *candA-C* mutants disagree with *cand1/A* knockouts of most other fungi. *C. albicans* *cand1* deletion has only morphological, growth and protein degradation alterations when the strain was additionally lacking Nedd8 (Sela *et al.*, 2012). Similar effects were observed in *S. cerevisiae* where *lag2* (longevity assurance gene, homolog of *cand1*) deletion had no effect but overexpression of *lag2/cand1* was lethal in strains lacking Nedd8 or Dcn1, but not when Csn5 was missing (Siergiejuk *et al.*, 2009). Deletion of *nedd8* in *A. nidulans* is lethal but a *dcaA* deletion strain was shown to have wild type-like development (von Zeska Kress *et al.*, 2012). Contradicting results were reported for an *N. crassa* *cand1* deletion strain. It was shown that the circadian clock is independent from Cand1 (Zhou *et al.*, 2012). Slight differences in rice tube experiments of a *cand1* knockout mutant compared to wild type and increased cullin neddylation were stated five years later, but are almost indistinguishable from controls (Liu *et al.*, 2017b). Cand1 is connected to auxin response, growth and development like leaf venation and crown root primordia development in plants like *A. thaliana* and *Oryzae sativa* (Chuang *et al.*, 2004; Alonso-Peral *et al.*, 2006; Zhang *et al.*, 2008; Aguilar-Hernández *et al.*, 2017). Furthermore, it was shown that Cand1 is essential in *O. sativa* as germlings survived only for two weeks when *cand1* was deleted (Wang *et al.*, 2011).

A. nidulans CandA-N and CandA-C have great impact on secondary metabolism as well as asexual and sexual development but the fungus is still able to survive under laboratory conditions without this protein complex (Figure 54). The *A. fumigatus* CanA-N and CanA C-terminal domain proteins are required for an appropriate production of conidia and are essential for spore germination at 30°C, which is below its growth optimum. These phenotypical alterations allow the analysis of CandA's impact on cellular pathways within eukaryotic cells.

4.2.3 *A. nidulans* CandA-C1 and the *A. fumigatus* CanA N-terminal domain are required for germination and vegetative growth

A. nidulans CandA-C is the ortholog to the *A. fumigatus* CanA C-terminal domain. *A. fumigatus* CanA has an N-terminal extension of 200 amino acids, encoded in the first exon. This extension corresponds to the separate protein CandA-C1 in *A. nidulans*. Deletion of only the first exon sequence of *A. fumigatus* *canA* or the *A. nidulans* orthologous gene *candA-C1* resulted in strains with vegetative growth defect (Figure 36, p. 108 and Figure 37, p. 111).

CandA-C1 and CanA^{NTE} are similarly required for conidia germination of their respective *Aspergillus* species at high temperature stress. In addition *A. fumigatus* CanA-N and CanA^{CTD} together are required for germination at 30°C. *A. nidulans* is more robust concerning growth

without *candA-N* and *candA-C* at different temperatures. Its growth optimum was reported to be between 35 to 37°C compared to *A. fumigatus* at 37°C (Trinci, 1969; Abad *et al.*, 2010; Krijgsheld *et al.*, 2013; Hagiwara *et al.*, 2017). Cold stress was shown to activate the HOG (high-osmolarity glycerol) pathway that transfers the stress signal to the nucleus to respond with transcriptional activation of for example thermotolerance genes followed by stabilization of the fungal cell wall (Ji *et al.*, 2012; Wong Sak Hoi *et al.*, 2012; Hagiwara *et al.*, 2016). These signaling pathways are interconnected with post-translational modifications and subsequently with CRLs. It is likely that CandA regulates the activity of CRLs, which are involved in modification of signaling pathway components, such as from the HOG pathway. Similar observations were made on the mammalian NF- κ B signaling pathway or other MAPK pathways (Sato *et al.*, 2003; Bayram *et al.*, 2012; Ahmed *et al.*, 2013; Ghosh and Dass, 2016) and are reviewed in Hagiwara *et al.*, 2016. Fungal cell wall homeostasis is also connected to TslA (trehalose regulatory-like) and TslB that support trehalose stability (Thammahong *et al.*, 2017). Trehalose is the major stress resistance factor for spores of *A. fumigatus* and *A. nidulans* (Al-Bader *et al.*, 2010; Fillinger *et al.*, 2018). Trehalose is a disaccharide of two α -glucose units found in high concentrations in asexual spores during dormancy and serves as energy source during germination (Leloir and Cabib, 1953; Cabib and Leloir, 1958; Hayer *et al.*, 2013; Hagiwara *et al.*, 2017). TslA is a dual function 'moonlighting' protein and besides its role in the trehalose synthesis it is also involved in chitin synthase activity (Thammahong *et al.*, 2017). Furthermore, it was reported that trehalose levels decrease at 25°C, which was explained by increased expression of the trehalose hydrolase gene *treB*, resulting in higher trehalose degradation efficiency (Svanström and Melin, 2013; Hagiwara *et al.*, 2017). CandA mediated UPS control might destabilize trehalose degrading enzymes and therefore improve stress resistance through stable trehalose levels. Additionally, CandA proteins seem to be required in general for the stress response by regulating the stability of signaling pathway components.

Observations on the sexual development of *A. nidulans* revealed that CandA-C1 is similarly required like CandA-N and CandA-C in cleistothecia development. The mutant strain without *candA-C1* is delayed in cleistothecia development and impaired in ascospore formation. Later during development the cleistothecia contained only hyphal structures that are most likely the ascogenous hyphae that failed to develop into asci filled with ascospores (Pontecorvo *et al.*, 1953; Braus *et al.*, 2002; Busch and Braus, 2007; Busch *et al.*, 2007; Pöggeler *et al.*, 2018). These results show that *A. nidulans* CandA-C1 supports the cleistothecia maturation in a later phase than CandA-N and CandA-C (Figure 54), which might be explained by CandA-N and CandA-C forming a dimeric CandA complex involved in most cellular processes and a trimeric CandA complex with CandA-C1 might be only required under certain conditions. *A. fumigatus*

CanA complex is required for spore germination at temperature stress conditions. The CanA N-terminal domain and *A. nidulans* CandA-C1 influences vegetative growth.

4.2.4 The *Aspergillus* specific CanA N-terminal extension and CandA-C1 are putative candidates for invasive aspergillosis treatment

Aspergillus spp. can have the potency for pathogenicity, allergy or toxicity to mammals, as immunocompromised patients are susceptible for invasive aspergillosis. Crops can be contaminated with mycotoxins such as aflatoxin (Dagenais and Keller, 2009; Bossou *et al.*, 2017; Challa, 2018). Specific treatment is difficult due to limited drug targets and emerging resistances e.g. against azoles (Bader *et al.*, 2015; Steinmann *et al.*, 2015; Gsaller *et al.*, 2016). Drug target search considered also components of the ubiquitin proteasome system, which is the most common cellular protein destruction pathway and contains essential elements that are mostly conserved through eukaryotes. Csn5/E is upregulated in many different cancers (Lee *et al.*, 2011) and thereof proteasome or CSN inhibitors like thiolutin and azaindoles are investigated with respect to pharmacological and therapeutic means (Schlierf *et al.*, 2016; Altmann *et al.*, 2017; Collins *et al.*, 2017; Lauinger *et al.*, 2017). Besides the CSN and the proteasome also other components of the ubiquitin degradation pathway are investigated upon their importance on *A. fumigatus* virulence like the fungal specific Fbx15 protein. Fbx15 is responsible for the nuclear localization of the SCF substrate adaptor SkpA and the transcriptional co-repressor SsnF, and thereby Fbx15 is required for fungal virulence (Jöhnk *et al.*, 2016). Trehalose is absent in humans and consequently in focus of a recent study that aims to find novel therapeutic targets against different kinds of mycosis (Thammahong *et al.*, 2017). The dependence of spore viability on trehalose (Ni and Yu, 2007; Park *et al.*, 2015) might also be responsible for germination deficiencies observed in *candA-C1/canA* deletion strains, but must be analyzed in future studies. The CanA NTE of *A. fumigatus* or the CandA-C1 separate subunit in *A. nidulans* are required for growth and germination at mild heat stress that would agree with fever as response of the host immune system to infection. This germination defect could be due to programmed cell death similar as reported by Shelzinger and co-workers. They showed that the immune system is able to induce an apoptosis-like programmed fungal cell death of conidia when a key mediator of the pathogenic virulence response is blocked (Shlezinger *et al.*, 2017). Mild-heat stress in combination with antifungal drugs was also shown to inhibit biofilm formation and thereby supported drug susceptibility (Zeng *et al.*, 2014). Biofilm formation in *A. fumigatus* is dependent on the transcription factor SomA that mediates invasive growth and adhesion required for pathogenicity (Lin *et al.*, 2015).

With this study the *Aspergillus* conserved novel component of the Cand1/A complex was identified and analyzed. This polypeptide of the Cand1/A complex is unique to Aspergilli and required for vegetative growth, sexual reproduction and activation of the ubiquitin labeling machinery. These features could make CandA-C1 an interesting candidate for target specific drug design without affecting the human ubiquitin-proteasome system. The human RNase P complex subunit Rpr2/Rpp21 might not be affected by targeting fungal CandA-C1 as their protein sequence identity is only 20 %. Inhibition of the fungal CandA complex would lead to early developmental and growth defects as it was proven by deletion mutants. This defect could be beneficial in the treatment of mycosis as tissue-invading spores have the potential for germination within 30 minutes (Paulussen *et al.*, 2017). Therefore, inhibitors must be explored that bind *A. nidulans* CandA-C1 or its orthologous peptide sequence in *A. fumigatus* to prevent CandA complex formation. Otherwise, the silencing of the corresponding gene could be achieved by for example RNA interference like the suggested internal transcriptional control mechanism with an antisense transcript. The microRNA miR-33a was shown to target *cand1*, which expression was increased in human lung cancer cells (Kang *et al.*, 2017). With this basis CandA-C1 could become a promising target to control fungal spreading.

4.3 CandA facilitates Cula neddylation

4.3.1 *A. nidulans* CandA mediates substrate-receptor-adaptor release on Cula containing SCFs

CSN and Cand1 were first described as negative regulators of CRL activity *in vitro* but *in vivo* experiments revealed CSN and Cand1 are required for proper CRL function (Wolf *et al.*, 2003; Busch *et al.*, 2007; Bosu and Kipreos, 2008; Dubiel, 2009; Beckmann *et al.*, 2015). Cand1 supports the dissociation of substrate-receptor complexes from SCF scaffolds and in turn it does not inhibit SCF assembly (Lydeard *et al.*, 2013). Different to *candA* deficient *A. nidulans* strains, deletion of any *csn* subunit causes accumulation of neddylated cullins (Busch *et al.*, 2007; von Zeska Kress *et al.*, 2012; Beckmann *et al.*, 2015). Double deletion strains of $\Delta csnE/\Delta candA$ resulted in the same amount of neddylated Cula as the single $\Delta csnE$ strain. Subsequently, the order of SCF inactivation is first deneddylation by CSN, followed by CandA binding for substrate-receptor disassembly, priming CRLs for new assembly with substrate-receptor units (Figure 55A).

The competition for CRL binding is shared by the CSN, Cand, neddylation pathway factors and adaptor-receptor units charged with substrates (Emberley *et al.*, 2012; Enchev *et al.*, 2012; Zheng and Shabek, 2017; Liu *et al.*, 2018). Thereby, Cand1 was found to mainly build complexes with Cul1 and is less associated with other cullins (Bennett *et al.*, 2010). This corroborates with results from this work that showed CulA as the only cullin associated with *A. nidulans* GFP-tagged CandA subunits in pull-down experiments. Pull-downs performed with *A. fumigatus* CanA-GFP identified besides CulA also CulC as putative interaction partner. The third *Aspergillus* cullin protein CulD was never identified as putative interaction partner of CandA/CanA. CulA, C and D were identified as interaction partners of Nedd8, underlining that all three cullins are neddylation to perform their ligase activity.

Deneddylation assays performed with Nedd8 antibody to observe levels of total neddylation cullins in *A. nidulans* did not show differences in neddylation status of total cullins in *candA-N* and *candA-C* deletion strains. An increase in total deneddylation cullins was observed in strains with *candA-C* deletion and simultaneous overexpression of *candA-C1*. Elevated levels of CandA-C1 in wild type background had no effect on CRL activity but seemed to have a rescuing effect when CandA-C was absent. The total number of ubiquitinated proteins was lower in all *candA* mutant strains, which underlines the importance of CandA for CRL activity. These results need to be further investigated in respect to the following questions: i) is CulA more abundant than other cullins and ii) does *A. nidulans* CandA have preferences for CulA containing SCFs and *A. fumigatus* CanA additionally to CulC SCFs? The second possibility would suggest that SCFs with other cullin scaffolds are differentially regulated concerning their substrate-adaptor-receptor exchange. *A. nidulans* CandA-C was reported to interact with CulD in yeast-two-hybrid assays, but to less extent than to CulA (Helmstaedt *et al.*, 2011). This observation would support that the CulC and CulD concentration was too low to identify CandA attached to both cullins in GFP-trap experiments but propose that CandA is in general able to interact with all types of SCFs.

So far, it is unclear how exactly CandA dissociation from CulA is triggered. It was shown that dephosphorylation of Fbx15 changes the SCF assembly in *A. fumigatus* (Jöhnk *et al.*, 2016). This might also trigger CandA disassembly from CulA allowing phosphorylated Fbx15-Skp1 binding. Post-translational modification as trigger for Cand1-Cul1 interaction and disassembly was also considered in studies with human Cand1 (Chua *et al.*, 2011). Further suggestions rely on the availability of substrate-receptor-adaptor complexes that lead to CandA dissociate from CulA (Pierce *et al.*, 2013). Different studies showed that accumulation of specific substrates forces their incorporation into the SCF as observed for the F-box protein Skp2. Skp2 accumulates in a specific phase of the cell cycle and then builds a SCF-Skp2 ligase that forces degradation of p27 and thereby ongoing cell cycle in human cell lines (Bornstein *et al.*, 2006; Lydeard *et al.*, 2013; Skaar *et al.*, 2013). Summarizing, *A. nidulans* CandA complex is

required for CRL activation with CulA scaffold. Furthermore, the novel third CandA-C1 subunit might have a stabilizing function for the complex and supports CRL activity when CandA-C is absent.

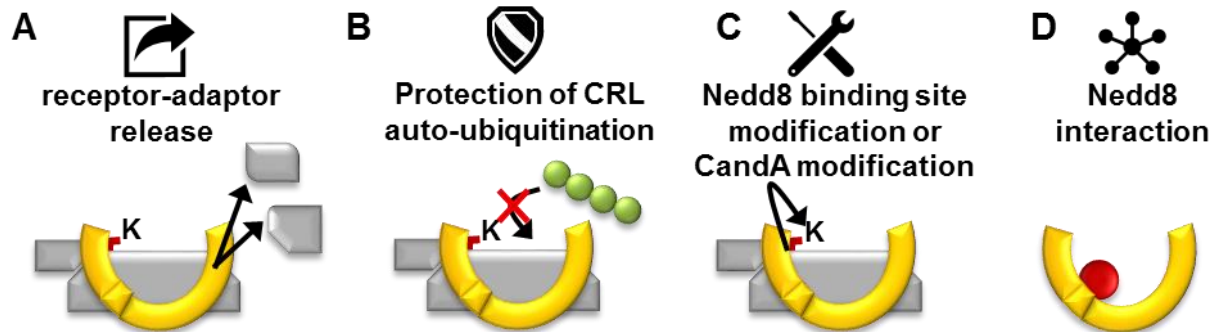


Figure 55. Possible functions of the CandA-CulA interaction for E3 ubiquitin ligase activity. **A** CandA complex formation on SCF complexes mediates adaptor-receptor release. **B** CandA might protect CRLs from auto-ubiquitination (green) when no substrates are available. **C** CandA-N is required for new neddylation putatively by post-translational modification of the cullin neddylation site or by facilitating E2 Nedd8 transfer. **D** All CandA subunits interact with Nedd8 in BiFC microscopy assays and Nedd8 pulls CandA-N and CandA-C in GFP-trap experiments, supporting the idea of CandA mediating CulA neddylation.

4.3.2 CandA might protect CRLs from autoubiquitination by a mechanism similar to CSN

CSN binding to a CRL does not only inactivate the ligase by deneddylation but also blocks substrate access and prevents autoubiquitination of CRL components when the CSN remains bound to the CRL (Bennett *et al.*, 2010; Emberley *et al.*, 2012; Enchev *et al.*, 2012; Zemla *et al.*, 2013). Autoubiquitination is not solely inhibited by CSN covering the CRL but also by deubiquitinating enzymes associated with the CSN such as Usp15 or Ubp12 (Heffeld *et al.*, 2005; Wu *et al.*, 2006; Huang *et al.*, 2009; Chou *et al.*, 2017). It is likely that also CandA has a stabilizing function on CRLs while they form a complex (Figure 55B) (Chua *et al.*, 2011). This would be required for maintaining the CRL repertoire until substrate receptor modules would compete for binding to cullins, followed by CandA dissociation allowing CRL activation. In case CandA cannot release substrate receptor modules from CRLs, the CRLs would be useless and targeted for degradation. However, this study showed increased amount of deneddylated cullins in *A. nidulans* strains lacking CandA. These observations suggest that the CSN remains bound to deneddylated cullins and by this the number of unemployed CRLs without substrates

increases. This increase of deneddylated cullin was not observed in other fungal species like *N. crassa* (Zhou *et al.*, 2012) indicating different CRL regulation by the CSN and CandA in *A. nidulans*.

4.3.3 *A. nidulans* CandA-N might modulate the cullin-Nedd8 binding site to facilitate neddylation

This work demonstrates accumulation of inactive, deneddylated CulA and decreased total ubiquitinated proteins in *candA* mutant strains. Previous findings suggested that CandA-C binds first to CRLs and only then CandA-N can join the complex, which correlates with the nuclear import dependence of CandA-N on CandA-C (Helmstaedt *et al.*, 2011). It was not yet solved when CandA-C1 joins the dimeric CandA complex and the CRL. For higher eukaryotes a different mechanism was reported. Studies showed that the N-terminus of a one subunit Cand1 binds first to the Nedd8 site and then the C-terminal part changes conformation to release the adaptor-receptor module (Lydeard *et al.*, 2013; Pierce *et al.*, 2013; Liu *et al.*, 2018). The different order of how CandA terminal ends bind cullins in *A. nidulans* might be a feature of the *Aspergillus* specific split-CandA.

The human Nedd8 E3 ligase Rbx1 requires additional auxiliary factors of the DCNL family for cullin neddylation (Kurz *et al.*, 2005, 2008; Scott *et al.*, 2010). DCNLs bind close to the cullin neddylation residue and simultaneously to the acetylated N-terminal amino acid residue of the Nedd8-E2 enzyme (Scott *et al.*, 2014; Enchev *et al.*, 2015). It is proposed that in this way DCNLs rearrange the Rbx1-E2~Nedd8 complex to orient it towards Nedd8 ligation to cullin (Scott *et al.*, 2010, 2011, 2017). Human Cand1 was co-purified with DCN1-5 and prevents DCNLs from neddylating cullin until substrate adaptor complexes compete for binding (Keuss *et al.*, 2016). *A. nidulans* as well as *S. cerevisiae* have only one DCN family protein (Scott *et al.*, 2011; von Zeska Kress *et al.*, 2012). The pull-downs performed in this study could not show a CandA-DcnA interaction neither a Nedd8-DcnA interaction, indicating minor importance of fungal DcnA in the neddylation process. *A. nidulans* DcnA is not essential and a mutant strain does not show altered development different to *candA* or *csn* deletion strains (Busch *et al.*, 2007; Helmstaedt *et al.*, 2011; von Zeska Kress *et al.*, 2012; Beckmann *et al.*, 2015), supporting that DcnA does not play a crucial role in the *A. nidulans* E3 ligase activity regulation. Recombinantly expressed *A. nidulans* CandA-N and CandA-C were not sufficient to restore SCF activity in fungal crude extracts in *in vitro* deneddylation assays. This strongly suggests that post-translational modifications are required for the CandA-CulA binding and adaptor-receptor exchange, which are not provided by the bacterial expression system. It was not yet tested, whether a recombinant trimeric CandA with CandA-C1 can complement the

CulA neddylation, because CandA-C1 could not be expressed and purified in sufficient amounts.

Poly(ADP)-ribosylation (PARylation) was described in human as post-translational modification of a RNF146 RING type E3 ubiquitin ligase, leading to allosteric activation similar as observed for neddylation (Wang *et al.*, 2012; DaRosa *et al.*, 2015). PARylation is found to regulate a plethora of biological processes as for example the Wnt signaling or DNA repair as well as transcription by histone PARylation (Leidecker *et al.*, 2016; Yang *et al.*, 2016; Liu *et al.*, 2017a). However, *A. nidulans* or *A. fumigatus* have no homolog of RNF146. Nevertheless, PARylation of CandA or CandA interacting proteins is likely as an ADP-ribosylation factor ArfA (AN1126, Afu1g11730) was identified in pull-downs with all *A. nidulans* CandA proteins or with *A. fumigatus* CanA. This study showed that CandA either itself is post-translationally modified or transfers a modification to the CRL, which allows neddylation (Figure 55C). PARylation or other post-translational modifications like phosphorylation can also be considered to induce CRL activation in a CandA-N dependent manner and are of interest for further studies on the regulation of CRL activity by CandA.

4.3.4 *A. nidulans* CandA physically interacts with Nedd8

Ubiquitin and ubiquitin polymers have many interacting proteins involved in recognition and downstream signaling (Komander and Rape, 2012; Zhao *et al.*, 2017; Zheng and Shabek, 2017). Therefore it is likely that also Nedd8 interacts with Nedd8 pathway enzymes and downstream effectors but so far the knowledge about Nedd8 interacting proteins is limited (Mergner and Schwechheimer, 2014; Enchev *et al.*, 2015). The best studied Nedd8 associated proteins are the cullins (Jones *et al.*, 2008) and Nedd8 activating enzymes UlaA and UbaC, which were found to be associated in GFP-Nedd8 pull-downs performed under native and denaturing conditions (Figure 33, p. 100). CandA-N and CandA-C were also pulled by GFP-Nedd8 but only under native conditions, indicating that the interaction is not due to CandA being covalently neddylated. A CandA-C1-Nedd8 interaction was also observed in a strain allowing bimolecular fluorescence complementation and Nedd8 was found in pull-down elution fractions of CandA-C1-GFP (Figure 25, p. 84 and Figure 34, p. 104). This Nedd8 interaction with the so called 'cullin-associated Nedd8-dissociated' protein and the fact that except for *S. cerevisiae*, Cand1/A was never found to be associated with Nedd8 refers to new research aspects including questions of where Nedd8 binds CandA and for which purpose (Siergiejuk *et al.*, 2009).

It is described that interactions with Nedd8 occur with the hydrophobic surface site around isoleucine 44, which is recognized by small domains of the interacting proteins (Bandau *et al.*, 2012; Singh *et al.*, 2012; Ma *et al.*, 2013; Enchev *et al.*, 2015). CandA putatively binds Nedd8

within this region and this might facilitate CRL neddylation (Figure 55D). The exact role of the CandA interaction with Nedd8 could not be solved so far. On the one hand, the CandA complex might bind Nedd8 as a transition step between CSN mediated deneddylation and CandA-CRL binding to keep Nedd8 close to the CRL for new cycles of CRL activation. On the other hand, CandA may directly participate in neddylation, remodeling the neddylation site like DCN proteins. The assumed nuclear transport dependence of Nedd8 on CandA-C could not be confirmed as Nedd8 localized to nuclei in a strain expressing *candA-C* without NLS.

It is also conceivable that CandA is not directly interacting with Nedd8 but through shared binding partners like CulA or one of the 16 other shared putative proteins identified by pull-down experiments. In summary, CandA is a Nedd8 associated protein different as described by its name. The exact role of this association is not clear but has probably a CRL regulatory function.

4.3.5 CandA mediated protein quality control is observed at the nucleus, in the cytosol and at mitochondria in *A. nidulans*

Protein quality control mediated by the ubiquitin-proteasome system is needed in many different cell components (Pines and Lindon, 2005). SCF E3 ligases and their regulatory elements (CSN and Cand1/A) as well as the 26S proteasome are for example localized at the mitochondria outer membrane for mitochondrial protein quality control (Azzu and Brand, 2010; Taylor and Rutter, 2011; Heo *et al.*, 2015). Ubiquitin-proteasome components are also present in the cytosol for degradation of proteins involved in e.g. translation (Wang *et al.*, 2013; Inobe and Matouschek, 2014; Williams and Dichtl, 2018). Furthermore, the endoplasmic reticulum (ER) detects misfolded proteins by the unfolded protein response leading for instance into the activation of the ER-associated degradation pathway, which secretes proteins into the cytosol for proteasomal degradation (Tsai and Weissman, 2010; Moore and Hollien, 2012; Hampel *et al.*, 2016). Protein degradation is also reported to take place in the nucleus where it ensures for example gene expression or DNA repair (von Mikecz *et al.*, 2006; Park *et al.*, 2013; Nielsen *et al.*, 2014; Chowdhury and Enenkel, 2015; Boban and Foisner, 2016).

This study revealed several aspects of the CandA complex being connected to mitochondrial activity, including the identification of putative interaction partners located in mitochondria. Deletion of *candA* genes caused fragmented mitochondria, similar as observed for a strain lacking the proteasome lid subunit SemA (Kolog Gulko *et al.*, 2018). This strain showed downregulation of the mitochondrial fusion protein encoding gene *fzoA* (Kolog Gulko *et al.*, 2018). FzoA was shown to be ubiquitinated and degraded at the outer mitochondrial membrane as substrate of the F-box protein Mdm30p in *S. cerevisiae* (Cohen *et al.*, 2008;

Livnat-Levanon and Glickman, 2011). CandA protein interaction studies with BiFC microscopy revealed that the CandA complex is not only localized in the nucleus but also at mitochondria. The mitochondrial associated degradation pathway regulates the stability of mistargeted, misfolded or no longer needed proteins in mammalian cells (Livnat-Levanon and Glickman, 2011; Taylor and Rutter, 2011). Those proteins are translocated to the outer membrane, which anchors ubiquitin E3 ligases like the parkin HECT E3 ligase (Heo *et al.*, 2015; Ordureau *et al.*, 2015; Mouton-Liger *et al.*, 2017) or even the proteasome (Azzu and Brand, 2010; Taylor and Rutter, 2011). This study indicates that CandA might serve as a regulator for mitochondria-connected SCFs supporting mitochondrial protein quality control.

Nuclear protein import requires importins that recognize and bind their cargo proteins by a nuclear localization sequences (NLS) (Görlich *et al.*, 1996; Ström and Weis, 2001; Kosugi *et al.*, 2009a). NLS are classified in two groups: i) monopartite NLS consist of a single sequence of basic amino acids and ii) bipartite NLS with two clusters of basic amino acids that are separated by 10-12 amino acids (Kosugi *et al.*, 2008). The monopartite NLS is predicted to have a conserved consensus sequence of K(K/R)X(K/R), where X means any amino acid and the bipartite NLS of (K/R)(K/R)X₁₀₋₁₂(K/R)_{3/5}, where at least three of five amino acids are either lysine or arginine (Dingwall and Laskey, 1991; Robbins *et al.*, 1991). It has also been stated that those sequences differ between species (Kosugi *et al.*, 2008).

NLS prediction (cNLS Mapper; (Kosugi *et al.*, 2009a)) and MUSCLE protein sequence alignment (Edgar, 2004) of eukaryotic Cand1/A proteins revealed that the presence of a canonical monopartite NLS is restricted to fungal Cand proteins (Figure 56A). The identified nuclear localization core-sequence RKRRR is conserved in *A. nidulans*, *A. fumigatus*, *P. chrysogenum*, *V. dahliae* and *N. crassa*. *U. maydis* has with LKRKR a different variant of the monopartite NLS. This monopartite NLS is in the N-terminal half of the CandA C-terminal subunit, which amino acids assemble HEAT repeat helix B9 in the afore mentioned fungi. Humans, *A. thaliana* and *C. albicans* have a putative bipartite NLS, which was predicted with a lower score than the monopartite NLS of fungal Cand proteins (Figure 56B) The score was determined by a reporter assay with different NLS motifs fused to GUS-GFP and high scores designate strong NLS activities (Kosugi *et al.*, 2009a, 2009b). The bipartite sequences are in the C-terminal end different to the fungal monopartite NLS's. The NLS mapper tool could not identify a NLS for Cand1 from *D. melanogaster* and *S. cerevisiae*, suggesting that either they have an unconventional NLS different to the core-sequence of other NLS's or they lack an NLS.



Figure 56. The monopartite NLS is conserved in most fungal CandA orthologs. A MUSCLE protein sequence alignment of the HEAT repeat helix 9 region with highlighted monopartite NLS. The NLS RKRRR core sequence (cyan) is conserved in *N. crassa* (Nc), *V. dahliae* (Vd), *P. chrysogenum* (Pc), *A. fumigatus* (Af) and *A. nidulans* (An) Cand1/A and has a high score (Kosugi *et al.*, 2009b). *U. maydis* (Um) has a different core sequence of LKRKR (green). *H. sapiens* (Hs), *D. melanogaster* (Dm), *A. thaliana* (At), *S. cerevisiae* (Sc) and *C. albicans* (Ca) do not have a monopartite NLS in this region. (pos. means amino acid position). **B** Bipartite NLS with low scores were identified for Hs, At and Ca which would be in the C-terminal end of the Cand1 proteins. Dm and Sc do not show any NLS. CandA-C1 has a putative bipartite NLS in the middle of its sequence. Basic amino acids lysine (K) and arginine (R) are highlighted in orange.

Nuclear localization of CandA-N and CandA-C was shown in this study as well as previously by Helmstaedt and co-workers, who also reported nuclear localization of CandA in complex with Cula (Helmstaedt *et al.*, 2011). In addition, they showed that CandA-N nuclear localization is dependent on CandA-C NLS as CandA-N has no own NLS (Helmstaedt *et al.*, 2011).

A strong monopartite NLS was not predicted for the novel third CandA subunit CandA-C1 either, but a bipartite NLS was predicted with low score to be in the middle of the protein sequence (Figure 56B). This work demonstrated that CandA-C1 nuclear import is independent of CandA-C, suggesting a different transport mechanism than for CandA-N.

The pull-down data revealed importins as putative interaction partners of CandA-C1. These findings suggest that CandA-C1 might be transported into the nucleus through direct interaction to the importin- α/β homologs KapA (AN2142) and KapB (AN0906). KapA and B are essential karyopherin- β superfamily members with nuclear localization of KapA and perinuclear localization of its adapter KapB (Fernández-Martínez *et al.*, 2003; Markina-

Iñárraegui *et al.*, 2011). In *A. nidulans* nuclear transport of the important regulator of sexual development and secondary metabolism VeA in complex with VelB is mediated by KapA (Stinnett *et al.*, 2007; Bayram *et al.*, 2008a; Sarikaya Bayram *et al.*, 2010). CandA-C1's nucleolar localization might be due to complex formation with the non-essential importin-4 homolog KapJ, that was reported to have a nucleocytoplasmic localization during interphase but is found in the nucleolus during mitosis (Markina-Iñárraegui *et al.*, 2011). The independence of CandA-C1 from CandA-N and CandA-C might be required for different subsets of CandA-C1 in different compartments to allow its putative second function in the RNase P complex. Furthermore, CandA complex formation with and without CandA-C1 as stoichiometric subunit could be transport dependent. It would be interesting for the future understanding of CandA complex dynamics, whether CandA-C1 loses its nucleolar localization in a *candA-C^{ΔNLS}/ΔkapJ* strain.

4.4 Conclusion and Outlook

This study shows that the CandA complex from *A. nidulans* and most other *Aspergillus* spp. has three subunits: CandA-N, CandA-C1 and CandA-C, whereas the CandA complex of *A. fumigatus* has two subunits CanA-N and CanA. CanA carries an N-terminal extension that is orthologous to *A. nidulans* CandA-C1. Investigations of the genetic locus of *A. nidulans candA* showed, that *candA-C1* is 269 bp upstream of the *candA-C* gene, which in turn is around 18 000 bp, including five open reading frames, upstream of *candA-N*. A similar arrangement of genes can be observed in *A. fumigatus*, but the *canA* gene includes the additional sequence information corresponding to *A. nidulans candA-C1* in the first exon (Figure 57 ①Af). These observations propose a common ancestor of *Aspergillus* spp., which had one gene including the information for the N- and C-terminal domains. Possibly a DNA double strand break and rearrangement of the DNA sequences encoding the C-terminal domain placed this sequence 18 000 nucleotides upstream and to *candA-C1*. *candA-C1* became a part of the *canA* gene in *A. fumigatus* but in *A. nidulans candA-C1* and *candA-C* are separate genes.

Expression of *A. nidulans candA-C1* and *candA-C* results into separate as well as into shared transcripts (Figure 57 ①An). The *candA-C1~candA-C* transcript can be an mRNA product from *candA-C1* terminator read-through or is a putative natural antisense transcript, which might regulate the generation of sufficient and equal amounts of both CandA subunits for complex formation.

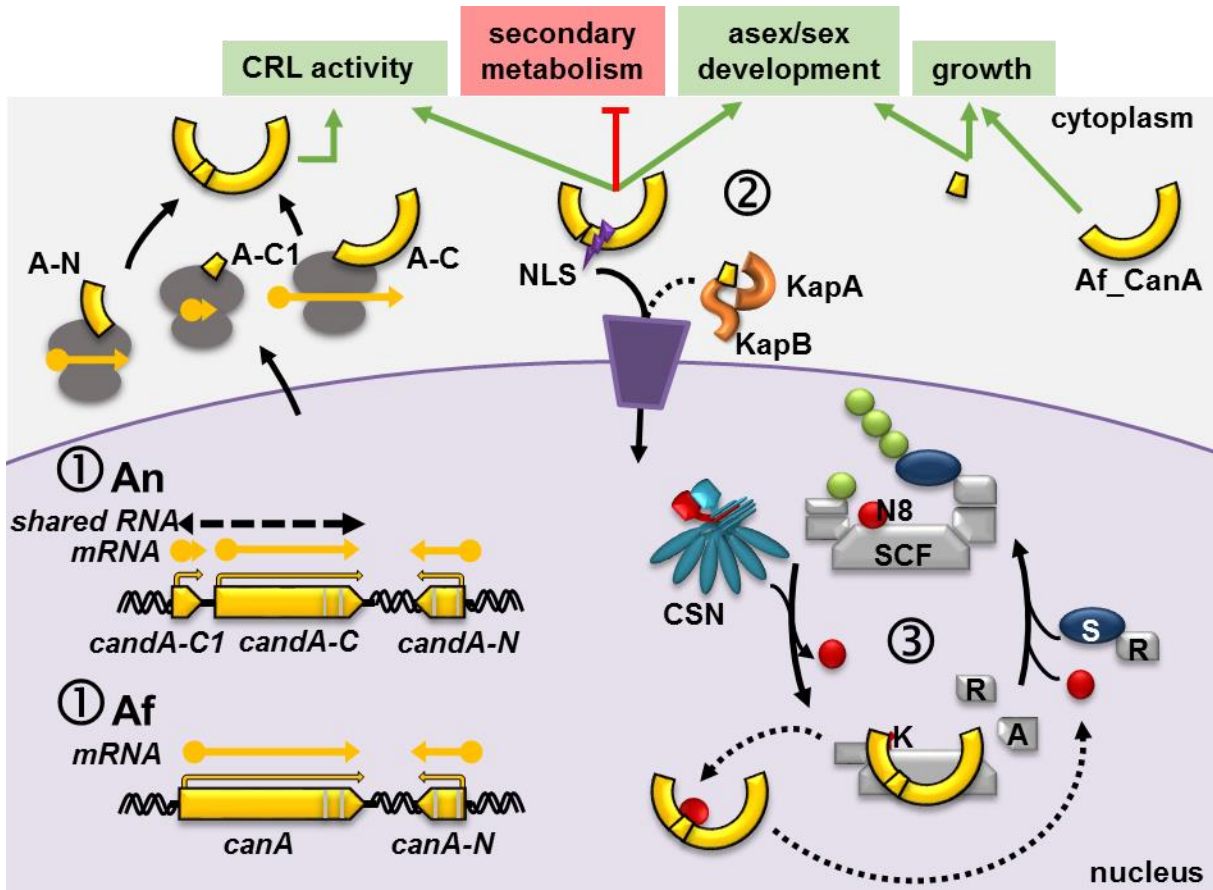


Figure 57. Comprehensive model of *candA* expression, nuclear transport and regulator of SCF activity. ①Af: *A. fumigatus* *canA* includes a *candA-C1* orthologous sequence and expresses two CanA proteins. ①An: *A. nidulans* *candA* genes are expressed separately and *candA-C1* and *candA-C* have additionally a shared transcript. *A. nidulans* dimeric CandA (A-N + A-C) promotes sexual and asexual development and prevents orsellinic acid secondary metabolism. *A. nidulans* dimeric and/or trimeric CandA (A-N + A-C + A-C1) supports CRL activity. CandA-C1 is required for sexual development and fungal growth. The *A. fumigatus* CanA is also required for vegetative growth. ②: CandA-C has an NLS and binds CandA-N for nuclear transport. CandA-C1 is putatively transported by KapA and KapB. ③: CandA assembles on CSN mediated deneddylated SCF complexes in the nucleus. Binding is followed by adaptor (A)-receptor (R) release and allows new activation of the CRL possibly by CandA~Nedd8 interaction.

CandA-C has an NLS and mediates the nuclear import of CandA-N. CandA-C1 nuclear import is independent from CandA-N and CandA-C but probably facilitated by the karyopherin's KapA and KapB (Figure 57 ②). *A. nidulans* CandA proteins bind to nuclear CulA containing SCF complexes that were first deneddylated by the CSN. *A. fumigatus* CanA can bind CulA and CulC containing SCFs. Binding of CandA to SCFs results in the release of the substrate-receptor-adaptor unit and supports new cycles of cullin neddylation (Figure 57 ③). By this

CandA ensures fast trade-off of adaptor-receptor units, which allows substrate variability of SCF complexes and thereby enhances the activity of those ubiquitin E3 ligases. Elevated levels of CandA-C1 have positive effects on CRL neddylation status and asexual development when *candA-C* is deleted, proposing a rescuing function. CandA complexes might also exist in different subunit assembly forms as CandA-C1 has also different functions than CandA-N and CandA-C. CandA-C1, as well as the N-terminal extension of *A. fumigatus* CanA support conidia germination and vegetative growth. CandA-N and CandA-C inhibit the synthesis of orsellinic acid secondary metabolite derivatives, support the asexual conidiophore formation and are essential for sexual multicellular development at the stage of primordia formation. Their orthologs from *A. fumigatus* CanA^{CTD} and CanA-N support conidia formation and are essential for germination at 30°C. CandA-C1 is similarly required for sexual development as other components of the ubiquitin pathway, like CSN, CandA-N and CandA-C but for a later step that includes ascospore formation. DenA has a similar role in ascospore formation like CandA-C1 but has no influence on asexual development. Together, these results highlight the requirement of a functional multi-subunit CandA complex for proper fungal growth, development and SCF ubiquitin ligase activity. These features and the conservation of CandA-C1 or CandA N-terminal extension in *Aspergillus* spp. suggest this sequence for drug target investigations to fight different kinds of mycosis or dysfunctions of SCFs of several cancer types and neurodegenerative diseases.

For a better understanding of the *Aspergillus* CandA subunit expression, assembly and function it is foremost important to investigate in the shared transcript of *candA-C1* and *candA-C*. It must be tested whether this is a read-through or antisense transcript. Furthermore, the regulation of SCF complexes by CandA interaction with Nedd8 and the re-activation by neddylation of CulA would be interesting to solve. Thereby, it could be useful to improve recombinant expression and purification of CandA subunits for crystallization and three-dimensional structure determination. Structural information coupled to the identification of post-translational modifications by LC-MS2 could help to explain CandA mediated SCF binding and activation. Virulence tests with the wax moth model *Galleria mellonella* or mice model must be performed to analyze the role of CanA in the pathogenicity of *A. fumigatus*. These experiments would then strengthen the possibility of CandA-C1/CanA becoming a putative drug target. Furthermore, it would be motivating to follow covalent interactions with Nedd8, as some interesting candidates were found in this study and other neddylation targets besides cullins are still not well known. All in all, there are still many open questions concerning the regulation of the ubiquitin proteasome system and this thesis identified a novel aspect of CandA mediated CRL regulation in *Aspergillus* spp. with the discovery and characterization of an additional CandA protein sequence, which supports CRL neddylation and is required for fungal growth.

Literature

- Abad, A, Victoria Fernández-Molina, J, Bikandi, J, Ramírez, A, Margareto, J, Sendino, J, Luis Hernando, F, Pontón, J, Garaizar, J, and Rementeria, A (2010). What makes *Aspergillus fumigatus* a successful pathogen? Genes and molecules involved in invasive aspergillosis. *Rev Iberoam Micol* 27, 155–182.
- Abinsworth, GC, and Bisby, GR (2008). Ascomycota. In: Ainsworth & Bisby's Dictionary of the Fungi, PM Kirked., Wallingford, UK: CABI, 55–56.
- Adams, TH, Boylan, MT, and Timberlake, WE (1988). *brlA* is necessary and sufficient to direct conidiophore development in *Aspergillus nidulans*. *Cell* 54, 353–362.
- Adams, TH, Hide, WA, Yager, LN, and Lee, BN (1992). Isolation of a gene required for programmed initiation of development by *Aspergillus nidulans*. *Mol Cell Biol* 12, 3827–3833.
- Adams, TH, and Timberlake, WE (1990). Developmental repression of growth and gene expression in *Aspergillus*. *Genetics* 87, 5405–5409.
- Adams, TH, Wieser, JK, and Yu, J-H (1998). Asexual sporulation in *Aspergillus nidulans*. 62, 35–54.
- Adhvaryu, KK, Gessaman, JD, Honda, S, Lewis, ZA, Grisafi, PL, and Selker, EU (2015). The cullin-4 complex DCDC does not require E3 ubiquitin ligase elements to control heterochromatin in *Neurospora crassa*. *Eukaryot Cell* 14, 25–28.
- Aguilar-Hernández, V, Kim, D-Y, Stankey, RJ, Scalf, M, Smith, LM, and Vierstra, RD (2017). Mass spectrometric analyses reveal a central role for ubiquitylation in remodeling the *Arabidopsis* proteome during photomorphogenesis. *Mol Plant* 10, 846–865.
- Ahmed, YL, Gerke, J, Park, H. S, Bayram, Ö, Neumann, P, Ni, M, Dickmanns, A, Kim, SC, Yu, JH, Braus, GH and Ficner, R. (2013). The velvet family of fungal regulators contains a DNA-binding domain structurally similar to NF- κ B. *PLoS Biol* 11, e1001750.
- Al-Bader, N, Vanier, G, Liu, H, Gravelat, FN, Urb, M, Hoareau, CM-Q, Campoli, P, Chabot, J, Filler, SG, and Sheppard, DC (2010). Role of trehalose biosynthesis in *Aspergillus fumigatus* development, stress response, and virulence. *Infect Immun* 78, 3007–3018.
- Alonso-Peral, MM, Candela, H, del Pozo, JC, Martínez-Laborda, A, Ponce, MR, and Micol, JL (2006). The HVE/CAND1 gene is required for the early patterning of leaf venation in *Arabidopsis*. *Development* 133, 3755–3766.
- Alpi, AF, and Echalièr, A (2017). ZOMES: the intriguing interplay of PCI complexes and the ubiquitin in protein homeostasis. *Cell Death Dis* 8, e3021.
- Altmann E, Erbel P, Rénatus M, Schaefer M, Schlierf A, Druet A, Kieffer L, Sorge M, Pfister K, Hassiepen U, Jones M, Ruedisser S, Ostermeier D, Martoglio B, Jefferson AB, Quancard J. (2017). Azaindoles as zinc-binding small-molecule inhibitors of the JAMM protease CSN5. *Angew Chemie - Int Ed* 56, 1294–1297.
- Andrade, MA, and Bork, P (1995). HEAT repeats in the Huntington's disease protein. *Nat Genet* 11, 115–116.
- Arthanari, Y, Heintzen, C, Griffiths-Jones, S, and Crosthwaite, SK (2014). Natural antisense transcripts and long non-coding RNA in *Neurospora crassa*. *PLoS One* 9, e91353.
- Axelrod, DE, Gealt, M, and Pastushok, M (1973). Gene control of developmental competence in *Aspergillus nidulans*. *Dev Biol* 34, 9–15.
- Azzu, V, and Brand, MD (2010). Degradation of an intramitochondrial protein by the cytosolic proteasome. *J Cell Sci* 123, 3616–3616.
- Bader, O, Tünnermann, J, Dudakova, A, Tangwattanachuleeporn, M, Weig, M, and Groß, U (2015). Environmental isolates of azole-resistant *Aspergillus fumigatus* in Germany. *Antimicrob Agents Chemother* 59, 4356–4359.
- Bai, C, Sen, P, Hofmann, K, Ma, L, Goebel, M, Harper, JW, and Elledge, SJ (1996). SKP1 connects cell

- cycle regulators to the ubiquitin proteolysis machinery through a novel motif, the F-Box. *Cell* 86, 263–274.
- Bainbridge, BW (1971). Macromolecular composition and nuclear division during spore germination in *Aspergillus nidulans*. *J Gen Microbiol* 66, 319–325.
- Bakti, F, Sasse, C, Heinekamp, T, Pócsi, I, and Braus, GH (2018). Heavy metal induced expression of PcaA provides Cadmium tolerance to *Aspergillus fumigatus* and supports its virulence in the *Galleria mellonella* model. *Front Microbiol* 9, 744.
- Bandau, S, Knebel, A, Gage, ZO, Wood, NT, and Alexandru, G (2012). UBXN7 docks on neddylated cullin complexes using its UIM motif and causes HIF1 α accumulation. *BMC Biol* 10, 36.
- Barth, E, Hübler, R, Baniahmad, A, and Marz, M (2016). The evolution of COP9 signalosome in unicellular and multicellular organisms. *Genome Biol Evol* 8, 1279–1289.
- Bartnicki-Garcia, S (2002). Molecular biology of fungal development. In: *Molecular Biology of Fungal Development*, Heinz D. Osiewacz ed., New York: Marcel Dekker, INC, 26–53.
- Bartnicki-Garcia, S, Bracker, CE, Gierz, G, López-Franco, R, and Lu, H (2000). Mapping the growth of fungal hyphae: orthogonal cell wall expansion during tip growth and the role of turgor. *Biophys J* 79, 2382–2390.
- Bayram Ö, Krappmann S, Ni M, Bok JW, Helmstaedt K, Valerius O, Braus-Stromeyer S, Kwon N-J, Keller NP, Yu J-H, Braus GH. (2008a). VelB/VeA/LaeA complex coordinates light signal with fungal development and secondary metabolism. *Science* 320, 1504–1506.
- Bayram, Ö, Bayram, ÖS, Ahmed, YL, Maruyama, J, Valerius, O, Rizzoli, SO, Ficner, R, Irrniger, S, and Braus, GH (2012). The *Aspergillus nidulans* MAPK module AnSte11-Ste50-Ste7-Fus3 controls development and secondary metabolism. *PLoS Genet* 8, e1002816.
- Bayram, O, Biesemann, C, Krappmann, S, Galland, P, and Braus, GH (2008b). More than a repair enzyme: *Aspergillus nidulans* photolyase-like CryA is a regulator of sexual development. *Mol Biol Cell* 19, 3254–3262.
- Bayram, Ö, and Braus, GH (2012). Coordination of secondary metabolism and development in fungi: the velvet family of regulatory proteins. *FEMS Microbiol Rev* 36, 1–24.
- Bayram, Ö, Braus, GH, Fischer, R, and Rodriguez-Romero, J (2010). Spotlight on *Aspergillus nidulans* photosensory systems. *Fungal Genet Biol* 47, 900–908.
- Bayram, Ö, Feussner, K, Dumkow, M, Herrfurth, C, Feussner, I, and Braus, GH (2016). Changes of global gene expression and secondary metabolite accumulation during light-dependent *Aspergillus nidulans* development. *Fungal Genet Biol* 87, 30–53.
- Beckmann, EA, Köhler, AM, Meister, C, Christmann, M, Draht, OW, Rakebrandt, N, Valerius, O, and Braus, GH (2015). Integration of the catalytic subunit activates deneddylase activity in vivo as final step in fungal COP9 signalosome assembly. *Mol Microbiol* 97, 110–124.
- Bedford, L, Paine, S, Sheppard, PW, Mayer, RJ, and Roelofs, J (2010). Assembly, structure, and function of the 26S proteasome. *Trends Cell Biol* 20, 391–401.
- Bennett, EJ, Rush, J, Gygi, SP, and Harper, JW (2010). Dynamics of cullin-RING ubiquitin ligase network revealed by systematic quantitative proteomics. *Cell* 143, 951–965.
- Bennett, JW (2010). An overview of the genus *Aspergillus*. In: *Aspergillus: Molecular Biology and Genomics*, M Machida, and K Gomied., Norfolk, UK: Caister Academic Press, 1–17.
- Bergkessel, M, and Guthrie, C (2013). Colony PCR. *Methods Enzymol* 529, 299–309.
- Bertani, G (1951). Studies on lysogenesis. I. The mode of phage liberation by lysogenic *Escherichia coli*. *J Bacteriol* 62, 293–300.
- Blumenstein, A, Vienken, K, Tasler, R, Purschwitz, J, Veith, D, Frankenberg-Dinkel, N, and Fischer, R (2005). The *Aspergillus nidulans* phytochrome FphA represses sexual development in red light. *Curr Biol* 15, 1833–1838.

- Boban, M, and Foisner, R (2016). Degradation-mediated protein quality control at the inner nuclear membrane. *Nucleus* 7, 41–49.
- Bornstein, G, Ganoth, D, and Hershko, A (2006). Regulation of neddylation and deneddylation of cullin1 in SCFSkp2 ubiquitin ligase by F-box protein and substrate. *Proc Natl Acad Sci U S A* 103, 11515–11520.
- Bossou, YM, Serssar, Y, Allou, A, Vitry, S, Momas, I, Seta, N, Menotti, J, and Achard, S (2017). Impact of mycotoxins secreted by *Aspergillus* molds on the inflammatory response of human corneal epithelial cells. *Toxins (Basel)* 9, 197.
- Bosu, DR, Feng, H, Min, K, Kim, Y, Wallenfang, MR, and Kipreos, ET (2010). *C. elegans* CAND-1 regulates cullin neddylation, cell proliferation and morphogenesis in specific tissues. *Dev Biol* 346, 113–126.
- Bosu, DR, and Kipreos, ET (2008). Cullin-RING ubiquitin ligases: global regulation and activation cycles. *Cell Div* 3, 7.
- Braumann, I, van den Berg, MA, and Kempken, F (2008). Strain-specific retrotransposon-mediated recombination in commercially used *Aspergillus niger* strain. *Mol Genet Genomics* 280, 319–325.
- Braus, GH, Irniger, S, and Bayram, Ö (2010). Fungal development and the COP9 signalosome. *Curr Opin Microbiol* 13, 672–676.
- Braus, GH, Krappmann, S, and Eckert, SE (2002). Sexual development in Ascomycetes fruit body formation of *Aspergillus nidulans*. In: *Molecular Biology of Fungal Development*, HD Osiewacz, New York: Marcel Dekker, INC., 200–226.
- Brockway, H, Balukoff, N, Dean, M, Alleva, B, and Smolikove, S (2014). The CSN/COP9 signalosome regulates synaptonemal complex assembly during meiotic prophase I of *Caenorhabditis elegans*. *PLoS Genet* 10, e1004757.
- Budenholzer, L, Cheng, CL, Li, Y, and Hochstrasser, M (2017). Proteasome structure and assembly. *J Mol Biol* 429, 3500–3524.
- Buonanno, M et al. (2017). Disclosing the interaction of carbonic anhydrase IX with cullin-associated NEDD8-dissociated protein 1 by molecular modeling and integrated binding measurements. *ACS Chem Biol* 12, 1460–1465.
- Busch, S, and Braus, GH (2007). How to build a fungal fruit body: from uniform cells to specialized tissue. *Mol Microbiol* 64, 873–876.
- Busch, S, Eckert, SE, Krappmann, S, and Braus, GH (2003). The COP9 signalosome is an essential regulator of development in the filamentous fungus *Aspergillus nidulans*. *Mol Microbiol* 49, 717–730.
- Busch, S, Schwier, EU, Nahlik, K, Bayram, Ö, Helmstaedt, K, Draht, OW, Krappmann, S, Valerius, O, Lipscomb, WN, and Braus, GH (2007). An eight-subunit COP9 signalosome with an intact JAMM motif is required for fungal fruit body formation. *Proc Natl Acad Sci U S A* 104, 8089–8094.
- Cabib, E, and Leloir, LF (1958). The biosynthesis of trehalose phosphate. *J Biol Chem* 231, 259–275.
- Calvo, AM, Wilson, RA, Bok, JW, and Keller, NP (2002). Relationship between secondary metabolism and fungal development. *Microbiol Mol Biol Rev* 66, 447–459.
- Carvalho, MDF, Baracho, MS, and Baracho, IR (2002). An investigation of the nuclei of hülle cells of *Aspergillus nidulans*. *Genet Mol Biol* 25, 485–488.
- Cavadini, S et al. (2016). Cullin–RING ubiquitin E3 ligase regulation by the COP9 signalosome. *Nature* 531, 598–603.
- Cerqueira, GC et al. (2014). The *Aspergillus* genome database: multispecies curation and incorporation of RNA-Seq data to improve structural gene annotations. *Nucleic Acids Res* 42, D705–10.
- Challa, S (2018). Pathogenesis and pathology of invasive aspergillosis. *Curr Fungal Infect Rep* 12, 23–32.
- Champe, SP, and Simon, LD (1992). Cellular differentiation and tissue formation in the fungus

- Aspergillus nidulans*. In: Morphogenesis: An Analysis of the Development of Biological Form, EF Rossomando, and S Alexandered., New York: Marcel Dekker, INC., 63–93.
- Chen, AJ, Frisvad, JC, Sun, BD, Varga, J, Kocsubé, S, Dijksterhuis, J, Kim, DH, Hong, S-B, Houbraken, J, and Samson, RA (2016). *Aspergillus* section *Nidulantes* (formerly *Emericella*): Polyphasic taxonomy, chemistry and biology. *Stud Mycol* 84, 1–118.
- Chou, C-K, Chang, Y-T, Korinek, M, Chen, Y-T, Yang, Y-T, Leu, S, Lin, I-L, Tang, C-J, and Chiu, C-C (2017). The regulations of deubiquitinase USP15 and its pathophysiological mechanisms in diseases. *Int J Mol Sci* 18.
- Chowdhury, M, and Enenkel, C (2015). Intracellular Dynamics of the Ubiquitin-Proteasome-System. *F1000Research* 4, 367.
- Christmann, M, Schmalzer, T, Gordon, C, Huang, X, Bayram, O, Schinke, J, Stumpf, S, Dubiel, W, and Braus, GH (2013). Control of multicellular development by the physically interacting deneddylases DEN1/DenA and COP9 signalosome. *PLoS Genet* 9, e1003275.
- Chua, YS, Boh, BK, Ponyeam, W, and Hagen, T (2011). Regulation of cullin RING E3 ubiquitin ligases by CAND1 *in vivo*. *PLoS One* 6, e16071.
- Chuang, H, Zhang, W, and Gray, WM (2004). Arabidopsis ETA2, an apparent ortholog of the human cullin-interacting protein CAND1, is required for auxin responses mediated by the SCF(TIR1) ubiquitin ligase. *Plant Cell* 16, 1883–1897.
- Chung, D, Dellaire, G, Heyer, W-D, Helleday, T, and Hanaoka, F (2015). The role of the COP9 signalosome and neddylation in DNA damage signaling and repair. *Biomolecules* 5, 2388–2416.
- Ciechanover, A (1998). The ubiquitin-proteasome pathway: on protein death and cell life. *EMBO J* 17, 7151–7160.
- Cohen, MMJ, Leboucher, GP, Livnat-Levanon, N, Glickman, MH, and Weissman, AM (2008). Ubiquitin-proteasome-dependent degradation of a mitofusin, a critical regulator of mitochondrial fusion. *Mol Biol Cell* 19, 2457–2464.
- Collins, I, Wang, H, Caldwell, JJ, and Chopra, R (2017). Chemical approaches to targeted protein degradation through modulation of the ubiquitin–proteasome pathway. *Biochem J* 474, 1127–1147.
- Cope, GA, and Deshaies, RJ (2003). COP9 signalosome: a multifunctional regulator of SCF and other cullin-based ubiquitin ligases. *Cell* 114, 663–671.
- Cox, J, and Mann, M (2008). MaxQuant enables high peptide identification rates, individualized p.p.b.-range mass accuracies and proteome-wide protein quantification. *Nat Biotechnol* 26, 1367–1372.
- Dagenais, TRT, and Keller, NP (2009). Pathogenesis of *Aspergillus fumigatus* in invasive aspergillosis. *Clin Microbiol Rev* 22, 447–465.
- DaRosa, PA, Wang, Z, Jiang, X, Pruneda, JN, Cong, F, Klevit, RE, and Xu, W (2015). Allosteric activation of the RNF146 ubiquitin ligase by a poly(ADP-ribosylation) signal. *Nature* 517, 223–226.
- Deribe, YL, Pawson, T, and Dikic, I (2010). Post-translational modifications in signal integration. *Nat Struct Mol Biol* 17, 666–672.
- Deshaies, RJ, and Joazeiro, CAP (2009). RING domain E3 ubiquitin ligases. *Annu Rev Biochem* 78, 399–434.
- Dickman, MB, and Yarden, O (1999). Serine/Threonine protein kinases and phosphatases in filamentous fungi. *Fungal Genet Biol* 26, 99–117.
- Dingwall, C, and Laskey, RA (1991). Nuclear targeting sequences--a consensus? *Trends Biochem Sci* 16, 478–481.
- Drocourt, D, Calmels, T, Reynes, JP, Baron, M, and Tiraby, G (1990). Cassettes of the *Streptoalloteichus hindustanus ble* gene for transformation of lower and higher eukaryotes to phleomycin resistance. *Nucleic Acids Res* 18, 4009.
- Duan, G, and Walther, D (2015). The roles of post-translational modifications in the context of protein

interaction networks. *PLOS Comput Biol* 11, e1004049.

Dubiel, D, Gierisch, ME, Huang, X, Dubiel, W, and Naumann, M (2013). CAND1-dependent control of cullin 1-RING Ub ligases is essential for adipogenesis. *Biochim Biophys Acta - Mol Cell Res* 1833, 1078–1084.

Dubiel, D, Ordemann, J, Pratschke, J, Dubiel, W, and Naumann, M (2015). CAND1 exchange factor promotes Keap1 integration into cullin 3-RING ubiquitin ligase during adipogenesis. *Int J Biochem Cell Biol* 66, 95–100.

Dubiel, W (2009). Resolving the CSN and CAND1 Paradoxes. *Mol Cell* 35, 547–549.

Dubois, EL, Gerber, S, Kisselev, A, Harel-Bellan, A, and Groisman, R (2016). UV-dependent phosphorylation of COP9/signalosome in UV-induced apoptosis. *Oncol Rep* 35, 3101–3105.

Duda, DM, Borg, LA, Scott, DC, Hunt, HW, Hammel, M, and Schulman, BA (2008). Structural insights into NEDD8 activation of cullin-RING ligases: conformational control of conjugation. *Cell* 134, 995–1006.

Duda, DM, Scott, DC, Calabrese, MF, Zimmerman, ES, Zheng, N, and Schulman, BA (2011). Structural regulation of cullin-RING ubiquitin ligase complexes. *Curr Opin Struct Biol* 21, 257–264.

Edgar, RC (2004). MUSCLE: multiple sequence alignment with high accuracy and high throughput. *Nucleic Acids Res* 32, 1792–1797.

Ellis, T, Reynolds, DR, and Alexopoulos, C (1973). Development in *Emericella nidulans*. *Mycologia* 65, 1028–1035.

Emberley, ED, Mosadeghi, R, and Deshaies, RJ (2012). Deconjugation of Nedd8 from Cul1 is directly regulated by Skp1-F-box and substrate, and the COP9 signalosome inhibits deneddylated SCF by a noncatalytic mechanism. *J Biol Chem* 287, 29679–29689.

Enchev, RI, Schreiber, A, Beuron, F, and Morris, EP (2010). Structural insights into the COP9 signalosome and its common architecture with the 26S proteasome lid and eIF3. *Structure* 18, 518–527.

Enchev, RI, Schulman, BA, and Peter, M (2015). Protein neddylation: beyond cullin–RING ligases. *Nat Rev Mol Cell Biol* 16, 30–44.

Enchev, RI, Scott, DC, da Fonseca, PCA, Schreiber, A, Monda, JK, Schulman, BA, Peter, M, and Morris, EP (2012). Structural basis for a reciprocal regulation between SCF and CSN. *Cell Rep* 2, 616–627.

Esakova, O, and Krasilnikov, AS (2010). Of proteins and RNA: the RNase P/MRP family. *RNA* 16, 1725–1747.

Etxebeste, O, Garzia, A, Espeso, EA, and Ugalde, U (2010). *Aspergillus nidulans* asexual development: making the most of cellular modules. *Trends Microbiol* 18, 569–576.

Faghihi, MA, and Wahlestedt, C (2009). Regulatory roles of natural antisense transcripts. *Nat Rev Mol Cell Biol* 10, 637–643.

Fang, L, Kaake, RM, Patel, VR, Yang, Y, Baldi, P, and Huang, L (2012). Mapping the protein interaction network of the human COP9 signalosome complex using a label-free QTAX strategy. *Mol Cell Proteomics* 11, 138–147.

Fernández-Martínez, J, Brown, C V., Díez, E, Tilburn, J, Arst Jr, HN, Peñalva, MÁ, and Espeso, EA (2003). Overlap of nuclear localisation signal and specific DNA-binding residues within the zinc finger domain of PacC. *J Mol Biol* 334, 667–684.

Fiddy, C, and Trinci, APJ (1976). Mitosis, septation, branching and the duplication cycle in *Aspergillus nidulans*. *J Gen Microbiol* 97, 169–184.

Fillinger, S, Chaverroche, M-K, Van Dijck, P, De Vries, R, Ruijter, G, Thevelein, J, and D'enfert, C (2018). Trehalose is required for the acquisition of tolerance to a variety of stresses in the filamentous fungus *Aspergillus nidulans*. *Microbiology* 1358, 40–1851.

Finn, RD et al. (2017). InterPro in 2017—beyond protein family and domain annotations. *Nucleic Acids Res* 45, D190–D199.

- Fischer, R, and Timberlake, WE (1995). *Aspergillus nidulans* *apsA* (anucleate primary sterigmata) encodes a coiled-coil protein required for nuclear positioning and completion of asexual development. *J Cell Biol* 128, 485–498.
- Fournier, D, Palidwor, GA, Shcherbinin, S, Szengel, A, Schaefer, MH, Perez-Iratxeta, C, and Andrade-Navarro, MA (2013). Functional and genomic analyses of alpha-solenoid proteins. *PLoS One* 8, e79894.
- Franciosini, A et al. (2015). The COP9 signalosome is required for postembryonic meristem maintenance in *Arabidopsis thaliana*. *Mol Plant* 8, 1623–1634.
- Frank, DN, and Pace, NR (1998). Ribonuclease P: unity and diversity in a tRNA processing ribozyme. *Annu Rev Biochem* 67, 153–180.
- Garzia, A, Etxebeste, O, Herrero-Garcia, E, Fischer, R, Espeso, EA, and Ugalde, U (2009). *Aspergillus nidulans* FlbE is an upstream developmental activator of conidiation functionally associated with the putative transcription factor FlbB. *Mol Microbiol* 71, 172–184.
- Garzia, A, Etxebeste, O, Rodríguez-Romero, J, Fischer, R, Espeso, EA, and Ugalde, U (2013). Transcriptional changes in the transition from vegetative cells to asexual development in the model fungus *Aspergillus nidulans*. *Eukaryot Cell* 12, 311–321.
- Gasteiger, E, Hoogland, C, Gattiker, A, Duvaud, S, Wilkins, MR, Appel, RD, and Bairoch, A (2005). The Proteomics Protocols Handbook. In: *The Proteomics Protocols Handbook*, JM Walkered., Totowa, NJ: Humana Press, 571–607.
- Geer, LY, Marchler-Bauer, A, Geer, RC, Han, L, He, J, He, S, Liu, C, Shi, W, and Bryant, SH (2010). The NCBI BioSystems database. *Nucleic Acids Res* 38, D492-6.
- Gerke, J, Bayram, Ö, Feussner, K, Landesfeind, M, Shelest, E, Feussner, I, and Braus, GH (2012). Breaking the silence: protein stabilization uncovers silenced biosynthetic gene clusters in the fungus *Aspergillus nidulans*. *Appl Environ Microbiol* 78, 8234–8244.
- Gerke, J, and Braus, GH (2014). Manipulation of fungal development as source of novel secondary metabolites for biotechnology. *Appl Microbiol Biotechnol* 98, 8443–8455.
- Ghosh, S, and Dass, JFP (2016). Study of pathway cross-talk interactions with NF- κ B leading to its activation via ubiquitination or phosphorylation: A brief review. *Gene* 584, 97–109.
- Goldenberg, SJ, Cascio, TC, Shumway, SD, Garbutt, KC, Liu, J, Xiong, Y, and Zheng, N (2004). Structure of the Cand1-Cul1-Roc1 complex reveals regulatory mechanisms for the assembly of the multisubunit cullin-dependent ubiquitin ligases. *Cell* 119, 517–528.
- Gorelik, M, and Sidhu, SS (2017). Specific targeting of the deubiquitinase and E3 ligase families with engineered ubiquitin variants. *Bioeng Transl Med* 2, 31–42.
- Görlich, D, Henklein, P, Laskey, RA, and Hartmann, E (1996). A 41 amino acid motif in importin-alpha confers binding to importin-beta and hence transit into the nucleus. *EMBO J* 15, 1810–1817.
- Grice, GL, and Nathan, JA (2016). The recognition of ubiquitinated proteins by the proteasome. *Cell Mol Life Sci* 73, 3497–3506.
- Grigoriev, I V. et al. (2012). The genome portal of the Department of Energy Joint Genome Institute. *Nucleic Acids Res* 40, D26-32.
- Grigoriev, I V et al. (2014). MycoCosm portal: gearing up for 1000 fungal genomes. *Nucleic Acids Res* 42, D699-704.
- Groves, MR, and Barford, D (1999). Topological characteristics of helical repeat protein. *Curr Opin Struct Biol* 9, 383–389.
- Groves, MR, Hanlon, N, Turowski, P, Hemmings, BA, and Barford, D (1999). The structure of the protein phosphatase 2A PR65/A subunit reveals the conformation of its 15 tandemly repeated HEAT motifs. *Cell* 96, 99–110.
- Gsaller, F et al. (2016). Sterol biosynthesis and azole tolerance is governed by the opposing actions of SrbA and the CCAAT binding complex. *PLoS Pathog* 12, e1005775.

- Gul, IS, Hulpiau, P, Saeys, Y, and van Roy, F (2017). Metazoan evolution of the armadillo repeat superfamily. *Cell Mol Life Sci* 74, 525–541.
- Gummlich, L, Kähne, T, Naumann, M, Kilic, E, Jung, K, and Dubiel, W (2016). New insights into the mechanism of COP9 Signalosome–Cullin-RING ubiquitin-ligase pathway deregulation in urological cancers. *Int Rev Cell Mol Biol* 323, 181–229.
- Gusmaroli, G, Figueroa, P, Serino, G, and Deng, XW (2007). Role of the MPN subunits in COP9 signalosome assembly and activity, and their regulatory interaction with *Arabidopsis* Cullin3-based E3 ligases. *Plant Cell* 19, 564–581.
- Hagiwara, D, Sakai, K, Suzuki, S, Umemura, M, Nogawa, T, Kato, N, Osada, H, Watanabe, A, Kawamoto, S, Gono, T, Kamei, K. (2017). Temperature during conidiation affects stress tolerance, pigmentation, and trypacidin accumulation in the conidia of the airborne pathogen *Aspergillus fumigatus*. *PLoS One* 12, e0177050.
- Hagiwara, D, Sakamoto, K, Abe, K, and Gomi, K (2016). Signaling pathways for stress responses and adaptation in *Aspergillus* species: stress biology in the post-genomic era. *Biosci Biotechnol Biochem* 80, 1667–1680.
- Hampel, M, Jakobi, M, Schmitz, L, Meyer, U, Finkernagel, F, Doehlemann, G, and Heimel, K (2016). Unfolded protein response (UPR) regulator Cib1 controls expression of genes encoding secreted virulence factors in *Ustilago maydis*. *PLoS One* 11, e0153861.
- Han, K-H, Han, K-Y, Yu, J-H, Chae, K-S, Jahng, K-Y, and Han, D-M (2001). The *nsdD* gene encodes a putative GATA-type transcription factor necessary for sexual development of *Aspergillus nidulans*. *Mol Microbiol* 41, 299–309.
- Hanahan, D, Jessee, J, and Bloom, FR (1991). Plasmid transformation of *Escherichia coli* and other bacteria. *Methods Enzymol* 204, 63–113.
- Harispe, L, Portela, C, Scazzocchio, C, Peñalva, MA, and Gorfinkiel, L (2008). Ras GTPase-activating protein regulation of actin cytoskeleton and hyphal polarity in *Aspergillus nidulans*. *Eukaryot Cell* 7, 141–153.
- Harris, SD, Read, ND, Roberson, RW, Shaw, B, Seiler, S, Plamann, M, and Momany, M (2005). Polarisome meets Spitzenkörper: microscopy, genetics, and genomics converge. *Eukaryot Cell* 4, 225–229.
- Harting, R, Bayram, Ö, Laubinger, K, Valerius, O, and Braus, GH (2013). Interplay of the fungal sumoylation network for control of multicellular development. *Mol Microbiol* 90, 1125–1145.
- Hartmann, E, and Hartmann, RK (2003). The enigma of ribonuclease P evolution. *Trends Genet* 19, 561–569.
- Hartmann, T, Dümig, M, Jaber, BM, Szewczyk, E, Olbermann, P, Morschhäuser, J, and Krappmann, S (2010). Validation of a self-excising marker in the human pathogen *Aspergillus fumigatus* by employing the beta-rec/six site-specific recombination system. *Appl Environ Microbiol* 76, 6313–6317.
- Hayer, K, Stratford, M, and Archer, DB (2013). Structural features of sugars that trigger or support conidial germination in the filamentous fungus *Aspergillus niger*. *Appl Environ Microbiol* 79, 6924–6931.
- Helmstaedt, K, Schwier, EU, Christmann, M, Nahlik, K, Westermann, M, Harting, R, Grond, S, Busch, S, and Braus, GH (2011). Recruitment of the inhibitor Cand1 to the cullin substrate adaptor site mediates interaction to the neddylation site. *Mol Biol Cell* 22, 153–164.
- Heo, J-M, Ordureau, A, Paulo, JA, Rinehart, J, and Harper, JW (2015). The PINK1-PARKIN mitochondrial ubiquitylation pathway drives a program of OPTN/NDP52 recruitment and TBK1 activation to promote mitophagy. *Mol Cell* 60, 7–20.
- Herrero-Garcia, E, Garzia, A, Cordobés, S, Espeso, EA, and Ugalde, U (2011). 8-Carbon oxylipins inhibit germination and growth, and stimulate aerial conidiation in *Aspergillus nidulans*. *Fungal Biol* 115, 393–400.
- Hershko, A, and Ciechanover, A (1998). The ubiquitin system. *Annu Rev Biochem* 67, 425–479.

- Hetfeld, BKJ, Helfrich, A, Kapelari, B, Scheel, H, Hofmann, K, Guterman, A, Glickman, M, Schade, R, Kloetzel, P-M, and Dubiel, W (2005). The zinc finger of the CSN-associated deubiquitinating enzyme USP15 is essential to rescue the E3 ligase Rbx1. *Curr Biol* 15, 1217–1221.
- Hipp, K, Galani, K, Batisse, C, Prinz, S, and Böttcher, B (2012). Modular architecture of eukaryotic RNase P and RNase MRP revealed by electron microscopy. *Nucleic Acids Res* 40, 3275–3288.
- Honda, T, Kakuta, Y, Kimura, K, Saho, J, and Kimura, M (2008). Structure of an archaeal homolog of the human protein complex Rpp21–Rpp29 that is a key core component for the assembly of active Ribonuclease P. *J Mol Biol* 384, 652–662.
- Horio, T, and Oakley, BR (2005). The role of microtubules in rapid hyphal tip growth of *Aspergillus nidulans*. *Mol Biol Cell* 16, 918–926.
- Howard, RJ, and Gow, NAR (2001). Gene nomenclature. In: *Biology of the Fungal Cell*, RJ Howard, and NAR Gowded., Berlin, Heidelberg: Springer, 288–289.
- Hua, Z, and Vierstra, RD (2011). The Cullin-RING Ubiquitin-Protein Ligases. *Annu Rev Plant Biol* 62, 299–334.
- Huang, DT, Hunt, HW, Zhuang, M, Ohi, MD, Holton, JM, and Schulman, BA (2007). Basis for a ubiquitin-like protein thioester switch toggling E1–E2 affinity. *Nature* 445, 394–398.
- Huang, X, Langelotz, C, Hetfeld-Pěchoč, BKJ, Schwenk, W, and Dubiel, W (2009). The COP9 signalosome mediates β -Catenin degradation by deneddylation and blocks adenomatous polyposis coli destruction via USP15. *J Mol Biol* 391, 691–702.
- Inobe, T, and Matouschek, A (2014). Paradigms of protein degradation by the proteasome. *Curr Opin Struct Biol* 24, 156–164.
- Inoue, H, Nojima, H, and Okayama, H (1990). High efficiency transformation of *Escherichia coli* with plasmids. *Gene* 96, 23–28.
- Jeram, SM, Srikumar, T, Zhang, X-D, Anne Eisenhauer, H, Rogers, R, Pedrioli, PGA, Matunis, M, and Raught, B (2010). An improved SUMOn-based methodology for the identification of ubiquitin and ubiquitin-like protein conjugation sites identifies novel ubiquitin-like protein chain linkages. *Proteomics* 10, 254–265.
- Ji, Y, Yang, F, Ma, D, Zhang, J, Wan, Z, Liu, W, and Li, R (2012). HOG-MAPK signaling regulates the adaptive responses of *Aspergillus fumigatus* to thermal stress and other related stress. *Mycopathologia* 174, 273–282.
- Jin, D, Wu, M, Li, B, Bücken, B, Keil, P, Zhang, S, Li, J, Kang, D, Liu, J, Dong, J, Deng, XW, Irish, V, Wei, N. (2018). The COP9 Signalosome regulates seed germination by facilitating protein degradation of RGL2 and ABI5. *PLOS Genet* 14, e1007237.
- Jöhnk, B, Bayram, Ö, Abelmann, A, Heinekamp, T, Mattern, DJ, Brakhage, AA, Jacobsen, ID, Valerius, O, and Braus, GH (2016). SCF ubiquitin ligase F-box protein Fbx15 controls nuclear co-repressor localization, stress response and virulence of the human pathogen *Aspergillus fumigatus*. *PLoS Pathog* 12, e1005899.
- Jones, J, Wu, K, Yang, Y, Guerrero, C, Nillegoda, N, Pan, Z-Q, and Huang, L (2008). A targeted proteomic analysis of the ubiquitin-like modifier Nedd8 and associated proteins. *J Proteome Res* 7, 1274–1287.
- Jumpertz, S, Hennes, T, Asare, Y, Schütz, AK, and Bernhagen, J (2017). CSN5/JAB1 suppresses the WNT inhibitor DKK1 in colorectal cancer cells. *Cell Signal* 34, 38–46.
- Jun Han, S, Jae Lee, B, and Sam Kang, H (1998). Purification and characterization of the nuclear ribonuclease P of *Aspergillus nidulans*. *Eur J Biochem* 251, 244–251.
- Kakuta, Y, Ishimatsu, I, Numata, T, Kimura, K, Yao, M, Tanaka, I, and Kimura, M (2005). Crystal structure of a ribonuclease P Protein Ph1601p from *Pyrococcus horikoshii* OT3: An archaeal homologue of human nuclear Ribonuclease P protein Rpp21. *Biochemistry* 44, 12086–12093.
- Kang, M, Li, Y, Zhao, Y, He, S, and Shi, J (2017). miR-33a inhibits cell proliferation and invasion by

- targeting CAND1 in lung cancer. *Clin Transl Oncol*.
- Karve, TM, and Cheema, AK (2011). Small changes huge impact: the role of protein posttranslational modifications in cellular homeostasis and disease. *J Amino Acids* 2011, 207691.
- Kato, JY, and Yoneda-Kato, N (2009). Mammalian COP9 signalosome. *Genes to Cells* 14, 1209–1225.
- Kelley, LA, Mezulis, S, Yates, CM, Wass, MN, and Sternberg, MJE (2015). The Phyre2 web portal for protein modeling, prediction and analysis. *Nat Protoc* 10, 845–858.
- Keuss, MJ, Thomas, Y, McArthur, R, Wood, NT, Knebel, A, and Kurz, T (2016). Characterization of the mammalian family of DCN-type NEDD8 E3 ligases. *J Cell Sci* 129, 1441–1454.
- Kim, J-M, Zeng, CJT, Nayak, T, Shao, R, Huang, A-C, Oakley, BR, and Liu, B (2009). Timely septation requires SNAD-dependent spindle pole body localization of the septation initiation network components in the filamentous fungus *Aspergillus nidulans*. *Mol Biol Cell* 20, 2874–2884.
- Kipreos, ET, and Pagano, M (2000). The F-box protein family. *Genome Biol* 1, reviews3002.1-3002.7.
- Knutson, BA (2010). Insights into the domain and repeat architecture of target of rapamycin. *J Struct Biol* 170, 354–363.
- Köhler, A, Meister, C, and Braus, G (2016). *In vitro* deneddylation assay. *Bio-Protocol* 6, e1756.
- Kolog Gulko, M, Heinrich, G, Gross, C, Popova, B, Valerius, O, Neumann, P, Ficner, R, and Braus, GH (2018). Sem1 links proteasome stability and specificity to multicellular development. *PLOS Genet* 14, e1007141.
- Komander, D (2009). The emerging complexity of protein ubiquitination. *Biochem Soc Trans* 37, 937–953.
- Komander, D, and Rape, M (2012). The Ubiquitin Code. *Annu Rev Biochem* 81, 203–229.
- Kosugi, S, Hasebe, M, Entani, T, Takayama, S, Tomita, M, and Yanagawa, H (2008). Design of peptide inhibitors for the importin α/β nuclear import pathway by activity-based profiling. *Chem Biol* 15, 940–949.
- Kosugi, S, Hasebe, M, Matsumura, N, Takashima, H, Miyamoto-Sato, E, Tomita, M, and Yanagawa, H (2009a). Six classes of nuclear localization signals specific to different binding grooves of importin alpha. *J Biol Chem* 284, 478–485.
- Kosugi, S, Hasebe, M, Tomita, M, and Yanagawa, H (2009b). Systematic identification of cell cycle-dependent yeast nucleocytoplasmic shuttling proteins by prediction of composite motifs. *Proc Natl Acad Sci U S A* 106, 10171–10176.
- Krappmann, S, Sasse, C, and Braus, GH (2006). Gene targeting in *Aspergillus fumigatus* by homologous recombination is facilitated in a nonhomologous end-joining-deficient genetic background. *Eukaryot Cell* 5, 212–215.
- Krijghsheld, P, Bleichrodt, R, van Veluw, GJ, Wang, F, Müller, WH, Dijksterhuis, J, and Wösten, HAB (2013). Development in *Aspergillus*. *Stud Mycol* 74, 1–29.
- Kück, U, and Hoff, B (2006). Application of the *nourseothricin acetyltransferase* gene (*nat1*) as dominant marker for the transformation of filamentous fungi. *Fungal Genet Rep* 53, 9–11.
- Kurz, T, Chou, Y-C, Willems, AR, Meyer-Schaller, N, Hecht, M-L, Tyers, M, Peter, M, and Sicheri, F (2008). Dcn1 functions as a scaffold-type E3 ligase for cullin neddylation. *Mol Cell* 29, 23–35.
- Kurz, T, Özlü, N, Rudolf, F, O'Rourke, SM, Luke, B, Hofmann, K, Hyman, AA, Bowerman, B, and Peter, M (2005). The conserved protein DCN-1/Dcn1p is required for cullin neddylation in *C. elegans* and *S. cerevisiae*. *Nature* 435, 1257–1261.
- Kwon-Chung, KJ, and Sugui, JA (2013). *Aspergillus fumigatus*--what makes the species a ubiquitous human fungal pathogen? *PLoS Pathog* 9, e1003743.
- Lafon, A, Seo, J-A, Han, K-H, Yu, J-H, and d'Enfert, C (2005). The heterotrimeric G-protein GanB(alpha)-SfaD(beta)-GpgA(gamma) is a carbon source sensor involved in early cAMP-dependent germination in *Aspergillus nidulans*. *Genetics* 171, 71–80.

- Lauinger, L, Li, J, Shostak, A, Cemel, IA, Ha, N, Zhang, Y, Merkl, PE, Obermeyer, S, Stankovic-Valentin, N, Schafmeier, T, Wever, WJ, Bowers, AA, Carter, KP, Palmer, AE, Tschochner, H, Melchior, F, Deshaies, RJ, Brunner, M, Diernfellner, A. (2017). Thiolutin is a zinc chelator that inhibits the Rpn11 and other JAMM metalloproteases. *Nat Chem Biol* 13, 709–714.
- Lee, CH (2017). A simple outline of methods for protein isolation and purification. *Endocrinol Metab* (Seoul, Korea) 32, 18–22.
- Lee, M-H, Zhao, R, Phan, L, and Yeung, S-CJ (2011). Roles of COP9 signalosome in cancer. *Cell Cycle* 10, 3057–3066.
- Lee, M-K, Kwon, N-J, Choi, JM, Lee, I-S, Jung, S, and Yu, J-H (2014). NsdD is a key repressor of asexual development in *Aspergillus nidulans*. *Genetics* 197, 159–173.
- Lee, SC, and Shaw, BD (2008). Localization and function of ADP ribosylation factor A in *Aspergillus nidulans*. *FEMS Microbiol Lett* 283, 216–222.
- Leidecker, O, Bonfiglio, JJ, Colby, T, Zhang, Q, Atanassov, I, Zaja, R, Palazzo, L, Stockum, A, Ahel, I, and Matic, I (2016). Serine is a new target residue for endogenous ADP-ribosylation on histones. *Nat Chem Biol* 12, 998–1000.
- Leiter, É, Park, HS, Kwon, NJ, Han, KH, Emri, T, Oláh, V, Mészáros, I, Dienes, B, Vincze, J, Csernoch, L, Yu, JH, Pócsi, I. (2016). Characterization of the *aodA*, *dnmA*, *mnSOD* and *pimA* genes in *Aspergillus nidulans*. *Sci Rep* 6, 20523.
- Leloir, LF, and Cabib, E (1953). The enzymic synthesis of trehalose phosphate. *J Am Chem Soc* 75, 5445–5446.
- Letunic, I, and Bork, P (2016). Interactive tree of life (iTOL) v3: an online tool for the display and annotation of phylogenetic and other trees. *Nucleic Acids Res* 44, W242–W245.
- Lin, C-J et al. (2015). Transcription factor SomA is required for adhesion, development and virulence of the human pathogen *Aspergillus fumigatus*. *PLoS Pathog* 11, e1005205.
- Lingaraju, GM, Bunker, RD, Cavadini, S, Hess, D, Hassiepen, U, Renatus, M, Fischer, ES, and Thomä, NH (2014). Crystal structure of the human COP9 signalosome. *Nature* 512, 161–165.
- Liu, C, Vyas, A, Kassab, MA, Singh, AK, and Yu, X (2017a). The role of poly ADP-ribosylation in the first wave of DNA damage response. *Nucleic Acids Res* 45, 8129–8141.
- Liu, J, Furukawa, M, Matsumoto, T, and Xiong, Y (2002). NEDD8 modification of CUL1 dissociates p120CAND1, an inhibitor of CUL1-SKP1 binding and SCF ligases. *Mol Cell* 10, 1511–1518.
- Liu, Q, Zhou, Y, Tang, R, Wang, X, Hu, Q, Wang, Y, and He, Q (2017b). Increasing the unneddylated cullin1 portion rescues the *csn* phenotypes by stabilizing adaptor modules to drive SCF assembly. *Mol Cell Biol* 37, e00109-17.
- Liu, W, Xie, Y, Ma, J, Luo, X, Nie, P, Zuo, Z, Lahrmann, U, Zhao, Q, Zheng, Y, Zhao, Y, Xue, Y, Ren, J. (2015). IBS: An illustrator for the presentation and visualization of biological sequences. *Bioinformatics* 31, 3359–3361.
- Liu, X, Reitsma, JM, Mamrosh, JL, Zhang, Y, Straube, R, and Deshaies, RJ (2018). Cand1-mediated adaptive exchange mechanism enables variation in F-Box protein expression. *Mol Cell* 69, 773–786.e6.
- Livak, KJ, and Schmittgen, TD (2001). Analysis of relative gene expression data using real-time quantitative PCR and the 2^{-ΔΔC_T} Method. *Methods* 25, 402–408.
- Livnat-Levanon, N, and Glickman, MH (2011). Ubiquitin-Proteasome System and mitochondria — Reciprocity. *Biochim Biophys Acta - Gene Regul Mech* 1809, 80–87.
- Lo, HC, Entwistle, R, Guo, CJ, Ahuja, M, Szewczyk, E, Hung, JH, Chiang, YM, Oakley, BR, and Wang, CCC (2012). Two separate gene clusters encode the biosynthetic pathway for the meroterpenoids austinol and dehydroaustinol in *Aspergillus nidulans*. *J Am Chem Soc* 134, 4709–4720.
- Lu, Y, Lee, B, King, RW, Finley, D, and Kirschner, MW (2015). Substrate degradation by the proteasome: a single-molecule kinetic analysis. *Science* 348, 1250834.

- Lydeard, JR, Schulman, BA, and Harper, JW (2013). Building and remodelling Cullin-RING E3 ubiquitin ligases. *EMBO Rep* 14, 1050–1061.
- Ma, T, Chen, Y, Zhang, F, Yang, C-Y, Wang, S, and Yu, X (2013). RNF111-dependent neddylation activates DNA damage-induced ubiquitination. *Mol Cell* 49, 897–907.
- Makalowska, I, Lin, C-F, and Makalowski, W (2005). Overlapping genes in vertebrate genomes. *Comput Biol Chem* 29, 1–12.
- Makino, Y, Yogosawa, S, Kayukawa, K, Coin, F, Egly, J-M, Wang, Z-X, Roeder, RG, Yamamoto, K, Muramatsu, M, and Tamura, T-A (1999). TATA-binding protein-interacting protein 120, TIP120, stimulates three classes of eukaryotic transcription via a unique mechanism. *Proc Natl Acad Sci USA* 96, 7951–7960.
- Markina-Iñarrairaegui, A, Etxebeste, O, Herrero-García, E, Araújo-Bazán, L, Fernández-Martínez, J, Flores, JA, Osmani, SA, and Espeso, EA (2011). Nuclear transporters in a multinucleated organism: functional and localization analyses in *Aspergillus nidulans*. *Mol Biol Cell* 22, 3874–3886.
- Meister, C, Kolog Gulko, M, Köhler, AM, and Braus, GH (2016). The devil is in the details: comparison between COP9 signalosome (CSN) and the LID of the 26S proteasome. *Curr Genet* 62, 129–136.
- Mergner, J, Heinzlmeir, S, Kuster, B, and Schwechheimer, C (2015). DENEDDYLASE1 deconjugates NEDD8 from non-cullin protein substrates in *Arabidopsis thaliana*. *Plant Cell* 27, 741–753.
- Mergner, J, Kuster, B, and Schwechheimer, C (2017). DENEDDYLASE1 protein counters automodification of neddylation enzymes to maintain NEDD8 protein homeostasis in *Arabidopsis*. *J Biol Chem* 292, 3854–3865.
- Mergner, J, and Schwechheimer, C (2014). The NEDD8 modification pathway in plants. *Front Plant Sci* 5, 103.
- Metzger, MB, Hristova, VA, and Weissman, AM (2012). HECT and RING finger families of E3 ubiquitin ligases at a glance. *J Cell Sci* 125, 531–537.
- Metzger, MB, Pruneda, JN, Klevit, RE, and Weissman, AM (2014). RING-type E3 ligases: Master manipulators of E2 ubiquitin-conjugating enzymes and ubiquitination. *Biochim Biophys Acta - Mol Cell Res* 1843, 47–60.
- Micheli, PA (1729). *Nova plantarum genera juxta Tournefortii methodum disposita*, Florence.
- von Mikecz, A, Wigley, WC, Thomas, PJ, and DeMartino, GN (2006). The nuclear ubiquitin-proteasome system. *J Cell Sci* 119, 1977–1984.
- Mims, CW, Richardson, EA, and Timberlake, WE (1988). Ultrastructural analysis of conidiophore development in the fungus *Aspergillus nidulans* using freeze-substitution. *Protoplasma* 144, 132–141.
- Min, K-W, Hwang, J-W, Lee, J-S, Park, Y, Tamura, T, and Yoon, J-B (2003). TIP120A associates with cullins and modulates ubiquitin ligase activity. *J Biol Chem* 278, 15905–15910.
- Moore, KA, and Hollien, J (2012). The unfolded protein response in secretory cell function. *Annu Rev Genet* 46, 165–183.
- Mosadeghi, R et al. (2016). Structural and kinetic analysis of the COP9-Signalosome activation and the cullin-RING ubiquitin ligase deneddylation cycle. *Elife* 5, 10.7554/eLife.12102.
- Mouton-Liger, F, Jacoupy, M, Corvol, J-C, and Corti, O (2017). PINK1/Parkin-dependent mitochondrial surveillance: from pleiotropy to Parkinson's disease. *Front Mol Neurosci* 10, 120.
- Nahlik, K et al. (2010). The COP9 signalosome mediates transcriptional and metabolic response to hormones, oxidative stress protection and cell wall rearrangement during fungal development. *Mol Microbiol* 78, 964–979.
- Nayak, T, Szewczyk, E, Oakley, CE, Osmani, A, Ukil, L, Murray, SL, Hynes, MJ, Osmani, SA, and Oakley, BR (2006). A versatile and efficient gene-targeting system for *Aspergillus nidulans*. *Genetics* 172, 1557–1566.
- Ni, M, and Yu, J-H (2007). A novel regulator couples sporogenesis and trehalose biogenesis in *Aspergillus nidulans*. *PLoS One* 2, e970.

- Nielsen, S V, Poulsen, EG, Rebula, CA, and Hartmann-Petersen, R (2014). Protein quality control in the nucleus. *Biomolecules* 4, 646–661.
- Novodvorska, M, Hayer, K, Pullan, ST, Wilson, R, Blythe, MJ, Stam, H, Stratford, M, and Archer, DB (2013). Transcriptional landscape of *Aspergillus niger* at breaking of conidial dormancy revealed by RNA-sequencing. *BMC Genomics* 14, 246.
- O’Gorman, CM, Fuller, HT, and Dyer, PS (2009). Discovery of a sexual cycle in the opportunistic fungal pathogen *Aspergillus fumigatus*. *Nature* 457, 471–474.
- Oiartzabal-Arano, E, Garzia, A, Gorostidi, A, Ugalde, U, Espeso, EA, and Etxebeste, O (2015). Beyond asexual development: modifications in the gene expression profile caused by the absence of the *Aspergillus nidulans* transcription factor FlbB. *Genetics* 199, 1127–1142.
- Oliveira, M (2014). *Aspergillus fumigatus*: a mere airborne particle or a powerful biohazard? *Nov Acta Científica Compostel* 64, 57–64.
- Ordureau, A, Heo, J-M, Duda, DM, Paulo, JA, Olszewski, JL, Yanishevski, D, Rinehart, J, Schulman, BA, and Harper, JW (2015). Defining roles of PARKIN and ubiquitin phosphorylation by PINK1 in mitochondrial quality control using a ubiquitin replacement strategy. *Proc Natl Acad Sci U S A* 112, 6637–6642.
- Oshero, N, and May, G (2000). Conidial germination in *Aspergillus nidulans* requires RAS signaling and protein synthesis. *Genetics* 155, 647–656.
- Pacurar, DI, Pacurar, ML, Lakehal, A, Pacurar, AM, Ranjan, A, and Bellini, C (2017). The *Arabidopsis* Cop9 signalosome subunit 4 (CSN4) is involved in adventitious root formation. *Sci Rep* 7, 628.
- Park, H-S, Man Yu, Y, Lee, M-K, Jae Maeng, P, Chang Kim, S, and Yu, J-H (2015). Velvet-mediated repression of β -glucan synthesis in *Aspergillus nidulans* spores. *Sci Rep* 5, 10199.
- Park, H-S, Ni, M, Jeong, KC, Kim, YH, and Yu, J-H (2012). The role, interaction and regulation of the velvet regulator VelB in *Aspergillus nidulans*. *PLoS One* 7, e45935.
- Park, S-H, Kukushkin, Y, Gupta, R, Chen, T, Konagai, A, Hipp, MS, Hayer-Hartl, M, and Hartl, FU (2013). PolyQ proteins interfere with nuclear degradation of cytosolic proteins by sequestering the Sis1p chaperone. *Cell* 154, 134–145.
- Paulussen, C, Hallsworth, JE, Álvarez-Pérez, S, Nierman, WC, Hamill, PG, Blain, D, Rediers, H, and Lievens, B (2017). Ecology of aspergillosis: insights into the pathogenic potency of *Aspergillus fumigatus* and some other *Aspergillus* species. *Microb Biotechnol* 10, 296–322.
- Perry, J, and Kleckner, N (2003). The ATRs, ATMs, and TORs are giant HEAT repeat proteins. *Cell* 112, 151–155.
- Petroski, MD, and Deshaies, RJ (2005a). Function and regulation of cullin-RING ubiquitin ligases. *Nat Rev Mol Cell Biol* 6, 9–20.
- Petroski, MD, and Deshaies, RJ (2005b). Mechanism of lysine 48-linked ubiquitin-chain synthesis by the cullin-RING ubiquitin-ligase complex SCF-Cdc34. *Cell* 123, 1107–1120.
- Pick, E, and Pintard, L (2009). In the land of the rising sun with the COP9 signalosome and related Zomes. Symposium on the COP9 signalosome, Proteasome and eIF3. *EMBO Rep* 10, 343–348.
- Pierce, NW, Lee, JE, Liu, X, Sweredoski, MJ, Graham, RL, Larimore, EA, Rome, M, Zheng, N, Clurman, BE, Hess, S, Shan, SO, Deshaies, RJ. (2013). Cand1 promotes assembly of new SCF complexes through dynamic exchange of F Box proteins. *Cell* 153, 206–215.
- Pines, J, and Lindon, C (2005). Proteolysis: anytime, any place, anywhere? *Nat Cell Biol* 7, 731–735.
- Pöggeler, S, Nowrousian, M, and Kück, U (2006). Fruiting-body development in Ascomycetes. In: *Growth, Differentiation and Sexuality*, U Kües, and R Fischered., Berlin/Heidelberg: Springer-Verlag, 325–355.
- Pöggeler, S, Nowrousian, M, Teichert, I, Beier, A, and Kück, U (2018). Fruiting-body development in Ascomycetes. In: *Physiology and Genetics*, 2nd Edition, The Mycota XV, T Anke, and A Schüfflered., Berlin, Heidelberg: Springer, 1–56.

- Pontecorvo, G, Roper, JA, Chemmons, LM, Macdonald, KD, and Bufton, AWJ (1953). The Genetics of *Aspergillus nidulans*. In: *Advances in Genetics*, M Demereced., Academic Press, Cambridge, Massachusetts, USA, 141–238.
- Portbury, AL, Ronnebaum, SM, Zungu, M, Patterson, C, and Willis, MS (2012). Back to your heart: ubiquitin proteasome system-regulated signal transduction. *J Mol Cell Cardiol* 52, 526–537.
- Punt, PJ, and van den Hondel, CAMJJ (1992). Transformation of filamentous fungi based on hygromycin b and phleomycin resistance markers. In: *Methods in Enzymology*, Academic Press, 447–457.
- Purschwitz, J, Müller, S, and Fischer, R (2009). Mapping the interaction sites of *Aspergillus nidulans* phytochrome FphA with the global regulator VeA and the White Collar protein LreB. *Mol Genet Genomics* 281, 35–42.
- Qian, T-M, Zhao, L-L, Wang, J, Li, P, Qin, J, Liu, Y, Yu, B, Ding, F, Gu, X-S, and Zhou, S-L (2016). miR-148b-3p promotes migration of Schwann cells by targeting cullin-associated and neddylation-dissociated 1. *Neural Regen Res* 11.
- Qian, Y, Ng, CL, and Schulz, C (2015). CSN maintains the germline cellular microenvironment and controls the level of stem cell genes via distinct CRLs in testes of *Drosophila melanogaster*. *Dev Biol* 398, 68–79.
- Rabl, J, Smith, DM, Yu, Y, Chang, S-C, Goldberg, AL, and Cheng, Y (2008). Mechanism of gate opening in the 20S proteasome by the proteasomal ATPases. *Mol Cell* 30, 360–368.
- Raper, KB, and Fennell, DI (1965). The genus *Aspergillus*, Pennsylvania: Williams and Wilkins.
- Rappsilber, J, Mann, M, and Ishihama, Y (2007). Protocol for micro-purification, enrichment, pre-fractionation and storage of peptides for proteomics using StageTips. *Nat Protoc* 2, 1896–1906.
- Reitsma, JM, Liu, X, Reichermeier, KM, Moradian, A, Sweredoski, MJ, Hess, S, and Deshaies, RJ (2017). Composition and regulation of the cellular repertoire of SCF ubiquitin ligases. *Cell* 171, 1326–1339.e14.
- Reverter, D, Wu, K, Erdene, TG, Pan, Z-Q, Wilkinson, KD, and Lima, CD (2005). Structure of a complex between Nedd8 and the Ulp/Senp protease family member Den1. *J Mol Biol* 345, 141–151.
- Robbins, J, Dilworth, SM, Laskey, RA, and Dingwall, C (1991). Two interdependent basic domains in nucleoplasmin nuclear targeting sequence: identification of a class of bipartite nuclear targeting sequence. *Cell* 64, 615–623.
- Rock, KL, Gramm, C, Rothstein, L, Clark, K, Stein, R, Dick, L, Hwang, D, and Goldberg, AL (1994). Inhibitors of the proteasome block the degradation of most cell proteins and the generation of peptides presented on MHC class I molecules. *Cell* 78, 761–771.
- Rodríguez-Urra, AB, Jiménez, C, Nieto, MI, Rodríguez, J, Hayashi, H, and Ugalde, U (2012). Signaling the induction of sporulation involves the interaction of two secondary metabolites in *Aspergillus nidulans*. *ACS Chem Biol* 7, 599–606.
- Ronau, JA, Beckmann, JF, and Hochstrasser, M (2016). Substrate specificity of the ubiquitin and Ubl proteases. *Cell Res* 26, 441–456.
- Ruger-Herreros, C, Rodríguez-Romero, J, Fernández-Barranco, R, Olmedo, M, Fischer, R, Corrochano, LM, and Canovas, D (2011). Regulation of conidiation by light in *Aspergillus nidulans*. *Genetics* 188, 809–822.
- Saiki, RK, Gelfand, DH, Stoffel, S, Scharf, SJ, Higuchi, R, Horn, GT, Mullis, KB, and Erlich, HA (1988). Primer-directed enzymatic amplification of DNA with a thermostable DNA polymerase. *Science* 239, 487–491.
- Samson, RA, Visagie, CM, Houbraken, J, Hong, SB, Hubka, V, Klaassen, CH, Perrone, G, Seifert, KA, Susca, A, Tanney, JB, Varga, J, Kocsubé, S, Szigeti, G, Yaguchi, T, Frisvad, JC. (2014). Phylogeny, identification and nomenclature of the genus *Aspergillus*. *Stud Mycol* 78, 141–173.
- Sanchez, JF, Chiang, Y-M, Szewczyk, E, Davidson, AD, Ahuja, M, Elizabeth Oakley, C, Woo Bok, J, Keller, N, Oakley, BR, and Wang, CCC (2010). Molecular genetic analysis of the orsellinic acid/F9775 genecluster of *Aspergillus nidulans*. *Mol BioSyst* 6, 587–593.

- Sarikaya-Bayram, Ö, Palmer, JM, Keller, N, Braus, GH, and Bayram, Ö (2015). One Juliet and four Romeos: VeA and its methyltransferases. *Front Microbiol* 6, doi: 10.3389/fmicb.2015.00001.
- Sarikaya Bayram, Ö, Bayram, Ö, Valerius, O, Park, HS, Irniger, S, Gerke, J, Ni, M, Han, K-H, Yu, J-H, and Braus, GH (2010). LaeA control of velvet family regulatory proteins for light-dependent development and fungal cell-type specificity. *PLoS Genet* 6, e1001226.
- Sato, N, Kawahara, H, Toh-e, A, and Maeda, T (2003). Phosphorelay-regulated degradation of the yeast Ssk1p response regulator by the ubiquitin-proteasome system. *Mol Cell Biol* 23, 6662–6671.
- Scheffner, M, and Kumar, S (2014). Mammalian HECT ubiquitin-protein ligases: Biological and pathophysiological aspects. *Biochim Biophys Acta - Mol Cell Res* 1843, 61–74.
- Schinke, J, Kolog Gulko, M, Christmann, M, Valerius, O, Stumpf, SK, Stirz, M, and Braus, GH (2016). The DenA/DEN1 interacting phosphatase DipA controls septa positioning and phosphorylation-dependent stability of cytoplasmatic DenA/DEN1 during fungal development. *PLOS Genet* 12, e1005949.
- Schlierf, A, Altmann, E, Quancard, J, Jefferson, AB, Assenberg, R, Renatus, M, Jones, M, Hassiepen, U, Schaefer, M, Kiffe, M, Weiss, A, Wiesmann, C, Sedrani, R, Eder, J, Martoglio, B. (2016). Targeted inhibition of the COP9 signalosome for treatment of cancer. *Nat Commun* 7, 13166.
- Schmidt, MW, McQuary, PR, Wee, S, Hofmann, K, and Wolf, DA (2009). F-Box-directed CRL complex assembly and regulation by the CSN and CAND1. *Mol Cell* 35, 586–597.
- Schreiner, P, Chen, X, Husnjak, K, Randles, L, Zhang, N, Elsasser, S, Finley, D, Dikic, I, Walters, KJ, and Groll, M (2008). Ubiquitin docking at the proteasome through a novel pleckstrin-homology domain interaction. *Nature* 453, 548–552.
- Schroeckh, V, Scherlach, K, Nutzmann, H-W, Shelest, E, Schmidt-Heck, W, Schuemann, J, Martin, K, Hertweck, C, and Brakhage, AA (2009). Intimate bacterial-fungal interaction triggers biosynthesis of archetypal polyketides in *Aspergillus nidulans*. *Proc Natl Acad Sci* 106, 14558–14563.
- Scott, DC, Rhee, DY, Duda, DM, Kelsall, IR, Olszewski, JL, Paulo, JA, de Jong, A, Ovaa, H, Alpi, AF, Harper, JW, Schulman, BA. (2016). Two distinct types of E3 ligases work in unison to regulate substrate ubiquitylation. *Cell* 166, 1198–1214.
- Scott, DC, Hammill, JT, Min, J, Rhee, DY, Connelly, M, Sviderskiy, VO, Bhasin, D, Chen, Y, Ong, SS, Chai, SC, Goktug, AN, Huang, G, Monda, JK, Low, J, Kim, HS, Paulo, JA, Cannon, JR, Shelat, AA, Chen, T, Kelsall, IR, Alpi, AF, Pagala, V, Wang, X, Peng, J, Singh, B, Harper, JW, Schulman, BA, Guy, RK. (2017). Blocking an N-terminal acetylation-dependent protein interaction inhibits an E3 ligase. *Nat Chem Biol* 13, 850–857.
- Scott, DC, Monda, JK, Bennett, EJ, Harper, JW, and Schulman, BA (2011). N-terminal acetylation acts as an avidity enhancer within an interconnected multiprotein complex. *Science* 334, 674–678.
- Scott, DC, Monda, JK, Grace, CRR, Duda, DM, Kriwacki, RW, Kurz, T, and Schulman, BA (2010). A dual E3 mechanism for Rub1 ligation to Cdc53. *Mol Cell* 39, 784–796.
- Scott, DC, Sviderskiy, VO, Monda, JK, Lydeard, JR, Cho, SE, Harper, JW, and Schulman, BA (2014). Structure of a RING E3 trapped in action reveals ligation mechanism for the ubiquitin-like protein NEDD8. *Cell* 157, 1671–1684.
- Sela, N, Atir-Lande, A, and Kornitzer, D (2012). Neddylation and CAND1 independently stimulate SCF ubiquitin ligase activity in *Candida albicans*. *Eukaryot Cell* 11, 42–52.
- Seo, J-A, Guan, Y, and Yu, J-H (2006). FluG-dependent asexual development in *Aspergillus nidulans* occurs via derepression. *Genetics* 172, 1535–1544.
- Seo, J-A, Han, K-H, and Yu, J-H (2004). The *gprA* and *gprB* genes encode putative G protein-coupled receptors required for self-fertilization in *Aspergillus nidulans*. *Mol Microbiol* 53, 1611–1623.
- Sewall, TC, Mims, CW, and Timberlake, WE (1990). *abaA* controls phialide differentiation in *Aspergillus nidulans*. *Plant Cell* 2, 731–739.
- Shen, L, Liu, H, Dong, C, Xirodimas, D, Naismith, JH, and Hay, RT (2005). Structural basis of NEDD8

- ubiquitin discrimination by the deNEDDylating enzyme NEDP1. *EMBO J* 24, 1341–1351.
- Sheppard, DC, and Filler, SG (2014). Host cell invasion by medically important fungi. *Cold Spring Harb Perspect Med* 5, a019687.
- Shevchenko, A, Wilm, M, Vorm, O, and Mann, M (1996). Mass spectrometric sequencing of proteins from silver-stained polyacrylamide gels. *Anal Chem* 68, 850–858.
- Shimizu, K, and Keller, NP (2001). Genetic involvement of a cAMP-dependent protein kinase in a G protein signaling pathway regulating morphological and chemical transitions in *Aspergillus nidulans*. *Genetics* 157, 591–600.
- Shin, Y-C, Chen, J-H, and Chang, S-C (2017). The molecular determinants for distinguishing between ubiquitin and NEDD8 by USP2. *Sci Rep* 7, 2304.
- Shlezinger, N, Irmer, H, Dhingra, S, Beattie, SR, Cramer, RA, Braus, GH, Sharon, A, and Hohl, TM (2017). Sterilizing immunity in the lung relies on targeting fungal apoptosis-like programmed cell death. *Science* 357, 1037–1041.
- Siergiejuk, E, Scott, DC, Schulman, BA, Hofmann, K, Kurz, T, and Peter, M (2009). Cullin neddylation and substrate-adaptors counteract SCF inhibition by the CAND1-like protein Lag2 in *Saccharomyces cerevisiae*. *EMBO J* 28, 3845–3856.
- Singh, RK, Gonzalez, M, Kabbaj, M-HM, and Gunjan, A (2012). Novel E3 ubiquitin ligases that regulate histone protein levels in the budding yeast *Saccharomyces cerevisiae*. *PLoS One* 7, e36295.
- Skaar, JR, Pagan, JK, and Pagano, M (2013). Mechanisms and function of substrate recruitment by F-box proteins. *Nat Rev Mol Cell Biol* 14, 369–381.
- Smith, BJ (1984). SDS Polyacrylamide gel electrophoresis of proteins. In: *Proteins*, New Jersey: Humana Press, 41–56.
- Smith, CA, Robertson, D, Yates, B, Nielsen, DM, Brown, D, Dean, RA, and Payne, GA (2008). The effect of temperature on Natural Antisense Transcript (NAT) expression in *Aspergillus flavus*. *Curr Genet* 54, 241–269.
- Southern, EM (1975). Detection of specific sequences among DNA fragments separated by gel electrophoresis. *J Mol Biol* 98, 503–517.
- Stajich, JE, Harris, T, Brunk, BP, Brestelli, J, Fischer, S, Harb, OS, Kissinger, JC, Li, W, Nayak, V, Pinney, DF, Stoeckert, CJ Jr, Roos, DS. (2012). FungiDB: an integrated functional genomics database for fungi. *Nucleic Acids Res* 40, D675-81.
- Steinberg, G (2007). Hyphal growth: a tale of motors, lipids, and the Spitzenkorper. *Eukaryot Cell* 6, 351–360.
- Steinmann, J, Hamprecht, A, Vehreschild, MJGT, Cornely, OA, Buchheidt, D, Spiess, B, Koldehoff, M, Buer, J, Meis, JF, and Rath, P-M (2015). Emergence of azole-resistant invasive aspergillosis in HSCT recipients in Germany. *J Antimicrob Chemother* 70, 1522–1526.
- Stinnett, SM, Espeso, EA, Cobeño, L, Araújo-Bazán, L, and Calvo, AM (2007). *Aspergillus nidulans* VeA subcellular localization is dependent on the importin α carrier and on light. *Mol Microbiol* 63, 242–255.
- Straube, R, Shah, M, Flockerzi, D, and Wolf, DA (2017). Trade-off and flexibility in the dynamic regulation of the cullin-RING ubiquitin ligase repertoire. *PLOS Comput Biol* 13, e1005869.
- Ström, AC, and Weis, K (2001). Importin-beta-like nuclear transport receptors. *Genome Biol* 2, REVIEWS3008.
- Stukenbrock, EH (2013). Evolution, selection and isolation: a genomic view of speciation in fungal plant pathogens. *New Phytol* 199, 895–907.
- Svanström, Å, and Melin, P (2013). Intracellular trehalase activity is required for development, germination and heat-stress resistance of *Aspergillus niger* conidia. *Res Microbiol* 164, 91–99.
- Swatek, KN, and Komander, D (2016). Ubiquitin modifications. *Cell Res* 26, 399–422.
- Szewczyk, E, and Krappmann, S (2010). Conserved regulators of mating are essential for *Aspergillus*

fumigatus cleistothecium formation. *Eukaryot Cell* 9, 774–783.

Szewczyk, E, Nayak, T, Oakley, CE, Edgerton, H, Xiong, Y, Taheri-Talesh, N, Osmani, SA, Oakley, BR, and Oakley, B (2006). Fusion PCR and gene targeting in *Aspergillus nidulans*. *Nat Protoc* 1, 3111–3120.

Taheri-Talesh, N, Horio, T, Araujo-Bazán, L, Dou, X, Espeso, EA, Peñalva, MA, Osmani, SA, and Oakley, BR (2008). The tip growth apparatus of *Aspergillus nidulans*. *Mol Biol Cell* 19, 1439–1449.

Taylor, EB, and Rutter, J (2011). Mitochondrial quality control by the ubiquitin-proteasome system. *Biochem Soc Trans* 39, 1509–1513.

Thammahong, A, Caffrey-Card, AK, Dhingra, S, Obar, JJ, and Cramer, RA (2017). *Aspergillus fumigatus* trehalose-regulatory subunit homolog moonlights to mediate cell wall homeostasis through modulation of chitin synthase activity. *MBio* 8, e00056-17.

The UniProt Consortium (2017). UniProt: the universal protein knowledgebase. *Nucleic Acids Res* 45, D158–D169.

Thompson, DM, and Parker, R (2009). The RNase Rny1p cleaves tRNAs and promotes cell death during oxidative stress in *Saccharomyces cerevisiae*. *J Cell Biol* 185, 43–50.

Thrower, JS, Hoffman, L, Rechsteiner, M, and Pickart, CM (2000). Recognition of the polyubiquitin proteolytic signal. *EMBO J* 19, 94–102.

Todd, RB, Davis, MA, and Hynes, MJ (2007). Genetic manipulation of *Aspergillus nidulans*: meiotic progeny for genetic analysis and strain construction. *Nat Protoc* 2, 811–821.

Trinci, AP (1969). A kinetic study of the growth of *Aspergillus nidulans* and other fungi. *J Gen Microbiol* 57, 11–24.

Tsai, YC, and Weissman, AM (2010). The unfolded protein response, degradation from the endoplasmic reticulum, and cancer. *Genes Cancer* 1, 764–778.

Tsuji, M, Okuda, S, Ishi, K, Madokoro, K, Takeuchi, M, and Yamagata, Y (2016). A long natural-antisense RNA is accumulated in the conidia of *Aspergillus oryzae*. *Biosci Biotechnol Biochem* 80, 386–398.

Tuch, BB, Mitrovich, QM, Homann, OR, Hernday, AD, Monighetti, CK, De La Vega, FM, and Johnson, AD (2010). The transcriptomes of two heritable cell types illuminate the circuit governing their differentiation. *PLoS Genet* 6, e1001070.

Tyanova, S, Temu, T, Sinitcyn, P, Carlson, A, Hein, MY, Geiger, T, Mann, M, and Cox, J (2016). The Perseus computational platform for comprehensive analysis of (prote)omics data. *Nat Methods* 13, 731–740.

Vallim, MA, Miller, KY, and Miller, BL (2000). *Aspergillus* SteA (Sterile12-like) is a homeodomain-C2/H2-Zn²⁺ finger transcription factor required for sexual reproduction. *Mol Microbiol* 36, 290–301.

van der Veen, AG, and Ploegh, HL (2012). Ubiquitin-Like Proteins. *Annu Rev Biochem* 81, 323–357.

Verma, R, Aravind, L, Oania, R, McDonald, WH, Yates, JR, Koonin, E V, and Deshaies, RJ (2002). Role of Rpn11 metalloprotease in deubiquitination and degradation by the 26S proteasome. *Science* 298, 611–615.

Verweij, PE, Snelders, E, Kema, GHJ, Mellado, E, and Melchers, WJG (2009). Azole resistance in *Aspergillus fumigatus*: a side-effect of environmental fungicide use? *Lancet Infect Dis* 9, 789–795.

Vienken, K, and Fischer, R (2006). The Zn(II)₂Cys₆ putative transcription factor NosA controls fruiting body formation in *Aspergillus nidulans*. *Mol Microbiol* 61, 544–554.

Vienken, K, Scherer, M, and Fischer, R (2005). The Zn(II)₂Cys₆ putative *Aspergillus nidulans* transcription factor repressor of sexual development inhibits sexual development under low-carbon conditions and in submerged culture. *Genetics* 169, 619–630.

Vierstra, RD (2012). The expanding universe of ubiquitin and ubiquitin-like modifiers. *Plant Physiol* 160, 2–14.

- de Vries, RP, Riley, R, Wiebenga, A, Aguilar-Osorio, G, Amillis, S, Uchima, CA, Anderluh, G, Asadollahi, M, Askin, M, Barry, K, Battaglia, E, Bayram, Ö, Benocci, T, Braus-Stromeier, SA, Caldana, C, Cánovas, D, Cerqueira, GC, Chen, F, Chen, W, Choi, C, Clum, A, dos Santos, RAC, Damásio, AR de L, Diallinas, G, Emri, T, Fekete, E, Flippi, M, Freyberg, S, Gallo, A, Gournas, C, Habgood, R, Hainaut, M, Harispe, ML, Henrissat, B, Hildén, KS, Hope, R, Hossain, A, Karabika, E, Karaffa, L, Karányi, Z, Kraševc, N, Kuo, A, Kusch, H, LaButti, K, Lagendijk, EL, Lapidus, A, Lévasseur, A, Lindquist, E, Lipzen, A, Logrieco, AF, MacCabe, A, Mäkelä, MR, Malavazi, I, Melin, P, Meyer, V, Mielnichuk, N, Miskei, M, Molnár, ÁP, Mulé, G, Ngan, CY, Orejas, M, Orosz, E, Ouedraogo, JP, Overkamp, KM, Park, H-S, Perrone, G, Piumi, F, Punt, PJ, Ram, AFJ, Ramón, A, Rauscher, S, Record, E, Riaño-Pachón, DM, Robert, V, Röhrig, J, Ruller, R, Salamov, A, Salih, NS, Samson, RA, Sándor, E, Sanguinetti, M, Schütze, T, Sepčić, K, Shelest, E, Sherlock, G, Sophianopoulou, V, Squina, FM, Sun, H, Susca, A, Todd, RB, Tsang, A, Unkles, SE, van de Wiele, N, van Rossen-Uffink, D, Oliveira, JV de C, Vesth, TC, Visser, J, Yu, J-H, Zhou, M, Andersen, MR, Archer, DB, Baker, SE, Benoit, I, Brakhage, AA, Braus, GH, Fischer, R, Frisvad, JC, Goldman, GH, Houbraken, J, Oakley, B, Pócsi, I, Scazzocchio, C, Seiboth, B, VanKuyk, PA, Wortman, J, Dyer, PS, Grigoriev, I V. (2017). Comparative genomics reveals high biological diversity and specific adaptations in the industrially and medically important fungal genus *Aspergillus*. *Genome Biol* 18, 28.
- Walker, SC, and Engelke, DR (2006). Ribonuclease P: the evolution of an ancient RNA enzyme. *Crit Rev Biochem Mol Biol* 41, 77–102.
- Wang, F, Durfee, LA, and Huijbregtse, JM (2013). A cotranslational ubiquitination pathway for quality control of misfolded proteins. *Mol Cell* 50, 368–378.
- Wang, J, Hu, Q, Chen, H, Zhou, Z, Li, W, Wang, Y, Li, S, and He, Q (2010). Role of individual subunits of the *Neurospora crassa* CSN complex in regulation of deneddylation and stability of cullin proteins. *PLoS Genet* 6, e1001232.
- Wang, X-F, He, F-F, Ma, X-X, Mao, C-Z, Hodgman, C, Lu, C-G, and Wu, P (2011). OsCAND1 is required for crown root emergence in rice. *Mol Plant* 4, 289–299.
- Wang, Z, Michaud, GA, Cheng, Z, Zhang, Y, Hinds, TR, Fan, E, Cong, F, and Xu, W (2012). Recognition of the iso-ADP-ribose moiety in poly(ADP-ribose) by WWE domains suggests a general mechanism for poly(ADP-ribosyl)ation-dependent ubiquitination. *Genes Dev* 26, 235–240.
- Wauer, T, and Komander, D (2014). The JAMM in the proteasome. *Nat Struct Mol Biol* 21, 346–348.
- Wei, N, Serino, G, and Deng, X-W (2008). The COP9 signalosome: more than a protease. *Trends Biochem Sci* 33, 592–600.
- Werner, A, and Swan, D (2010). What are natural antisense transcripts good for? *Biochem Soc Trans* 38, 1144–1149.
- Whitby, FG, Xia, G, Pickart, CM, and Hill, CP (1998). Crystal structure of the human ubiquitin-like protein NEDD8 and interactions with ubiquitin pathway enzymes. *J Biol Chem* 273, 34983–34991.
- Wiborg, O, Pedersen, MS, Wind, A, Berglund, LE, Marcker, KA, and Vuust, J (1985). The human ubiquitin multigene family: some genes contain multiple directly repeated ubiquitin coding sequences. *EMBO J* 4, 755–759.
- Wight, M, and Werner, A (2013). The functions of natural antisense transcripts. *Essays Biochem* 54, 91–101.
- Williams, NK, and Dichtl, B (2018). Co-translational control of protein complex formation: a fundamental pathway of cellular organization? *Biochem Soc Trans* 46, 197–206.
- Wolf, DA, Zhou, C, and Wee, S (2003). The COP9 signalosome: an assembly and maintenance platform for cullin ubiquitin ligases? *Nat Cell Biol* 5, 1029–1033.
- Wong Sak Hoi, J, Beau, R, and Latgé, J-P (2012). A novel dehydrin-like protein from *Aspergillus fumigatus* regulates freezing tolerance. *Fungal Genet Biol* 49, 210–216.
- Wu, J-T, Chan, Y-R, and Chien, C-T (2006). Protection of cullin-RING E3 ligases by CSN-UBP12. *Trends Cell Biol* 16, 362–369.
- Wu, K, Yamoah, K, Dolios, G, Gan-Erdene, T, Tan, P, Chen, A, Lee, CG, Wei, N, Wilkinson, KD, Wang, R, Pan, ZQ. (2003). DEN1 is a dual function protease capable of processing the C terminus of Nedd8

- and deconjugating hyper-neddylated CUL1. *J Biol Chem* 278, 28882–28891.
- Wu, S, Zhu, W, Nhan, T, Toth, JI, Petroski, MD, and Wolf, DA (2013). CAND1 controls *in vivo* dynamics of the cullin 1-RING ubiquitin ligase repertoire. *Nat Commun* 4, 1642.
- Xu, S, Abbasian, M, Patel, P, Jensen-Pergakes, K, Lombardo, CR, Cathers, BE, Xie, W, Mercurio, F, Pagano, M, Giegel, D, Cox, S. (2007). Substrate recognition and ubiquitination of SCFSkp2/Cks1 ubiquitin-protein isopeptide ligase. *J Biol Chem* 282, 15462–15470.
- Yan, J, Walz, K, Nakamura, H, Carattini-Rivera, S, Zhao, Q, Vogel, H, Wei, N, Justice, MJ, Bradley, A, and Lupski, JR (2003). COP9 signalosome subunit 3 is essential for maintenance of cell proliferation in the mouse embryonic epiblast. *Mol Cell Biol* 23, 6798–6808.
- Yang, E, Tacchelly-Benites, O, Wang, Z, Randall, MP, Tian, A, Benchabane, H, Freemantle, S, Pikielny, C, Tolwinski, NS, Lee, E, Ahmed, Y. (2016). Wnt pathway activation by ADP-ribosylation. *Nat Commun* 7, 11430.
- Yen, H-CS, Xu, Q, Chou, DM, Zhao, Z, and Elledge, SJ (2008). Global protein stability profiling in mammalian cells. *Science* 322, 918–923.
- Yogosawa, S, Makino, Y, Yoshida, T, Kishimoto, T, Muramatsu, M, and Tamura, T (1996). Molecular cloning of a novel 120-kDa TBP-interacting protein. *Biochem Biophys Res Commun* 229, 612–617.
- Yu, J-H (2006). Heterotrimeric G protein signaling and RGSs in *Aspergillus nidulans*. *J Microbiol* 44, 145–154.
- Yu, J-H (2010). Regulation of development in *Aspergillus nidulans* and *Aspergillus fumigatus*. *Mycobiology* 38, 229–237.
- Yu, Z et al. (2011). Dual function of Rpn5 in two PCI complexes, the 26S proteasome and COP9 signalosome. *Mol Biol Cell* 22, 911–920.
- Zemla, A, Thomas, Y, Kedziora, S, Knebel, A, Wood, NT, Rabut, G, and Kurz, T (2013). CSN- and CAND1-dependent remodelling of the budding yeast SCF complex. *Nat Commun* 4, 1641.
- Zeng, R, Li, M, Chen, Q, Wang, L, Zhan, P, Wang, C, Lv, G, Shen, Y, and Liu, W (2014). *In vitro* analyses of mild heat stress in combination with antifungal agents against *Aspergillus fumigatus* biofilm. *Antimicrob Agents Chemother* 58, 1443–1450.
- von Zeska Kress, MR, Harting, R, Bayram, Ö, Christmann, M, Irmer, H, Valerius, O, Schinke, J, Goldman, GH, and Braus, GH (2012). The COP9 signalosome counteracts the accumulation of cullin SCF ubiquitin E3 RING ligases during fungal development. *Mol Microbiol* 83, 1162–1177.
- Zhang, J, van den Heuvel, J, Debets, AJM, Verweij, PE, Melchers, WJG, Zwaan, BJ, and Schoustra, SE (2017). Evolution of cross-resistance to medical triazoles in *Aspergillus fumigatus* through selection pressure of environmental fungicides. *Proceedings Biol Sci* 284, 20170635.
- Zhang, S, Huang, J, Shi, T, Hu, F, Zhang, L, Zhou, P-K, Ma, D, Ma, T, and Qiu, X (2016). DCUN1D3 activates SCFSKP2 ubiquitin E3 ligase activity and cell cycle progression under UV damage. *Oncotarget* 7, 58483–58491.
- Zhang, W, Ito, H, Quint, M, Huang, H, Noël, LD, and Gray, WM (2008). Genetic analysis of CAND1-CUL1 interactions in *Arabidopsis* supports a role for CAND1-mediated cycling of the SCFTIR1 complex. *Proc Natl Acad Sci U S A* 105, 8470–8475.
- Zhao, X, Lutz, J, Höllmüller, E, Scheffner, M, Marx, A, and Stengel, F (2017). Identification of proteins interacting with ubiquitin chains. *Angew Chemie Int Ed* 56, 15764–15768.
- Zheng, J, Yang, X, Harrell, JM, Ryzhikov, S, Shim, EH, Lykke-Andersen, K, Wei, N, Sun, H, Kobayashi, R, and Zhang, H (2002a). CAND1 binds to unneddylated CUL1 and regulates the formation of SCF ubiquitin E3 ligase complex. *Mol Cell* 10, 1519–1526.
- Zheng, N et al. (2002b). Structure of the Cul1-Rbx1-Skp1-F boxSkp2 SCF ubiquitin ligase complex. *Nature* 416, 703–709.
- Zheng, N, and Shabek, N (2017). Ubiquitin Ligases: Structure, Function, and Regulation. *Annu Rev Biochem* 86, 129–157.

Zhou, C, Wee, S, Rhee, E, Naumann, M, Dubiel, W, and Wolf, DA (2003). Fission yeast COP9/signalosome suppresses cullin activity through recruitment of the deubiquitylating enzyme Ubp12p. *Mol Cell* 11, 927–938.

Zhou, Z, Wang, Y, Cai, G, and He, Q (2012). *Neurospora* COP9 signalosome integrity plays major roles for hyphal growth, conidial development, and circadian function. *PLoS Genet* 8, e1002712.

List of abbreviations

%	percent
α	alpha
aa	amino acid(s)
Af	<i>A. fumigatus</i>
ah	aerial hyphae
An	<i>A. nidulans</i>
β	beta
BiFC	bimolecular fluorescence complementation
BLAST	basic local alignment search tool
bp	base pair
c	cleistothecium
$^{\circ}\text{C}$	degree Celsius
CandA	cullin-associated Nedd8-dissociated protein A
cDNA	complementary DNA
COP9	constitutive photomorphogenesis 9
CRL	cullin-RING ligase
CSN	COP9 signalosome
CulA/C/D	cullin A/C/D
Δ	delta, deletion
d	day
DAPI	4',6-Diamidin-2-phenylindol
DenA	deneddylase A
dH ₂ O	deionized water
DIC	differential interference contrast (microscopy)
DNA	deoxyribonucleic acid
e.g.	<i>exempli gratia</i> = for example
<i>et al.</i>	<i>et alii</i> , and others
ex1	exon 1
Fbx	F-box
g	gram
GG	die-glycine motif
gDNA	genomic DNA
GFP	green fluorescent protein
GST	glutathione-S-transferase
h	hour(s) or Hülle cells
<i>h2A</i>	<i>histone 2A</i>
HEAT	Huntington, EF3, PP2A, TOR1
HPLC	high performance liquid chromatography
<i>igr</i>	<i>intergenic region</i>
kDa	kilo Dalton
kb	kilo base pair
l	liter
LB	lysogeny broth
LC-MS	liquid chromatography coupled with mass spectrometry
LFQ	label free quantification
Lys, K	lysine

List of abbreviations

M	Molar (mol/l)
mAu	milliabsorption unit
mg	milligram
min	minute
ml	milliliter
mM	millimolar
mm	millimeter
mRNA	messenger RNA
NAE	Nedd8 activating enzyme
<i>natR</i>	nourseothricin resistance marker
<i>nat-RM</i>	nourseothricin recyclable resistance marker
Nedd8, N8	Neural precursor cell expressed developmentally down-regulated protein 8
NLS	nuclear localization sequence/signal
ns	non-significant
NTE	N (amino)-terminal extension
OE	over expression
ORF	open reading frame
^P	promoter
p.c.	personal communication
PCR	polymerase chain reaction
<i>phleo</i> ^R	phleomycin resistance marker
<i>phleo-RM</i>	phleomycin recyclable resistance marker
PTM	post-translational modification
<i>ptrA-RM</i>	pyrithiamine recyclable resistance marker
qRT-PCR	quantitative real-time PCR
^R	resistance
RbxA/Rco1	RING-box protein / regulator of cullins
RFP	red fluorescent protein
RING	really interesting new gene
RNA	ribonucleic acid
RNase P	Ribonuclease P
rpm	rounds per minute
Rpr2/Rpp21	RNase P ribonucleoprotein/ribonuclease P/MRP subunit P21
SCF	SkpA, CulA, F-box
SDS	sodium dodecyl sulfate
SEM	standard error of the mean
SkpA	S-phase kinase-associated protein A
spp.	species
^T	terminator
μl	micro liter
μm	micro meter
Ub	ubiquitin
UBL	ubiquitin-like
UPS	ubiquitin proteasome system
v/v	volume per volume
wt	wild type
w/v	weight per volume
YFP	yellow fluorescent protein

List of figures

Figure 1.	Conidia of <i>A. nidulans</i> and <i>A. fumigatus</i>	6
Figure 2.	<i>Aspergillus nidulans</i> life cycle.....	7
Figure 3.	The central regulatory pathway of <i>A. nidulans</i> asexual development.	10
Figure 4.	Comparison of ubiquitin and Nedd8.	14
Figure 5.	Neddylation and ubiquitination cascades.	16
Figure 6.	Types of E3 ligases.....	17
Figure 7.	Ubiquitin proteasome system.	19
Figure 8.	The CRL cycle and its regulation.	22
Figure 9.	The COP9 signalosome subunit architecture.	24
Figure 10.	Csn5/E activation upon CRL binding.....	25
Figure 11.	Domain properties and crystal structure of Cand1 in complex with Cul1-Rbx1.	27
Figure 12.	Cand1 has conserved Nedd8 and Skp1 blocking sites.	29
Figure 13.	Scheme of <i>in locus</i> integration of a recyclable marker cassette and its recycling.	42
Figure 14.	<i>A. nidulans</i> CandA has three genes coding for three subunits and <i>A. fumigatus</i> CanA has two genes coding for two CanA proteins.....	68
Figure 15.	Comparison of single and split Cand proteins in human and fungi.	69
Figure 16.	Comparative analysis of CandA-C1 and CandA-C orthologs in different <i>Aspergillus</i> spp.	71
Figure 17.	The genomic environment of the <i>candA</i> genes within Aspergilli.....	72
Figure 18.	<i>A. nidulans candA-C1</i> and <i>candA-C</i> have a shared transcript and the <i>intergenic</i> <i>region</i> promotes <i>candA-C</i> transcription.	74
Figure 19.	Expression of <i>candA-C</i> is independent from <i>candA-C1</i> expression.....	75
Figure 20.	A synthetic fusion protein of <i>A. nidulans</i> CandA-C migrates at similar molecular weight like the <i>A. fumigatus</i> CanA.....	77
Figure 21.	<i>A. nidulans</i> CandA proteins are localized in nuclei.....	78
Figure 22.	CandA-C1 and Nedd8 nuclear localization are independent from the CandA-C NLS in <i>A. nidulans</i>	79
Figure 23.	CandA-C1 is found in nuclei independent of CandA-N and CandA-C and <i>vice</i> <i>versa</i>	81
Figure 24.	CandA-C1 interacts with CandA-C and CandA-N.....	83
Figure 25.	<i>A. nidulans</i> CandA-C1 pulls Nedd8, CulA and CSN subunits as components of SCF regulation.....	84
Figure 26.	Perseus workflow.....	85

List of figures

Figure 27.	Pull-downs coupled to LC-MS of CandA-N, CandA-C and CandA-C1 supports the existence of a trimeric CandA complex in <i>A. nidulans</i>	87
Figure 28.	<i>A. fumigatus</i> CanA pulls CulaA and CulC.	91
Figure 29.	CandA is required for CulaA neddylation in <i>A. nidulans</i>	93
Figure 30.	Recombinant CandA-N and CandA-C form a complex.	95
Figure 31.	Recombinantly expressed CandA-N and CandA-C are not sufficient to reduce accumulated unneddylated CulaA in <i>candA</i> deletion strains.	96
Figure 32.	CandA-C1 supports the reduction of deneddyated CulaA accumulation in <i>candA-C</i> deletion strains of <i>A. nidulans</i>	98
Figure 33.	Nedd8 pulls CandA-N and CandA-C but not CandA-C1 under native buffer conditions.	100
Figure 34.	Nedd8 interacts with CandA-N, CandA-C and CandA-C1 in nuclei and cytoplasm.	104
Figure 35.	<i>A. fumigatus canA</i> mutants are delayed in development.	106
Figure 36.	<i>A. fumigatus</i> CanA proteins are required for germination of asexual spores at different temperatures.	108
Figure 37.	<i>A. nidulans</i> CandA-C1 is required for spore germination at 42°C.	111
Figure 38.	<i>candA-C1</i> and <i>igr</i> are required for growth and sexual development and the <i>igr</i> is possibly the promoter for <i>candA-C</i>	112
Figure 39.	Asexual development is dependent on <i>candA-C1</i>	113
Figure 40.	Overexpression of <i>candA-C1</i> reduces the colony growth of <i>candA-C</i> defective mutants.	115
Figure 42.	<i>A. fumigatus</i> and <i>A. nidulans</i> gene orthologs for <i>candAC-1</i> complement each other.	116
Figure 41.	CandA and CsnE together are required for growth, development and coordinated secondary metabolism.	118
Figure 43.	Mitochondria of Δ <i>candA</i> deletion strains are fragmented.	119
Figure 44.	Overexpression <i>candA-C1</i> increases conidiospore production of strains defective in <i>candA-C</i> and <i>candA-N/C</i>	121
Figure 45.	Colony of Δ <i>candA-C1</i> has a volcano-like growth in sexual development.	122
Figure 46.	Ascospore formation is dependent on <i>candA-C1</i>	124
Figure 47.	CandA and DenA are required for sexual development.	126
Figure 48.	Orsellinic acid derivative production is independent of CandA-C1.	128
Figure 49.	3D structure prediction of <i>A. nidulans</i> CandA-C1 shows similarities to Rpr2/Rpp21.	132
Figure 50.	<i>A. nidulans</i> CandA-C and <i>A. fumigatus</i> CanA C-terminal proteins have the same sequence features.	133

List of figures

Figure 51.	Overview of RNase P/RNase MRP subunits.	135
Figure 52.	Scheme of a putative <i>Aspergillus</i> ancestor and DNA rearrangement of the <i>candA</i> loci.	137
Figure 53.	CandA-C1 and CandA-C have a shared transcript.	139
Figure 54.	CandA/CanA are required for growth and development of <i>Aspergillus</i> spp. ...	142
Figure 55.	Possible functions of the CandA-CuIA interaction for E3 ubiquitin ligase activity.	148
Figure 56.	The monopartite NLS is conserved in most fungal CandA orthologs.	153
Figure 57.	Comprehensive model of <i>candA</i> expression, nuclear transport and regulator of SCF activity.	155

List of tables

Table 1. <i>E. coli</i> strains used in this study.....	33
Table 2. <i>A. fumigatus</i> strains used in this study.....	34
Table 3. <i>A. nidulans</i> strains used in this study.....	35
Table 4. Oligonucleotides used for qRT-PCR.....	40
Table 5. qRT-PCR program used in this study	40
Table 6. Oligonucleotides used for cDNA amplification assay	41
Table 7. Oligonucleotides designed and used in this study	43
Table 8. Plasmids designed and used in this study	46
Table 9. Identified proteins in CandA-N, CandA-C and CandA-C1 pull-downs.	88
Table 10. Identified proteins of Nedd8 pull-downs.	101

Acknowledgements

First and foremost, I would like to thank Prof. Dr. Gerhard H. Braus for his extensive support while I was working on my PhD project. I am grateful for many fruitful discussions, his expertise and helpful advice and all together he provided me with an excellent supervision. I appreciate that I could attend national as well as international meetings, where he introduced me to outstanding researchers.

I am thankful to Prof. Dr. Kai Tittmann for being a member of my thesis committee. He always gave helpful advices and had motivating suggestions.

I want to thank Dr. Achim Dickmanns for being a member of my thesis committee. I appreciate his expertise on protein research already since my Bachelor thesis and I benefit from the discussions we had during the last years, which helped me with my research projects.

Furthermore, I would like to thank Prof. Dr. Stefanie Pöggeler for helpful discussions and advices during the progress reports and that she deputized Prof. Dr. Kai Tittmann for my 4th thesis committee meeting.

Additionally, I thank Prof. Dr. Stefanie Pöggeler, Jun. Prof. Dr. Kai Heibel and PD. Dr. Michael Hoppert for being members of my examination board.

I am very grateful to be enrolled in the doctoral program 'Microbiology and Biochemistry' of the Göttingen Graduate School for Neuroscience, Biophysics and Molecular Biosciences (GGNB). The GGNB allowed me to attend method and soft skill courses as well as gave me the opportunity to visit companies, from which I learned a lot for my PhD and future career. Furthermore, I thank the GGNB for financial support by providing me with travel grants.

Additionally, I am very thankful for the participation in the project B06 of the SFB860 'Integrative Structural Biology of Dynamic Macromolecular Assemblies'. I am thankful for funding and additional support in means of travel grants. Furthermore, I am grateful to Prof. Dr. Gerhard H. Braus that he involved me in grant writing as well as oral and poster presentations within the SFB860, from which I learned a lot.

I appreciate the discussions, advises, expertise as well as mental and experimental support of Dr. Rebekka Harting. I am deeply grateful for her supervision, especially during the final phase of my PhD thesis.

Furthermore, I would like to thank Gabriele Heinrich, Cindy Meister, Fruzsina Bakti, Dr. Mirit Kolog Gulko and the former members Dr. Elena Beckmann and Dr. Josua Schinke of my lab. I enjoyed the working atmosphere, coffee and cake breaks and discussions we had together. I could always count on your help and advice. My gratitude goes to Gaby for her kindness and excellent technical support with experiments. I thank Dr. Mirit Kolog-Gulko for helpful discussions and successful cooperation, which resulted in an inspiring review article. I am thankful for Fruzsina Bakti that she kindly introduced me to the work in the S2 lab with *A. fumigatus*, also for having open ears for discussing experiments, the sewing projects we shared in our free time and for her friendship. Special thanks to Cindy, I could count on her suggestions and support from the first day of our Master thesis till now. Together we experienced many milestones, like successful publications and scientific meetings as well as difficult times when lab work was not easy. All in all, this friendship helped me a lot during my PhD. Furthermore, I would like to thank my Master student Annika Langeneckert. She was an excellent student and I enjoyed working with her.

Acknowledgements

I thank Sabine Thieme for her long friendship, expertise and help. During the time we first met in the early beginning of our studies in 2007 until now we shared many of our interests and therefore we ended up together in the same working group for our PhD and we will hopefully kiss the Gänseliesel together as Sabine proposed four years ago.

Additionally, I want to thank our lunch group, which was kind of a daily therapy meeting that helped all of us to calm down from lab work and I benefited from the fruitful discussions. Especially, I want to thank Karl Thieme for his advises and the friendship.

For the proofreading of my thesis I would like to thank Rebekka, Karl, Fruzsina, Anja and Sabine.

I am very grateful to Dr. Oliver Valerius and Dr. Kerstin Schmitt who performed the LC-MS measurements and taught me the data analysis. I also thank them for providing protocols and working solutions and for the corrections of the materials and methods section in this work.

I want to thank Dr. Jennifer Gerke for the HPLC measurements of secondary metabolites and that she provided me with BiFC and recyclable marker plasmids, which supported my experiments. Thank you for proofreading the respective materials and methods section.

I thank Dr. Christoph Sasse for his expertise in the work with *A. fumigatus* that he shared with me and for providing me a cloning plasmid with *ptrA* marker cassette.

I am also very thankful for all other members of the department of 'Molecular Microbiology and Genetics' who were always kind and helpful. A special thank you to Heidi Northemann, Andrea Wäge, Nicole Scheiter, Verena Große and Katharina Ziese-Kubon for supporting administrative issues as well as everyday lab life. Furthermore, I am thankful for the technical support provided by the maintenance facility.

Besides my colleagues from the institute of 'Microbiology and Genetics', I would like to thank my friends from outside of the lab. I especially appreciate the close ten-years friendship with the 'Bachelor Mädels' Bine, Steffi, Ronja, Ramona und Natalie! Every Tuesday I cannot wait for our dinner evening to take place. These meetings always motivated me during the last years. Furthermore, I would like to thank the 'Master Mädels' for their friendship and mental support. A special thank you to Sandra Keiper and Berit Hassing, for open ears and discussions. I think a lot about our exciting travel through the New Zealand north island, Berits new home! This travel provided me with energy for the last year of my PhD.

Last but not least, I want to express my deepest gratitude to my family. I especially honor my parents and my grandmother for their constant support and love during my studies. I also thank my sister and brother with his little family for motivation and that you are always there for me. I excuse myself for not attending several family gatherings of my huge and harmonic family, as I was mostly busy with PhD work.

Finally, I want to thank my boyfriend Christian for his love, encouragement and endless patience. He has been there for me the past ten years and has always supported me with all my wishes and aims. Thank you for everything!

Curriculum vitae

Anna Maria Köhler

born on June 1st, 1988

in Fritzlar, Germany

Higher education and academic qualification

04/2014 – 2018

PhD student in the doctoral program “Microbiology and Biochemistry” of the Göttingen Graduate School of Neuroscience, Biophysics and Molecular Biosciences (GGNB) at the Georg-August-Universität Göttingen, Germany.

PhD thesis at the Institute for Microbiology and Genetics, Department of Molecular Microbiology and Genetics (Prof. Dr. Gerhard H. Braus). Title: “Specific ubiquitin-dependent protein degradation requires a trimeric CandA complex in *Aspergillus nidulans*”

10/2011 – 11/2013

Master of Science in Microbiology and Biochemistry at the Georg-August-Universität Göttingen, Germany.

Master thesis at the Institute for Microbiology and Genetics, Department of Molecular Microbiology and Genetics (Prof. Dr. Gerhard H. Braus). Title: “Structural insights into *A. nidulans* CSN-DenA interactions.”

10/2007 – 09/2011

Bachelor of Science in Biology at the Georg-August-Universität Göttingen, Germany.

Bachelor thesis at the Institute for Microbiology and Genetics, Department of Molecular Structural Biology (Prof. Dr. Ralf Ficner). Title: “Interaktionen zwischen den eukaryotischen Translations-Initiationsfaktoren eIF2 und eIF5 aus *Saccharomyces cerevisiae*.”

Scientific Teaching

- 03/2016 – 05/2016 Supervision of a laboratory internship of a Bachelor student Martin Dollinger
- 04/2015 – 10/2015 Supervision of a Master thesis of Annika Elise Langeneckert
- 01/2015 – 02/2015 Supervision of a laboratory internship of Annika Elise Langeneckert

Publications

- 2016 **Köhler, A.M.**, Meister, C., and Braus, G.H. (2016) In vitro Deneddylation Assay. *Bio-protocol* 6(6): e1756. DOI: 10.21769/BioProtoc.1756.
- 2016 Meister, C*, Kolog Gulko, M*, **Köhler, A.M.***, and Braus, G.H. (2016) The devil is in the details: comparison between COP9 signalosome (CSN) and the LID of the 26S proteasome. *Curr Genet* 62: 129–136 (* equally contributed)
- 2015 Beckmann, E.A., **Köhler, A.M.**, Meister, C., Christmann, M., Draht, O.W., Rakebrandt, N., *et al.* (2015) Integration of the catalytic subunit activates deneddylase activity in vivo as final step in fungal COP9 signalosome assembly. *Mol Microbiol* 97: 110–124

Further scientific and work experiences

- 2016 – 2018 Collaboration with Dahlia Shamir and Joel Hirsch, Department of Biochemistry & Molecular Biology, George S. Wise Faculty of Life Sciences, Tel Aviv University and Daniel Chamovitz, Department of Plant Science, Tel Aviv University. Project: COP9 signalosome
- 11/2016 – 2018 Member of the Bio-Protocol reviewer board
- 01/2015 – 05/2015 Scientific assistant at the research group of Chromatin Biochemistry (Prof. Dr. Wolfgang Fischle), Max Planck Institute for Biophysical Chemistry Göttingen, Germany. Scope of duty: DNA giga-preparations for chromatin studies.

10/2012 – 12/2012
and
11/2011 – 12/2011

Student assistant at the Department of Molecular Structural Biology (Prof. Dr. Ralf Ficner), Georg-August-Universität Göttingen, Germany. Scope of duty: Supervision of the Biochemistry tutorial of Bachelor Students

04/2012 – 11/2012

Student research project within the 'International Genetically Engineered Machine Competition' (iGEM), Team Göttingen 2012 supervised by Prof. Dr. Heinz Neumann, Project title: Homing Coli

School education

1998 – 2007

Secondary school and attainment of the university-entrance diploma (Abitur) at the CJD Oberurff Jugenddorf-Christophorusschule, Bad Zwesten, Germany

1994 – 1998

Elementary school at the Altenburgschule Bad Zwesten, Germany

Awards

03/2017

Poster award at the 14th International Aspergillus Meeting of the 29th Fungal Genetics Conference, Pacific Grove, CA, USA

10/2012

iGEM Gold Award at the regional jamboree: Europe, Amsterdam, Netherlands